Structure and molecular function of WD-40 repeat-containing autophagy proteins Atg18, Atg21 and Hsv2

Dissertation

For the award of the degree

"Doctor rerum naturalium"

Of the Georg-August University Göttingen

Within the doctoral program "Molecular Medicine" of the Georg-August University School of Science (GAUSS)

Submitted by

Matthew Faber Taylor

Göttingen 2022

Members of the thesis committee and examination board

Prof. Dr Michael Thumm (Supervisor and first referee)	Department of Cellular Biochemistry Centre for Cellular Biochemistry University Medical Centre Göttingen
Prof. Dr Ralph Kehlenbach (Second referee)	Department of Molecular Biology Centre for Molecular Biology University Medical Centre Göttingen
Prof. Dr Ralf Ficner	Department of Molecular Structural Biology Institute for Microbiology and Genetics University Medical Centre Göttingen

Further members of the examination board

Prof. Dr Peter Schu	Department of Cellular Biochemistry University Medical Centre Göttingen
Prof. Dr Silvio O. Rizzoli	Department of Neuro- and Sensory Physiology University Medical Centre Göttingen
Dr Alex Faesen	Department of Biochemistry of Signal Dynamics Max Planck Institute for Multidisciplinary Sciences

Date of oral examination: 28.04.2022

Affidavit

I hereby declare that the thesis entitled "**Structure and molecular function of WD-40 repeat containing autophagy proteins Atg18, Atg21 and Hsv2**" has been written independently and with no other sources and aids than quoted.

Matthew Faber Taylor

Göttingen, March 2022

Table of Contents

List of Figures

List of Tables

List of Abbreviations

5-FOA:	5-fluoroorotic acid
AIM:	Atg8-interacting motif
Amp:	Ampicillin
Ams1:	α-mannosidase
Ape1:	Aminopeptidase 1
Ape4:	Aminopeptidase 4
ARM:	Armadillo repeat
ATG:	Autophagy-related
Atg11BRs:	Atg11-binding regions
ATP:	Adenosine triphosphate
BioID:	Proximity-dependant biotin identification
BirA*	$BirA^{R118G}$
BFP:	Blue fluorescent protein
C-terminal:	Carboxyterminal
C-terminus:	Carboxyterminus
CBB:	Coomassie brilliant blue
CM:	Complete minimal
CMA:	Chaperone-mediated autophagy
Co-IP:	Coimmunoprecipitation
COPII:	Coat protein complex II
C_{ub}:	Carboxyterminal half of ubiquitin
Cvt:	Cytoplasm-to-vacuole tragetting
ddH_2O:	Double-distilled water
DAPI:	4’,6-diamidino-2-phenyliindole
DIC:	Differential interference contrast
DMSO:	Dimethyl sulfoxide
DNA:	Desoxyribonucleic acid
DTT:	Dithioreitol
ER:	Endoplasmic reticulum
ERES:	Endoplasmic reticulum exit sites

ESCRT:	Endosomal sorting complexes required for transport
FAM:	5(6)-carboxyfluorescein
GDP:	Guanosine diphosphate
GEF:	Guanine nucleotide exchange factor
GFP:	Green fluorescent protein
GTP:	Guanosine triphosphate
GTPase:	Guanosine triphosphatase
GUV:	Giant unilamellar vesicle
HA:	Human influenza hemagglutinin
HEPES:	4-(2-hydroxyethyl)-1-piperazineethanesulfonic acid
His:	Histidine
HORMA domain:	Hop1, Rev7 and Mad2 domain
HOPS:	Homotypic vacuole fusion and protein sorting
HRP:	Horseradish peroxidase
IDR:	Intrinsic disordered region
Kl:	*Kluyveromyces lactis*
LB:	Lysogeny broth
LC-MS:	Liquid chromatography-mass spectrometry
mApe1:	Mature aminopeptidase 1
mCherry:	Monomeric Cherry
MCS:	Multiple cloning site
MIT domain:	Microtubule-interacting and transport domain
MOP:	Meiosis II outer plaque
MS:	Mass spectrometry
MV:	Minimal plus vitamins
MVB:	Multi-vesicular bodies
N-terminal:	Aminoterminal
N-terminus:	Aminoterminus
N_{ub}:	Aminoterminal half of ubiquitin
NVJ:	Nucleus-vacuole junction
ns:	Not significant
pApe1:	Precursor aminopeptidase 1

PAS:	Pre-autophagosomal structure
PBS:	Phosphate buffered saline
PCR:	Polymerase chain reaction
PDB:	Protein databank
PE:	Phosphatidylethanolamine
PEG:	Polyethylene glycol
pH:	Potential of hydrogen
PI:	Phosphatidylinositol
PI3-kinase:	Phosphatidylinositol 3-kinase
PI3P:	Phosphatidylinositol 3-phosphate
$PI(3,5)P_2$:	Phosphatidylinositol 3,5-bisphosphate
PKA:	Protein kinase A
PMN:	Piecemeal microautophagy of the nucleus
PMSF:	Phenylmethane sulfonyl fluoride
PROPPIN:	β-propellers that bind polyphosphoinositides
PSM:	Prospore membrane
PVDF:	Polyvinylidene difluoride
RT:	Room temperature
S. cerevisiae:	*Saccharomyces cerevisiae*
SEC:	Size exclusion chromatography
SD-N:	Synthetic defined medium without nitrogen
SDS:	Sodium dodecyl sulphate
SDS-PAGE:	Sodium dodecyl sulphate polyacrylamide gel electrophoresis
SEM:	Standard error of the mean
SILAC:	Stable isotope labelling by amino acids
SNARE:	Soluble N-ethylmaleimide-sensitive-factor attachment receptor
SOC:	Super optimal broth with catabolite repression
TAE:	Tris base, acetic acid, EDTA
TBST:	Tris buffered saline with triton X-100
TCA:	Trichloroacetic acid
TEMED:	Tetramethylethylendiamin
Tris:	Tris(hydroxymethyl)aminomethane

Trp:	Tryptophan
TORC1:	Target of rapamycin complex 1
Ura:	Uracil
UV:	Ultra violet
v/v:	volume per volume
WIPI:	WD40 repeat-containing proteins that interact with phosphoinositides
w/o:	Without
WT:	Wildtype
w/v:	Weight per volume
yEGFP:	Yeast optimised, enhanced GFP
Ymr1:	Yeast myotubularin-related PI3P phosphatase
YPD:	Yeast peptone dextrose

Units

A:	Ampere(s)
a.u.:	Arbitrary unit(s)
bp:	Basepair(s)
°C:	Degree(s) Celsius
Da:	Dalton(s)
g:	Gram(s)
x g:	Times gravity
hrs:	Hour(s)
L:	Litre(s)
µ:	Micro
m:	Milli
M:	Mole(s) per litre
mins:	Minute(s)
n:	Nano

OD_{600}:	Optical density/absorbance at 600 nm wavelength
pI:	Isoelectric point
rpm:	Revolutions per minute
s:	Seconds
V:	Volt

1. Summary

Autophagy is a highly regulated cellular degradation and recycling process conserved from yeast to higher eukaryotes. This process is constitutively active at a low level, and non-selectively degrades portions of the cytosol in response to internal or external stimuli. This process begins with the *de novo* formation of a cup-shaped membrane structure at the pre-autophagosomal structure (PAS) termed the isolation membrane or phagophore. The phagophore expands to fully engulf the cargo before closing to form the double-membrane structure known as the autophagosome which then fuses with the vacuole to release its cargo into the vacuolar lumen for degradation and recycling.

The biogenesis of the autophagosomes requires the generation of phosphatidylinositol 3-phosphate (PI3P) at the PAS. The presence of PI3P at the PAS allows for the binding of β-propellers that bind polyphosphoinositides (PROPPIN). The PROPPINs are a highly conserved family of WD40-repeat proteins and structurally fold as seven-bladed β-propellers. WD40 domains are key components of proteins that mediate protein-protein interactions, including scaffolding, cooperative assembly, and regulation of dynamic multi-subunit complexes. PROPPINs also have a conserved FRRG-motif at the circumference of the propeller that allows for binding phosphoinositides.

In *Saccharomyces cerevisiae,* there are three PROPPINs: Atg18, Atg21 and Hsv2. They are highly homologous but have different autophagic subtypes specificities. Atg18 is a core autophagy protein required for all autophagy in a PI3P-dependent manner. Atg18 has a secondary role at the vacuole binding to $PI(3,5)P_2$, where it carries out nonautophagic functions in regulating vacuolar morphology. Atg21 is not essential for unselective autophagy but is crucial for selective types of autophagy, including the Cvt pathway, which targets vacuolar hydrolases like prApe1 to the vacuole. Hsv2 is the least functionally characterised PROPPIN which is required for efficient piecemeal microautophagy of the nucleus. So far, this is the only observation that has been seen to affect autophagic activity.

This study focused on investigating the molecular function of the *S. cerevisiae* Hsv2. As very little is known about the role of Hsv2, a proximity-dependent biotin identification assay in combination with a stable isotope labelling by amino acids based approach was used to identify potential interactors of Hsv2. In this approach, 50 proteins were identified as potential interactors of Hsv2. To confirm these interactions, Hsv2-GFP and identified proteins tagged with HA were tested for coimmunoprecipitation using a GFP-Trap. Yck3, Vtc3, Vps35 and Vac14 are all confirmed interaction partners of Hsv2 using these methods. Many of these proteins localise to the vacuolar membrane which correlates with the localisation of Hsv2. In parallel, a split ubiquitin assay was also used to further the understanding of the Hsv2 interactome. Using this method we saw an interaction between Hsv2 and Vps21, Sso1, Pep12, Tlg1, and Snc1. These potential interacting partners of Hsv2 provide a promising basis for elucidating the role of Hsv2 within the cell.

In addition, we determined the potential interaction site between Atg21 and Atg8. By purifying *Saccharomyces cerevisiae* Atg8 and with the subsequent binding assays with a synthetic peptide of Atg21, we found the binding affinity to be 42.5 nM. Once the binding affinity had been determined, crystallisation trials were initiated to deduce the crystal structure of *Kluyveromyces lactis* Atg21 in a complex with ScAtg8. Crystals that formed were tested using X-ray crystallography, these were found to be formed of salt and not protein. Computational modelling of the known crystal structures of KlAtg21 and ScAtg8 confirmed that residue D146 of Atg21 could be essential for binding to Atg8.

Finally, part of this study was to dissect the functional role of Atg18 with the retromer complex in regulating vacuolar morphology. Using hyperosmotic stress to induce vacuolar fragmentation, we found that Vps35, Vps29 and Vps26 are required for efficient Atg18 fission activity at the vacuolar membrane. Additionally, in the absence of Vps5 and Vps17, there was unregulated fission activity at the vacuolar membrane that was not dependent on hyperosmotic conditions. These results suggest the importance of Vps35, Vps29 and Vps26 in the efficient fission activity of Atg18 as well as the value of Vps5 and Vps17 in impeding the fission activity of Atg18.

2. Introduction

2.1 Autophagy

The etymology of autophagy comes from the Ancient Greek' αὐτόφαγος', directly translating to 'self-devouring'. Degradation and recycling of cellular components are achieved by autophagy, an evolutionarily conserved process in eukaryotes. Macromolecules and organelles are transported via vesicles from the cytosol to the lytic compartment, which in higher eukaryotes is the lysosome and for fungi and plants is the vacuole. Once in the lysosome/vacuole, these components are degraded and recycled, providing the cell with energy and vital amino acids to synthesise new proteins. A basal level of autophagy occurs constitutively; however, this process can be further induced in response to various stimuli including starvation, hypoxia and hormonal changes [1]. It is also an essential mechanism in many crucial cellular functions, including the quality control of proteins and organelles, organelle remodelling, destruction of pathogens, cell differentiation, and the regulation of inflammation and immunity. Due to its diverse roles, it is not surprising that many diseases have been linked to autophagic dysfunction, including cancer, diabetes, myopathies, neurodegeneration, and liver and heart diseases [2], [3].

Transmission electron microscopy first revealed autophagy in the early 1960s. In rat liver cells, membrane-bound dense bodies containing partial organelles, like mitochondria and endoplasmic reticulum (ER) membranes, were observed [4]–[6]. Then in the 1990s, autophagy was first described in the yeast *Saccharomyces cerevisiae* (*S. cerevisiae*). With the use of genetic screens, the first autophagy-related (Atg) genes were identified [7]–[9]. Currently, 42 Atg proteins have been identified of which ~20 are essential for autophagic function.

Autophagy in yeast can be categorised into two main types: microautophagy and macroautophagy, which can be further divided into selective and nonselective depending on the conditions. All eukaryotes share the core autophagic machinery, and many of the Atgs found in mammalian cells have orthologs in yeast and plants. Interestingly, the autophagic machinery is shared between micro- and macroautophagy. An additional third type of autophagy, which is mechanistically distinct has been seen in mammalian cells and was

identified as chaperone-mediated autophagy [10]. Although all three differ morphologically, they share a common objective: delivering cargo to the lytic compartment for degradation.

2.2 The Yeast *S. cerevisiae* as a Model Organism

Saccharomyces cerevisiae is one of the most widely used eukaryotic model organisms. *S. cerevisiae* has been used as a model for studying ageing [11], regulation of gene expression [12], signal transduction [13], [14], cell cycle [15], metabolism [16], apoptosis [17], neurodegenerative disorders [18], and many other biological processes [19]. It began with one of the most extensive international collaborations, consisting of over 600 scientists, to fully sequence the genome of *Saccharomyces cerevisiae*; which made it the first fully sequenced eukaryote [20]. Finding that a typical haploid cell contains roughly 12,000 kb of genomic DNA distributed across 16 chromosomes. Once fully sequenced, this led to the development of molecular tools for quick and straightforward genetic manipulations, using homologous recombination to tag proteins, alter promotors and remove genes [21]–[23]. Subsequently, large databases of plasmids and deletion strains have been generated, like the Yeast Knockout Collection, containing over 20,000 deletion strains corresponding to 5,916 genes (http://www-sequence.stanford.edu/group/yeast_deletion_project/deletions3.html).

S. cerevisiae is a unicellular organism that is oval in shape with a diameter of 5-10 µm and a member of the Fungi kingdom. *S. cerevisiae* can exist as a haploid cell that can multiply by mitotic division via budding. In addition, *S. cerevisiae* can be diploid and multiply by meiotic division via sporulation. *S. cerevisiae* has a short generation time under nutrient-rich conditions, doubling every 90 mins at 30°C. In the presence of nutrients, both haploid and diploid cells undergo mitotic division. During nutrient depletion, specifically in the absence of nitrogen and the presence of a nonfermentable carbon source, diploid cells will exit the mitotic cycle, undergo meiosis and sporulate to give rise to four stress-resistant haploid spores [24], [25]. Sporulation and budding are explained further in chapter 2.10.

Since every analysed eukaryotic organism uses part of the autophagic machinery already present in yeast, the knowledge obtained through fungal research is highly transferable and potentially relevant for studying human diseases.

2.3 Macroautophagy

The best-characterised type of autophagy is macroautophagy involving the sequestration of bulk cellular material. It is constitutively active at a low level and non-selectively degrades portions of the cytosol in response to internal and external stimuli. The process of autophagy starts with the *de novo* formation of a cup-shaped membrane structure at the pre-autophagosomal structure (PAS) termed the isolation membrane (IM) or phagophore (Figure 2-1). The phagophore then expands to fully engulf the cargo before closing to form a double-membrane structure called the autophagosome, with a diameter of 400-900 nm [26], [27]. The autophagic body and its contents are released into the vacuolar lumen by fusion of its membrane with the vacuole's outer membrane. Within the vacuole, the autophagic body requires lysis in order for the vacuole hydrolases to have access to its contents. The metabolic precursors can then be transported back into the cytosol for the synthesis of new proteins and organelles. The whole cycle from initiation to fusion with the vacuole takes roughly 10 minutes [28], [29].

Macroautophagy can also selectively degrade specific cargo using the core autophagic machinery in addition to selective autophagy receptors (SARs) that are able to recognise and bind particular cargo. Specific cargos can be damaged or superfluous mitochondria (mitophagy), ribosomes (ribophagy), ER (ER-phagy) or peroxisomes (pexophagy) [30]–[33]. Among the core autophagic proteins is Atg8. A ubiquitin-like protein that conjugate to autophagosome membranes to facilitate cargo recruitment, transport and autophagosome biogenesis [34]. Atg8 is attached to both the inner and outer autophagosome membranes, this is explained further in chapter 2.6.3. Atg8 on the inner membrane surface interacts with specific cargo receptors which are key mediates of selective autophagy [35]. On the outer membrane Atg8 binds to adaptor proteins to facilitate transport and fusion to the vacuole [36].

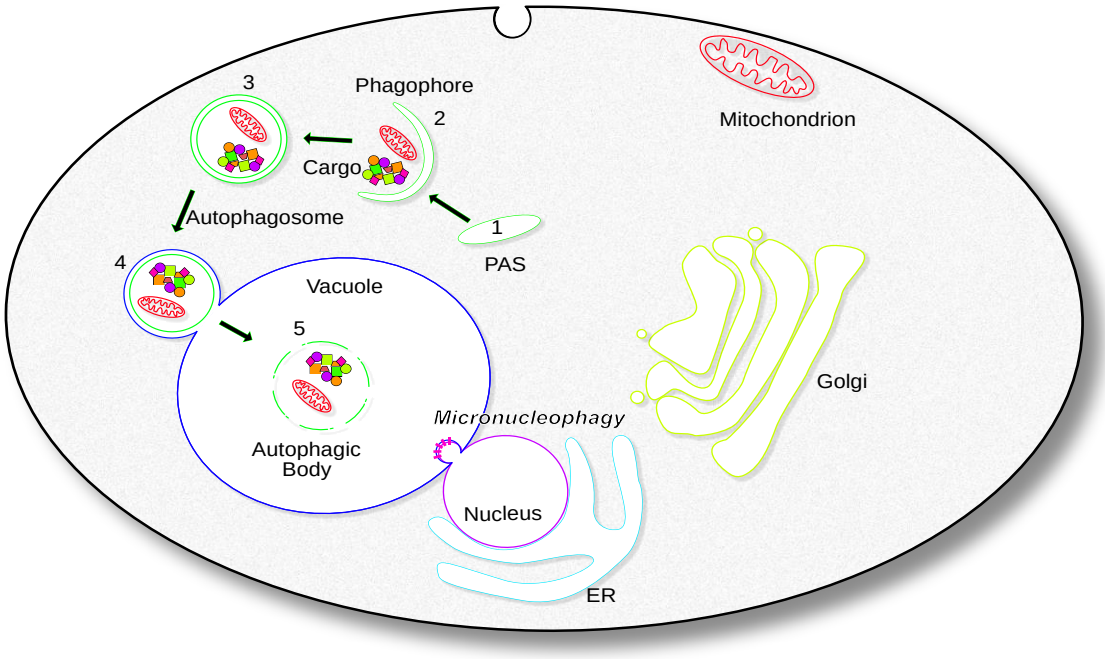

Figure 2-1: A Model of the different stages of macroautophagy in yeast.

In this process, nucleation at the phagophore assembly site (PAS) starts the de novo formation of a double-membraned structure within the cytosol. Phagophores engulf cellular components and expand to form an autophagosome, which eventually fuses with the vacuolar membrane. Which releases the inner membrane or autophagic body, with the cargo inside, into the vacuole lumen. The autophagic body is then lysed exposing the cargo to the vacuolar hydrolases. The degradation products are recycled back into the cytosol for reuse.

The SARs can be soluble receptors, like Atg19 and Atg34, or they can be membrane-associated receptors like Atg32 and Atg39. SARs are not only crucial in cargo recruitment but also bind to Atg8, through the Atg8 interacting motifs (AIM), and to the scaffold protein Atg11 via the Atg11-binding region (Atg11BRs) [30], [37], [38]. However, the Atg11BRs in SARs are close to the AIMs, and this precludes simultaneous binding of both Atg8 and Atg11 to the receptor [39]. Each of the SARs are responsible for mediating selective autophagy of specific cargo. Mitophagy is mediated by Atg32 [40], nucleophagy relies on Atg39 [41], and Atg19 and Atg34 mediate cargo binding in the cytoplasm-to-vacuole targeting pathway (Cvt) [42].

2.4 Cytoplasm-to-Vacuole Targeting Pathway

The cytoplasm-to-vacuole targeting pathway is one type of selective autophagy. The primary cargo of the Cvt pathway is precursor aminopeptidase I (pApe1), which is synthesised in the cytosol and assembles into a dodecamer, as shown in Figure 2-2. The dodecamer

subsequently associates into an oligomer that is termed the pApe1 complex. The pApe1 complex, in combination with Atg19, a selective autophagy receptor protein, and small oligomers formed by α-mannosidase (Ams1), constitutes the Cvt complex [43]. The pApe1 contains a N-terminal propeptide to ensure enzyme inactivity in the cytosol. The amino acid sequence within the propeptide binds to Atg19 [42]. The C-terminus of Atg19 contains binding sites for both Atg11 and Atg8 [43], where the WXXL motif allows binding to Atg8 linking the cargo complex with the phagophore and its subsequent selective sequestration [44]. Additionally, Atg19 functions as a receptor for aspartyl aminopeptidase 4 (Ape4) and Ams1, two more resident vacuolar hydrolases that are part of the Cvt complex [45], [46].

In various types of selective autophagy, Atg11 acts as a scaffold protein, interacting with receptors, Atg1 kinase complex and itself. Atg11 is essential for the organisation of Atg proteins at the PAS during autophagy. In terms of the core autophagic proteins, Atg9 is the only multipass transmembrane protein, which is believed to be important for delivering membranes necessary for the formation of the sequestering vesicles, this is explained further in chapter 2.6.4 [47]. Atg11 interacts with Atg9 and causes some membranes positive for Atg9 to be relocated form the peripheral pool to the perivacuolar site which serves as the PAS [48], [49]. By interacting directly with the Arp2/3 complex, Atg11 guides movement of Atg9-Atg11 molecules [50], [51].

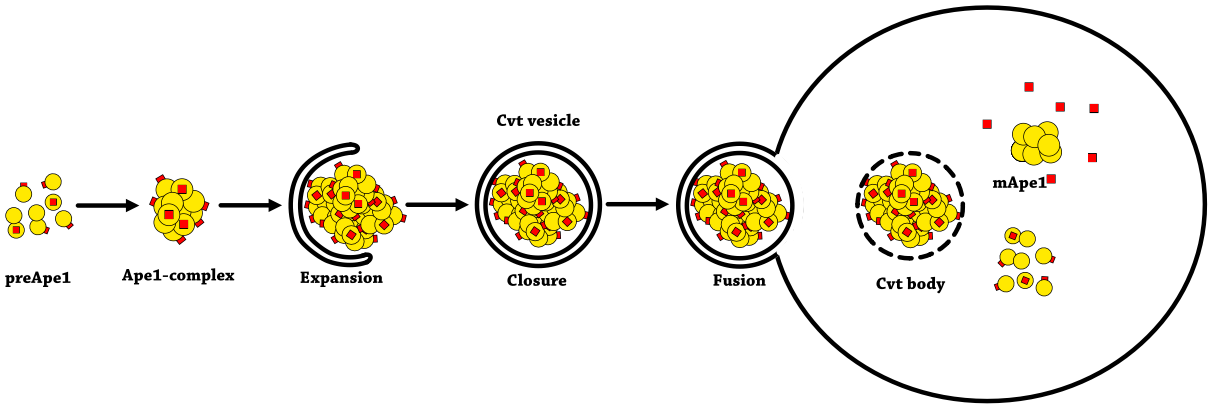

Figure 2-2: Cytoplasm-to-vacuole targeting pathway in yeast S. cerevisiae.

The Cvt pathway is constitutively active under nutrient rich conditions and selectively transports hydrolases to the vacuole. The core cargo is the inactive precursor form of aminopeptidase 1 which contains an N-terminal propeptide. PreApe1 aggregates into a large oligomeric structure called the Ape1 complex which is engulfed by a double membrane layered vesicle. After it is transported to the vacuole Ape1 is matured by cleaving off the propeptide. Upon starvation the transport of Ape1 to the vacuole is taken over by autophagy.

2.5 Microautophagy

Microautophagy is much less understood than macroautophagy. Microautophagy is a form of autophagy that does not require autophagosome formation to transport cargo to the vacuole. Instead, the vacuolar membrane invaginates to sequester the autophagic cargo [52], [53]. Once invagination is complete, the vacuolar membrane fuses and releases the microautophagic body into the vacuolar lumen for degradation. Most forms of selective microautophagy has been found to require the core autophagic machinery but micro-ER-phagy instead relies on the ESCRTs [54], [55]. Several selective microautophagy processes have been described, such as micro-ER-phagy [32], [56], micropexophagy [57], piecemeal micronucleophagy (PMN) [58], micromitophagy [59] and microlipophagy [60].

Nucleus-vacuole junction (NVJ) serves as a contact site between the vacuolar membrane and the nuclear envelope. This contact site is formed by the interaction between Nvj1 on the nuclear envelope and Vac8 on the vacuolar membrane [61]. Upon starvation, the NVJ expands and buds outwards towards the vacuolar lumen, creating a complex microautophagic body that is ~1 µm in diameter and consists of three different membranes; the inner nuclear membrane, the outer nuclear membrane and the vacuolar membrane [58], [62]. PMN requires some of the core autophagic machinery and involves a different intermediate stage where detached nuclear fragments are contained within vacuole invaginations (Krick *et al.*, 2008). Atg8 has been found to accumulate at the necks of these invaginations, suggesting the presence of a phagophore related structure. In addition to Atg8, Atg11 and Atg39 are also required for micronucleophagy [64].

2.6 Induction of Autophagy

Induction of autophagy begins with the regulation of the PAS formation. PAS formation requires the Atg1 kinase complex, which is regulated by two kinases: the target of rapamycin complex 1 (TORC1) and the cyclic adenosine monophosphate (cAMP)-dependent protein kinase A (PKA). Both kinases react to specific cellular conditions; TORC1 inactivation occurs during nitrogen or amino acid starvation, and in response to rapamycin treatment, PKA inactivation occurs during glucose starvation [65], [66].

Upon nutrient-rich conditions, Atg13 is hyperphosphorylated by TORC1, inhibiting the tight interaction between Atg1 and Atg17 and therefore inhibiting autophagy [67]. Nutrient starvation or treatment with rapamycin activates autophagy by inhibiting TORC1, leading to the dephosphorylation of Atg13 and subsequent interaction with Atg1 and Atg17 (Figure 2-3 Step 1) [68], [69]. Both Atg13 and Atg1 are phosphorylated by PKA under high glucose conditions, at non-TORC1-target sites [70], [71].

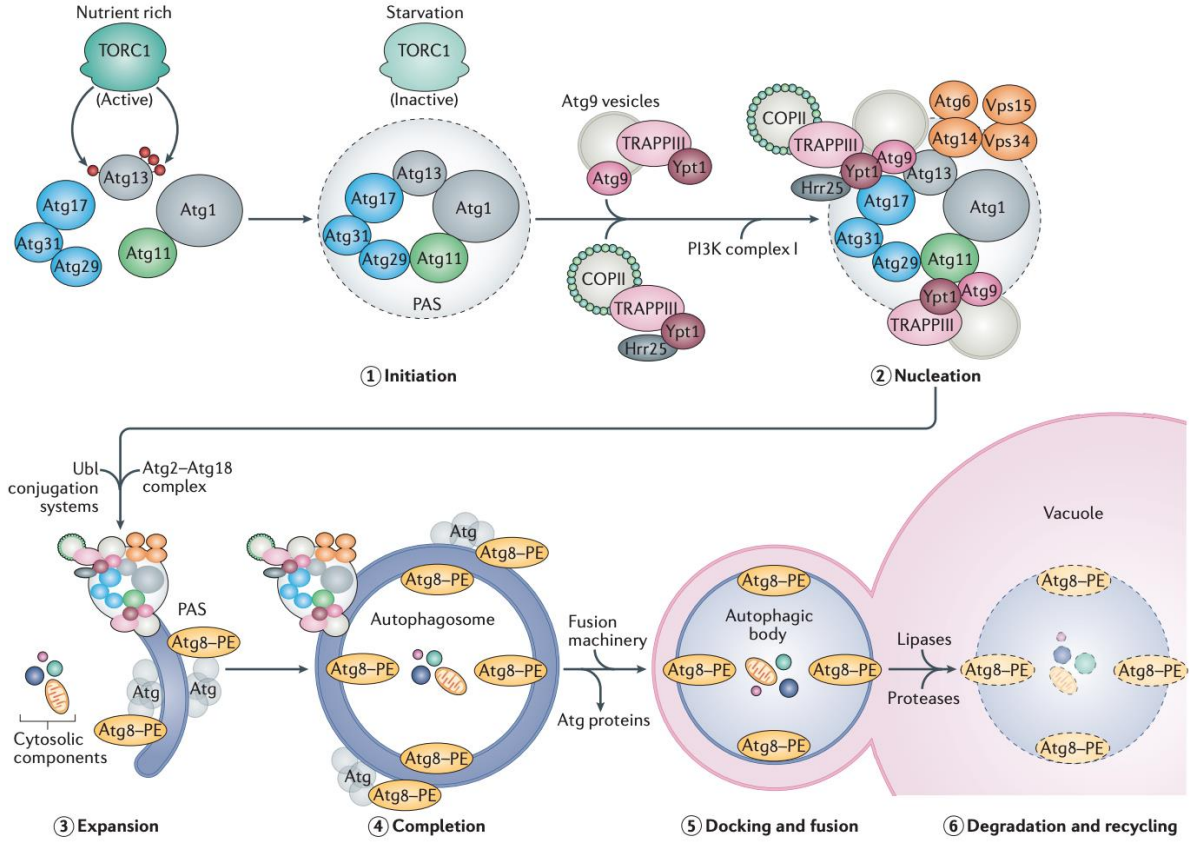

Figure 2-3: A model of the different stages of macroautophagy in yeast.

In yeast, macroautophagy can be divided into six stages. Under nutrient-rich conditions, TORC1 is active and inhibits autophagy via the hyperphosphorylation of Atg13. Nutrient starvation or treatment with rapamycin causes TORC1 inactivity leading to the dephosphorylation of Atg13 and subsequent interaction with Atg1 and Atg17, step 1 initiation. Step 2 nucleation involves the recruitment of core autophagic machinery to the PAS. Transport protein particle III (TRAPPIII) and Ypt1, recruited by scaffold components, contain coat protein complex II (COPII) and Atg9 vesicles that support the expansion of the phagophore. The development also requires the activity of phosphoinositide 3-kinase (PI3K) complex I, generating the PI3P to recruit the ubiquitin-like conjugation systems, resulting in the closure of the autophagosome (Step 4). Upon arriving at the vacuole, the vacuole's outer membrane fuses with the autophagosome, releasing the autophagic body into the vacuolar lumen (Step 5). Finally, hydrolases degrade and recycle the macromolecular components (Step 6). Taken from Farre & Subramani, 2016

The yeast Atg protein family consists of 42 proteins, of which 18 are essential for autophagosome formation and the degradation of cargoes. These proteins are classified as the core components of the autophagic machinery [72]. Several functional complexes are

recruited to the PAS, and they can be categorised into five groups: Atg1 kinase complex, Atg9-containing vesicles, the phosphatidylinositol 3-kinase (PI3-kinase) complex, and the two ubiquitin-like conjugation systems [72], [73]. The following chapters describe the structures and molecular functions of yeast's core autophagic machinery based on *S. cerevisiae,* the model organism used in this study.

2.6.1 The Atg1 Kinase Complex

Atg1, Atg13, and the Atg17-Atg31-Atg29 subcomplex are components of the Atg1 kinase complex, which is a fundamental unit facilitating autophagy initiation; depicted in Figure 2-4. By regulating the post-translation of downstream autophagy proteins and by providing a structural backbone for autophagosome formation, this complex promotes autophagosome formation [74]–[76].

The Atg17-Atg31-Atg29 complex is constitutively present at the PAS and upon initiation of autophagy provide a platform for Atg1 and Atg13 to bind to; forming the Atg1 kinase complex [77]. In recent years, the Atg1 kinase complex has been involved in multiple structural and biochemical studies. These revealed a highly dynamic self-assembling propensity for recognising and integrating Atg9-positive vesicles at the PAS [77]–[80].

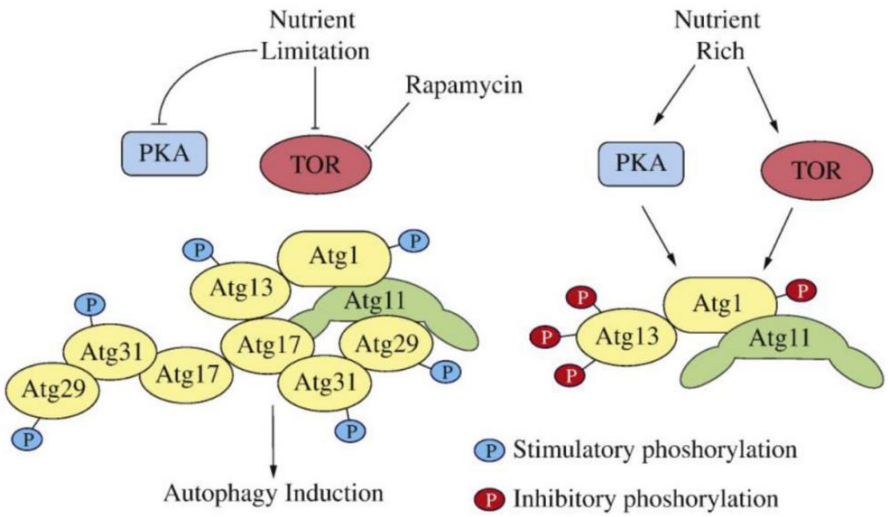

Figure 2-4: The interactome of the Atg1 kinase complex in S. cerevisiae.

When autophagy is induced, the Atg17-Atg31-Atg29 subcomplex and Atg13 are brought together. As there is no binding site on Atg1 for the subcomplex, Atg13 can directly bind to Atg1 as well as the Atg17-Atg31-Atg29 subcomplex. The scaffold protein Atg11 can bind Atg1 as well as Atg17 and Atg29. Taken from Wen & Klionsky 2017.

Atg1 contains an N-terminal serine/threonine kinase domain, linked to two carboxyterminal microtubule-interacting and transport (MIT) domains and a single early autophagy targeting (EAT) domain. Both the MIT and EAT domains are situated within the intrinsically disordered region (IDR) of Atg1 [81]. Within the Atg1 kinase complex sits the regulatory protein Atg13 at the centre of the interacting proteins. It is predicted that the IDR within the C-terminal of Atg13 is the region of phosphorylation and the binding regions for Atg1 and Atg17.

2.6.2 The Class III PI3K Complex I

Phosphatidylinositol 3-phosphate (PI3P), an important signalling molecule for concentrating PI3P-binding proteins to the phagophore. PI3P is found at autophagic membranes and is crucial for autophagosome formation. Vps34 is the only PI3-kinase in budding yeast that phosphorylates phosphatidylinositol at position 3 [82]. The product PI3P is essential for autophagosome formation and for vacuolar protein sorting (VPS) pathways in yeast [83]. To function in these processes, Vps34 forms at least two protein complexes that direct the synthesis of PI3P (Figure 2-5) [84]. Both of these complexes include the regulatory kinase Vps15, a PI3-kinase Vps34, and Vps30/Atg6; as seen in Figure 2-5 [85]–[88].

PI3K complex I is crucial for selective and nonselective autophagic processes. A crucial component of the PI3K complex I is Atg14 and is required for targeting the complex towards the PAS specifically in autophagy, while Vps15 mediates membrane association of the complex. In contrast, PI3K complex II contains Vps38 and is involved in endosomal trafficking, endocytosis, and the VPS pathway [84]. The role of Vps30/Atg6 is unknown; however, it directly interacts with Atg14, which directs the localisation of the complex to the PAS [87], [89]. Some Atg proteins bind to PI3P, and it has been speculated that phosphoinosides assists in the recruitment of proteins involved in autophagy and phagophore formation [90].

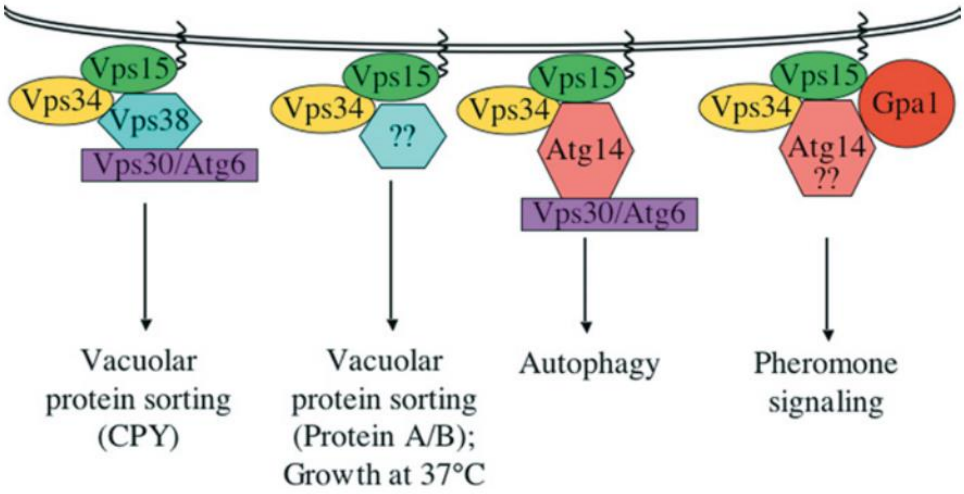

Figure 2-5: Vps34 signalling complexes in yeast.

The tetrameric complexes formed by Vps34, Vps15, Vps30 and either Atg14 or Vps38 regulate vacuolar protein sorting and autophagy. Taken from Backer, 2008.

2.6.3 The Ubiquitin-like Conjugation Systems

Atg8 and Atg12 are two specific ubiquitin-like protein conjugation complexes involved in autophagy. Among the core autophagic proteins is Atg8, a ubiquitin-like protein [91]. To expose the carboxyl-terminal glycine residue of newly synthesised Atg8, Atg4 acts as a cysteine protease [92], [93]. As soon as Atg8 has been processed, it is activated by Atg7, an ATP-dependent activating enzyme, and later transferred to Atg3, an E2-like conjugating enzyme; depicted in Figure 2-6 [92], [94], [95]. Once the C-terminal of Atg8 has been processed, a covalent bond is formed between the exposed C-terminal glycine residue of Atg8 and phosphatidylethanolamine (PE) by Atg3 [91]. This process allows for recruitment of soluble Atg8 to the membrane where it is fixed to PE. Atg8 can initially be found on both sides of the growing phagophore. Atg4 can subsequently cleave Atg8-PE in a deconjugation step, freeing Atg8, occurring mainly to the population on the external surface of the autophagosome. Thus, allowing for Atg8 to cycle through the conjugation process again in another round of autophagic flux.

Atg12, Atg5 and Atg16 combine to form a multimeric protein complex that facilitates the conjugation of Atg8 to PE [96], [97]. Atg7 and Atg10, E1-like and E2-like enzymes respectively, attach to the ubiquitin-like Atg12 and Atg5, thus forming this complex [98], [99].

The covalent bond between Atg12's C-terminal glycine and Atg5's internal lysine is formed by the activation of Atg12 by Atg7, which is then transferred to Atg10 catalysing the reaction [100], [101]. A unique feature of the Atg10-conjugating activity is that Atg12 conjugated to Atg5 is independent of the E3 ligase [102]. Atg5, and especially its Atg12-Atg5 conjugate, form a noncovalent interaction with Atg16. This noncovalent interaction promotes Atg16 self-interaction and ultimately generates a Atg12-Atg5-Atg16 dimer [99], [103], [104].

This complex is proposed to function as an E3-like enzyme for Atg8 conjugation, but Atg8-PE can be created without these proteins [97], [105], [106]. Activated Atg8 in the Atg8-Atg3 conjugate is thought to be brought into close contact to the acceptor PE via the Atg12-Atg5-Atg16 complex [107], [108]. Atg16 is not required for Atg12-Atg5 to exert E3-like activity, but is required for the complex to localise to autophagy-related membranes [109]. In 2012, it was found that Atg5 contains a membrane-binding domain that is negatively regulated by Atg12, and mutating this region inhibits macroautophagy [110]. It was also determined that recruitment of the components of the Atg8 conjugate system is dependent upon the Atg12-Atg5-Atg16 complex being able to associate with lipid bilayers.

Two mechanisms exist for Atg12-Atg5-Atg16 complex to act as an E3 for Atg8 lipidation. The most important is the interaction of Atg16 with Atg21 that localises this complex to close proximity to PE [62]. The second and less important is the interaction of Atg12 with the Atg1 complex that serves as a scaffold for PAS organisation [111].

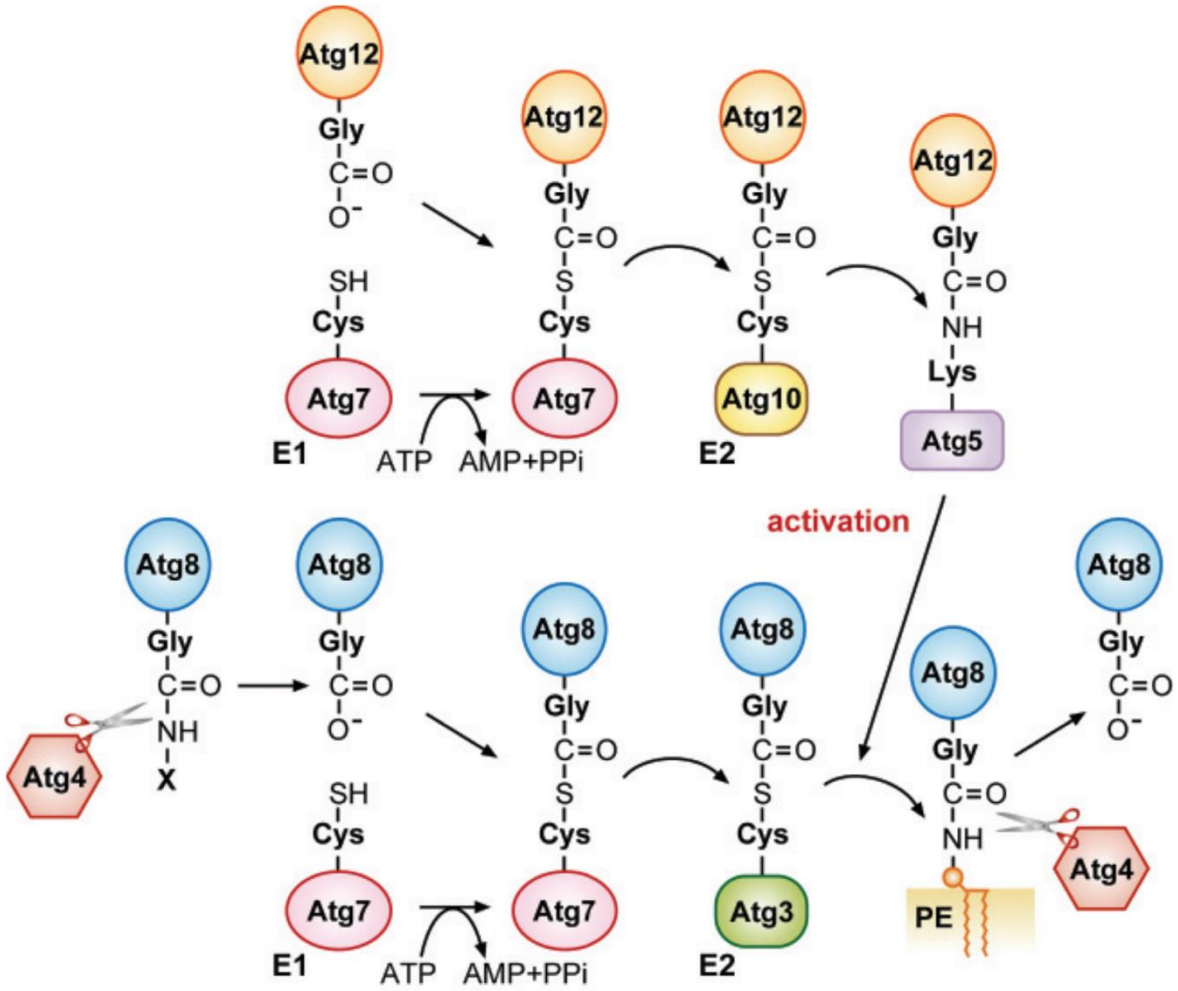

Figure 2-6: The Atg8 and Atg12 conjugation systems in S. cerevisiae.

After Atg7 activates the ubiquitin-like protein Atg8, Atg8 is then transferred to the E2-like enzyme Atg3 resulting in conjugation to PE via an amide bond. Atg4 handles the processing of Atg8's C-terminal in the deconjugation of PE from Atg8. Atg7 is also required for the activation of Atg12's C-terminus resulting in the enzyme's catalytic cysteine residue being passed onto the E2-like enzyme Atg10. Subsequently, an isopeptide bond is formed between this cysteine residue and the lysine residue of Atg5. The activity of the E2-like enzyme Atg3 is enhanced by the conjugation of Atg12-Atg5. Taken from [109]

Atg8 is located on both sides of the phagophore and therefore has two separate functions once at the phagophore. Atg8-PE on the concave face of the phagophore functions as a cargo receptor by binding AIM-containing proteins and is delivered to the vacuole with the cargo for degradation [112], [113]. Atg8-PE is predominantly located on the convex face of the phagophore, and upon autophagosome completion is recycled by proteolytic cleavage mediated by Atg4 [28], [92]. The function of this convex pool of Atg8-PE is poorly understood, but it has been suggested to recruit membrane tethering factors. Furthermore, Atg16 drives the two-dimensional meshing of Atg8-PE/Atg12-Atg5 complex to produce an ordered

membrane scaffold [114]. Due to the competition between cargo receptors and Atg12-Atg5 for Atg8-PE binding, cargo receptors can counteract scaffold formation. This explains how Atg8-PE can simultaneously act as a rigid membrane scaffold element and as a flexible cargo adaptor.

2.6.4 Multimembrane Spanning Proteins

During autophagosome formation, the only transmembrane protein crucial for this process is Atg9 [113]. The protein has been detected at multiple locations within the cell, including the ER, Golgi apparatus, as well as at the PAS and parts of the secretory pathway [48], [115], [116]. Atg9 is believed to deliver membranes from donor sites to the expanding phagophore through these peripheral sites, shown in Figure 2-7 [113], [117]. By supplying the initial membranes necessary to recruit and organise Atg proteins at the PAS, Atg9 is thought to act as a regulartor of autophagy initiation [48], [116]. It is known that Atg9 can self-interact which supports the idea of Atg9 being a landmark scaffold protein [118], [119]. Atg9 is primarily found on the external surface of the growing phagophore, where it is likely to be retrieved from the autophagosome membrane shortly before or after fusion of the autophagosome with the vacuole [116].

Upon being synthesised, Atg9 is transported to the ER before being packaged into vesicles in the Golgi [120]. In support of this hypothesis, it was observed in the *sso1Δ* strain, where the soluble N-ethylmaleimide-sensitive-factor attachment receptor (SNARE) Sso1 involved in protein secretion was deleted, Atg9 is only detected in small vesicles and not located at the PAS [121]. A SNARE-mediated membrane fusion event may be necessary for effective antegrade movement of peripheral Atg9-containing vesicles to the PAS. The purpose of these Atg9-containing vesicles continues to be a widely debated topic. One hypothesis is that they remain independent vesicles, and upon induction of autophagy are recruited to the PAS [116].

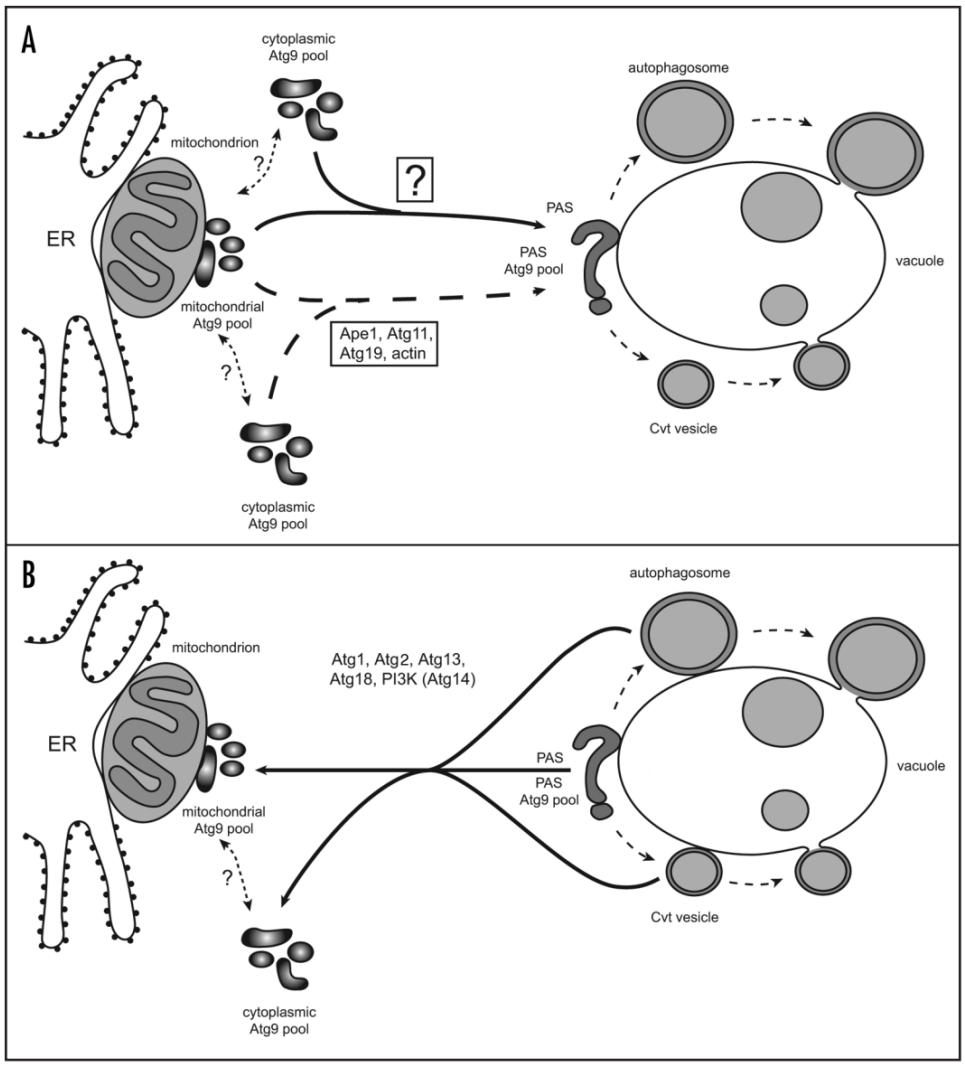

Figure 2-7: Proposed trafficking routes of Atg9 in S. cerevisiae.

A) The anterograde transport of Atg9. Atg9 is delivered to the PAS from a post Golgi pool during phagophore formation. Within the Cvt pathway (large dotted arrow), Atg9 anterograde transport requires the presence of the Ape1 oligomer, Atg19, Atg11 and actin. During starvation (continuous arrow), Atg9 trafficking becomes independent of these proteins. The mechanisms underlying this delivery is currently unknown. B) The retrograde transport of Atg9. Once the autophagosome is complete and the function of Atg9 is no longer required, the Atg1-Atg13 complex triggers the retrograde transport of Atg9 from the PAS. Also, Atg2, Atg18 and PI3P are thought to participate in the retrograde transport of Atg9. Taken from [122].

Another possibility is that the Atg9-containing vesicles gather at the peripheral sites in a SNARE-dependent process and one of these structures relocates near the vacuolar surface in order to form the PAS [48], [121]. In addition Atg23 and Atg27, which are non-conserved peripheral and integral membrane proteins, Atg9 requires Atg23 and Atg27 to function efficiently at the PAS [123]–[125]. In particular, Atg23 and Atg27 appear to play a vital role in mediating Atg9 sorting from the Golgi.

Induction of autophagy results in the inactivation of TORC1 and PKA, which dephosphorylates Atg13 and enables interactions with Atg1 and Atg17. By binding two molecules of Atg17 to Atg13, at least three hexamers of Atg17, Atg13 and Atg28 can be molecularly bridged producing an oligomeric structure. Once at the PAS, the IDR in the N-terminal of Atg9 interacts with the HORMA domain of Atg13, as seen in Figure 2-8 [126]. Atg9-containing vesicles are also associated with Atg17 and, as a result, are incorporated into the supra complex Atg1-Atg13-Atg17-Atg31-Atg29. It is the vesicles containing Atg9 that are tethered together by the S-shaped Atg17 homodimer, resulting in their fusion and subsequent formation of the phagophore [74], [76]. It has been reported that Atg9-containing vesicles are only recruited to the PAS, and no additional Atg9-containing vesicles are involved in the later stages of autophagosome formation [116].

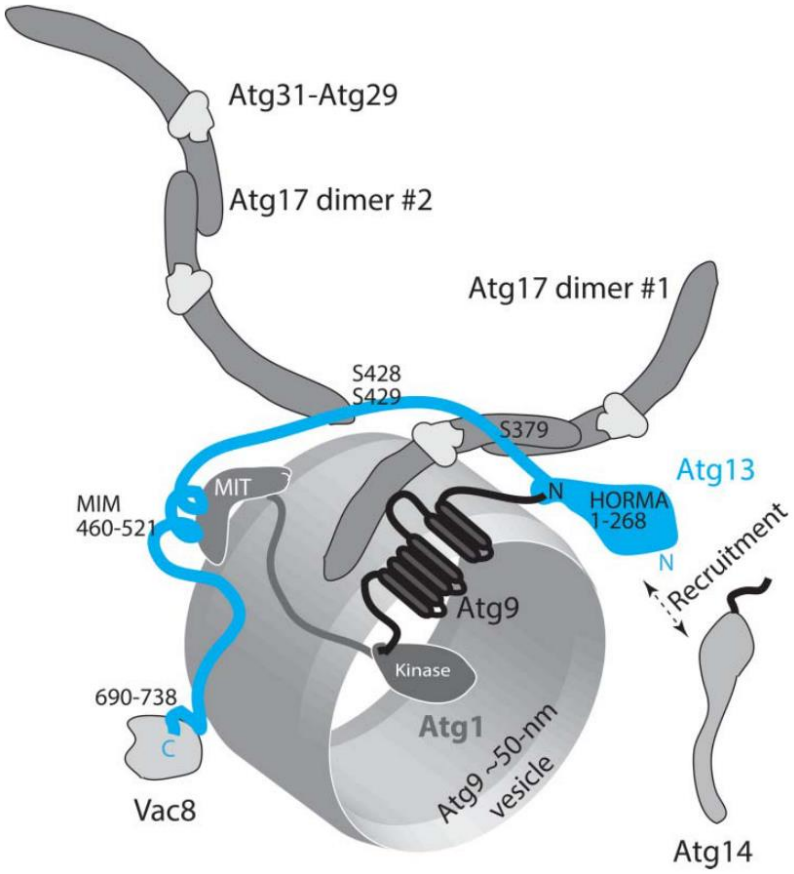

Figure 2-8: A model of Atg13 during autophagy induction.

Atg13, in blue, is depicted interacting with Atg1, Atg9, Atg17, Atg14 and Vac8. As well as recruiting Atg14 directly or indirectly, the HORMA domain of Atg13 binds to the N-terminus of Atg9. The IDR of Atg13 contains at least two Atg17 binding motifs. Atg13 binds to the Atg17 dimer interface where it activates Atg17-Atg31-Atg29 trimer and promotes a pivoting movement. This movement leads to the activation of Atg9-Atg17 complex interaction. Taken from [79].

2.6.5 Atg2-Atg18 complex

The peripheral membrane proteins Atg18 and Atg2 interact with each other and associate with Atg9 at the PAS [47], [127]. The absence of either Atg18 or Atg2 results in a defect in Atg9 localisation, similar to that seen in an *atg1Δ* strain. As with the mechanism by which Atg9 is retrogradely transported from the vacuole, it is unclear how Atg18 plays a role in autophagosome biogenesis. The recruitment and localisation of Atg18 and Atg2 to the PAS is dependent on each other, Atg9, the Atg1-Atg13 kinase complex, and the presence of PI3P generated by the PI3-kinase complex I [73], [128]. The interaction between Atg18 and Atg2 is PI3P independent, but appropriate targeting of the Atg18-Atg2 complex to the PAS is PI3P dependent [127].

2.6.6 Late Stages of Macroautophagy

In order for autophagosome expansion and sealing to be regulated, a signal must be applied that signals fusion with the vacuole. It is not known how this is accomplished. The edges of the expanding phagophore likely requires scission and subsequent fusion to separate the inner and outer membranes for the completion of the autophagosome. Unfortunately, the mechanism involved in the closing of the phagophore still need to be determined [129]. The edges of the expanding phagophore that contain the Atg2-Atg18 complex with their interacting partner Atg9, and the ubiquitin-like protein Atg8 have been implicated as possible closure factors [130]. Most of the Atg proteins are still on the surface of the autophagosomes that have just been sealed. These proteins may affect the activation of the fusion machinery, and so they must be removed and recycled. A study revealed that Atg8 on the surface of autophagosomes leads to inefficient fusion with the vacuole [131], [132]. After closure but before fusion with the vacuole maturation of autophagosomes needs to occur, this is defined as the removal of all Atg proteins from their surface. Atg8 and PI3P are removed from the surface membrane of autophagosomes during maturation, which is thought to facilitate the subsequent separation of Atg proteins from the surface of the autophagosome [133].

As described previous, the protease Atg4 is not only involved in cleaving the C-terminal arginine of Atg8 to promote its conjugation to PE but is also required for hydrolysis of the amino bond between Atg8 and PE and thereby releasing Atg8 from its lipid anchor [92], [134].

PI3P is dephosphorylated by the yeast enzyme myotubularin-related PI3P phosphatase (Ymr1) to yield PI which is an essential step in autophagosome maturation [135]. In yeast cells absent of *YMR1*, there is an accumulation of autophagosomes in the cytosol which still contain Atg proteins of their surface and are PI3P-positive [136]. Upon induction of autophagy Ymr1 localises to the PAS. At the moment, it is unknown how Ymr1 activity is controlled during autophagosome maturation and formation [135], [137].

The fusion of matured autophagosomes with the vacuole involves machinery that is common to other transport networks that terminate at the vacuole. This involves the action of specific Rab guanosine triphosphatase (GTPase) in combination with its respective guanine nucleotide exchange factor (GEF), a tethering factor, as well as SNARE proteins [133]. To regulate intracellular membrane traffic Rab GTPases are known to act as a molecular switch by cycling between their soluble guanosine diphosphate (GDP)-bound (inactive) form and the membrane associated guanosine triphosphate (GTP)-bound (active) form. GEFs mediate the replacement of GDP with GTP and lead to membrane association as well as the activation of the Rab GTPase which in turn is able to recruit effector proteins [138].

The machinery involved includes the Rab-like protein Ypt7 as the specific Rab GTPase which requires the GEF Mon1-Ccz1 complex for activation. Once activated, Ypt7 can interact with the vacuolar membrane via the homotypic vacuole fusion and protein sorting (HOPS) complex. Ypt7-positive membranes are tethered to this hexameric complex, which triggers SNARE protein assembly to facilitate the fusion of the tethered membranes [139]. The SNARE proteins Vam3, Vam7, Vti1 and Ykt6 have been found to be essential for the vacuolar fusion of autophagosomes [140]–[143].

The final fusion event of the outer autophagosome membrane with the vacuole-limiting membrane releases the inner vesicle into the vacuolar lumen, which is named to autophagic body. The membrane of the autophagic bodies is lysed through the action of the putative vacuolar lipase Atg15 [144], [145]. Allowing for resident hydrolases, that are present in the vacuolar lumen, to degrade cargo for subsequent transportation into the cytosol for recycling.

2.7 PROPPINs

β-propellers that bind polyphosphoinositides (PROPPIN) are a family of eukaryotic PI3P and PI(3,5)P_2 binding proteins which are involved in autophagy. They contain two PIP binding sites and a conserved phenylalanine-arginine-arginine-glycine (FRRG) motif essential for binding to PIP [146]–[149]. Yeast contain three homologous PROPPINs; Atg18, Atg21 and Hsv2. In mammalian cells, there are four orthologs known as the WD40 repeat-containing proteins that interact with PIs (WIPI). WD40 repeat proteins are characterised by the presence of tandem repeats of 40-60 amino acids having tryptophan (W) and aspartic acid (D) at the C-terminus; first identified in the bovine β subunit of transducin, a GTP binding protein [150], [151]. Structurally, PROPPINs are characterised by a β propeller fold comprising of 4-8 antiparallel sheets, where each sheet consists of 4 β strands; depicted in Figure 2-9. These sheets are arranged as blades of the propeller around a central cavity. The WD repeat is a part of the antiparallel strands. It is well known that WD40 domains can mediate diverse protein-protein interactions, such as scaffolding and cooperative assembly and regulation of multisubunit complexes. WD40 proteins are also present in bacteria, but the abundance of WD40 proteins in eukaryotes is much greater, where they perform a wide range of functions, such as signal transduction, cytoskeleton assembly, cell division, RNA processing and chemotaxis [152], [153].

The WD40 repeats are among the top ten most abundant domains in eukaryotes [154]. In contrast to other members of the β-propeller family, and despite often residing in enzymatic complexes, no WD40 protein is currently known to possess catalytic activity. WD40 propellers are large domains of ~300 amino acids and can be considered to have three distinct surfaces available for interaction: the top region of the propeller, which is defined as the part of the structure where the loops connecting D and A strands of the WD-repeats lie, the bottom area, and the circumference (Figure 2-9). Interestingly, most protein-protein interactions involve the top region of the propeller, corresponding to the 'supersite' for the β-propeller superfold [155].

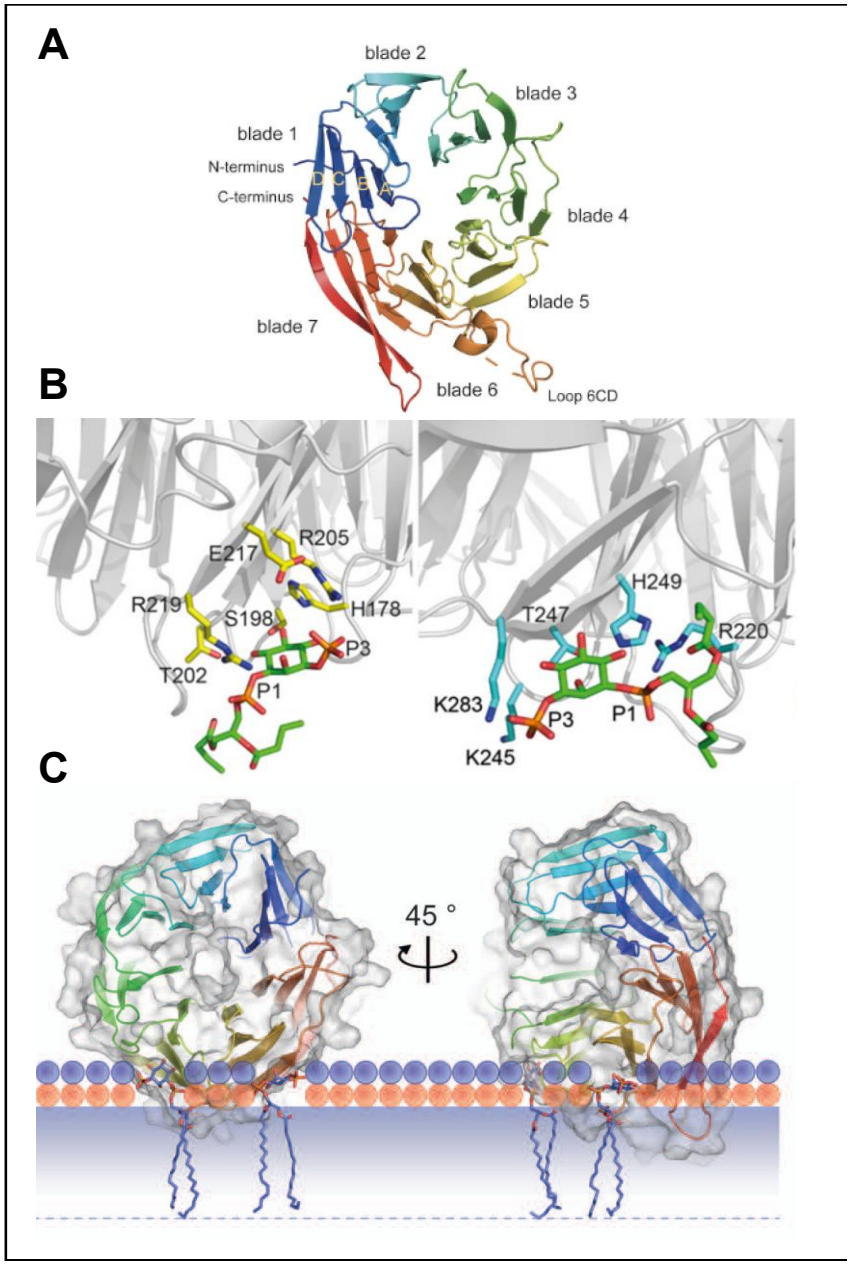

Figure 2-9: Structure for PI3P binding within KlHsv2.

A) Ribbon structure of Kluyveromyces lactis *Hsv2 where blue represents the N-terminal and in red is the C-terminal. KlHsv2 forms as a seven-bladed β-propeller, where each blade consists of a four-stranded antiparallel β-sheet. The blades are numbered from the N-terminal to the C-terminal, and the β-strands are ordered from inner to outer strand using A-D. The orientation of the ribbon structure in A is a view of the bottom of the protein. B) Showing the two binding sites for PI3P, the residues important for this interaction are shown in yellow and cyan. C) Model for membrane association of KlHsv2. The β-propeller is perpendicular to the membrane allowing for loop 6CD to insert into the membrane and provide support for the association. A) and B) taken from* [156] *C) taken from* [157].

The crystal structure of *Kluyveromyces lactis* Hsv2 revealed that PROPPINs contain two PIP binding sites and fold as a seven-bladed β-propeller [158]–[160]. The rim of the β-propeller contains the conserved FRRG motif, where each arginine forms a PIP binding site. Therefore, all PROPPINs can bind to two molecules of PIP. The binding to PIP allows the PROPPINs to be

localised to their active sites. In addition, PROPPINs can also penetrate the membrane via a loop at 6CD that protrudes from the β-propeller core. This membrane insertion loop is required for membrane binding using hydrophobic and electrostatic interactions [161]. The β-strands are linked by a short loop connecting to one another as well as between the blades, except for the last blade that exhibits a non-Velcro closure as these blades are not linked. The seventh blade consists of the WD40-repeat and does not share any β-strands with the first blade [156], [162]. The phosphorylation of the membrane insertion loop of Atg18 modulates the binding to membranes [163]. PROPPIN membrane binding is also dependent on the membrane curvature and proposed to bind perpendicular to the membrane through both PIP binding sites in addition to the membrane insertion loop 6CD [161].

Atg18 consists of seven WD40-repeats that fold into a seven-bladed β-propeller [148], [164]. Atg18 is also able to bind both PI3P and PI(3,5)P_2 through the conserved phenylalanine-arginine-arginine-glycine (FRRG) motif within its β-propeller [148], [149]. Atg18 localises in a PI3P dependent manner to the PAS for autophagosome formation [47]. Additionally, Atg18 forms a complex with Atg2, which is also crucial for autophagy progression. As a secondary function, PI(3,5)P_2 binding of Atg18 mediates its localisation to the vacuole [148]. Atg18 is involved in non-autophagic functions in regulating retrograde transport from the vacuole to the Golgi. Also, Atg18 has a regulatory role as part of the Fab1-containing PI3P 5-kinase complex at the vacuole, and has a direct effect on vacuolar fragmentation and homeostasis [165]–[167].

Atg21 is not essential for nonselective autophagy; nonselective autophagy in an *atg21Δ* strain is only impaired and not entirely blocked. However, Atg21 is crucial for selective autophagy, including the Cvt pathway, PMN and mitophagy [168], [169]. Atg21 is required for the recruitment of Atg5, Atg8 and Atg16 to the PAS. It was found that Atg21 organises Atg8 lipidation at the phagophore by binding to PI3P and recruiting Atg8 and the Atg8 lipidation complex, as shown in Figure 2-10 [170]. This is regulated by the loop 2D to 3A on the top side of Atg21 that allows for interaction with Atg8. The bottom side of Atg21 allows for binding with Atg16 via two negatively charged residues, D101 and E102 of Atg16 [171].

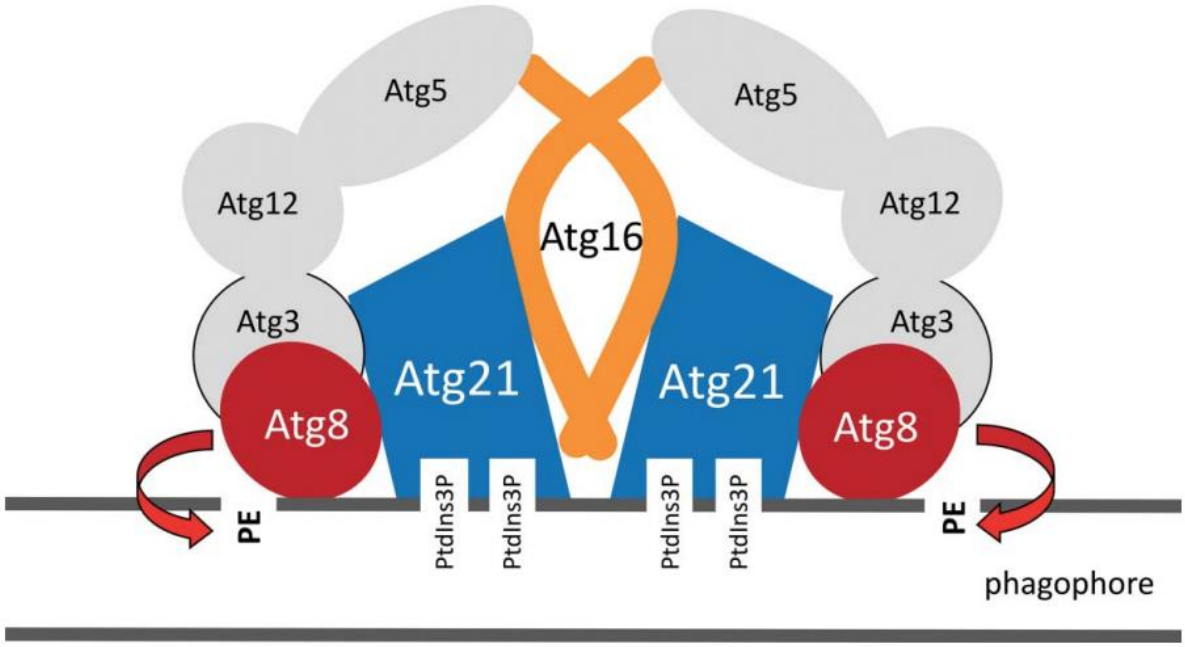

Figure 2-10: Model for protein interactions revolving around Atg21 at the phagophore.

Atg21 localises to PI3P at the phagophore membrane and defines the sites for Atg8 lipidation. Atg21 also binds PI3P at endosomes, here no Atg8 lipidation occurs, thus PI3P is not the only factor affecting Atg8 lipidation. Atg21 binds to the N-terminal arm-like domain of Atg8 which subsequently recruits the Atg8-Atg3 conjugate. On the opposite side of the Atg8 binding site, Atg21 recruits the Atg12-Atg5-Atg16 complex by interaction with Atg16. The dimeric coiled-coil domain of Atg16 is suggested to bind to two Atg21 molecules, this enhances the association of the complex with the autophagic membrane. Taken from [170]

Of the three yeast PROPPINs Hsv2 is functionally the least characterised. A partial impairment of PMN progression was seen in a *hsv2Δ* strain suggesting that Hsv2 could be a regulator of some selective types of autophagy. Recently, Hsv2 was implicated in the alternative autophagy termed Golgi membrane-associated degradation (GOMED) pathway, explained further in chapter 2.8.1. Furthermore, a defect in sporulation has been seen in a *hsv2Δ* strain compared to wildtype, where a third less asci were present under sporulation conditions. The mechanistic role of Hsv2 in sporulation is currently unknown.

2.8 Transport Pathways

S. cerevisiae has a multitude of complex trafficking pathways to ensure intracellular organisation. All newly synthesised membrane proteins are directed towards the Golgi, where they are sorted into destination compartments, whether that is to the PM or the external medium via exocytosis, to the vacuole through endosomes using the VPS pathway, or directly using the AP-3 pathway [172].

2.8.1 GOMED

The Golgi apparatus is an organelle responsible for the transport of proteins and lipids to the plasma membrane, vacuole and the cell exterior. In the Golgi, proteins are phosphorylated, modified by sugar chains, packaged, and sorted according to their destinations. A novel involvement has been reported that Golgi membranes are utilised in an intracellular proteolysis mechanism termed the GOMED pathway [173]. This process was originally called alternative autophagy due to the morphological and functional similarities to canonical autophagy (Figure 2-11). However, upon investigation there were some differences in proteins involved, the cargo degraded and biological roles uncovered.

GOMED is induced not only in yeast but also in mammals. Upon treatment with amphotericin B1 (AmB), an antifungal reagent, Golgi membranes become gathered and stacked with autophagosome-like structures, which are generated at the distal Golgi membranes, as seen in Figure 2-11. These autophagosome-like structures were found to engulf Golgi and cytosolic proteins and even organelles as autophagic cargo [173]. Amphotericin B1, a membrane-active antibiotic, increases the permeability of fungal membranes by binding to ergosterols. AmB has high affinity for ergosterol at membranes and upon association forms hydrophilic pores [174]. The presence of such structures on membranes increases the permeability and causes damages that could result in cell death. The molecular mechanisms behind AmB perturbing membranes is still poorly understood.

Ergosterol within the ER regulates phosphatidylinositol 4-phosphate (PI4P) levels on Golgi membranes [175], [176]. Yamaguchi *et al.*, 2016 examined whether AmB treatment reduced the levels of PI4P. Using a PI4P-monitoring protein in healthy cells localised to the Golgi and PM however, upon treatment with AmB the PI4P-monitoring protein was absent from the Golgi and spread throughout the cytosol. They then investigated if a reduction in PI4P was sufficient to induce GOMED. The deletion of Golgi PI4-phosphatases, Inp52 and Inp53, resulted in supressed AmB-induced GOMED; indicating that a reduction in PI4P levels is crucial for the induction of GOMED [173].

At the Golgi PI4P plays a direct role in controlling trafficking and Golgi morphology [177], [178]. Interestingly, the deletion of Atg1 suppressed GOMED even though no involvement of other autophagy genes has been observed. Additionally, defects in lipid sorting induced by Osh1 and Osh4 deletions and defects in retrograde trafficking caused by Vps74 deletion did not activate GOMED. However, the temperature-sensitive deletion of Gga1 and Gga2, proteins responsible for the anterograde transport in combination with PI4P, did induce GOMED [173], [179]. Upon further investigation by Yamaguchi's group, they found that only disruptions in the Golgi to PM trafficking induced GOMED and not disruptions in Golgi to vacuole or endosome to Golgi trafficking.

Recently, Hsv2 was implicated in GOMED [180]. This was verified by the absence of GOMED in AmB treated *hsv2Δatg5Δ* yeast cells. GOMED can function in the absence of the core Atg proteins and to avoid simultaneous activation of macroautophagy and GOMED, typically an *atg5Δ* background is used when measuring GOMED activity. In these cells, AmB treatment caused Golgi membrane stacking, but Golgi membrane elongation was blocked, suggesting that Hsv2 is required for membrane elongation during GOMED [180]. Furthermore, *hsv2Δatg5Δ* cells had significantly fewer autophagosome-like and autophagic body-like structures than *atg5Δ* cells. However, the Golgi membrane stacks were unchanged, suggesting that Hsv2 is required for the formation of the autophagosome-like structures and not the stacking of Golgi membranes. Additionally, Hsv2 may interact with *trans*-Golgi membranes via its PI3P interacting motif upon Golgi stimulation and may function in the formation of phagophore-like structures from Golgi membranes upon GOMED induction.

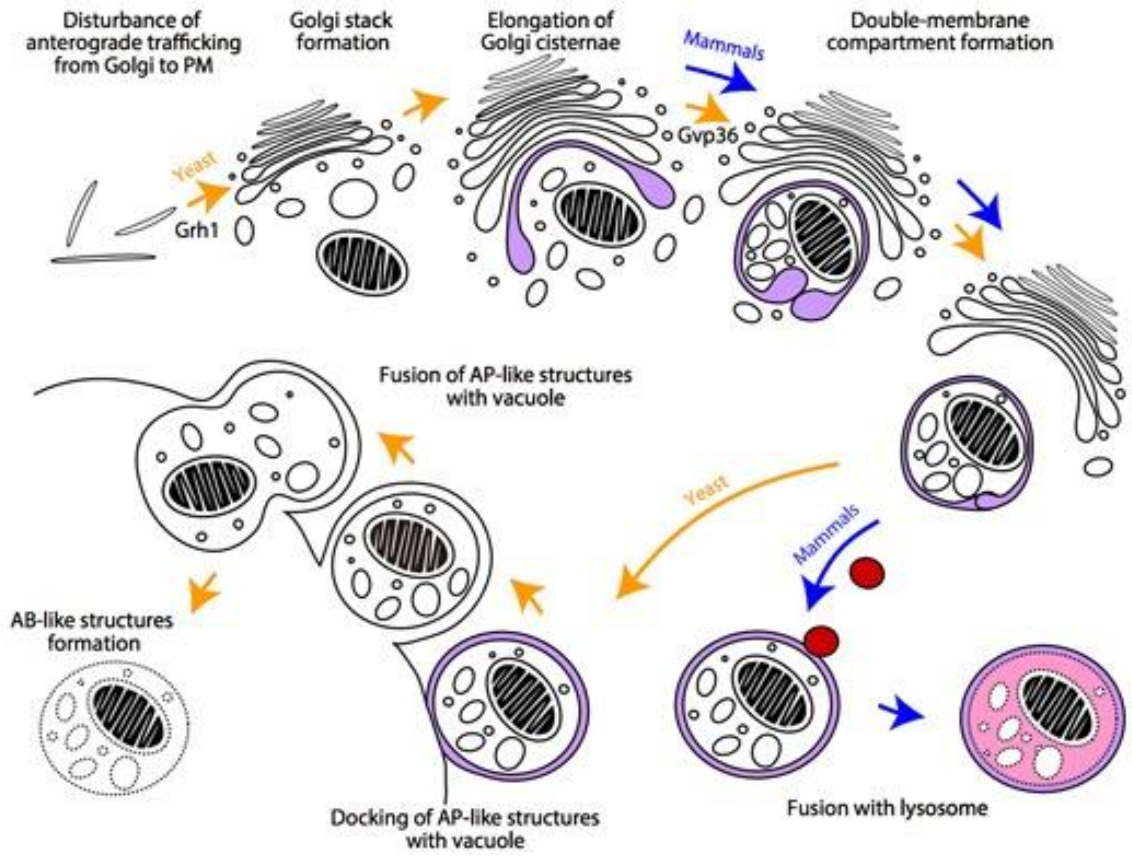

Figure 2-11: Golgi membrane-associated degradation pathway in yeast and mammals.

Upon disturbance of anterograde transport from the Golgi to the PM, Golgi membranes begin forming as stacks. These stacks then elongate around the cargo before fusing to form a double membraned compartment. The autophagosome-like structures then translocate to the vacuole for docking and lysis of cargo. Taken from Yamaguchi et al. 2016.

2.8.2 SNAREs

SNAREs are key components in mediating vesicle fusion with target membranes. Critical to the formation of SNARE complexes is the SNARE motif that is present in both v-SNAREs and t-SNAREs and consists of a 65 amino acid sequence characterised by heptad repeats of hydrophobic residues generally located on the C-terminal transmembrane anchor [181]. In order for efficient bilayer fusion to occur, four SNARE motifs have to bundle together in a parallel α-helical coil and thereby bringing the membranes into close proximity [182], [183]. This *trans* SNARE complex is referred to as a SNAREpin, with the target membrane t-SNAREs and the vesicle membrane v-SNAREs [184]. Within the coiled-coil of the SNAREpin, the contacts between the helices largely rely on hydrophobic interactions, with the exception of the middle of the bundle that contains an ionic layer [185]. Here each helix typically displays

either an arginine (R) or a glutamine (Q) residue, where three Q-SNAREs interact with one R-SNARE at the ionic layer within the SNAREpin.

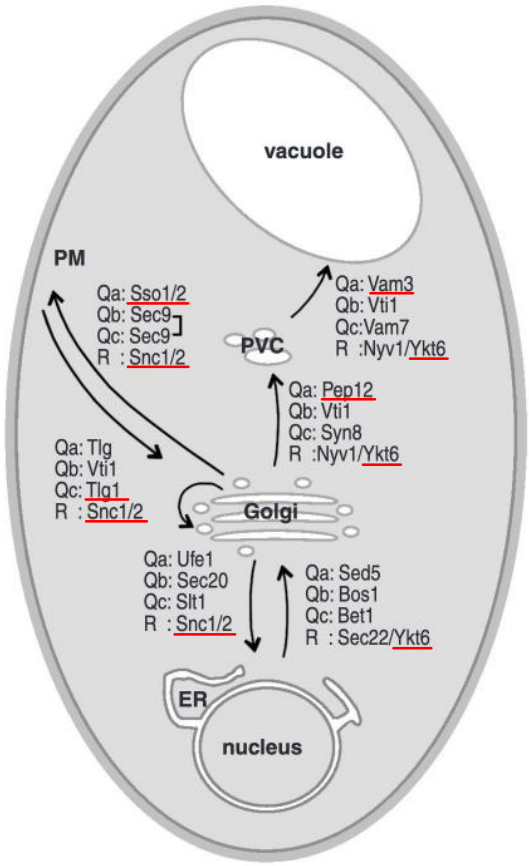

Figure 2-12: Subcellular location of S. cerevisiae Yeast SNAREs.

Showing SNAREs responsible for anterograde and retrograde trafficking between ER and Golgi, from Golgi to PVC and vacuole to PM. Endocytic transport makes use of the Golgi SNAREs to deliver cargo to an endosomal compartment. SNAREs that potentially interact with Hsv2 are underlined in red. Modified from [186].

2.8.3 Endomembrane System

The secretory and endocytic pathways are part of the endomembrane system within yeast *S. cerevisiae.* These pathways are the main routes to and from the *trans*-Golgi network (TGN) in order to maintain a homeostatic balance between anabolic and catabolic processes [187]. The endocytic and secretory pathways intersect at the Golgi apparatus, which is the central sorting organelle. Newly synthesised proteins and lipids are transported from the ER to the Golgi to begin the secretory pathway. Once at the TGN, cargo is sorted and packaged based on their destination, either for delivery to the plasma membrane, directly to the vacuole, back to the Golgi or into endosomes [188], [189].

Conversely, proteins and lipids are taken up at the plasma membrane and stored in endosomes during the first steps of endocytosis. These endocytosed cargoes are destined for recycling or degradation in the vacuole. En route to the vacuole, these cargoes pass through two distinct types of endosomes where components are recycled for further rounds of endocytosis [190], [191]. The best-characterised type of yeast endosome is the prevacuolar compartment, resembling a late endosome and localised next to the vacuole [192]. The early and recycling endosomes in yeast are less well described. The sorting of cargo at endosomes is initiated at the tubular endosomal network (TEN), a network of tubules that emanate from the vacuolar domain of the endosome [193]. The SNX-BAR family is a major family recruited to the TEN to facilitate cargo sorting; they are characterised by their ability to scaffold at high membrane curvatures such as that found at the TEN and endosomal transport carriers (ETCs). At the C-terminus, they contain a BAR domain and at the N-terminus, a phox homology domain for recognising PI3P.

The docking and fusion of membrane vesicles to their destined compartments has to be strictly regulated. Several families of proteins are required to guarantee fusion specificity, such as syntaxins, synaptobrevin and SNAP-25-like molecules. Synaptobrevins, v-SNAREs, on the surface of vesicles provide specificity for docking and fusion by interacting with syntaxins, t-SNAREs, on the target membrane [194]. Following this interaction, the involvement of specific cytosolic factors, *N*-ethylmaleimide sensitive factor (NSF) and soluble NSF-attachment proteins (SNAPs), have been implicated in vesicle docking and fusion [195].

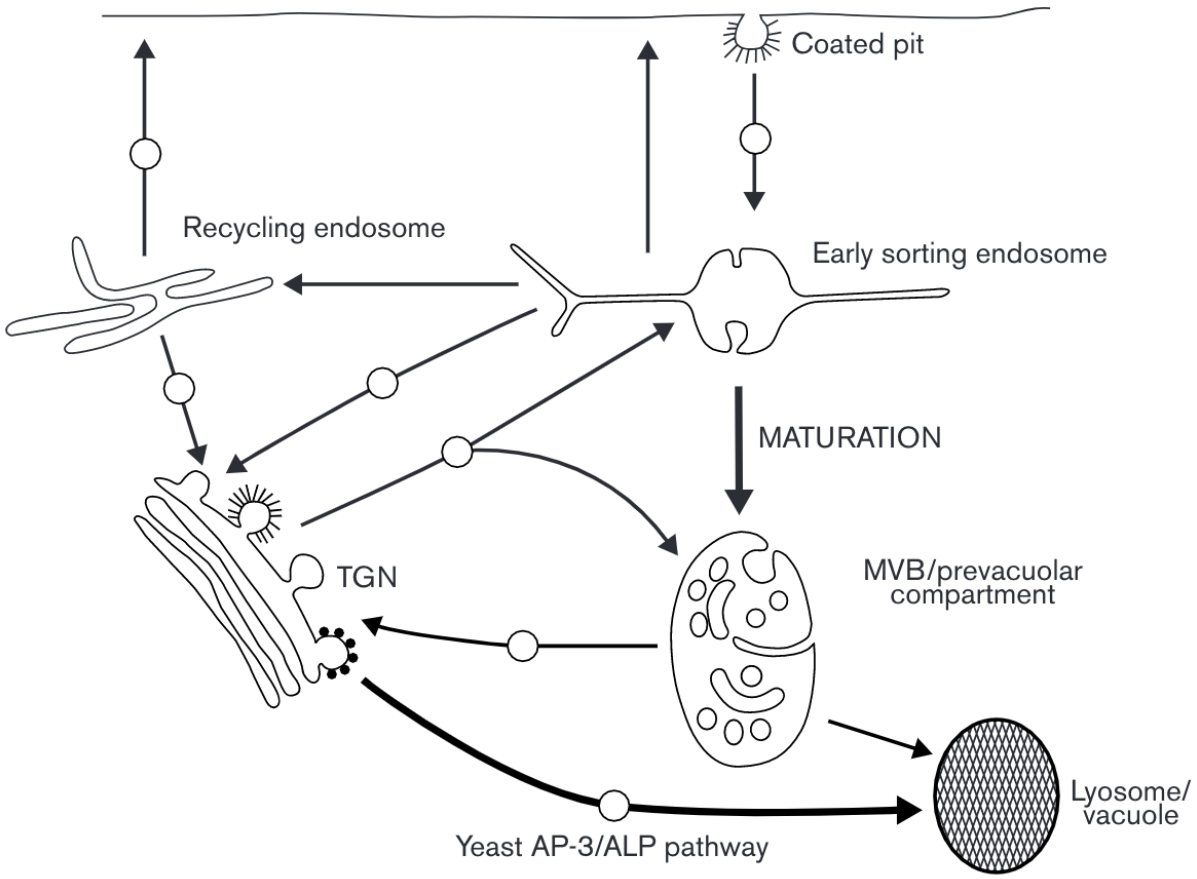

Figure 2-13: Schematic representation of the endosomal system in yeast S. cerevisiae.

The main trafficking routes of the endosomal system in yeast S. cerevisiae. The spheres within the lines represent an intermediate step required for transportation. Initially, sequestered cargo is packaged into the early sorting endosomes. Over time, as the early endosome matures it loses the ability to store cargo from PM-derived vesicles but not that from the TGN. This is part of the maturation process of multi-vesicular bodies (MVB). Taken from [196].

The TGN functions as the first destination for both bulk endocytosis and signal-dependent endocytosis. The formation of late endosomes is mediated by Vps21 via the recruitment of the CORVET tethering complex, consisting of Vps11, Vps16, Vps18 and Vps33, and the t-SNARE Pep12. Membrane fusion events are mediated by tethering factors and SNARE proteins and have been suggested to control the homotypic fusion of endosomes to create a large late endosome containing multiple intra-luminal vesicles. It is currently unclear which of these events are regulated by Vps21. It has been speculated that Vps21 could mediate the maturation of early endosomes to late endosomes, which are also known as MVBs. During this process, the early endosomal membrane invaginates to form pockets and sealing these pockets results in the formation of intraluminal vesicles inside the multi-vesicular bodies [197], [198].

2.8.4 ESCRT

The events relating to autophagosome closure are thought to be similar to the biogenesis of MVBs, virus budding and cytokinesis. The endosomal sorting complex required for transport (ESCRT) machinery is involved in these cellular membrane scission processes [199], [200]. Over a decade ago, the ESCRT machinery was implicated in autophagy progression, where ESCRT-depleted cells were observed to accumulate autophagic membrane structures [201], [202].

In *S. cerevisiae*, Snf7, a component of the ESCRT subunit, in conjunction with Vps4 promotes the budding of membranes away from the cytoplasm. Yeast cells depleted of Snf7 and Vps4 result in the accumulation of immature autophagosomes containing multiple Atg proteins [203]. The localisation of the ESCRT machinery to the isolation membrane is Vps21-dependant [204], [205]. Additionally, the interaction between Snf7 and Atg17 is crucial for the recruitment of the ESCRT machinery to the isolation membrane. Although these studies have highlighted the importance of the ESCRT machinery in the maturation of autophagosomes, the mechanisms behind these events remain poorly understood. Snf7 has also been seen to interact with the scaffold protein Atg11, potentially recruiting the ESCRT machinery to the isolation membrane in selective autophagy [206]. Interestingly, this interaction is Vps21 independent, suggesting different recruitment mechanisms between selective and nonselective autophagy.

2.8.5 The Retromer Complex

The sorting and export of cargo from the endosomal system is initiated by cargo identification and selection. The cargo selection machinery was first identified in budding yeast as a heteropentameric complex composed of Vps5, Vps17, Vps26, Vps29 and Vps35. The retromer complex was discovered to be required for endosome to Golgi retrieval of Vps10, an integral membrane sorting receptor that mediates sorting of carboxypeptidase Y (CPY) [207]. Seaman et al., 1997 found that in cells lacking any retromer components, Vps10 accumulated on the vacuolar membrane and was depleted at the Golgi, resulting in the improper secretion of newly synthesised CPY. The heteropentameric retromer complex can be dissociated into two

subcomplexes. The cargo selection complex (CSC) trimer consists of Vps35, Vps26 and Vps29, responsible for cargo recognition and mediating packaging of cargo into endosome-derived transport carriers (ETC) [208]. The other subcomplex is composed of a dimer of sorting nexins Vps5 and Vps17 that are proposed to mediate endosome recruitment of CSC and promote the formation of ETCs [209].

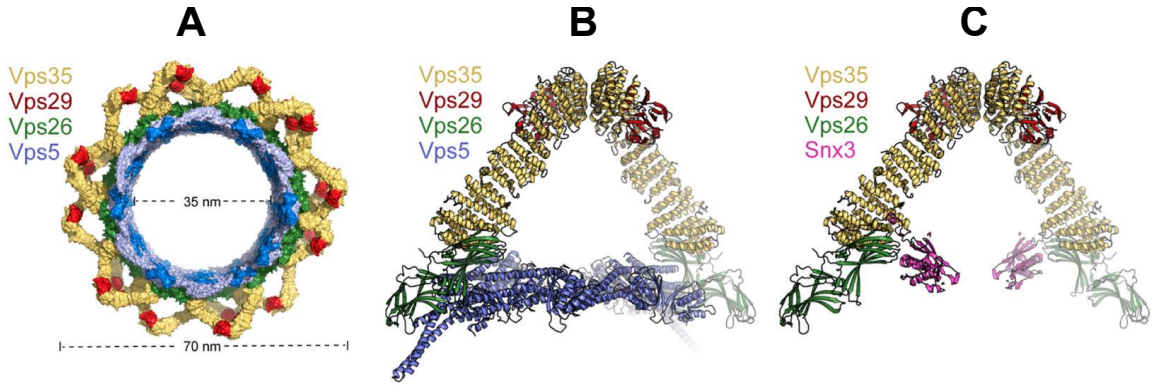

Figure 2-14: Model of the retromer complex in yeast S. cerevisiae.

A) A cross-section of the Vps5-retromer complex shows that the inner membrane coat is formed by SNX dimers while the outer layer is composed of retromer arches of Vps35 and Vps29. B) Showing the SNX Vps5-retromer complex. C) Showing the SNX3-retromer complex. The interaction of Vps35-Vps35 (yellow) interface with Vps29 (red) binding the opposite face forms a retromer dimer. The retromer dimer forms an arch by the extended α-helical solenoid of Vps35 projecting away from the membrane. This model shows a Vps5 dimer on the inner coat of the complex whereas in vivo a Vps5-Vps17 dimer is used. Alignment of crystal structures shows that the retromer complex forms mutually exclusive complexes with either SNX dimers or SNX3. Taken from [210]

Structural analyses of the CSC complex show that it is flexible and a long dumbbell-shaped complex, with Vps26 and Vps29 bound to sites near the N- and C-terminal of Vps35, respectively [211]. Vps29 has a metallophosphodiesterase fold containing two sites for metal ions to bind. Vps29 can bind Zn^{2+} and Mn^{2+} but at a very low affinity and with no functional explanation; therefore, Vps29 is not a metal-dependent phosphatase enzyme [212], [213]. Vps29 serves as a scaffold for the α-helical solenoid structure of Vps35 and is essential for stabilisation. Vps26 has a combination of exposed hydrophobic and basic residues, which is a hallmark of membrane-binding structures and was suggested to interact with membranes via this motif. However, upon observation, there was no noticeable interaction with PI3P or other acidic lipids. This suggests that although Vps26 could bind to membranes, it is too weak to localise to membranes on its own [214]. The folding of Vps26 closely resembles that of the arrestin family, despite the absence of sequence similarity [215]. However, one of the defining features of the arrestin family is the existence of a polar core embedded between two domains, and the domain interface of Vps26 contains clusters of buried polar

interactions. Although, the functional significance of this is unclear. It was suspected that this is required for interaction with clathrin coats and adaptor protein complexes, but mutations of the polar cores did not interfere with CPY sorting [214]. Vps26 interacts directly with Vps35 through a mobile loop and adjacent residues near the distal tip of the C-terminal domain and is essential for the assembly of the retromer complex.

The retromer complex does not possess intrinsic membrane-binding activity and, therefore, must be recruited to the endosome membrane via interaction with sorting nexins and integral membrane cargo [216], [217]. Sorting nexins contain a Phox-homology (PX) domain which is typically recognised by PI3P [218], [219]. Within the sub-family 'PX-only' sorting nexins is Snx3, which can bind to PI3P but is unable to induce membrane tubulation. Snx3 is known to interact with the retromer complex as it is required for the Golgi localisation of Ste13 and Kex2 [220]. The interaction between Snx3 with Vps35 and Vps26 is required for sequestering cargo proteins and for membrane recruitment of the retromer complex.

In unpublished work from our group, a model was proposed where Atg18 and probably another PROPPIN can replace the SNX-BAR proteins Vps5 and Vps17 [221]. This complex would allow for cargo recruitment via Snx3 and the retromer, membrane association via Snx3 and Atg18, and the induction of membrane tubulation via Atg18. Atg18's unstructured hydrophobic 6CD loop undergoes a conformational change into an amphipathic α-helix upon contact with lipids; at PI3P or PI(3,5)P_2 positive membranes this loop is necessary and sufficient to induce tubulation of giant unilamellar vesicles [167].

2.9 Vacuolar Morphology

A complex regulatory network maintains vacuolar morphology in response to environmental stimuli. Under starvation conditions, the vacuoles fuse together to form one large vacuole. Conversely, the volume of the vacuole is reduced during nutrient rich conditions by the fission of the vacuole into several smaller organelles. This process is regulated by the synthesis and regulation of PI(3,5)P_2 and the PI(3,5)P_2-binding protein Atg18. Furthermore, this process requires the dynamin-like GTPase Vps1, the interacting SNARE Vam3, the ATPase Sec18 and

a subunit of the COVERT complex Vps3. Yck3 is also essential to prevent the immediate re-fusion of the vacuoles [222].

PI3P controls protein sorting and membrane dynamics at early endosomes. In comparison, PI(3,5)P_2 appears to govern events associated with the later endosomal compartments such as the vacuole in yeast [82], [223]. Cells that are absent of PI(3,5)P_2 exhibit vacuolar defects, including nonacidic vacuoles, abnormal vacuolar inheritance and impaired retrograde transport [224], [225]. Atg18 has an FRRG motif on the β-barrel which is thought to be the site of direct interaction with PI(3,5)P_2. Mutation of the double arginines disrupts the binding to PI(3,5)P_2 and mislocalises Atg18 to the cytosol [148]. Due to the function differences seen by Atg18 interacting with PI3P and PI(3,5)P_2, it has been suggested that PROPPINs have two fundamentally different functional faces. The binding to PI3P causes tubulation of the endosomal membrane. Conversely, binding to PI(3,5)P_2 triggers insertion of the CD loop, oligomerisation, cooperative fission and tubulation of the membrane.

The acute vacuolar response to osmotic stress involves the rapid and transient 20-fold increase in PI(3,5)P_2. This requires the activation of Fab1 lipid kinase by Vac7 and the Vac14-Fig4 complex [226]–[228]. The rise in PI(3,5)P_2 levels are necessary for the fragmentation of the vacuole during osmotic stress. Both the rise and fall of PI(3,5)P_2 levels are dependent on Fig4 phosphatase activity [229]. Interestingly, *atg18Δ* cells that have been subjected to osmotic stress have PI(3,5)P_2 levels 60 times that of wildtype even though the vacuolar size is unchanged [148], [165].

2.10 Sporulation and budding

Saccharomyces cerevisiae is a single-celled organisms capable of rapid division on a defined medium. The cells are heterozygous for the mating-type locus and can respond to changes in the nutrient status of the environment in a variety of ways. Yeast cells enter the developmental pathway of meiosis and sporulation in the absence of a nitrogen source combined with the presence of a nonfermentable carbon source [25], [230]. Sporulation is an essential process that, like autophagy, is triggered due to stress conditions. The process of spore formation is entirely different from that of mitotic cell division [231], [232]. When under

nutrient rich conditions, the yeast cells undergo mitosis and multiply. Mitosis causes the dividing of the chromosomes, and the mother and daughter cells split by a cytokinetic event at the bud neck. However, in sporulation, the four haploid nuclei are produced from the segregation of the chromosomes by meiosis. *De novo* formation of the plasma membrane is formed around each nucleus within the cytoplasm of the mother cell to form immature spores. Once spores are fully developed, the anucleate but still intact mother cell becomes the ascus encasing the four spores of the tetrad [233]. The vegetative machinery is altered during these morphogenetic events to carry out several cellular functions, including RNA synthesis, chromosomal segregation, the cell cycle, and organellar segregation.

The yeast cell wall is composed of glucan, mannan, dityrosine and protein with small amounts of chitin. The bud wall is newly synthesised and not derived from the material of the mother cell wall [234], [235]. The glucan and mannan components of the cell wall are synthesised continuously throughout the cell cycle [236]. Dityrosine within the spore wall provides resistance to digestive enzymes and are present in the outer most layer of the spore wall [237]. Throughout the mitotic cycle, the nuclear envelope, a pair of double membranes, remains intact around the nucleus of a yeast cell. A portion of the nucleus stains differently and has a crescent shape during part of the mitotic cycle, and this is believed to be the nucleolus [238]. When the mature bud separates from the parent cell at the termination of the cell cycle, a permanent birth scar remains on the surface of both the bud and the parent cell [239], [240].

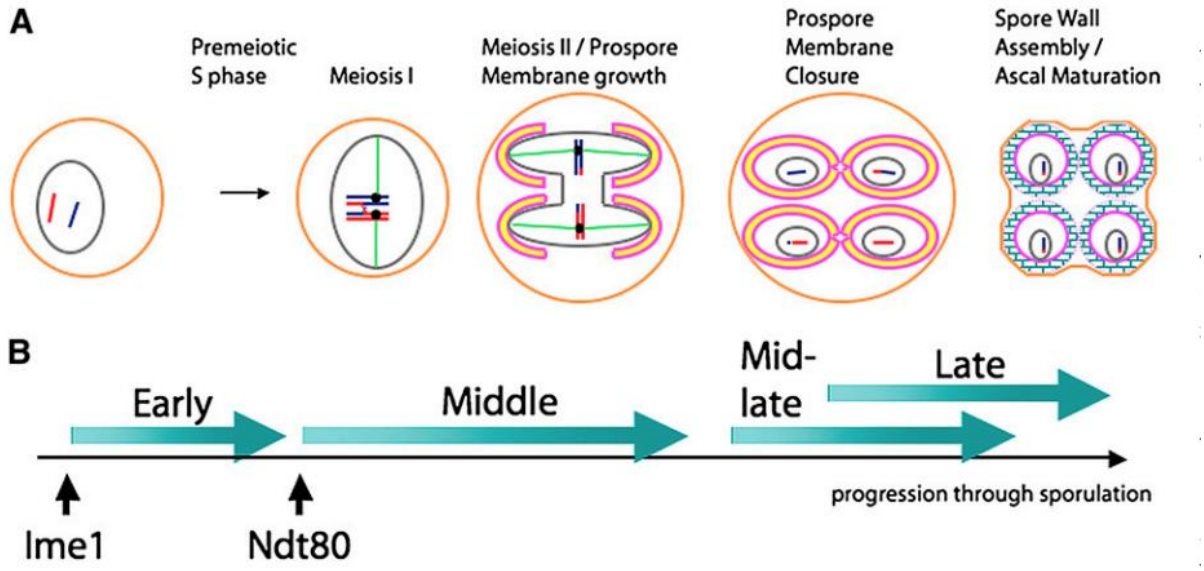

Figure 2-15: The events of spore formation in yeast S. cerevisiae.

(A) Following the events of meiosis and sporulation in chronological order. The orange lines indicate the plasma membrane of the original mother cell. The grey lines indicate the nuclear envelope. The green lines represent the spindle microtubules. The blue and red lines indicate the homologous chromosomes. The pink lines indicate the prospore membrane with the lumen highlighted in yellow. After the closure of the prospore membrane it is separated into two distinct membranes. The plasma membrane is the one closest to the nucleus, while the outer membrane is broken down during the assembly of the spore wall. The blue bricks represent the spore wall. (B) The chronological order of events and the transcription factors causes the events in A. Taken from [233]

Sporulation occurs in three major phases, as seen in Figure 2-15. The early phase begins when the cells differentiate into spores due to a lack of nitrogen or a fermentable carbon source [241]. This results in exiting from the mitotic cycle G1 and entry into the premeiotic S phase. Once the DNA is replicated, homolog recombination and pairing occur in the meiotic prophase. Alterations in both the cell cycle machinery and RNA processing are required for cells to begin meiosis [242], [243]. Meiotic division begins with the replication of DNA and the generation of the four spindle pole bodies (SPBs), ultimately producing four haploid nuclei from one mother cell. This phase requires a multitude of changes to the cell cytoplasm. Initially, the four spindle pole bodies present in meiosis are modified and become the new sites for the formation of the new membrane compartments, termed prospore membrane [244], [245]. Each prospore membrane grows and engulfs the forming haploid nucleus adjacent to it. Also, during this phase, organelles such as mitochondria migrate into the cytoplasmic space between the nuclear envelope and the prospore membrane [231]. During the meiosis II phase, the SPBs act as a recruitment platform for several sporulation specific proteins; this leads to the expansion of this face, known as the meiosis II outer plaque (MOP).

Once the prospore membrane has elongated around the nucleus and organelles a cytokinetic event is required for the ends of the prospore membrane to fuse. This double membraned compartment is termed an ascus and is surrounded by the cytoplasm of the original mother cell. This process happens at each MOP leading to the generation of the four asci from one original mother cell. The assembly of a spore wall around each spore begins only after the membrane fusion and is crucial for the maturation of the spore [246], [247]. In addition, closure causes the compaction of chromatin in the spore nucleus as well as the regeneration of organelles [248], [249]. This occurs in the cytoplasm of the ascus, and once the assembly of the spore wall is complete, the original mother cell collapses around the spore to produce the tetrahedral mature ascus [250]. The progression of sporulation is mediated by a transcription regulatory cascade that affects both meiosis and spore formation [251], [252]. Ime1 is the first transcription factor used to trigger the differentiation process within the cell. Once Ime1 is expressed this acts as a master switch for the sporulation process to begin [253].

Both autophagy and sporulation are induced during stress conditions and negatively regulated by TOR [254], [255]. Upon induction the *de novo* formation of a double membraned structure at the PAS or MOP termed phagophore or prospore membrane, respectively. These double membraned structures both expand to engulf material, cargo in autophagy and SPB in sporulation. These similarities suggest some cross-talk between autophagy and sporulation, this is explained further in chapter 5.3.

In unpublished data, a sporulation defect has been seen in the absence of Hsv2 when compared to wildtype. Under sporulation conditions *hsv2Δ* diploid cells contained a third less asci than wildtype cell, the role of Hsv2 in sporulation is still to be determined. It has also been observed that *hsv2Δ* cells have reduced levels of both D- and L-dityrosine with the majority located in the soluble fraction compared to the spore wall fraction [237].

2.11 Aim of the Study

The PROPPIN family are important PI3P and PI(3,5)P_2 adaptor proteins that often act as platforms to promote and coordinate protein-protein interactions, which are involved in autophagy and other vesicular transport pathways. All PROPPINs are structurally well characterised, although their molecular functions are still not fully comprehended. Atg18 is a

component of the core autophagic machinery, and Atg21 is crucial for selective autophagy such as the Cvt pathway. Hsv2 is the least functionally characterised protein within the PROPPIN family, although a mild defect has been observed on PMN and sporulation in the absence of Hsv2. However, the mechanistic function of Hsv2 in these processes is unknown.

There were three main aims to this study: First, to identify potential interaction partners of Hsv2 using proximity-dependent labelling assays. Uncovering the interactome of Hsv2 should give us a better understanding of its function.

Second, to deduce the molecular interaction between KlAtg21 and ScAtg8, we started with the purification of ScAtg8 to determine the binding affinity with KlAtg21. We used crystallisation trails to get a crystal structure of the Atg8-Atg21 complex to determine the residues of Atg21 responsible for interacting with Atg8.

Lastly, determine the role of Atg18 with the retromer complex in maintaining vacuolar morphology. We used hyperosmotic conditions to initiate vacuolar fragmentation to deduce which components of the retromer complex in conjunction with Atg18 are responsible for maintaining vacuolar morphology.

3. Methodology

3.1 Materials

3.1.1 Equipment

Table 3-1: Equipment used in this study

Equipment	Manufacturer
Agarose Gel Chamber Mini-Sub® cell GT	Bio-Rad Laboratories GmbH (DE)
Amersham™ Hybond™ PVDF Blotting membrane	GE Healthcare GmbH (DE)
Autoclave Systec DX-200	Systec GmbH (DE)
BioPhotometer 6132 Spectrophotometer	Eppendorf AG (DE)
Blotting Paper (MN218B 58 x 60 cm)	Macherey-Nagel (DE)
Blot Shaker GFL® 3019	GFL (DE)
Centrifuge 5415D	Eppendorf AG (DE)
Centrifuge 5415R	Eppendorf AG (DE)
Centrifuge 5417C	Eppendorf AG (DE)
Centrifuge 5804	Eppendorf AG (DE)
Centrifuge 5804R	Eppendorf AG (DE)
Clean Bench	BDK (DE)
Cuvettes (10 x 4 x 45 mm)	Sarstedt (DE)
DeltaVision®, Olympus IX71	Applied Precision (USA)
Diaphragm Vacuum Pump	Vacuubrand GmbH & Co. KG
Disruptor Genie Vortex-Shaker	Scientific Industries (USA)
Eppendorf Safe-Lock tubes, 1.5 mL	Eppendorf AG (DE)
Eppendorf Safe-Lock tubes, 2.0 mL	Eppendorf AG (DE)
Freezer (-20°C)	Heraeus Holding GmbH (DE)
Freezer (-80°C)	Heraeus Holding GmbH (DE)
Glass Beads, Acid Washed (425-600 µm)	Merck KGaA (DE)
Innova 4200 Incubator-Shaker	New Brunswick Scientific GmbH (DE)
Lab pH Meter inoLab® pH 7110	Xylem Analytics Germany Sales GmbH (DE)

Lab Shaker LS-X	Kühner Shaker GmbH (DE)
Lab Shaker SBM/SS-X	Kühner Shaker GmbH (DE)
LAS-300 Intelligent Dark Box	FUJIFILM Europe GmbH (DE)
Magnetic Stirrer MR 2002	Heidolph Elektro Gmbh & Co. KG (DE)
Magnetic Stirrer MR 3001	Heidolph Elektro Gmbh & Co. KG (DE)
Menzel Microscope Coverslips (24 x 24 mm)	Thermo Fisher Scientific (DE)
Menzel Microscope Slides (76 x 26 mm), Cut Edges	Thermo Fisher Scientific (DE)
Microwave R-939	Sharp Electronics GmbH (DE)
Mini Trans-Blot® Cell	Bio-Rad Laboratories GmbH (DE)
Mini-PROTEAN® Tetra Vertical Electrophoresis Cell	Bio-Rad Laboratories GmbH (DE)
Minisart® Filters (0.2 µm)	Sartorius AG (DE)
Nalgene Rapid-Flow, 500 mL	Thermo Fisher Scientific GmbH (DE)
NanoVue UV/Visible Spectrophotometer	GE Healthcare GmbH (DE)
PCR Mastercycler® Gradient	Eppendorf AG (DE)
Pipette Controllers Accu-Jet® Pro	Brand GmbH & Co KG (DE)
Pipettes Eppendorf Research® Plus	Eppendorf AG (DE)
PowerPac Basic Power Supply	Bio-Rad Laboratories GmbH (DE)
PowerPac HC Power Supply	Bio-Rad Laboratories GmbH (DE)
Protein LoBind Tubes 1.5 mL	Eppendorf (DE)
Refridgerator (4°C)	Liebherr (Bulle, Switzerland)
Roto Shake Genie	Scientific Industries Inc. (USA)
Sartorius Handy H51-D Lab Balance	Sartorius AG (DE)
Sartorius Universal U4100 Lab Balance	Sartorius AG (DE)
Savant SpeedVac Concentrator	Thermo Fisher Scientific GmbH (DE)
Semi-Dry Western-Blot Chambers	UMG (DE)
Shaking Water Bath SWB25	Thermo Haake GmbH (DE)
Thermo Mixer® Comfort	Eppendorf AG (Hamburg, Germany)

VICTOR Nivo Multimode Microplate Reader	Perkin Elmer (Massachusetts, USA)
Vortex Genie 2	Scientific Industries (USA)
Whatman Gel Blot Paper	GE Healthcare GmbH (DE)
Xtal Concepts SpectroLight 600	Xtal Concepts GmbH (Hamburg, Germany)

3.1.2 Software

Table 3-2: Software used in this study

Software	Reference
Affinity Designer	Serif Europe (Nottingham, UK)
Fiji ImageJ	[256]
GraphPad Prism 7	GraphPad Software (USA)
Keynote	Apple (California, USA)
MaxQuant 1.5.1.0	Max Planck Institute of Biochemistry [257]
Mendeley Desktop 1.19.8	Mendeley Ltd (London, UK)
Microsoft Office for Mac OS 2018	Microsoft (USA)
Perseus	Max Planck Institute of Biochemistry
Proteome Discoverer™ 2.2	Thermo Fisher Scientific (Bremen, Germany)
SnapGene	GSL Biotech LLC (USA)
SoftWoRx	Applied Precision (USA)
OmniGraffle	Omni Group (Washington, USA)
VICTOR NIVO system	Perkin Elmer (Massachusetts, USA)

3.1.3 Commercial Kits

Table 3-3: Commercial Kits used in this study

Kit Name	Manufacturer
Amersham™ ECL™ Western-Blotting Detection Reagents	GE Healthcare (DE)

DreamTaq Green PCR MasterMix	Thermo Fisher Scientific (DE)
NucleoSpin® Microbial SNA	Macherey-Nagel (DE)
Pierce ECL Plus Western-Blotting Substrates	Thermo Fisher Scientific (DE)
QIAquick® Gel Extraction Kit	Qiagen (DE)
QIAquick® PCR Purification Kit	Qiagen (DE)
Wizard® Plus SV Miniprep System	Promega (DE)
µMACS GFP Isolation Kit	Miltenyl Biotec (DE)

3.1.4 Enzymes

Table 3-4: Enzymes used in this study

Enzyme	Manufacturer
Alkaline Phosphatase, Calf Intestinal (CIP)	New England Biolabs (DE)
KOD Hot Start DNA Polymerase	Merck (DE)
KOD XL Polymerase	Merck (DE)
Restriction Enzymes	New England Biolabs (DE)
T4 DNA Ligase	New England Biolabs (DE)
Zymolyase 100T	Seikagaku Biobusiness (JP)

3.1.5 Antibodies

Table 3-5: Primary Antibodies used in this study

Primary Antibody	Dilution	Manufacturer
Anti-Ape1 (Rabbit IgG)	1:5,000	Eurogentec (BE)
Anti-GFP (Mouse IgG1κ)	1:1,000	Roche (DE)
Anti-HA (Mouse IgG_{2a} F-7)	1:10,000	Santa Cruz Biotechnology (USA)
Anti-MyC (Mouse IgG)	1:500	Gift from the group of Prof. P. Rehling (Dept. Cellular Biochemistry, University Göttingen)

Table 3-6: Secondary Antibodies used in this study

Secondary Antibody	Dilution	Manufacturer
Goat Anti-Mouse (H+L)-HRPO	1:10,000	Dianova (DE)
Goat Anti-Rabbit IgG (H+L)	1:5,000	Thermo Fisher Scientific (DE)
Strep-Tag HRP Conjugate	1:50,000	Iba (DE)

3.1.6 Medium & Buffers

Table 3-7: Medium used in this study

Medium	Composition		Reference
CM (pH 5.6)	2% (w/v)	D-glucose	[258]
	0.2% (w/v)	drop-out mix	
	0.67% (w/v)	Yeast nitrogen base w/o a.a	
CM excluding met (pH 5.6)	2% (w/v)	D-glucose	[258]
	0.2% (w/v)	drop-out mix excluding met	
	0.67% (w/v)	Yeast nitrogen base excluding a.a	
LB (pH 7.5)	0.5% (w/v)	Sodium Chloride	[259]
	1% (w/v)	Bacto™ tryptone	
	0.5% (w/v)	Bacto™ yeast extract	
MV	2% (w/v)	D-glucose	[260]
	0.67% (w/v)	Yeast nitrogen base w/o a.a	
SD-N	2% (w/v)	D-glucose	[7]
	0.67% (w/v)	Yeast nitrogen base w/o a.a & ammonium sulphate	
SOC (PH 7.5)	2% (w/v)	Bacto™ tryptone	[259]
	0.5% (w/v)	Bacto™ yeast extract	
	0.4% (w/v)	D-glucose	
	10 mM	Magnesium Chloride	
	10 mM	Magnesium Sulphate	
	10 mM	Sodium Chloride	
	2.5 mM	Potassium Chloride	

Sporulation	0.01% (w/v)	a.a supplement powder	[261]
	0.1% (w/v)	Bacto™ yeast extract	
	0.05% (w/v)	D-glucose	
	1% (w/v)	Potassium acetate	
YPD (pH 5.5)	2% (w/v)	Bacto™ peptone	[260]
	1% (w/v)	Bacto™ yeast extract	
	2% (w/v)	D-glucose	

Table 3-8: Buffers used in this study

Buffer	**Composition**	
Alkaline Lysis Buffer	0.28 M	Sodium Hydroxide
	1.125% (v/v)	β-mercaptoethanol
Atg8 Lysis Buffer	10 mM	Magnesium Chloride
	0.02% (v/v)	Benzonase
	3.6% (w/v)	Protease Inhibitor Cocktail
	1 x	PBS pH 7.4
BioID Lysis Buffer	10 mM	HEPES pH 7.9
	10 mM	Potassium Chloride
	1.5 mM	Magnesium Chloride
	1 mM	PMSF
	1 x	25 x cOmplete
	0.5 mM	DTT
CBB Fixing Solution I	40% (v/v)	Ethanol
	10% (v/v)	Methanol
	10% (v/v)	Orthophosphoric acid
CBB Fixing Solution II	10% (w/v)	Ammonium sulphate
	1% (v/v)	Orthophosphoric acid
CBB Staining Solution	0.125% (w/v)	CBB G-250
	45% (v/v)	Ethanol
	10% (v/v)	Orthophosphoric acid

CBB Destaining Solution	40% (v/v)	Ethanol
	5% (v/v)	Orthophosphoric acid
GFP TRAP Lysis buffer	1 mM	EDTA
	1 mM	PMSF
	50 mM	Tris/HCl
	0.5% (w/v)	Tween20
LiOAc-Sorb buffer (pH 8.0)	1 M	D-sorbitol
	1 mM	EDTA
	100 mM	Lithium acetate
	10 mM	Tris/acetic acid
PEG in LiTE buffer (pH 8.0)	1 mM	EDTA
	100 mM	Lithium acetate
	10 mM	Tris/acetic acid
	40% (w/v)	PEG 3350
1 x PBS (pH 7.4)	10 mM	Disodium phosphate
	1.8 mM	Monopotassium phosphate
	2.7 mM	Potassium chloride
	140 mM	Sodium chloride
SDS running buffer	200 mM	Glycine
	25 mM	Tris
	0.1% (w/v)	SDS
SDS sample buffer (pH 7.5)	20 mM	DTT
	10% (v/v)	Glycerol
	2% (w/v)	SDS
	100 mM	Tris/HCl
Silver Nitrate Fixing Solution	10% (v/v)	Acetic acid
	40% (v/v)	Ethanol
Silver Nitrate Staining Solution	0.2% (w/v)	Silver Nitrate
	0.02% (v/v)	Formaldehyde
TAE buffer (pH 8.1)	0.114% (v/v)	Acetic acid
	2 mM	EDTA

	40 mM	Tris
TBST buffer (pH 7.6)	137 mM	Sodium chloride
	20 mM	Tris/HCl
	0.1% (w/v)	Tween20
Western Blotting buffer	20% (v/v)	Ethanol
	192 mM	Glycine
	25 mM	Tris

3.1.7 Strains

Table 3-9: Strain backgrounds used in this study

Strain	Genotype	Reference
WCG4a (WT)	MATα *his*2-11,15 *leu*2-3,112 *ura*3	[8]
BY4741	WT DIPLOID	Euroscarf
SEY6210 (SEY WT)	SEY6210 *MATα ura3-52 leu2-3,112 his2-Δ200 lys2-801 trp1-Δ901 suc2-Δ9 mel GAL*	[9]

Table 3-10: S. Cerevisiae WCG strains used in this study

Strain	Genotype	Reference
atg1Δ	WCG4a *atg1Δ*::KAN	[262]
atg21Δ	WCG4a *atg21Δ*::KAN	[263]
hsv2Δ	WCG4a *hsv2Δ*::KAN	This study
atg18Δ	WCG4a *atg18Δ*::KAN	Euroscarf
atg18Δ hsv2Δ	WCG4a *atg18Δ*::KAN *hsv2Δ*::hphNT1	Dr Lena Munzel
atg21Δ hsv2Δ	WCG4a *atg21Δ*::KAN *hsv2Δ*::hphNT1	Dr Lena Munzel
atg18Δ atg21Δ hsv2Δ	WCG4a *atg18Δ*::KAN *atg21Δ*::natNT2 *hsv2Δ*::hphNT1	Dr Lena Munzel
Atg21-HA *hsv2Δ*	WCG4a Atg21-3xHA::HIS5 *hsv2Δ*::hphNT1	Dr Lena Munzel
Atg18-HA *hsv2Δ*	WCG4a Atg18::HA::HIS5 *hsv2Δ*::hphNT1	Dr Lena Munzel

hsv2Δ arg4Δ lys1Δ	WCG4a *hsv2Δ*::KAN *arg4Δ*::hphNT1 *lys1Δ*::natNT2	This study
Lsb6-6xHA *hsv2Δ*	Lsb6-6xHA::natNT2 *hsv2Δ*::hphNT1	This study
Pib2-6xHA *hsv2Δ*	Pib2-6xHA::natNT2 *hsv2Δ*::hphNT1	This study
Yck3-6xHA *hsv2Δ*	Yck3-6xHA::natNT2 *hsv2Δ*::hphNT1	This study
Vac14-6xHA *hsv2Δ*	Vac14-6xHA::natNT2 *hsv2Δ*::hphNT1	This study
Vtc3-6xHA *hsv2Δ*	Vtc3-6xHA::natNT2 *hsv2Δ*::hphNT1	This study
Avt4-6xHA *hsv2Δ*	Avt4-6xHA::natNT2 *hsv2Δ*::hphNT1	This study
Vps35-6xHA *hsv2Δ*	Vps35-6xHA::natNT2 *hsv2Δ*::hphNT1	Dr Lisa Marquardt

Table 3-11: **S. Cerevisiae BY4741** *strains used in this study*

Strain	Genotype	Reference
hsv2Δ	BY4741 *hsv2Δ*::KAN	Euroscarf
atg18Δ	BY4741 *atg18Δ::*KAN	Euroscarf
atg21Δ hsv2Δ	*BY4741 atg21Δ*::KAN *hsv2Δ*::LEU2	Euroscarf
atg21Δ atg18Δ hsv2Δ	*BY4741 atg21Δ*::KAN *atg18Δ*::HIS3 *hsv2Δ*::LEU2	Euroscarf
vps35Δ	BY4741 *vps35Δ::KAN*	Euroscarf
vps29Δ	BY4741 *vps29Δ::KAN*	Euroscarf
vps26Δ	BY4741 *vps26Δ::KAN*	Euroscarf
vps17Δ	BY4741 *vps17Δ::KAN*	Euroscarf
vps5Δ	BY4741 *vps5Δ::KAN*	Euroscarf
fab1Δ	BY4741 *fab1Δ::KAN*	Euroscarf
snx3Δ	BY4741 *snx3Δ::KAN*	Euroscarf

Table 3-12: **S. Cerevisiae SEY6210** *strains used in this study*

Strain	Genotype	Reference
atg5Δ	*SEY6210 atg5Δ::natNT2 pho8::pTDH3-GFP-pho8Δ60-URA3*	This study
atg5Δ hsv2Δ	*SEY6210 atg5Δ::natNT2 hsv2Δ::hphNT1 pho8::pTDH3-GFP-pho8Δ60-URA3*	This study

Table 3-13: E. coli strains used in this study

Strain	Genotype	Reference
XL1-Blue	recA1 endA1 gyrA96 thi-1 hsdR17 supE44 relA1 lac [F' proAB lacI^{q}ZΔM15 Tn10 (tet^{r})]	Agilent (Santa Clara, USA)
BL21	*fhuA2 [lon] ompT gal [dcm] ΔhsdS*	New England BioLabs

3.1.8 Plasmids

Table 3-14: Plasmids used in this study

Plasmid	Genotype	Reference
pME2783	CEN/ARS AmpR ori *URA3* PMET25-lacZ'/MCS	[264]
pUG36-Ygr223c	CEN/ARS AmpR ori *URA3* pUG36 P_{MET25}-GFP-Ygr223c-$T_{YGR223c}$	This study
pUG36-Myc-BirA*-Hsv2	CEN/ARS AmpR ori *URA3* pUG36 P_{MET25}-Myc-BirA*-Hsv2-T_{CYC1}	This study
pUG35-Hsv2-Myc-BirA*	CEN/ARS AmpR ori *URA3* pUG35 P_{MET25}-Hsv2-Myc-BirA*-T_{CYC1}	This study
pFA6a-Myc-BirA*	AmpR ori *TRP1* Myc-BirA*	H. D. Schmitt (Department of Neuroscience MPI)
pGEX-4T3-nGST-Atg8	pGEX-4T3 P_{PTAC}-nGST-Atg8-T_{ATG8}	Dr Roswitha Krick (AG Thumm)
pUG35-Hsv2-GFP	CEN/ARS AmpR ori URA3 P_{HSV2}-Hsv2-GFP-T_{CYC1}	This study
pRS426-Hsv2-GFP	2µ AmpR ori *URA3* P_{HSV2}-Hsv2-GFP-T_{CYC1}	This study
pRS416-Pep12-GFP	2µ AmpR ori *URA3* P_{TPI}-Pep12-GFP-T_{PEP12}	[265]
pUG36	CEN/ARS AmpR ori *URA3* P_{MET25}-yEGFP–lacZ'–T_{CYC1}	[266]
pFa6a-HISMX6	AmpR ori P_{TEF1}-HIS3-T_{CYC1}	[267]
pFa6a-hphNT1	AmpR ori P_{TEF1}-HygR-T_{CYC1}	[22]

pFa6a-kanMX6	AmpR ori P_{TEF1}-Kan-T_{CYC1}	[267]
pFa6a-natNT2	AmpR ori P_{TEF1}-Nrs-T_{ADH1}	[22]
pRS313	CEN/ARS AmpR ori lacZ' HIS3	[268]
pRS315	CEN/ARS AmpR ori lacZ' LEU2	[268]
pRS316	CEN/ARS AmpR ori lacZ' URA3	[268]
MET25-Ste14-Cub	CEN/ARS AmpR ori *HIS3* P_{MET25}-Ste14-C_{ub}	Dr Fulvio Reggiori (Groningen, NL)
MET25-Atg9-Cub	CEN/ARS AmpR ori *HIS3* P_{MET25}-Atg9-C_{ub}	Dr Fulvio Reggiori (Groningen, NL)
MET25-Hsv2-Cub	CEN/ARS AmpR ori *HIS3* P_{MET25}-Hsv2-C_{ub}	Dr Roswitha Krick (AG Thumm)
CUP1-Nui-Ubc6	CEN/ARS AmpR ori *TRP1* P_{CUP1}-N_{ui}-Ubc6	Dr Fulvio Reggiori (Groningen, NL)
CUP1-Nui-Atg1	CEN/ARS AmpR ori *TRP1* P_{CUP1}-N_{ui}-Atg1	Dr Fulvio Reggiori (Groningen, NL)
CUP1-Nui-Atg2	CEN/ARS AmpR ori *TRP1* P_{CUP1}-N_{ui}-Atg2	Dr Fulvio Reggiori (Groningen, NL)
CUP1-Nui-Atg6	CEN/ARS AmpR ori *TRP1* P_{CUP1}-N_{ui}-Atg6	Dr Fulvio Reggiori (Groningen, NL)
CUP1-Nui-Atg9	CEN/ARS AmpR ori *TRP1* P_{CUP1}-N_{ui}-Atg9	Dr Fulvio Reggiori (Groningen, NL)
CUP1-Nui-Atg14	CEN/ARS AmpR ori *TRP1* P_{CUP1}-N_{ui}-Atg14	Dr Fulvio Reggiori (Groningen, NL)
CUP1-Nui-Atg18	CEN/ARS AmpR ori *TRP1* P_{CUP1}-N_{ui}-Atg18	Dr Fulvio Reggiori (Groningen, NL)
CUP1-Nui-Atg20	CEN/ARS AmpR ori *TRP1* P_{CUP1}-N_{ui}-Atg20	Dr Fulvio Reggiori (Groningen, NL)
CUP1-Nui-Atg21	CEN/ARS AmpR ori *TRP1* P_{CUP1}-N_{ui}-Atg21	Dr Fulvio Reggiori (Groningen, NL)
CUP1-Nui-Atg23	CEN/ARS AmpR ori *TRP1* P_{CUP1}-N_{ui}-Atg23	Dr Fulvio Reggiori (Groningen, NL)

CUP1-Nui-Pep12	CEN/ARS AmpR ori *TRP1* P_{CUP1}-N_{ui}-Pep12	Dr Fulvio Reggiori (Groningen, NL)
CUP1-Nui-Pex10	CEN/ARS AmpR ori *TRP1* P_{CUP1}-N_{ui}-Pex10	Dr Fulvio Reggiori (Groningen, NL)
CUP1-Nui-Rcy1	CEN/ARS AmpR ori *TRP1* P_{CUP1}-N_{ui}-Rcy1	Dr Fulvio Reggiori (Groningen, NL)
CUP1-Nui-Sec62	CEN/ARS AmpR ori *TRP1* P_{CUP1}-N_{ui}-Sec62	Dr Fulvio Reggiori (Groningen, NL)
CUP1-Nui-Sed5	CEN/ARS AmpR ori *TRP1* P_{CUP1}-N_{ui}-Sed5	Dr Fulvio Reggiori (Groningen, NL)
CUP1-Nui-Snc1	CEN/ARS AmpR ori *TRP1* P_{CUP1}-N_{ui}-Snc1	Dr Fulvio Reggiori (Groningen, NL)
CUP1-Nui-Snx4	CEN/ARS AmpR ori *TRP1* P_{CUP1}-N_{ui}-Snx4	Dr Fulvio Reggiori (Groningen, NL)
CUP1-Nui-Sso1	CEN/ARS AmpR ori *TRP1* P_{CUP1}-N_{ui}-Sso1	Dr Fulvio Reggiori (Groningen, NL)
CUP1-Nui-Tlg1	CEN/ARS AmpR ori *TRP1* P_{CUP1}-N_{ui}-Tlg1	Dr Fulvio Reggiori (Groningen, NL)
CUP1-Nui-Tlg2	CEN/ARS AmpR ori *TRP1* P_{CUP1}-N_{ui}-Tlg2	Dr Fulvio Reggiori (Groningen, NL)
CUP1-Nui-Tom5	CEN/ARS AmpR ori *TRP1* P_{CUP1}-N_{ui}-Tom5	Dr Fulvio Reggiori (Groningen, NL)
CUP1-Nui-Tom22	CEN/ARS AmpR ori *TRP1* P_{CUP1}-N_{ui}-Tom22	Dr Fulvio Reggiori (Groningen, NL)
CUP1-Nui-Trs85	CEN/ARS AmpR ori *TRP1* P_{CUP1}-N_{ui}-Trs85	Dr Fulvio Reggiori (Groningen, NL)
CUP1-Nui-Vam3	CEN/ARS AmpR ori *TRP1* P_{CUP1}-N_{ui}-Vam3	Dr Fulvio Reggiori (Groningen, NL)
CUP1-Nui-Vps5	CEN/ARS AmpR ori *TRP1* P_{CUP1}-N_{ui}-Vps5	Dr Fulvio Reggiori (Groningen, NL)
CUP1-Nui-Vps15	CEN/ARS AmpR ori *TRP1* P_{CUP1}-N_{ui}-Vps15	Dr Fulvio Reggiori

		(Groningen, NL)
CUP1-Nui-Vps45	CEN/ARS AmpR ori *TRP1* P_{CUP1}-N_{ui}-Vps45	Dr Fulvio Reggiori (Groningen, NL)
CUP1-Nui-Vps52	CEN/ARS AmpR ori *TRP1* P_{CUP1}-N_{ui}-Vps52	Dr Fulvio Reggiori (Groningen, NL)
CUP1-Nui-Vps34	CEN/ARS AmpR ori *TRP1* P_{CUP1}-N_{ui}-Vps34	Dr Fulvio Reggiori (Groningen, NL)
CUP1-Nui-Vti1	CEN/ARS AmpR ori *TRP1* P_{CUP1}-N_{ui}-Vti1	Dr Fulvio Reggiori (Groningen, NL)
CUP1-Nui-Vps21	CEN/ARS AmpR ori *TRP1* P_{CUP1}-N_{ui}-Vps21	Dr Roswitha Krick (AG Thumm)
CUP1-Nui-Vac1	CEN/ARS AmpR ori *TRP1* P_{CUP1}-N_{ui}-Vac1	Dr Roswitha Krick (AG Thumm)
CUP1-Nui-Vac17	CEN/ARS AmpR ori *TRP1* P_{CUP1}-N_{ui}-Vac17	Dr Roswitha Krick (AG Thumm)
CUP1-Nui-Atg8	CEN/ARS AmpR ori *TRP1* P_{CUP1}-N_{ui}-Atg8	Dr Roswitha Krick (AG Thumm)
CUP1-Nui-Atg5	CEN/ARS AmpR ori *TRP1* P_{CUP1}-N_{ui}-Atg5	Dr Roswitha Krick (AG Thumm)
CUP1-Nui-Vps21(S21N)	CEN/ARS AmpR ori *TRP1* P_{CUP1}-N_{ui}-Vps21(S21N)	Dr Roswitha Krick (AG Thumm)
CUP1-Nui-Vps21(Q66L)	CEN/ARS AmpR ori *TRP1* P_{CUP1}-N_{ui}-Vps21(Q66L)	Dr Roswitha Krick (AG Thumm)
CUP1-Nui-Hsv2	CEN/ARS AmpR ori *TRP1* P_{CUP1}-N_{ui}-Hsv2	Dr Roswitha Krick (AG Thumm)

Table 3-15: Oligonucleotides used in this study

Name	**Sequence**

Avt1_S2	AGAGCTAATGTAAATGAATTTTAAGTAGAGTAAGTATGCCCCTCGTCGAcgtacgctgcaggtcgac
Avt1_S3	GTGTTGTCCACATTAGGTGTTGGTGCTGCAATTATTTCAcgtacgctgcaggtcgac
Hsv2_S3	GAGCCCACCAGATGGGAGTTGGTGAGAGAATCATGGAGAGAGCTTCGTACGCTGCAGGTCGAC
Ygr125w_S2	GCAATACGCCGGCAATAAAAGAAATTAAATAAATATACGTGTACGCTCatcgatgaattcgagctcg
Ygr125w_S3	ATCAAGGACACCAGATTCAAAGAATTACTAGGTTACACACTTGTTAGCGCAcgtacgctgcaggtcgac
VPS74_S2	GCTTGACTTTTCCTTATGTTTCAAAGAGAGGATTTTTGTTGTTATTTTCAatcgatgaattcgagctcg
VPS74_S3	TTATTGCTGGTGTATTTGAAGTCTTTTCAAGAATGGATATGCTATTAcgtacgctgcaggtcgac
BamH1_GFP_rev	GGATCCGGGTTATTTGTACAATTCATC
EcoRI-Hsv2-rev	TTGACTGAATTCAAGCTCTCTCCATGATTCTCTCACC
SacI_Hsv2-for	AGTCAAGAGCTCTGCAAGAAAGGGGCCTGAGT
Xba1_Hsv2_for	GGGTCTAGAATGGATGTTCGTCGACCTATA
Mut-BamH1_Hsv2_for	GCATACATAACTAGCAGGGATCCATGGATGTTCGTCGACCTATAAGGG
Mut-BamH1_Hsv2_rev	CCCTTATAGGTCGACGAACATCCATGGATCCCTGCTAGTTATGTATGC

3.1.9 Consumables & Chemicals

Table 3-16: Consumables and chemicals used in this study

Chemical	Manufacturer

$^{13}C_6$-L-Arginine HCL (Arg-6:HCl)	Silantes (DE)
$^{13}C_6$,$^{15}N_2$-L-Lysine HCl (Lys6:HCl)	Silantes (DE)
$^{13}C_6$,$^{15}N_4$-L-Arginine HCl (Arg-10:HCl)	Silantes (DE)
4,4,5,5-D_4-L-Lysine 2HCl (Lys-4D:2HCl)	Silantes (DE)
5-Fluoroorotic acid	Thermo Fisher Scientific (DE)
Agarose NEEO Ultra-Qualität	Carl Roth GmbH (DE)
Amicon Ultra-15 Centrifugal Units 3,000 MWCO	Merck Millipore (USA)
Ampicillin Sodium Salt	Thermo Fisher Scientific (DE)
Bacto™ Agar	Becton Dickinson (DE)
Bacto™ Peptone	Becton Dickinson (DE)
Bacto™ Tryptone	Becton Dickinson (DE)
Bacto™ Yeast Extract	Becton Dickinson (DE)
Biotin	Sigma-Aldrich (DE)
BufferW (10x) (Strep-Tactin®)	IBA Lifesciences (DE)
Calcofluor-White Staining	Sigma-Aldrich (DE)
cOmplete™, EDTA-free	Roche (DE)
Coomassie® Brilliant Blue G 250	Serva Electrophoresis GmbH (DE)
DeltaVision Immersion Oil (N=1.520)	GE Healthcare (DE)
Difco™ Yeast Nitrogen Base w/o a.a	Becton Dickinson (DE)
Difco™ Yeast Nitrogen Base w/o a.a & ammonium sulphate	Becton Dickinson (DE)
Drop-Out Mix Synthetic w/o Ade, Arg, His, Leu, Met, Trp, Ura & Yeast Nitrogen Base	USBiological (USA)
Frema Reform Instant Skim Milk Powder	Granovita (DE)
Gravity Flow Strep-Tactin® Sepherose® Column (1 ml)	IBA Lifesciences (DE)
GST-HiTrap® Column (5 ml)	Sigma Aldrich (DE)
Herring Sperm DNA	Promega (DE)
Hygromycin B Solution	Carl Roth GmbH (DE)

Invitrogen™ Molecular Probes™ FM4-64 Dye	Thermo Fisher Scientific (DE)
Nourseothricin-dihydrogen sulphate / clonNAT powder	Werner BioAgents (DE)
Ponceau S	Serva Electrophoresis GmbH (DE)
Precision Plus Protein™ All Blue Prestained Protein Standard	Bio-Rad (DE)
Purple Gel Loading Dye (6x)	New England Biolabs (DE)
SEC 16/600 SuperDex 75 pg	Sigma Aldrich (DE)
SnakeSkin™ Dialysis Tubing 7,000 MWCO	Thermo Fisher Scientific (DE)
Strep-Tactin® Spin Column	IBA Lifesciences (DE)
Rapamycin	LC Laboratories (USA)
Roti® GelStain 1 ml	Carl Roth GmbH (DE)
TriDye™ 1 kb DNA Ladder	New England Biolabs (DE)
Thrombin Protease	Merck Millipore (USA)

3.2 Methods

3.2.1 Cultivation Conditions

Saccharomyces Cerevisiae strains were cultivated under nutrient-rich conditions in a yeast peptone dextrose (YPD) medium. Complete minimal (CM) medium, supplemented with the appropriate amino acids, was used to select auxotrophic markers. Cultures were grown at 30°C and shaking at 220 rpm. Precultures were inoculated using a sterile toothpick from an agar plate and were incubated overnight until stationary phase was reached. Cell density was measured using a photometer OD_{600}. Precultures were used to inoculate main cultures to the targeted growth phase. Strains were stored for six weeks on agar plates at 4°C with the correct selection. Cryo-stocks were used for long term storage of yeast cells, freezing stationary cells to -80°C in an appropriate medium containing 15% (v/v) glycerol.

E. coli strains XL1-Blue and BL21 was used for molecular biological methods. Cultures were grown in liquid lysogeny broth (LB) medium or on LB agar plates, supplemented with

ampicillin (Amp). Cultures were grown at 37°C while shaking at 220 rpm overnight. For the selection of plasmid positive clones, each clone was patched onto a fresh LB_{AMP} plate and incubated at 37°C. Strains were stored at 4°C on LB_{Amp} plates for up to 6 weeks for short term storage. Cryo-stocks were used for long term storage in LB_{Amp} containing 30% (v/v) glycerol and stored at -80°C.

3.2.2 Sporulation

Diploid cells were grown in a preculture containing a selective CM medium appropriate for plasmid selection and incubated at 30°C overnight. Cells were harvested at 2,000 rpm for 5 min and washed with 1% potassium acetate. Once cleaned, the pellet was resuspended in sporulation medium and incubated at 30°C for 3-5 days. Cells were stained with calcofluor white 30 mins before visualisation using the DeltaVision®.

3.2.3 Chromosomal DNA Isolation from Yeast

DNA isolation from yeast cells was done using the NucleoSpin® Microbial DNA Kit (Macherey-Nagel). A 5 ml culture was grown overnight at 30°C, and 2 ml was harvested by centrifugation, 13,200 rpm for 1 min, and processed according to the manufacturer's instructions. The concentration of isolated DNA was measured using the NanoVue™ UV/Visible spectrophotometer.

3.2.4 Isolation of Plasmid DNA from *E.coli*

E. coli cultivated with plasmids were grown overnight in a 5 ml culture. Plasmids were isolated using the Wizard® Plus SV Miniprep System (Promega). 5 ml were harvested by centrifugation, 5,000 rpm for 5 min, and processed according to the manufacturer's instructions. The concentration of isolated plasmids was measured using the NanoVue™ UV/Visible spectrophotometer.

3.2.5 Polymerase Chain Reaction (PCR)

Polymerase Chain Reaction was used to amplify fragments of DNA using oligonucleotide primers that flank the target sequence. KOD Hot Start DNA Polymerase was used to generate

target DNA fragments for transformation or genomic integration, and DreamTaq™ Polymerase was used for control PCRs to verify modifications to the genome. All PCRs were performed on the MasterCycler® and following the manufacturer's instructions based on amplicon length and primer specifications.

3.2.6 Agarose Gel Electrophoresis

Separation of specific DNA fragments for analysis or isolation was performed using gel electrophoresis. 0.8% (w/v) agarose gels were used with the addition of 1% RotiStain to make the DNA visible under UV light. DNA samples were mixed with 6 x Purple Gel Loading Dye (NEB) and loaded with TriDye™ 1 kb DNA ladder (NEB) as a size marker. Electrophoresis was run at 110 V for 25 min. A UV transilluminator was used to visualise and photograph the DNA bands. Gel extraction was performed on fragments of interest using the QIAquick® Gel Extraction Kit for agarose gels. Excised agarose gel was processed in accordance with the manufacturer's instructions.

3.2.7 Molecular Cloning

All plasmids created in this study are listed in Table 3-11. Specifically generated oligonucleotides were synthesised up- and downstream of the ORF in combination with DNA from WCG wildtype strain. Oligonucleotides contained overhangs with sequences appropriate for cutting with selected restriction enzymes according to [269]. PCR products were validated by size using DNA electrophoresis and purified using the QIAquick® Gel Extraction Kit. Approximately 10 µg of PCR product and target plasmid were digested with restriction enzymes according to the manufacturer's protocol. To inhibit the ligation of the vector, 1 µl CIP was included in the vector setup. The insert and vector concentrations were measured to determine the correct volumes for a 5:1 ratio, respectively. T4 DNA ligase was used to perform the ligation according to the manufacturer's protocol [270]. Chemically competent XL1-Blue cells were transformed with the ligation reaction. All cloned plasmids were verified by sequencing.

3.2.8 Restriction of DNA

Restriction digestion of DNA for cloning or validation of constructs was performed using restriction endonucleases and buffers from NEB. If available, the High-Fidelity versions of the enzymes were used. All restriction digestions were performed according to the manufacturer's protocol.

3.2.9 Sequencing of DNA

All constructs were verified via sequencing performed by Microsynth AG (Balgach, Switzerland). Samples containing 1,000 ng of purified DNA and 30 pmol of specific oligonucleotide primers were sent for evaluation. SnapGene® was used to check the sequencing data and the validity of the constructs.

3.2.10 Transformation of *E.coli*

Aliquots of XL1-Blue cells were thawed on ice for 20 min. 50 µl of XL1-Blue cells were used per transformation. 10 µl of plasmid DNA or ligation mix was incubated with the cells while on ice for 30 mins. Cells were then heat shocked for 40 seconds at 42°C in a water bath before being placed back on the ice for 2 mins. 450 µl SOC medium was added to the cells and incubated at 37°C for 1 hr while shaking. Cells were pelleted at 2,000 rpm for 5 min and then plated onto LB_{Amp} agar plates with appropriate antibiotics. Plates were left to grow overnight at 37°C. Clones were used to inoculate 5 ml LB-Amp so that plasmids could be isolated and tested for the correct transformation.

3.2.11 Transformation of Yeast

Two different methods were used to introduce DNA into yeast cells. Transforming yeast cells with plasmid DNA was done using a 'quick & dirty' method. 300 µl of PEG in LiTE buffer, 10 µl herring sperm DNA and 5 µl of the selected plasmid. Yeast cells were added using a sterile toothpick directly from the agar plate. The reaction was incubated at 30°C for 30 min, followed by 42°C for 15 min. Cells were pelleted, 2,000 rpm for 5 min, resuspended in 50 µl sterile ddH_2O and plated on CM plates with the appropriate selection. Plates were incubated at 30°C for three days for colonies to grow.

Transforming yeast cells with chromosomal DNA for homologous recombination requires high transformation efficiency. Cells were grown to log-phase in 50 ml YPD and harvested at 2,000 rpm for 5 min. The pellet was mixed and washed twice with sterile ddH_2O, followed by once with LiOAc-Sorb buffer. The pellet was resuspended in 50-250 µl LiOAc-Sorb and incubated at 30°C for 15 min. Transformation reactions were done in 50 µl aliquots with 300 µl PEG in LiTE buffer, 10 µl herring sperm DNA and 10 µl of the chromosomal DNA. The reaction was mixed and incubated at 30°C for 30 min, followed by 42°C for 15 min. Cells were pelleted, 2,000 rpm for 5 min, and resuspended in 2 ml YPD for regeneration at 30°C for 3 hrs shaking at 220 rpm. Cells were pelleted, 2,000 rpm for 5 min, and resuspended in 50 µl ddH_2O before being plated onto the appropriate selection plate. Plates were incubated at 30°C for three days before clones were patched onto a fresh selection plate and incubated at 30°C overnight. 5 ml YPD was inoculated with the clones for chromosomal isolation and verification via PCR or sequencing.

3.2.12 Alkaline Lysis

Between 2-10 OD_{600} yeast cells were harvested, 5,000 rpm for 5 min, resuspended in 1 ml Alkaline Lysis Buffer and incubated on ice for 10 min. The sample was occasionally vortexed throughout the experiment. 150 µl 50% TCA was added, and samples were incubated for a further 10 min on ice. Precipitated proteins were then pelleted at 12,700 rpm for 10 min at 4°C and washed twice with -20°C Acetone. Pellets were then dried at 37°C to remove all remaining acetone within the sample. Pellet was resuspended in 50-100 µl 2 x Lämmli buffer and agitated at 30°C for 30 min.

3.2.13 SDS-PAGE

SDS-PAGE was performed according to [271]. Protein samples were prepared by the addition of 2 x Lämmli buffer and denaturation at 95°C for 5 min, followed by vortex and 12,700 rpm for 1 min. Sample volumes of 10-20 µl were loaded to a 10-15% SDS gel with 10 µl of Precision Plus Protein™ All Blue prestained protein standard. The SDS gel was run in a Mini-PROTEAN® Tetra Vertical electrophoresis cell at a constant 150 V for 90 min, or until the blue running line was leaving the bottom of the gel. Once finished, the gel was either stained with Coomassie Brilliant Blue or Silver Nitrate Staining or used for immunoblotting.

3.2.14 pApe1 Maturation

To monitor bulk unselective autophagy, cultures were starved of nitrogen for up to 6 hr. The main culture of yeast was harvested at 2,000 rpm for 5 min and washed with SD-N. The pellet was resuspended in 2 ml SD-N and incubated at 30°C, shaking at 220 rpm. 2 OD_{600} samples were taken at 0, 2, and 4 hrs, cells were harvested and processed following the Alkaline Lysis protocol. Both premature and mature Ape1 was detected using the anti-Ape1 antibody.

3.2.15 Amphotericin B1 Treatment

To monitor the novel alternative autophagy GOMED, GFP-pho8Δ60 expressing stationary phase SEY 6210 cultures were treated with 1-25 µg/ml of Amphotericin B1, antifungal drug. 10 OD_{600} samples were taken at 0 and 24 hrs, cell were harvested and processed following the Alkaline lysis protocol. GFP-pho8Δ60 was detected using the GFP antibody. Initial protocol was obtained from Yamaguchi *et al.,* 2020.

3.2.16 Immunoblotting

Protein was transferred from SDS gel to PVDF membrane via a Mini Trans-Blot® cell. PVDF membrane requires activation in ethanol and sandwiched with the SDS gel between blotting paper soaked in blotting buffer. Proteins were transferred at 75 mA per SDS gel at 4°C for 10 hrs. The PVDF membrane was then saturated in a blocking solution containing 10% (w/v) skim milk powder in 1 x TBST at room temperature for 1 hr. The PVDF membrane was washed three times for 5 min with TBST. Subsequently, the primary antibody was added and incubated at room temperature for 3 hrs or 4°C overnight. The PVDF membrane was washed once again with TBST before the addition of the secondary antibody and incubated for a further 1 hr at room temperature. The excess antibody was washed off with TBST before Pierce™ ECL Plus Western-Blotting Substrate was used to treat the PVDF membrane according to the manufacturer's protocol. PVDF membranes were developed using the LAS-3000 and quantified using Fiji [256]. To strip the PVDF membranes of bound antibodies, 10% (v/v) acetic acid was used for 10 mins; this meant that the membrane could be redecorated with a different antibody.

3.2.17 Coomassie Brilliant Blue Staining

All steps were done at room temperature and under constant shaking according to [272], [273]. First, the proteins were fixed within the SDS gel by incubating the gel for 1 hr in Fixing Solution I. The SDS gel was then transferred to Fixing Solution II for 2 hrs. The Staining Solution was used overnight to maximise the staining of the unspecific proteins within the gel. The gel was then destained for 1 hr in Destaining Solution before further destaining in ddH_2O for 24 hrs. Once good contrast between protein bands and background was obtained, the gel was scanned using the Epson Scanner.

3.2.18 Silver Nitrate Staining

First, the proteins were fixed within the SDS gel by incubation with Silver Nitrate Fixing Solution at room temperature for 1 hr or 4°C overnight. The gel was then washed twice with Washing Solution, 30% (v/v) ethanol, at room temperature for 20 mins. The gel was transferred to a solution containing 0.8 mM Thiosulphate for 1 min before being washed three times with ddH_2O. The gel was incubated in Silver Nitrate Staining Solution at room temperature for 1 hr, followed by three quick washes with ddH_2O. The gel was moved to 4°C to slow down the subsequent reaction. The gel was incubated in 283 mM Sodium Carbonate with 0.02% (v/v) Formaldehyde until bands were seen, at which point this solution was poured off, and the reaction was stopped with a 5% (v/v) acetic acid solution for 10 min. The gel was then washed with ddH_2O three times before being scanned on the Epson Scanner.

3.2.19 Split Ubiquitin System

The split-ubiquitin system was used to determine protein-protein interactions *in vivo*. This technique requires the reassembly of the C-terminal, C_{ub}, and the N-terminal, N_{ub}, half of the ubiquitin. Tagging your bait protein with one half of ubiquitin and the protein of interest with the other half, if these two proteins come into close proximity, then ubiquitin will reassemble. The promotors for each half of ubiquitin differ, while N_{ub} contains a *CUP1* promotor C_{ub} contains a *MET25* promotor. Yeast strain SEY 6210 were transformed with the respective halves of ubiquitin tagged to specific proteins. The preculture in the selection medium without histidine and tryptophan was used to maintain the strains and their plasmids. A cell density of 1 OD_{600} per ml was used for the dilution series. A dilution series from 1:10 to

1:10,000 was prepared in sterile ddH_2O. 4 µl from each dilution were dropped onto three different agar plates:

The first plate served as a growth control and consisted of selective CM medium without His and Trp. The second plate was used for negative interactions and consisted of selective CM medium without Histidine, Tryptophan and Uracil but with the addition of 250 µM methionine and 100 µM copper sulphate. The third plate was for positive interactions and consisted of selective CM medium without His and Tryptophan supplemented with 1 mg/ml 5-fluoroorotic acid, 250 µM methionine and 100 µM copper sulphate.

After the dilutions were dropped onto the three plates, they were incubated at 30°C for three days. The plates were scanned at the Epson Scanner on days two and three.

3.2.20 Proteomics Analysis

Proteomic analysis was carried out to look at the changes between wildtype and *hsv2Δ.* Cells were grown to stationary phase in YPD medium before being starved in SD-N. 4 OD_{600} cells were harvested at 8 and 24 hrs, 5,000 rpm for 5 min, followed by lysis of the cells with Alkaline lysis buffer. The protocol is the same as 3.2.13, but the dried pellets were resuspended in SDS loading buffer without bromophenol blue and agitated at 30°C for 30 min. The samples were then centrifuged at 13,000 rpm for 10 min, and the top 50 µl of the supernatant was transferred to a low binding Eppendorf before freezing in liquid nitrogen and storing at -80°C. These samples were further handled by Prof. Dr Henning Urlaub's group for proteomic analysis.

3.2.21 Co-Immunoprecipitation

Miltenyi Biotec's µMACS System was used for co-immunoprecipitation. This system uses superparamagnetic microbeads conjugated to monoclonal antibodies against specific tags, GFP, HA, MyC and GST. This allows for proteins of interest to be isolated within the magnetic field. The bait proteins were tagged with GFP, and the prey proteins were tagged with 3x/6xHA. The manufacturer's protocol was followed, but the buffers used were modified according to the proteins being isolated.

Precultures were grown to ensure the target growth phase, OD_{600} of 2-3, was reached for the main culture. Main cultures consisted of 100-150 ml of selective medium. 200-250 OD_{600} cells were harvested, 2,000 rpm at 4°C for 5 min before being washed twice with cold 50 mM Tris/HCl pH 7.5. The pellet was resuspended in 750 µl GFP TRAP lysis buffer, 400 µl glass beads were added to lyse the cell walls, and the cells were harshly agitated at 4°C for 30 min. Cell debris was removed via centrifugation, 10,000 x g at 4°C for 10 min, and the supernatant was transferred to a fresh Eppendorf. 25 µl of the supernatant was taken as the 'INPUT' and mixed with 25 µl 2x Lämmli buffer, and samples were boiled at 95°C for 5 min. The remaining supernatant was incubated with 50 µl µMACS anti-GFP microbeads on ice for 30 min. The gravity columns containing magnetic beads provided by Miltenyi Biotec were equilibrated with 500 µl GFP TRAP lysis buffer before the supernatant was loaded onto the column. Columns were washed with GFP TRAP lysis buffer twice and once with 50 mM Tris/HCl pH 7.5 before proteins were eluted. Elution was done in two steps: first, 2x Lämmli buffer was heated to 95°C, and 20 µl was added to the column; after 5 min, a further 50 µl was added to elute the proteins off the column. The addition of SDS to both the lysis buffer and washing buffers was changed depending on the protein on interest and whether transmembrane domains were present.

3.2.22 Atg8 Purification

A culture of BL21 cells expressing GST-Atg8 were incubated in $LB_{Amp/CM}$ medium at 30°C overnight. 2.0 L $LB_{Amp/CM}$ medium was inoculated to an OD_{600} of 0.2 and incubated at 30°C for 90 min. The culture was induced with 100 mM PMSF and 0.2 mM IPTG and incubated at 30°C for a further 5 hrs. Cells were harvested at 5,000 rpm for 10 min, the supernatant was discarded, and the pellets were frozen in liquid nitrogen and stored at -80°C.

For each gram of pellet, 5 ml of Atg8 lysis buffer was used. The pellet was resuspended and kept on ice for 5 min before being transferred to a JA-20 tube, and the addition of 1% Triton X-100 was gently mixed in. Tubes were centrifuged at 14,000 rpm for 40 min at 4°C. The supernatant was transferred to a precooled 50 ml falcon. A 5 ml GSTrap™ HP column was attached to the Äkta system and equilibrated with 1 x PBS pH 7.4 before the crude cell lysate

was applied. The column was washed with 1 x PBS pH 7.4 and eluted with 10 mM reduced glutathione in 1 x PBS pH 8.0. The elution was poured into SnakeSkin™ dialysis tubing (7,000 MWCO) and dialysed against 1 x PBS and 1 mM DTT pH 7.4 overnight at 4°C to remove the reduced glutathione.

Contents were poured into a fresh 50 ml falcon and spun, 500 x g for 3 min, to remove any precipitated proteins. A_{280} measurement was done to calculate the concentration of GST-Atg8. Between the GST tag and the Atg8 protein was a Thrombin cleavage site, 100 units of Thrombin was used for every 10 mg of GST-Atg8 and incubated at 4°C for 24 hrs. A 50% slurry of glutathione sepharose 4B beads was made with 1 x PBS pH 7.4. 1 ml of 50% slurry was added per 10 mg GST-Atg8 and incubated at 4°C for 30 min on a roller. The glutathione sepharose 4B beads were pelleted at 500 x g for 3 min, and the supernatant was transferred to a fresh falcon. The glutathione sepharose 4B beads should bind all the free GST that has been cleaved by Thrombin. The beads were washed twice with 1 x PBS 1 mM DTT pH 7.4, and all solutions were pooled and concentrated to 10 ml using Amicon Ultra-15 Centrifugal Units with a 3,000 Dalton molecular weight cut off.

Size exclusion chromatography was used to clean the sample so that only Atg8 remains. The 16/600 SuperDex 75 pg was attached to the Äkta system and equilibrated with 1 x PBS pH 7.4 before the sample was loaded. Proteins were mainly eluted in 4 peaks; the first peak contained large molecular weight chaperones, the second peak contained the remaining GST tag that the glutathione sepharose 4B beads didn't bind, the third peak contained Atg8, and the final peak had very small molecular weight proteins.

All aliquots from the third peak were pooled and concentrated to 1 ml. A_{280} measurement was done again to determine the final concentration of isolated Atg8. The samples were then split into 70 µl aliquots and frozen in liquid nitrogen before being stored at -80°C. Throughout this purification process, samples were taken to ensure sample integrity.

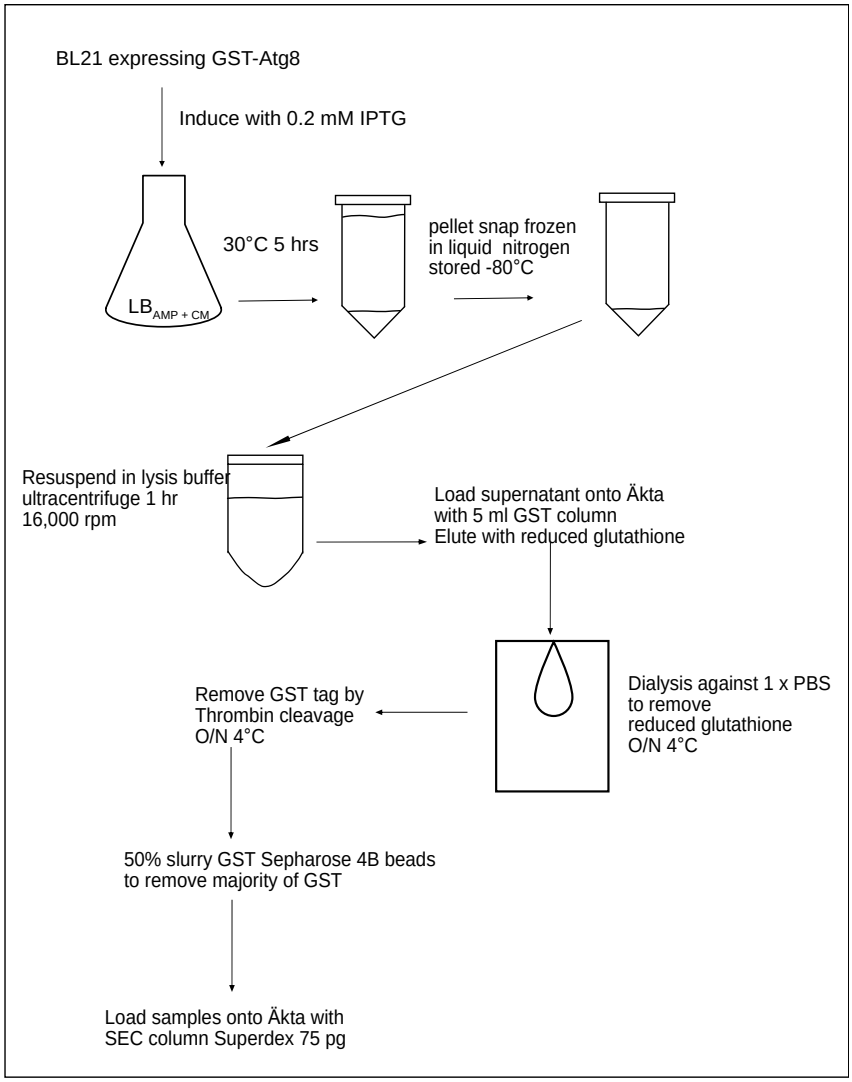

Figure 3-16: Work flow scheme for Atg8 purification in E. coli.

3.2.23 Protein Binding Assay

To determine the optimal conditions for Atg8 and Atg21 binding, three different buffers were tested: 1 x PBS pH 7.4, 50 mM Tris/HCl 1 mM EDTA and 30 mM HEPES 150 mM NaCl pH 7.5. A synthetic peptide of Atg21 (CEIVFPHEIVKVVMND(FAM)) was ordered from EMC containing the region hypothesised to be required for binding to Atg8. The peptides were bound to the fluorescent tag FAM in order to monitor the activity.

1 µM of the Atg21 peptide was incubated with 50 nM, 100 nM and 500 nM of Atg8 in a 96 well plate at room temperature for 5 min. The 96 well plate was loaded into the Victor Nivo multimode plate reader, where the quenching of the fluorescent signal was measured. Once the correct buffer was found, a full binding assay was done to determine the K_d value. This was done in the same format, but Atg8 concentrations went as low as 0.5 nM.

3.2.24 Dynamic Light Scattering

Dynamic light scattering was used to determine solution homology. After centrifugation at max speed for 10 min, 1 µl of the solution was transferred to a well containing liquid paraffin oil. The plate was loaded into Xtal Concepts SpectroLight 600, the settings were kept as default with 15 iterations for 20 seconds.

3.2.25 Crystallography

In order to try to get Atg8 to crystallise with the Atg21 active peptide, a 20 M excess of the active peptide was used with numerous crystallisation conditions. 30 mM HEPES 150 mM NaCl pH 7.5 was the buffer used for all conditions. 20 M excess of the active peptide was incubated with Atg8 at room temperature for 30 min before being plated onto a 12x96 well crystallisation plate.

Each well within the 12x96 well plate contains four separate wells as seen in Figure 3-2. The reservoir contains the screening conditions, which differs from well to well. The buffer contains 30 mM HEPES 150 mM NaCl pH 7.5. The 1:1 ratio well contains equal parts Atg8 with the active Atg21 peptide and screening condition within the reservoir. The 2:1 ratio well contains two parts Atg8 with the active Atg21 peptide and one part screening condition from the reservoir.

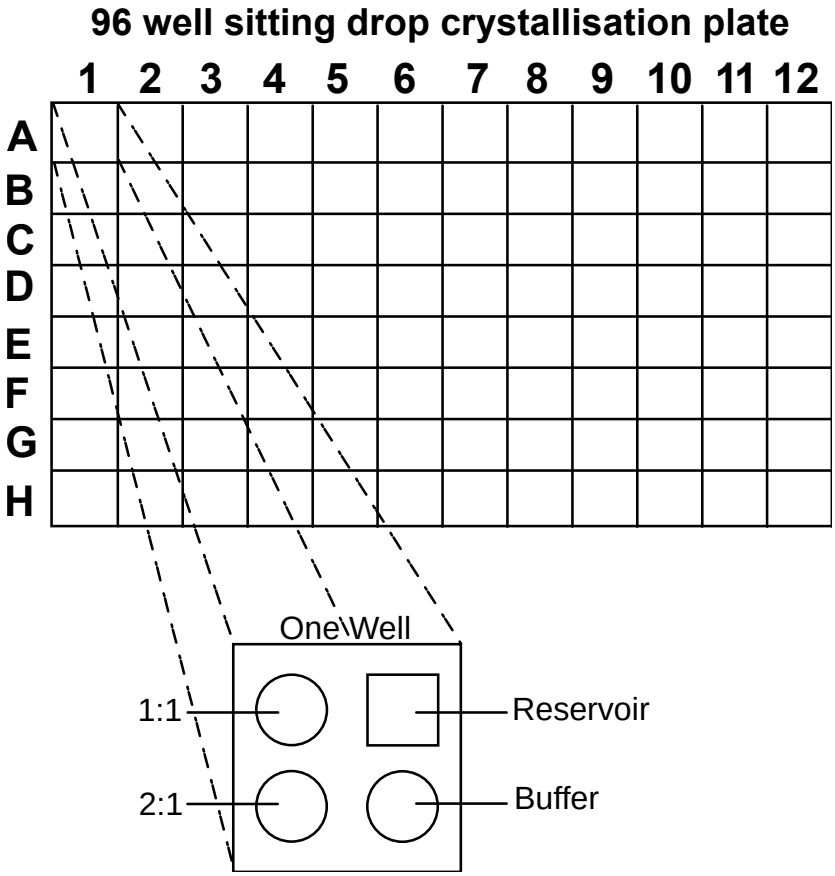

Figure 3-17: 96 well crystallisation plate for crystallisation trials with a magnified well.

The screening conditions used were Midas, Nuc Pro, Pact^{++}, Midas dilution, JB6, JB1, JCSG, Pro Plex, $AmSO_4$, Natrix, Morpheus and PGA. Once all the solutions have been pipetted into the wells, the plate is sealed with a clear plastic sheet and stored at room temperature. Conditions were checked every six weeks under a microscope for crystal growth.

3.2.26 DeltaVision®

For monitoring live cell activity, fluorescence microscopy was used. 6 µl of yeast culture was dropped onto a microscope slide and fixed with a coverslip. DeltaVision® immersion oil was applied to the coverslip for a better connection between the objective and the microscope slide. The DeltaVision® setup included an inverted IX71 microscope, equipped with the UPlanSApo x 100,1.4 numerical aperture, an oil immersion objective and a CoolSNAP$_{HQ2}$™ couple-charged device camera. Images were captured with the 100 x objective and stacks along the z-axis of 24-30 images, separated by 0.2 µm. With the appropriate filter set, the sample could be excited and the emissions recorded. The differential interference contrast (DIC) images were either recorded at the centre of the stack or at every stack along the z-axis

by applying the transmitted light source. Deconvolution of the images was processed by the softWoRx® software, any further evaluation was done using Fiji [256].

Table 3-17: Filter Sets for DeltaVision®

Filter Set	Excitation Wavelength	Emission Wavelength	Fluorophores
Blue	390/18 nm	435/48 nm	BFP, Calcofluor-White
Green	475/28 nm	525/50 nm	GFP, yeGFP
Red	575/25 nm	632/69 nm	mCherry, RFP, FM4-64

3.2.27 Vacuolar Fragmentation

Vacuolar morphology was assessed using the DeltaVision®, cells were grown until log phase and stained with FM4-64 for 30 mins. Cells were harvested at 700 x g for 3 mins and split, half the cells were resuspended in YPD and the other half were resuspended in YPD + 0.4 M NaCl. Cells were incubated at 30°C for 1 hour before 5 µl were dropped on a cover slip and imaged using the DeltaVision®. For each condition 200 cells were imaged and analysed using Fiji.

3.2.28 Proximity-Dependent Biotin Identification (BioID) Assay

For studying the interactions between proteins, Opitz et al., 2017 came up with a proximity-dependent assay involving the promiscuous protein Biotin. Whereby proteins that have been biotinylated could be elucidated via mass spectrometry. A detailed protocol was provided by Dr Oliver Valerius and Dr Nadine Opitz and modified for our experimental approach by Dr Lena Munzel.

Three strains were used during this experiment: Myc-BirA*-Hsv2, BirA* alone and an empty plasmid. A preculture was made for each strain in a selective CM medium grown at 30°C overnight. A second preculture was used to introduce the SILAC amino acids; this culture was inoculated from the first preculture in a 1:100 dilution and grown at 30°C overnight. The main culture consisted of selective CM medium, SILAC amino acids and 10 µM Biotin and was inoculated from the second preculture and grown at 30°C overnight.

Between 200-300 OD_{600} were harvested per strain, 2,000 rpm at 4°C for 5 min, and washed with cold 10 mM HEPES pH 7.9. Pellets were resuspended in cold 10 mM HEPES pH 7.9 and pooled in a 1:1:1 ratio. The pooled culture was pelleted at 2,000 rpm at 4°C for 5 min and resuspended in BioID lysis buffer with 400 µl glass beads in low-binding Eppendorf. Cells were agitated at 4°C for 30 mins, 4% SDS was added, and the solution was inverted to mix before incubating at 65°C for 10 min. Reactions were centrifuged, 3,000 x g for 5 min, and the supernatants were pooled in a fresh Eppendorf.

Biotinylated proteins were isolated using 1 ml strep-tactin columns, which, before the cell lysate can be loaded, need to be equilibrated with 2 ml Buffer W and 0.4% SDS. After the cell lysate had run through the column, it was washed with 50 ml Buffer W and 0.4% SDS. Elution of the proteins from the column was done with 1 ml Buffer W and 10 mM Biotin; this was done three times with each elution collected in a separate low binding Eppendorf.

Proteins were then precipitated using 10% TCA on ice for 30 min, followed by centrifugation at 13,200 rpm at 4°C for 10 min. Pellets were washed twice with -20°C acetone, and the pellet was left to dry at 37°C. Each pellet was resuspended in 10 µl 2 x Lämmli and agitated at 30°C for 30 min before being loaded on a 10% SDS gel. The SDS gel was only run for a short time until the running line was 3-4 cm into the resolving gel; the gel was then stained with Coomassie Brilliant Blue staining compatible with mass spectrometry.

The stained gel was then handled by Olaf Bernhard (Department of Cellular Biochemistry, University Medical Centre Göttingen), where the gel was cut into 10 sections and digested with trypsin. The samples were then placed in a SpeedVac to remove all liquid and preserve the peptides for analysis via mass spectrometry.

3.2.29 Mass Spectrometry

Liquid chromatography-mass spectrometry analysis was performed by Dr Oliver Valerius and Dr Kerstin Schmitt (Department of Molecular Microbiology and Genetics, Georg-August-University Göttingen). The dried peptides were resuspended in fresh LC-MS sample buffer

and incubated for 3 min in an ultrasonic bath before being measured with a Q exactive™ HF Hybrid Quadrupole-Orbitrap™ mass spectrometer (Thermo Fisher Scientific).

Quantification of mass spectrometry results was performed using MaxQuant 1.5.1.0 and further processed using Perseus software. A second software, Proteome Discoverer™ 2.2, was also used to identify candidates. All parameters were set according to Opitz el al., 2017, and the SequestHT and Mascot algorithms were used for database searching against the SGD database for *S. cerevisiae* (SGD, 6110 entries, including common contaminants, S288C_ORF_database release version 2011, Stanford University).

3.2.30 Statistics

All evaluation and plotting of data were done using GraphPad Prism®; unless stated otherwise. Graphs were plotted using the mean value of data together with the standard error of the mean as error bars. Asterisks indicate P-values: ns, not significant P>0.05.* for P<0.05. ** for P<0.01. *** for P<0.001. **** for P<0.0001.

4. Results

Despite being in the PROPPINs family, Hsv2 remains poorly understood, and its mechanisms of action are not well defined. Published data regarding Hsv2 are rare and few groups are actively working with the protein. Homologues of Hsv2, Atg18 and Atg21, play crucial roles in autophagy and Hsv2 could have a similar function. To elucidate the molecular function of Hsv2, proximity-dependent assays such as the BioID and split ubiquitin assays were used to determine potential interaction partners. Additionally, a proteomic analysis was used to establish which proteins were affected by the absence of Hsv2. Furthermore, monitoring the maturation of Ape1 is an excellent way to measure the Cvt pathway or bulk degradation activity depending on the conditions used. Starving the cells of nitrogen causes unselective autophagy, whereas nutrient-rich conditions allow for selective autophagy.

4.1.1 Ape1 Maturation

To better understand the function of Hsv2, various deletion strains were made to see the effects on Ape1 maturation. Vacuolar aminopeptidase 1 accumulates in the cytosol before being transported to the vacuole via a selective autophagic process named the Cvt pathway [275]. Once in the vacuole, the protein is processed from an inactive precursor, preApe1, to an active mature form, mApe1, which can be seen by a shift in size after immunoblotting. Cells were grown to an OD_{600} of 4, starved in SD-N for up to 4 hrs and lysed with alkaline lysis buffer (see Figure 4-1).

Various deletion strains were generated to determine the effect of Hsv2 on autophagy. The single deletions of Atg18 and Atg21 were used to determine if the assay functions as expected, as the functions of these proteins is already known. The double deletions *hsv2Δatg18Δ* and *hsv2Δatg21Δ* were generated to see if there is an epistatic effect of knocking out multiple PROPPINs. Finally, the triple deletion *hsv2Δatg21Δatg18Δ* was developed to determine if the complete absence of PROPPINs had any additional impact on autophagic activity.

Most of the deletion strains showed a significant deficit in the maturation of Ape1. *atg1Δ* strain was included as a negative control, as Atg1 is crucial to autophagy, and without it,

preApe1 cannot be processed. *hsv2Δ* cells processed preApe1 at the same rate as wildtype for all time points; suggesting that Hsv2 is not involved in the Cvt pathway. *atg21Δ* cells at 0 hrs had a significant reduction in mature Ape1; it is well established that Atg21 is crucial for selective autophagy [263]. Although, after 2 hrs, this reduction had disappeared due to the switch from selective to bulk autophagy in which Atg21 is no longer required, so maturation of preApe1 returned to wildtype levels. *atg18Δ* cells caused a significant reduction in processed Ape1 for all time points. This was to be expected as Atg18 is crucial for all autophagic activity.

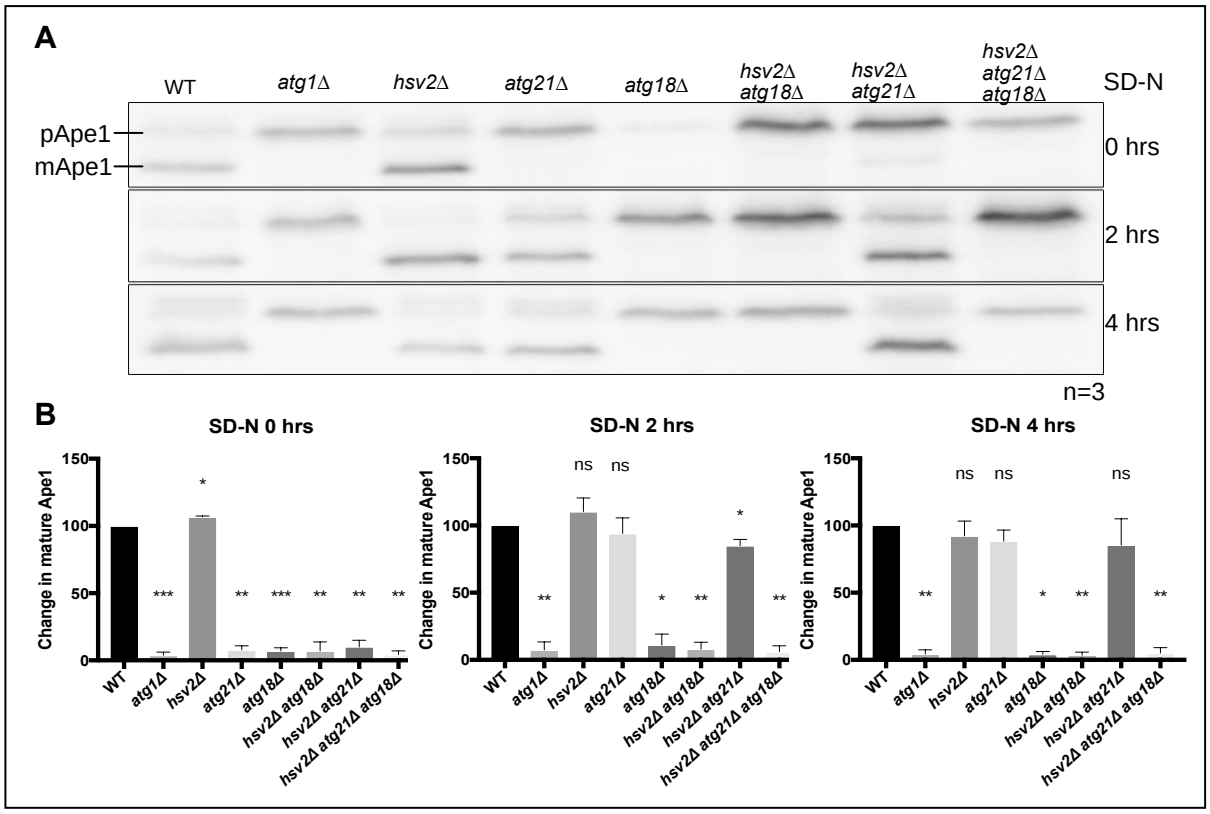

Figure 4-18: Preliminary experiments to determine Hsv2 role in autophagy.

(A) Ape1 assay to determine the effect on preApe1 maturation. Constructs were grown to OD_{600} 4, starved in SD-N and harvested, followed by alkaline lysis. Cell extracts were run on SDS gels, blotted and decorated with Ape1 antibody. (B) The quantification of the ratio between mApe1 to total Ape1 was measured in Western-Blot analysis of three independent experiments and was performed using FIJI and GraphPad Prism. WT ratios were set to 100%. Asterisks indicate P-values: ns, not significant P>0.05. for P<0.05. ** for P<0.01. *** for P<0.001. **** for P<0.0001.*

The double deletion *hsv2Δatg18Δ* resulted in similar levels of matured Ape1 as *atg18Δ* alone. This is to be expected as Atg18 is required for all autophagy activity. *hsv2Δatg21Δ* cells had reduced autophagic activity at 0 hrs but to the same degree as *atg21Δ*. As Atg21 is necessary for the Cvt pathway under nutrient rich conditions it was expected that the absence of Hsv2 caused no additional effect on the maturation of Ape1. At 2 hrs, the double deletion still

causes a reduction in autophagic activity, which was not present in the *atg21Δ* strain alone. However, at 4 hrs, the autophagic activity has returned to wildtype levels as during starvation induced autophagy Atg18 is required for the maturation of Ape1 and not Atg21. The triple deletion showed significant reductions in autophagic activity for all time points, which is not surprising since *atg18Δ* cells already showed a defect in preApe1 processing. These results suggest that Hsv2 is not required for the autophagic processing of preApe1, but in the event that Atg21 is absent, then Hsv2 could partially substitute in.

4.1.2 GOMED

In order to investigate the role of Hsv2 in GOMED as described by Yamaguchi *et al.* 2020 we first tried to reproduce their results. In a *atg5Δhsv2Δ* strain a defect was observed in the processing of GFP-pho8Δ60 compared to a *atg5Δ* strain when treated with AmB. Using the SEY 6210 background *atg5Δ* and *atg5Δhsv2Δ* strains were generated. Strains were cultivated in nutrient rich conditions and treated with 10 µg/ml AmB for 24 hrs. This assay utilises a genetically engineered version of Pho8 that lacks the N-terminal transmembrane domain. Thus, pho8Δ60 remains in the cytosol and is delivered to the vacuole through nonspecific autophagy. Using a *atg5Δ* strain allows us to block autophagy and therefore access GOMED activity.

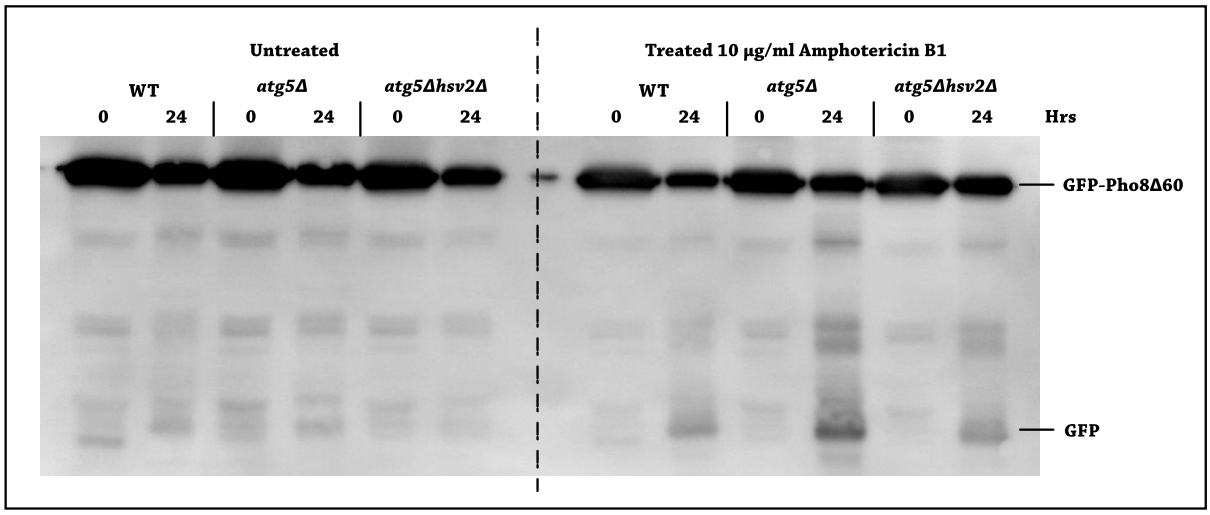

Figure 4-19: Hsv2 involvement in GOMED.

GFP-pho8Δ60 expressing WT, atg5Δ and atg5Δhsv2Δ cells were treated with or without Amphotericin B1 (10 µg/ml for 24 hrs)

Unexpectedly, these results contradict the results observed by Yamaguchi *et al.* 2020. Less GFP-pho8Δ60 is processed in the *atg5Δhsv2Δ* strain compared to *atg5Δ* strain. However, it was reported that this process is completely blocked in the double deletion. Different concentrations of AmB (1-25 µg/ml) were used to treat the cells but this did not affect the processing of GFP-pho8Δ60 in the double deletion strain as free GFP was always observed. The reasons why the results are not reproducible is still to be determined.

4.1.3 Split Ubiquitin System

The split ubiquitin assay is based on the *in vivo* reassembly of ubiquitin. Each half of ubiquitin is fused to the proteins of interest, with the C-terminal (C_{ub}) tagged to the 'bait', and the N-terminal (N_{ub}) tagged to the 'prey'. If the proteins directly interact or come within close proximity to one another, the two halves of ubiquitin are able to interact, forming a quasi-native ubiquitin [276].

A Ura3 protein with an additional N-terminal arginine is attached to the C-terminus of the C_{ub} fragment. Ura3 catalyses an important step in the synthesis of Uracil. In a *ura3* defective strain, the expression of Ura3 restores their growth on a medium lacking uracil. Also, Ura3 converts the nontoxic 5-FOA into the toxic 5-fluorouracil. The functions of Ura3 allow us to use both positive and negative readouts for protein interaction in the split ubiquitin system [277].

Once recombined, the quasi-native ubiquitin can be recognised by specific ubiquitin proteases. These proteases cleave off the R-Ura3 that is attached to the C_{ub}; with the now exposed N-terminal arginine, rapid proteasomal degradation of the protein according to the N-end rule occurs. Therefore, these strains show uracil auxotrophy and are resistant to 5-FOA. The strains that show no interaction between proteins of interest can grow in a medium that does not contain any uracil but are sensitive to 5-FOA [277].

Using the split ubiquitin system, Hsv2-C_{ub} was tested for its interaction with a library of both Atg and non-Atg proteins, as indicated in Figure 4-3 and Figure 4-4 respectively. As a positive control for interacting proteins, SEY 6210 WT strain expressing STE14-C_{ub} and N_{ub}-UBC6 was

used. As the interaction of these two proteins is known, this was used as an indicator of interaction strength when comparing the growth against the other strains.

SEY 6210 WT strain was transformed with the plasmid expressing Hsv2-C_{ub} and N_{ub}-Prey with the selection markers His and Trp, respectively. Hsv2-C_{ub} was expressed under the control of a *MET25* promotor, and N_{ub}-'prey' were expressed under the control of a *CUP1* promotor. Methionine and copper sulphate were not included in the growing medium and were only used on the selective medium plates at a concentration of 250 µM methionine and 100 µM $CuSO_4$.

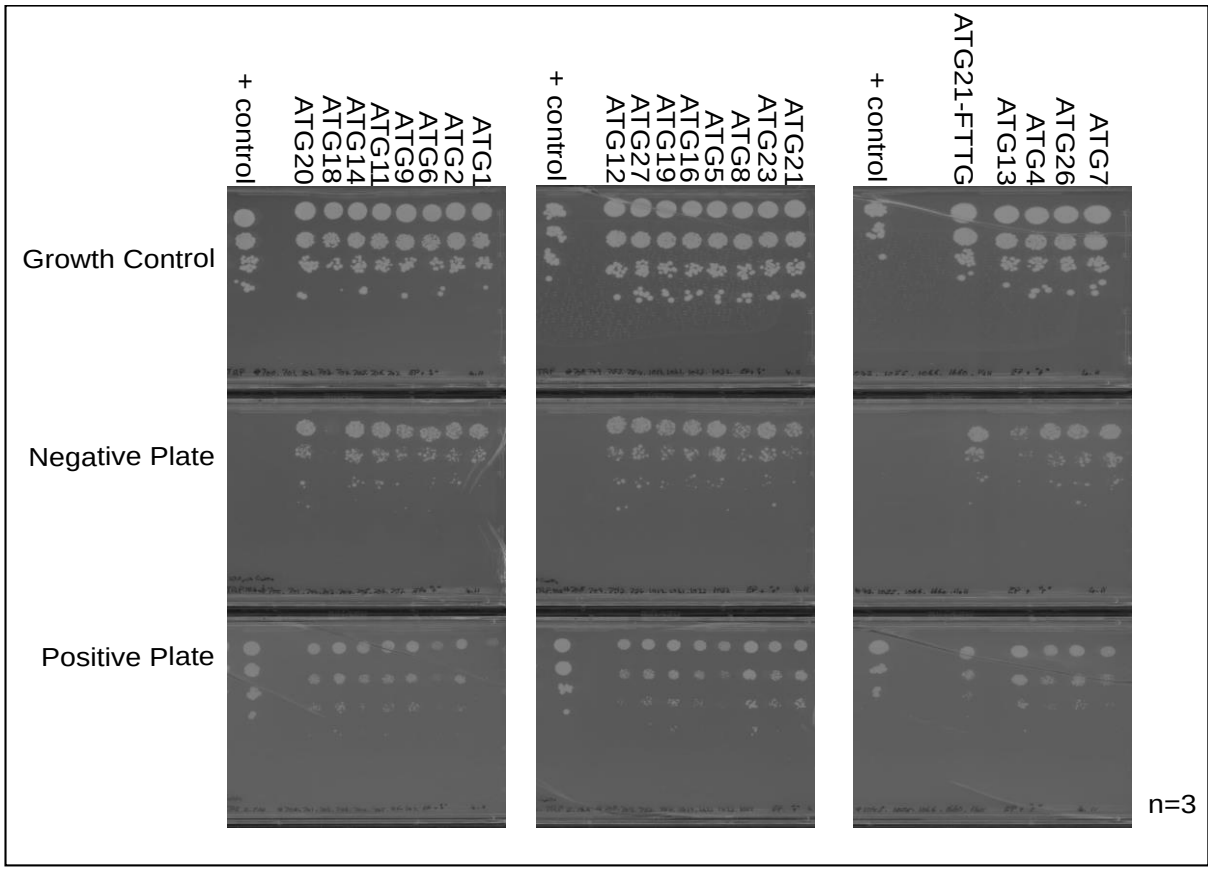

Figure 4-20: Examining the interaction of Hsv2 with Atg proteins in a split ubiquitin assay.

Hsv2-C_{ub} was used as bait, and all prey Atg constructs were tagged with N_{ub}. Each yeast preculture was dropped onto the CM-His-Trp plate (growth control), MV-His-Trp-Ura plate (growth indicates no interaction) and CM-His-Trp+5-FOA plate (growth indicates interaction). Images were taken five days after dropping, allowing for growth at 30°C. The positive control used was Ste14-C_{ub} + N_{ub}-Ubc6. All plates contained 250 µM methionine and 100 µM $CuSO_4$.

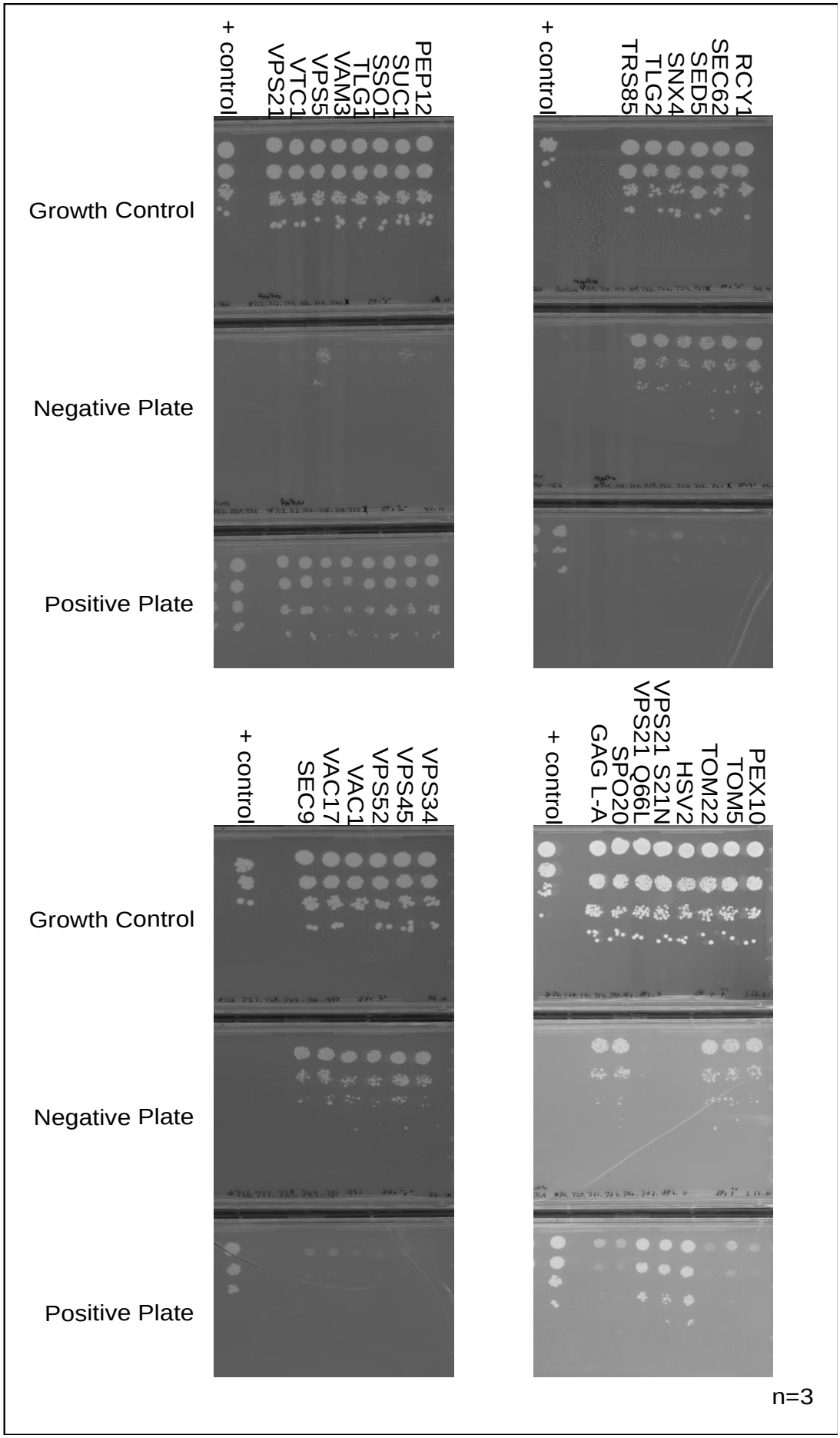
Growth Control
Negative Plate
Positive Plate
+ control
RCY1
SEC62
SED5
SNX4
TLG2
TRS85
+ control
PEP12
SUC1
SSO1
TLG1
VAM3
VPS5
VTC1
VPS21
+ control
PEX10
TOM5
TOM22
HSV2
VPS21 S21N
VPS21 Q66L
SPO20
GAG L-A
+ control
VPS34
VPS45
VPS52
VAC1
VAC17
SEC9
n=3

Figure 4-21: Examining the interaction of Hsv2 with non-Atg proteins in a split ubiquitin assay.

Hsv2-C_{ub} was used as bait, and all prey constructs were tagged with N_{ub}. Each yeast preculture was dropped onto the CM-His-Trp plate (growth control), MV-His-Trp-Ura plate (growth indicates no interaction) and CM-His-Trp+5-FOA plate (growth indicates interaction). Images were taken five days after dropping, allowing for growth at 30°C. The positive control used was Ste14-C_{ub} + N_{ub}-Ubc6. All plates contained 250 µM methionine and 100 µM $CuSO_4$.

In this shotgun approach, quite a few proteins interacting with Hsv2 were identified. The most substantial growth was seen for Vps21, Vtc1, Sso1, Pep12 and Hsv2 (See Table 4-1). It is known that PROPPINs interact with themselves, so the significant growth on the 5-FOA containing plate seen for Hsv2 was a suitable proof of concept. There was also a strong interaction with Atg18, Atg8 and Atg13. A slightly weaker interaction was seen with Atg21, Atg9 and Atg2. Interaction between members of the PROPPIN family detected with the split ubiquitin approach has been described before [169]. However, interaction with Atg9, Atg2 and Atg13 may suggest a role in the recycling of proteins.

After the split ubiquitin assays were analysed, each protein was ranked based on the growth at the different dilutions seen on the CM-His-Trp+5-FOA containing plate. For the non-Atg proteins, growth was mainly seen on one plate or the other depending on whether the proteins interact. Unfortunately, this was not the case for the Atg proteins, where a lot of growth is seen on both plates (see Figure 4-3). This was unexpected, as one of the main benefits of this assay was that the strains would either grow on the positive plate or the negative plate depending on protein interaction.

This made the Atg protein results more complicated to understand than the non-Atg proteins. This could potentially show close proximity to one another rather than direct interaction of the proteins. After repeating the experiment three times and no change to the growth patterns was seen, the evaluation of the growth was done at each dilution, seen in Table 4-1. If the strains were able to grow at the highest dilution on CM-His-Trp+5-FOA containing plates, then ++++ was given to the protein. If growth was seen at the third dilution then +++ was given to the protein. If there was growth at the first and second dilutions and weak growth at the third dilution then the protein was given ++. If there was growth at the first dilution and no growth in the rest of the dilution series then the protein was given +. Finally, if no growth was seen on the 5-FOA containing plate then the protein was given – to denote

no interaction.

Protein	Bait	Interaction Strength
Vps21	Hsv2	++++
Vtc1	Hsv2	++++
Sso1	Hsv2	++++
Pep12	Hsv2	++++
Hsv2	Hsv2	++++
Vps21 S21N	Hsv2	++++
Tlg1	Hsv2	+++
Snc1	Hsv2	+++
Vam3	Hsv2	+++
Vps21 Q66L	Hsv2	+++
Vps5	Hsv2	++
Snx4	Hsv2	+
Sec9	Hsv2	+
Vac17	Hsv2	+
Trs85	Hsv2	+
Tom5	Hsv2	+
Spo20	Hsv2	+
Vac1	Hsv2	-
Vps52	Hsv2	-
Vps45	Hsv2	-
Vps34	Hsv2	-
Vps15	Hsv2	-
Tlg2	Hsv2	-
Sed5	Hsv2	-
Sec62	Hsv2	-
Rcy1	Hsv2	-
Pex10	Hsv2	-
Tom22	Hsv2	-
GAG L-A	Hsv2	-
Atg18	Hsv2	++++
Atg8	Hsv2	++++
Atg13	Hsv2	++++
Atg2	Hsv2	+++
Atg9	Hsv2	+++
Atg21	Hsv2	+++
Atg11	Hsv2	++
Atg14	Hsv2	++
Atg20	Hsv2	++
Atg23	Hsv2	++
Atg19	Hsv2	++
Atg27	Hsv2	++
Atg26	Hsv2	++
Atg21-FTTG	Hsv2	+
Atg6	Hsv2	+
Atg16	Hsv2	+
Atg12	Hsv2	+
Atg7	Hsv2	+
Atg4	Hsv2	+
Atg1	Hsv2	-
Atg5	Hsv2	-

Table 4-18: Split Ubiquitin assay interaction strengths.

The split ubiquitin assay was repeated three times, and the growth was quantified by growth on both the CM-His-Trp+5-FOA and MV-His-Trp-Ura. The growth at each dilution was also taken into consideration. The interaction strength ranged from no interaction (-), only growth seen on MV-His-Trp-Ura, to full interaction (++++), growth at all dilutions on the CM-His-Trp+5-FOA.

These results suggest Hsv2 involvement in protein sorting and recycling and potentially involved in specific selective forms of autophagy. Further experimentation is required to determine the exact role of Hsv2 with these proteins of interest.

4.1.4 Mislocalisation of Pep12

Due to the strong interaction found with Vps21, Sso1 and Pep12, further investigation was done to see if these proteins were mislocalised in the absence of Hsv2. Green fluorescent protein (GFP) was tagged to the C-terminal of each protein and transformed into haploid and diploid wildtype and *hsv2Δ* strains. GFP is one of the best fluorophores for detection with a microscope and allow for the visualisation of proteins with a low abundance. GFP is also a very bright fluorophore that is highly resistant to photobleaching and non-toxic to the cells. The fusion of GFP to proteins very rarely alters their function and allows for observation in their natural state. Pep12-GFP was expressed under a constitutive *TPI* promotor, and Vps21-GFP and Sso1-GFP were expressed under *MET25* promotors. These promotors share a constant activity pattern ensuring consistent gene expression.

GFP can only be degraded slowly in the vacuole by resident proteases, and this can be used to determine autophagic activity. If a protein is not being correctly sorted or trafficked, then the GFP signal will accumulate in the vacuole as the protein has been missorted for degradation. Live-cell microscopy was performed under starvation conditions. Yeast cells were grown to a stationary phase and switched to a minimal synthetic media lacking nitrogen (SD-N) for up to 4 hrs before evaluation under the microscope.

Vps21-GFP and Sso1-GFP were not affected by the deletion of *HSV2* in either haploid or diploid cells (data not shown). However, Pep12-GFP was mislocalised in diploid hsv2Δ cells, as seen by the accumulation of GFP signal in the vacuole (Figure 4-5). Interestingly, Pep12-GFP in haploid *hsv2Δ* cells showed correct localisation suggesting that Hsv2 might have a different role in diploid cells compared to haploid cells. As these cells were starved of nitrogen, we initiated an autophagy response and not sporulation, implying that additional autophagic mechanisms could be at play in diploid cells compared to haploid cells.

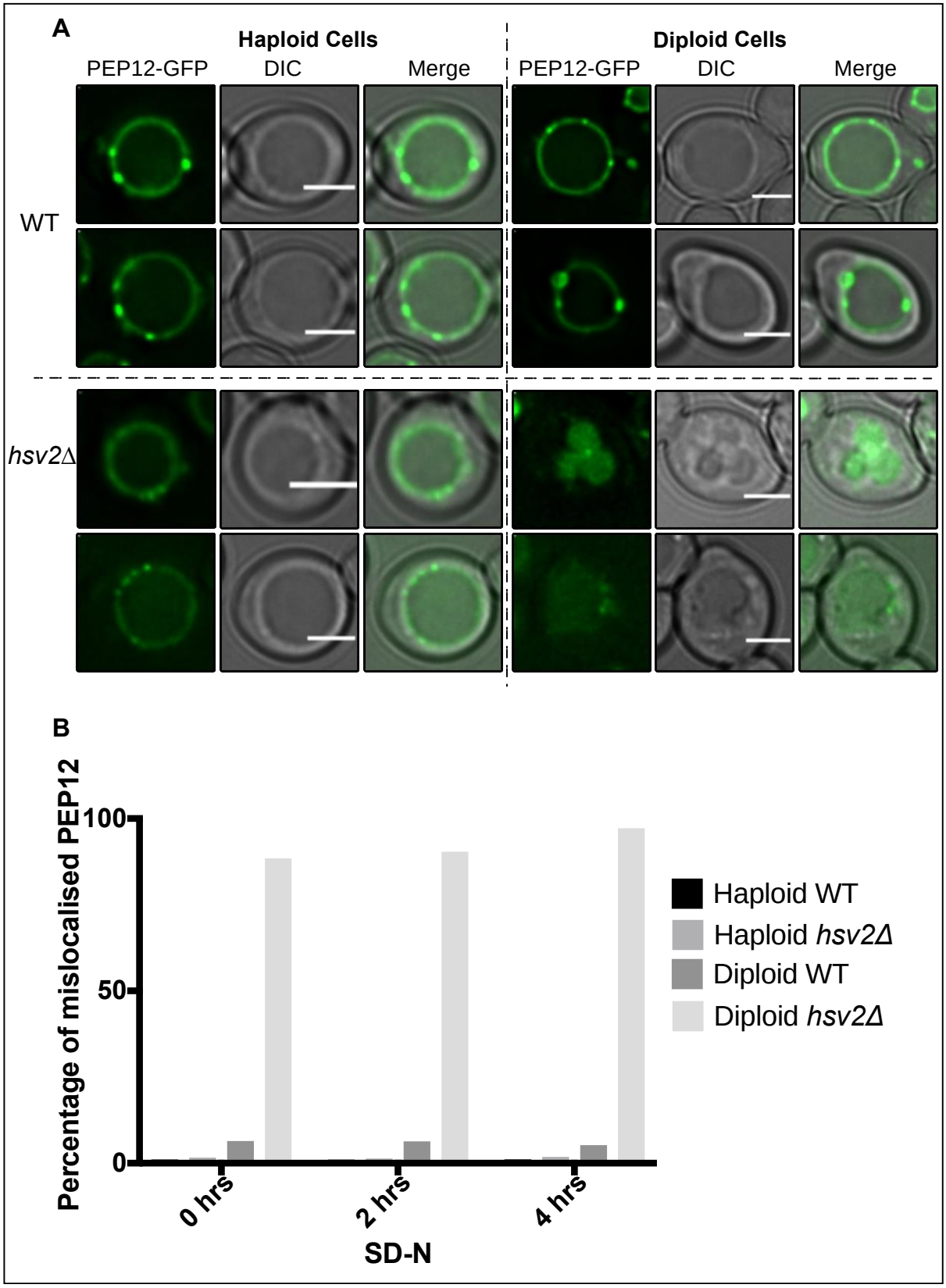

Figure 4-22: Localisation of Pep12 by fluorescence microscopy.

(A) Pep12-GFP localisation in wildtype and hsv2Δ haploid and diploid cells. A differential interference contrast (DIC) image is shown along with a merged overlay with GFP. (B) Bar graph depicting the percentage of cells showing a mislocalisation of Pep12-GFP. Scale bar = 2.5 µm. 100 cells were counted for each condition.

This is a fascinating discovery as it was previously thought that autophagy and transport systems functioned similar in haploid and diploid cells. This suggests that Hsv2 potentially has a more functional role in diploid cells than in haploid cells. It would be interesting to repeat this experiment but under sporulation conditions rather than starvation conditions.

4.1.5 Proteomics Analysis of WT vs *hsv2Δ*

In order to better understand the function of Hsv2 and uncover potential cargoes, a different approach was performed. In collaboration with Henning Urlaub's group, we did a proteomic analysis of *hsv2Δ* cells compared to wildtype. In this method, cells from *hsv2Δ* and wildtype cells were lysed and labelled with stable isotope reagents before mass spectrometry analysis. The expression levels of cargo proteins are often affected by the presence or absence of their respective transport or degradation systems. Therefore, the expression patterns of potential cargo proteins in cells depleted of Hsv2 compared to wildtype could indicate an additional function of Hsv2.

Wildtype and *hsv2Δ* cells were nitrogen starved and samples were taken after 8 and 24 hrs. Samples were alkaline lysed and were resuspended in SDS sample buffer without bromophenol blue. Triplicates of each strain were made and in the Urlaub group stable isotope reagents were added to each sample before being analysed via tandem mass tag-based quantification.

The analysis revealed 87 proteins that had been up- or down-regulated in Hsv2 depleted cells compared to wildtype. A select few genes where chosen based on their level of up- or down-regulation and whether they had a connection to autophagy, these can be seen in Table 4-2. The Gene Ontology Slim Mapper of the *Saccharomyces* Genome Database, was used to determine the most affected compartments within the cell. 21% of the genes are found in the mitochondria and the cytoplasm, 17% of the genes are located at membranes, 15% are found

at the vacuole or nucleus and 11% in the endoplasmic reticulum. Almost all compartments seem to be partially affected by the absence of Hsv2.

Log Change	8 Hrs SD-N	Protein
0.7665	Up-Regulated	FMP23
0.6400	Up-Regulated	VPH1
0.6187	Up-Regulated	URA2
-1.1462	Down-Regulated	VPS15
-1.2834	Down-Regulated	ROM2
-1.3216	Down-Regulated	ELM1
-1.3815	Down-Regulated	MFα1
-1.5887	Down-Regulated	HSV2

Log Change	24 Hrs SD-N	Protein
1.2525	Up-Regulated	SCE1
0.7921	Up-Regulated	VPS15
0.7848	Up-Regulated	ELO3
0.7828	Up-Regulated	URA2
0.7798	Up-Regulated	ELM1
0.7300	Up-Regulated	NOP8
0.6362	Up-Regulated	VPS13
-0.5942	Down-Regulated	ATG42
-0.6754	Down-Regulated	APE1
-0.6874	Down-Regulated	ATG33
-0.8033	Down-Regulated	PRC1
-0.8737	Down-Regulated	YPT53
-0.9491	Down-Regulated	MFα1
-1.0100	Down-Regulated	STF2
-1.2041	Down-Regulated	ACM1
-1.8325	Down-Regulated	HSV2
-2.3362	Down-Regulated	INO1
-10.8485	Down-Regulated	SKN1

Table 4-19: Proteomic Analysis WT vs hsv2Δ.

In both the 8 and 24 hrs samples, the expression of *HSV2* is down-regulated; this served as an excellent control that the experiment worked. Interestingly, the expression of *VPS15* was down-regulated in the 8 hrs sample but up-regulated in the 24 hrs sample. Vps15 plays a role in protein sorting at the vacuole and is part of the PI3-kinase complex. The down-regulation of both *ATG42* and *ATG33* was unexpected as Hsv2 was thought not to be involved in autophagy. Atg42 is a most recently discovered Atg protein, is a vacuolar serine-type carboxypeptidase involved in vacuolar zymogen activation and autophagic body breakdown [278]. Atg33 is a mitophagy-specific protein, and this could suggest Hsv2 is involved in regulating mitophagy or in the recycling of some mitophagy components. The down-regulation of Ape1 was unforeseen, considering the Ape1 maturation assays did not hint

towards an involvement of Hsv2 in the Cvt pathway. *SKN1* was massively down-regulated in the 24 hrs sample. Skn1 is involved in sphingolipid biosynthesis of the cell wall and could be linked to Hsv2 involvement in GOMED.

Further experimentation is required to narrow the list of candidates down to elucidate a molecular function for Hsv2. It should be mentioned that this experiment was done using haploid cells and in light of the previously described effects of *HSV2* deletion in haploid cells compared to diploid cells (see chapter 4.1.4), it would be interesting to see if this also has an impact on expression patterns. This experiment should also be performed with diploid cells.

4.1.6 Bio ID

The *in vivo* identification and characterisation of protein-protein interactions are essential to understanding mechanisms of action. More recently, enzymatic proximity-labelling protocols, including ascorbate peroxidase (APEX) tagging and proximity-based biotin identification (BioID), have been developed as additional methods to study the interactome of a protein of interest. The original biotin ligase (BirA) for the BioID was based on the E. *coli* biotin ligase. The original biotin ligase is both an enzyme and a sequence-specific DNA-binding protein. As an enzyme, BirA adenylates biotin and transfers it to a unique lysine residue on the biotin carboxyl protein subunit of acetyl-CoA carboxylase [279]. As a DNA-binding protein, it represses the expression of genes that encode the biotin biosynthetic enzymes [280]. BirA was mutated by replacing an arginine with glycine at residue 118, R118G, disrupting the DNA-binding domain. This mutation, BirA*, also caused the 'activated' biotin to be loosely bound at the active site, allowing for the highly reactive biotinoyl-5'-AMP to diffuse and indiscriminately biotinylate proteins in approximately a 10 nm radius [281]. The biotinylated proteins can be recovered using streptavidin columns and subsequently identified by mass spectrometry.

A second generation biotin ligase was created, BioID2, which lacks the DNA-binding domain and is approximately one-third smaller than BioID. BioID2 requires less biotin to accomplish similar levels of biotinylation and can be attached to an extended flexible linker to increase the labelling range to 15 nm [282]. A former member of the lab, Dr Lena Munzel, optimised

the BioID protocol for yeast *Saccharomyces cerevisiae* from a protocol provided by Opitz et al., 2017.

4.1.6.1 Preliminary BioID experiments

Functional experiments were done on the Hsv2 BioID constructs to determine whether Hsv2 tagged C- or N-terminally with BirA* were functionally viable. A Myc tag was included in the constructs at the C-terminal of BirA*; this allowed expression levels to be assessed via immunoblotting. To ensure maximal functionality of the Hsv2 tagged BirA* constructs, two separate experiments were used to test this; first, a mild phenotype has been seen during sporulation of *hsv2Δ* diploid cells. Asci formation is reduced in *hsv2Δ* cells, therefore sporulation in cells expressing BirA* tagged Hsv2 constructs were analysed to determine the functionality of the proteins. *hsv2Δ* strains were transformed with either an empty plasmid, Hsv2-GFP, Myc-BirA*-Hsv2 or Hsv2-Myc-BirA*, grown to an OD_{600} of 2.0 and stained with Calcofluor white to visualise the cell walls of sporulating yeast cells using the DeltaVision®.

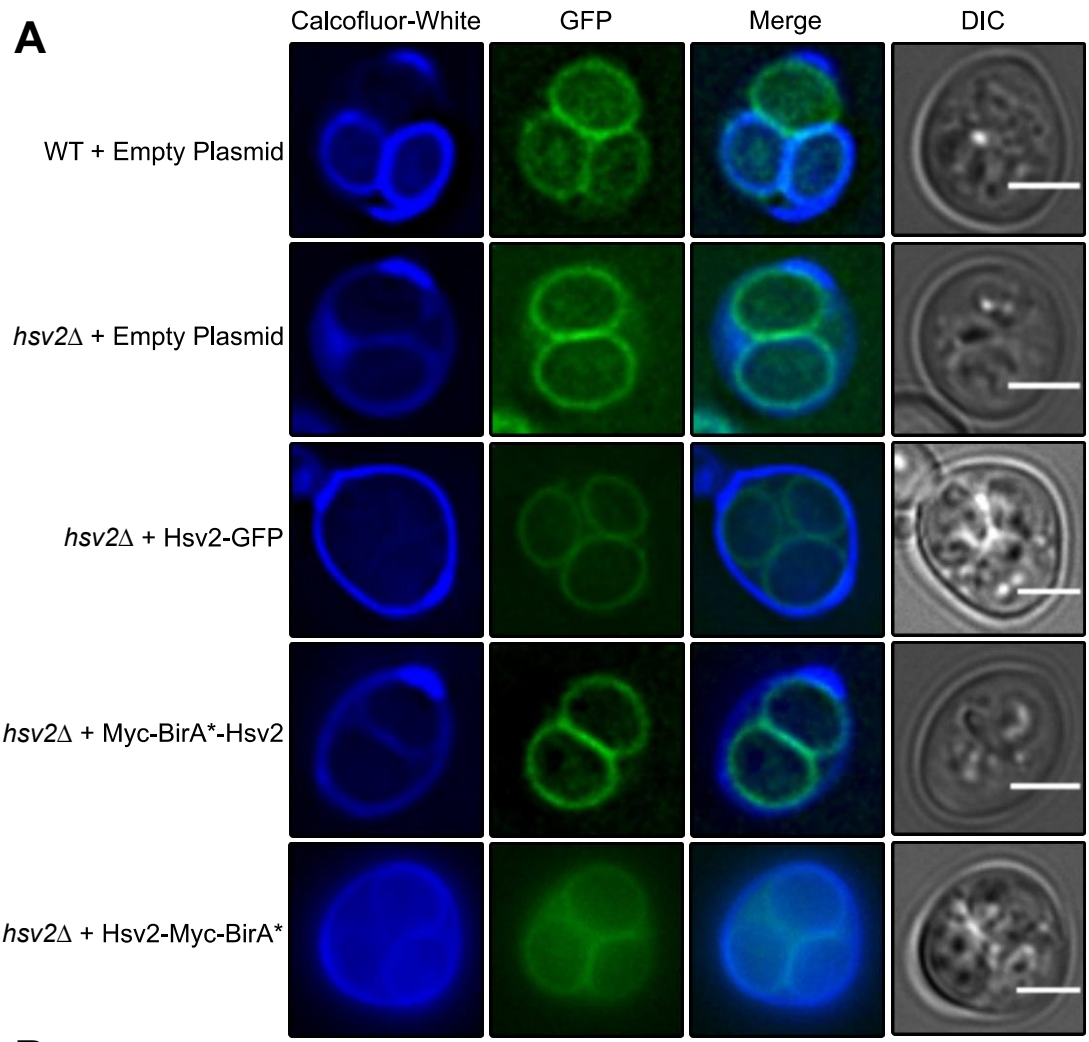

B

Day 5

	Total Cells	Total Spores	Spores/ Cells(%)
WT + Empty Plasmid	199	39	19.60
hsv2Δ + Empty Plasmid	149	10	6.71
hsv2Δ + Hsv2- GFP	166	10	6.02
hsv2Δ + Myc- BirA*- Hsv2	137	22	16.06
hsv2Δ + Hsv2- Myc- BirA*	233	31	13.30

Day8

	Total Cells	Total Spores	Spores/ Cells(%)
WT + Empty Plasmid	273	90	32.97
hsv2Δ + Empty Plasmid	163	30	18.40
hsv2Δ + Hsv2- GFP	134	41	30.60
hsv2Δ + Myc- BirA*- Hsv2	156	54	34.62
hsv2Δ + Hsv2- Myc- BirA*	137	37	27.01

Figure 4-23: Sporulation test using BioID constructs.

(A) Images of the asci of sporulating yeast cells with different BioID constructs. Scale bar = 2.5 µm (B) Table showing the total number of cells and spores seen for each BioID construct.

Figure 4-6 (B) shows quite a difference in spores seen between the two constructs. After five days, both the N- and C-terminally tagged Hsv2 were more similar to wildtype than *hsv2Δ*. However, the rate of sporulation seen with Hsv2-GFP was more similar to *hsv2Δ* than the wildtype strain. This changed in the day eight samples where the Hsv2-GFP strain was very close to that of the wildtype strain. Both BirA* constructs were also similar to the wildtype strain, although the Myc-BirA*-Hsv2 was more functional compared to Hsv2-Myc-BirA* as the sporulation rate was even higher than the wildtype.

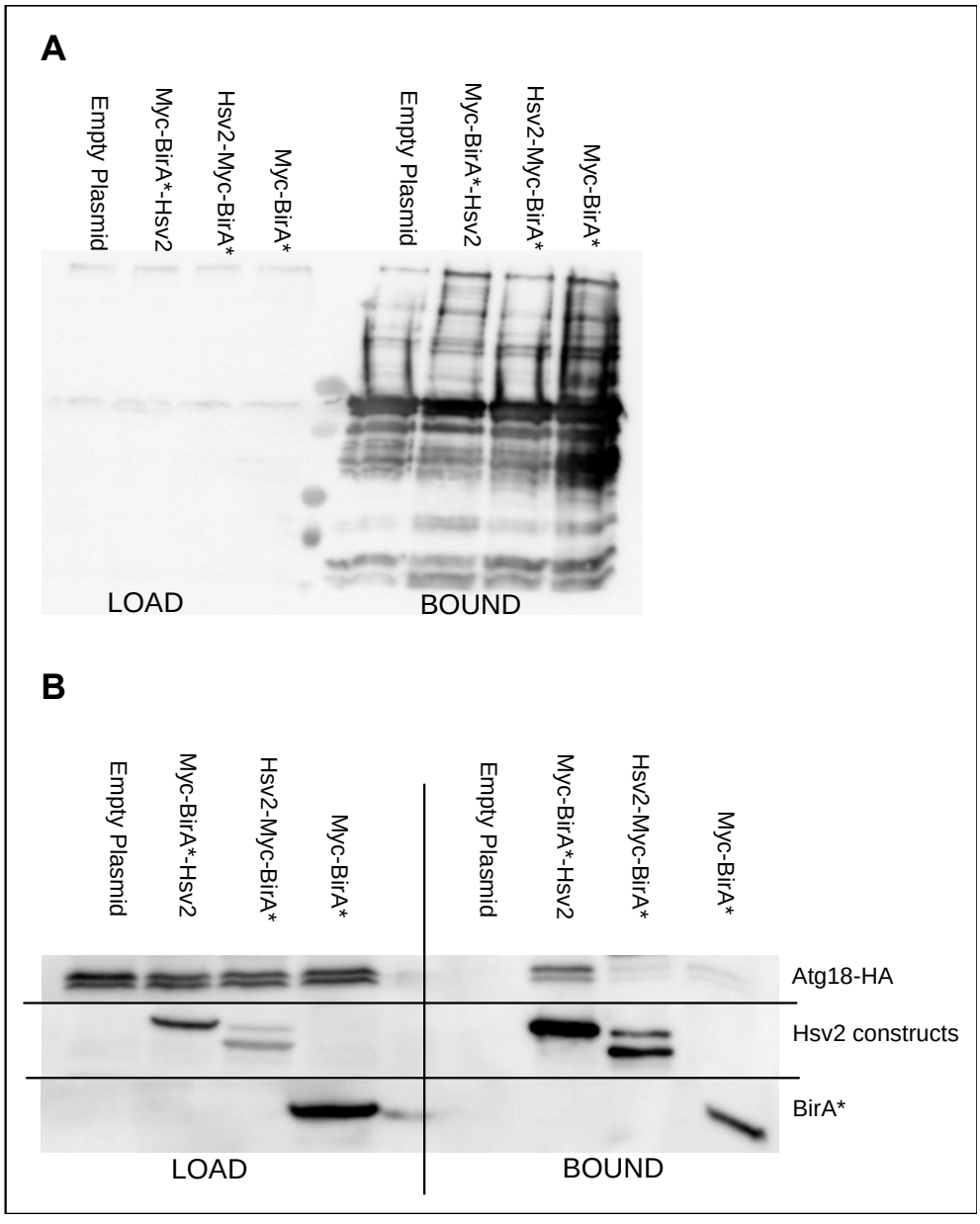

Figure 4-24: Small Scale BioID.

(A) *Atg18-HA hsv2Δ strain transformed with the BioID constructs before and after affinity purification using streptavidin column, blot decorated with Strep-tag HRP-conjugate to observe biotinylated proteins. (B) The same samples were also tested with known interacting partner Atg18-HA, blots decorated with HA and Myc.*

With both BioID constructs performing quite similarly, we tried a second experiment where we attempted a small-scale BioID with an already known interaction partner of Hsv2. Atg18, previously shown to interact with Hsv2, was chromosomally tagged with HA in a *hsv2Δ* strain and transformed with the BioID constructs and Myc-BirA* alone as a control. All biotinylated proteins were recovered using a streptavidin column (Figure 4-7 (A)) and decorated with Strep-tag HRP-conjugate, and imaged using the LAS-3000. This allows us to visualise all biotinylated proteins within the sample. Both Hsv2-Myc-BirA* and Myc-BirA*-Hsv2 show a similar pattern of biotinylated proteins.

Figure 4-7 (B) shows a blot decorated with an anti-Myc and anti-HA antibodies to visualise the BioID constructs and Atg18-HA, respectively. Atg18-HA can be found in the load of all BioID constructs but can only be found in the bound fraction of Myc-BirA*-Hsv2. Interestingly, blots decorated with anti-Myc show one band for Hsv2 in the bound fraction of Myc-BirA*-Hsv2, but in the Hsv2-Myc-BirA* construct, an additional band can be seen, which indicates degradation. The Myc-BirA* was seen in both the input and the bound fractions, which functioned as good controls. These results together with the sporulation experiment suggest that the Myc-BirA*-Hsv2 construct is much more stable and functionally viable, and therefore this construct was used for the main experiment.

4.1.6.2 BioID Results

Biotinylation of proteins occurs naturally within organisms and in order to differentiate between naturally occurring biotinylation and proteins biotinylated by BirA* itself; a stable isotope labelling by amino acids in cell culture (SILAC) approach was required. The used yeast strains are unable to synthesise the essential amino acids arginine and lysine. Knowing this, we are able to use different isotopes of arginine and lysine in the growth medium, which will be transported into the cells and used in protein synthesis. Cells expressing the entire construct, Myc-BirA*-Hsv2, were grown in a medium containing 'light' amino acids, L-arginine and L-lysine with a natural isotope abundance. The cells expressing the control Myc-BirA* were grown in medium containing 'medium' amino acids, ^{13}C L-arginine and 4,4,5,5-D_4-L-lysine, and finally, cells transformed with the empty vector control were grown in medium containing 'heavy' amino acids, ^{13}C ^{15}N L-arginine and ^{13}C ^{15}N L-lysine. This allows for a direct

comparison of biotinylated proteins from the three different strains via mass spectrometry. The control strain containing the empty plasmid should reveal naturally biotinylated proteins. Myc-BirA* alone served as a control for unspecific biotinylation of proteins. The combination of both these controls should allow us to determine proteins specifically biotinylated by Myc-BirA*-Hsv2.

Once the samples had been analysed via liquid chromatography coupled to electrospray and tandem mass spectrometry by Dr Oliver Valerius and Dr Kerstin Schmitt (Department of Molecular Microbiology and Genetics, Georg-August-University Göttingen), the data was subjected to numerous database searches using the MaxQuant software. MaxQuant uses the MS spectra data that contains the peptide mass and intensity information to deduce the identity of the proteins using the Mascot algorithm. Identified proteins were filtered and organised based on relative enrichment from the strain expressing Myc-BirA*-Hsv2 against both control strains using Perseus software, as described by [274]. In order for a protein to be filtered for further analysis, there must be at least 20% enrichment in two out of the three Myc-BirA*-Hsv2 samples when compared to the controls.

Hsv2 had the highest enrichment when compared to the controls (Table 4-3). This acted as a reasonable control as BirA* also biotinylates the protein it is fused to, and therefore Hsv2 should contain multiple biotinylation sites. No Atg proteins were detected as enriched in two of the three samples; this was unexpected considering Hsv2 is known to interact with Atg18 and Atg21. Without any other interacting partners known for Hsv2, it is difficult to determine if the experiment worked as expected.

Of the 50 proteins that were filtered as enriched, 15% are associated with the structural integrity of a complex, 12% are involved in lipid binding, and 8% are transmembrane transporters. Several of the hits are located at the vacuolar membrane, including vacuolar transporters Avt1, Avt4 and Vtc3, and the SNARE protein Ykt6, as well as phospholipid-binding protein Pib2. Hsv2 localises to the vacuolar membrane, increasing the possibility that these hits are interacting partners of Hsv2. From the 50 proteins a ranked list was created based on enrichment, as seen in Table 4-3.

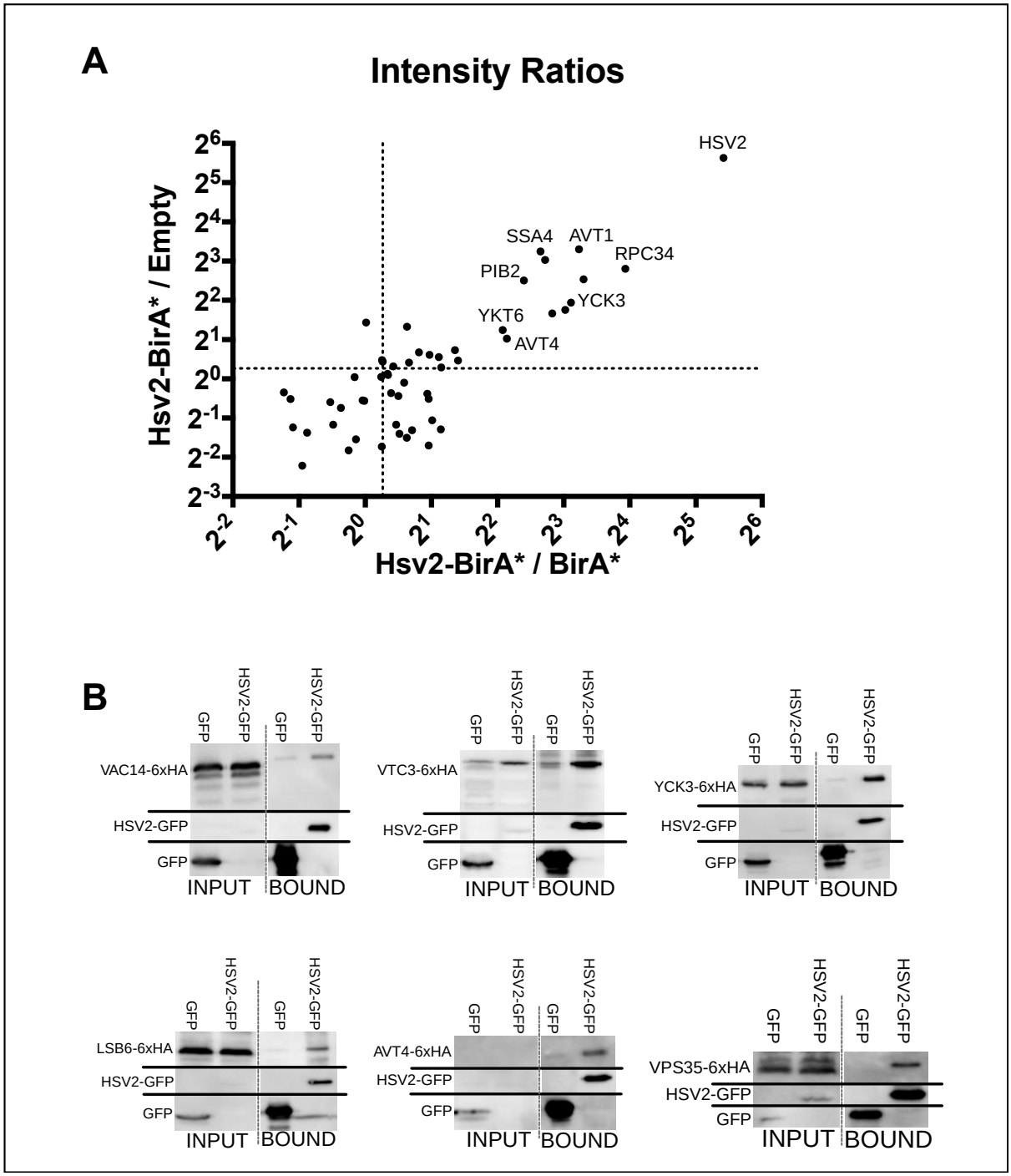

Figure 4-25: BioID results and confirmation.

(A) Scatterplot of the top 50 proteins identified in the BioID assay. The signal ratio of BirA-Hsv2 to empty plasmid was plotted against the signal ratio of BirA*-Hsv2 to BirA* alone. Dotted lines represent the 20% enrichment compared to the controls. (B) Confirmation of BioID candidates by co-immunoprecipitation using GFP-Traps. Hsv2-GFP was used as the 'bait', and all the 'prey' proteins were chromosomally tagged with 6xHA. The blots show cell lysate as the 'input' to the columns and the 'bound' fraction that was eluted off the GFP column. All experiments were done in triplicates.*

As very little is known about Hsv2, confirming any interacting partners would give us an insight into the possible function of Hsv2. In order to confirm the hits from the BioID co-immunoprecipitation assays (Co-IPs) were done using GFP traps. This was achieved using Hsv2-GFP as 'bait' on a low copy plasmid, and the BioID hits, the 'prey', were chromosomally tagged with 6xHA at the C-terminal. This allowed for the expression of all proteins to be under their endogenous promotors. Each experiment was done in parallel with a plasmid containing only GFP as a control.

Gene Name	***Enrichment***	***Function***
HSV2	4.67630	
AVT1	3.21813	Amino acid vacuolar transporter
YCK3	2.82007	Kinase
VTC3	2.54223	Vacuolar transporter
YGR125W	2.26776	Vacuolar transporter
SSA4	2.09307	Protein sorting
MAM3	2.067875	Mitochondria morphology
TFC7	1.84558	DNA binding
AVT4	1.6257785	Vacuolar transporter
YKT6	1.09683	v-SNARE
SEC16	0.91317	Protein transport
PIB2	0.463808	Lipid binding
LSB6	0.21489	Kinase
VAC14	0.10471	Vacuolar morphology

Table 4.20: List of BioID candidates sorted by enrichment.

The Co-IPs were performed using the µMACS system from Miltenyi. Of the candidates tested, Vac14 and Vtc3 could be found in the bound fraction of Hsv2-GFP and with a faint band in the control. Although, the signal ratio between the GFP and HA bands is much higher in the Hsv2-GFP compared to the GFP alone. This suggests that there is an interaction between Hsv2 and Vac14 and Vtc3. Vac14 is part of the phosphatidylinositol 3,5-bisphosphate (PI (3,5)P2) regulatory complex and regulates both the synthesis and turnover of PI (3,5)P2. This complex

contains the scaffold protein Vac14, the lipid kinase Fab1 and the counteracting lipid phosphatase Fig4. This is essential for the control of trafficking proteins to the vacuolar lumen via the MVB, as well as the maintenance of vacuole size and acidity [283], [284]. Vtc3 is a component of the vacuolar transporter chaperone (VTC) complex, which is involved in vacuolar polyphosphate homeostasis, membrane trafficking, microautophagy and non-autophagic vacuolar fusion. Vtc3 is not necessary for priming or formation of the trans-complex, but it is required for fusion and release in the terminal phase of docking. Thus, it is thought to mediate a very late, post-docking function of the VTC complex [285]–[287].

Lsb6 could be shown to co-precipitate with Hsv2 and not with GFP alone. Lsb6 is a type II phosphatidylinositol 4-kinase involved in actin patch assembly and actin polymerisation [177]. Yck3 has also been found in the bound fraction of Hsv2-GFP, but not in the control. Yck3 is a palmitoylated vacuolar membrane-localised casein kinase I that negatively regulates vacuole fusion during hypertonic stress [288]. Although Avt4 can be seen to co-precipitate with Hsv2 the signal is very weak. The expression levels of Avt4 are quite low so it may be worth using a MET25 promotor instead of the endogenous promotor. Avt4 is a vacuolar transporter that exports sizeable neutral amino acids from the vacuole [289]. Vps35 was also shown to co-precipitate with Hsv2 and not with the control. Additionally, Vps35 was found to co-precipitate with all PROPPINs. Vps35 is a component of the retromer complex required for the retrieval of cargo from endosomes to the late-Golgi [209], [290]. These results hint towards Hsv2 having a function at the vacuolar membrane, potentially in vacuolar protein homeostasis or recycling of proteins transported to the vacuole. Although, further experimentation is required to determine what Hsv2 is doing at these locations.

4.2.1 Atg8 Purification

To better understand the interaction between Atg8 and Atg21, we wanted to isolate these proteins to perform binding assays and crystallisation trials. Atg21 has already been isolated from *K. lactis* in collaboration with Karin Kühnel's group. A plasmid containing GST-ScAtg8 was transformed into *E. coli* BL21 cells. Plasmid expression was induced using IPTG, and cells were incubated at 30°C, the optimal temperature for Atg8 stability, rather than 37°C, which

is optimal for *E. coli* growth. Cultures were harvested 6 hrs after induction and stored at -80°C to preserve the protein.

The Äkta system was used to aid in loading and eluting the sample from the purification columns. All fractions that were eluted from the 5 ml GST column contained the fusion protein GST-Atg8 (Figure 4-9 (A+B)). Although some of the earlier fractions include contaminations, this was not a problem at this stage. Subsequent, dialysis was required for the removal of the reduced glutathione that was used to elute the GST from the column. Unfortunately, during this step proteins precipitated (Figure 4-9 (C) DP); which was slightly reduced with the addition of 1 mm DTT. A thrombin cleavage site is located between the GST tag and Atg8 protein, allowing for the removal of the GST tag. Initially, thrombin cleavage was done at room temperature, but this caused massive precipitation of protein, so instead, cleavage was done at 4°C for 24 hrs. Protein still precipitated, but this was a significantly decreased compared to cleavage at room temperature (Figure 4-9 (C) CP). A 50% slurry glutathione sepharose 4B beads were used to remove the free GST tags after cleavage (Figure 4-9 (C) 4B). This was done to reduce the overall protein concentration within the solution rather than the full removal of the free GST tags, as this will be accomplished by size exclusion chromatography (SEC). The glutathione sepharose 4B beads were washed twice with 1 x PBS to clean the beads of Atg8. The washes were pooled, and the solutions were concentrated for SEC.

The load volume of the SuperDex 75 pg is 5 ml. It was found that concentrating the solution too much before SEC precipitated proteins. To conserve more protein the SEC SuperDex 75 pg was loaded in two separate runs, and the elution fractions were pooled. SEC columns elute proteins based on their size, with the larger proteins eluting first and the smaller proteins eluting later. The fraction A6 contained mostly unwanted proteins, although there is still a GST-Atg8 band showing that not all of the fusion construct was cleaved by thrombin. The fraction A12 had the majority of the remaining GST tags in the sample. The fractions D4-9 contained most of the Atg8 (Figure 4-9 (D)). Once the fractions containing Atg8 were pooled,

Amicon Ultra Centrifugal filter units with a molecular cut off size of 3,000 Da was used to concentrate the solution to 1 ml.

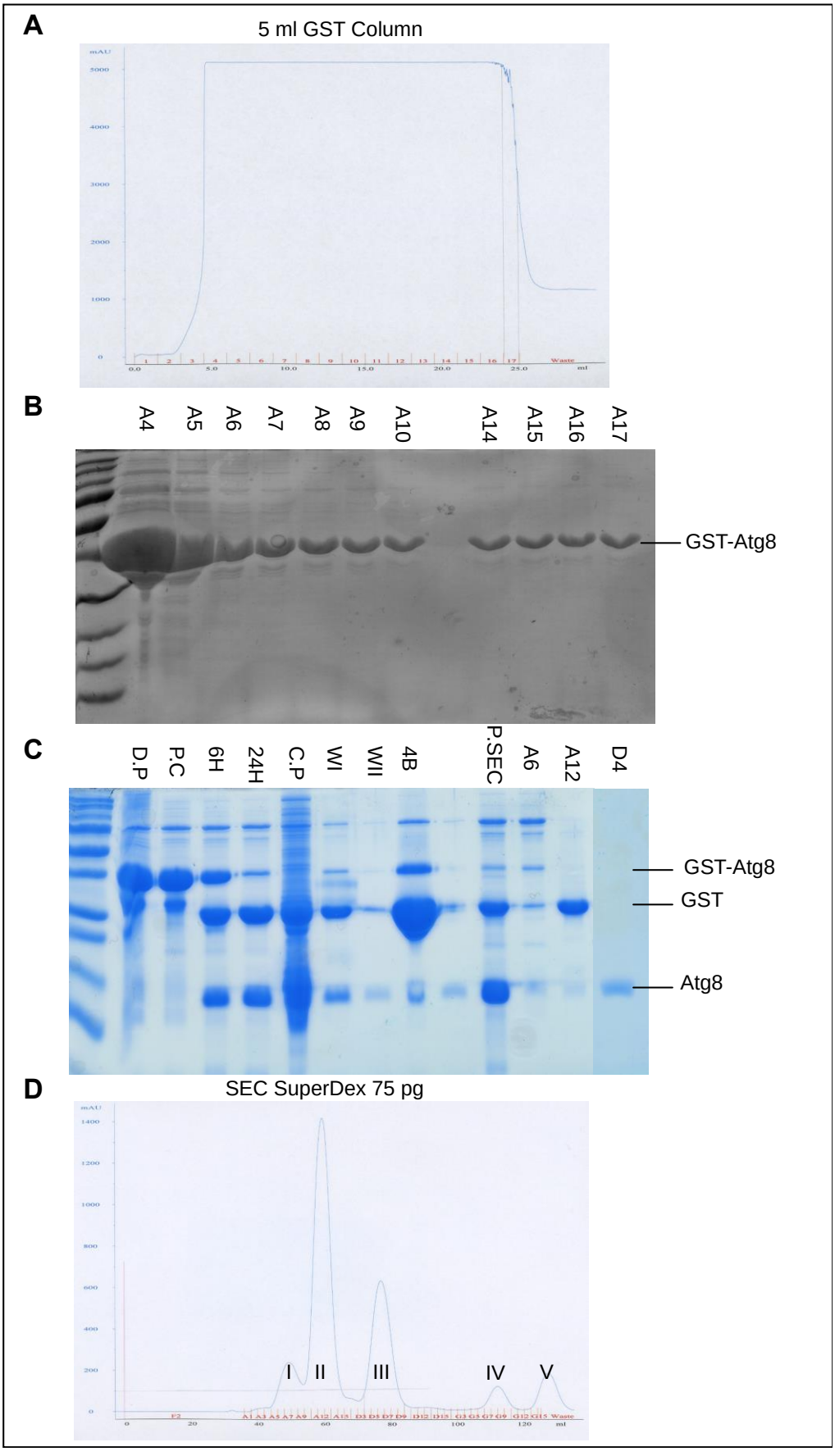

Figure 4-26: Purification of Atg8.

*(A) Elution profile from 5 ml GST column (B) Elution fractions from 5 ml GST column run on 10% SDS gel and stained with Coomassie. (C) Samples were taken throughout the purification process. DP = protein precipitation after dialysis. PC = sample before thrombin cleavage. 6H and 24H = samples during thrombin cleavage. C.P = protein precipitation after thrombin cleavage. WI = first wash from the glutathione sepharose 4B beads. WII = second wash from the glutathione sepharose 4B beads. 4B = glutathione sepharose 4B beads. P.SEC = sample before size exclusion chromatography. A6, A12 and D4 = fraction samples from SEC. (D) Elution profile from size exclusion chromatography column SuperDex 75 pg. Fraction **I** contained high molecular weight proteins, fraction **II** contained mainly free GST, fraction **III** contained Atg8 and fractions **IV** and **V** contained low molecular weight proteins. Samples were run on 10% SDS gel and stained with Coomassie.*

The concentration of purified Atg8 was measured using the Bradford assay and the Nanodrop A_{280} value. Protein concentrations can be estimated by measuring the UV absorbance at 280 nm. Proteins tend to show a strong peak at 280 nm due to the absorbance from tryptophan and tyrosine residues. Unfortunately, Atg8 does not contain any of these residues so the A_{280} value alone is not sufficient to accurately measure the concentration. Therefore, the Atg8 A_{280} value was used in conjunction with the Atg8 extinction coefficient and molecular weight in the Beer-Lambert's law to determine the concentration of purified Atg8. This, in combination with the Bradford assay, determined final concentration of Atg8 to be 15.6 mg/ml. The Atg8 sample was divided into 70 µl aliquots and snap-frozen in liquid nitrogen and stored at -80°C to preserve the protein. Aliquots were thawed on ice before use.

4.2.2 Atg8 Binding Assay

To determine the best conditions for Atg21 and Atg8 binding, a synthetic peptide of Atg21 was created, CEIVFPHEIVKVVMND(FAM), with a 5(6)-carboxyfluorescein (FAM) fluorophore tagged at the C-terminal. The FAM fluorophore is a tag small enough not to interfere with protein dynamics but still allow for visualisation. *K. lactis* Atg21 was purified using 30 mM HEPES 150 mM NaCl pH 7.5 buffer, whereas Atg8 was purified using 1 x PBS pH 7.4. So, the first experiment was to determine which buffer allowed for the best binding conditions for the two proteins.

To test this, three buffers were selected; 1 x PBS pH 7.4, 50 mM Tris 1 mM EDTA, and 30 mM HEPES 150 mM NaCl pH 7.5. 1 µM of the Atg21 peptide was used in each experiment with 50, 100 and 500 nM Atg8. 96 well plates were incubated for 5 min at room temperature before fluorescence anisotropy and intensity were measured using a VictorNiro Plate reader with

assistance from Dr Alaa Shaikhqasem (Group of Prof. Dr R. Ficner, Molecular Structural Biology, Georg-August-University Göttingen).

In 2016, a library of synthetic peptides corresponding to the loops of Atg21 were screened for binding with Atg8. It was observed that the peptide corresponding to loop 2D to 3A of Atg21 was binding to Atg8 [170]. We expected a correlation between the concentration of Atg8 and the number of Atg21 peptides in a bound state and therefore the fluorescence intensity would decrease as the fluorophore is within the binding pocket of Atg8. As well as fluorescence intensity we also measured the fluorescence anisotropy. Here, the FAM fluorophore is excited with vertically polarised light at 494 nm that selectively excites a subset of the fluorophores according to their relative orientation with the incoming beam. The resulting emission at 518 nm also has a directionality whose relationship in the vertical and horizontal planes defines anisotropy. The anisotropy should increase as more molecules enter a bound conformation. The 1 x PBS buffer did not follow either of these trends, which was unexpected (Figure 4-10 (Left)). The 50 mM Tris buffer did increase in anisotropy as the concentration of Atg8 increased, but the fluorescence intensity did not decrease over time (Figure 4-10 (Middle)). Finally, the 30 mM HEPES buffer increased in anisotropy and decreased in fluorescence intensity as the concentration of Atg8 increased (Figure 4-10 (Right)). The results using the HEPES buffer were as expected, therefore these conditions were chosen for a full binding assay.

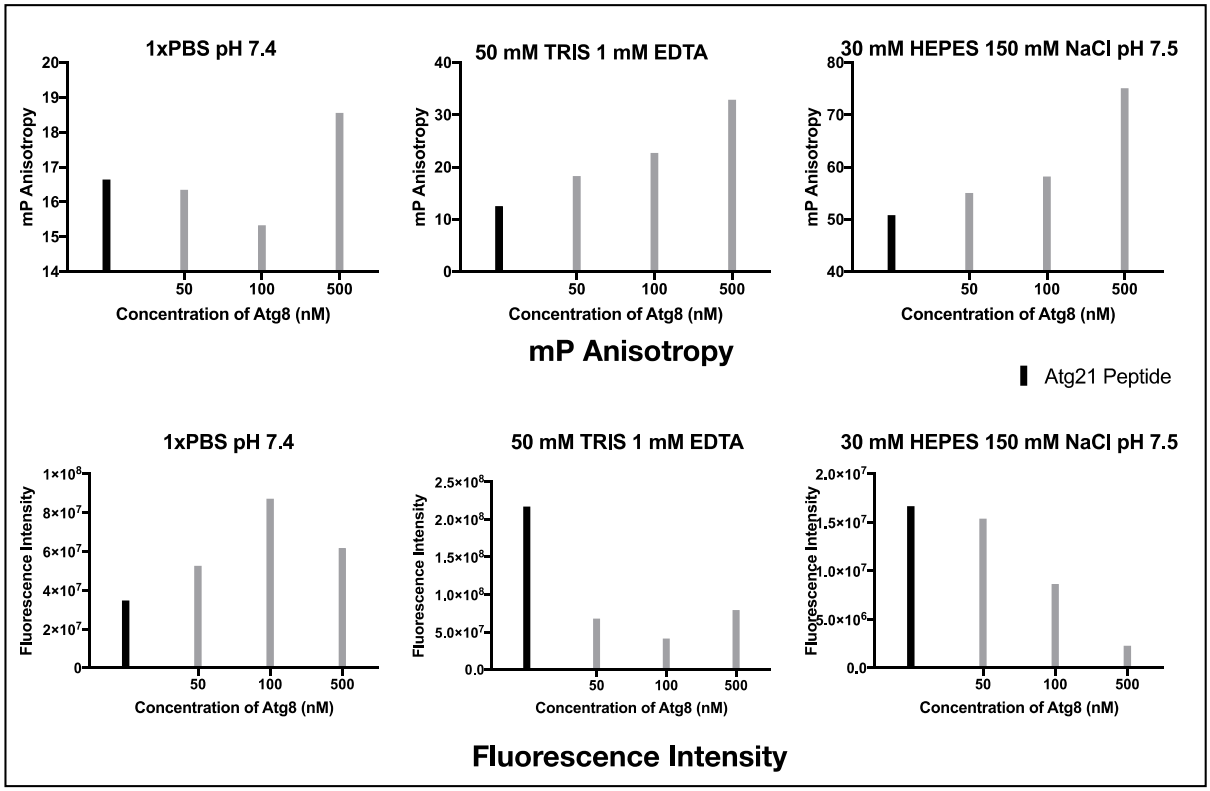

Figure 4-27: Buffer test for Atg8 Atg21 binding.

Fluorescence anisotropy and intensity of triplicate samples were measured within each buffer. Using 1 µM of the Atg21 peptide and 50, 100 and 500 nM Atg8, incubated at room temperature for 5 mins before measuring. Black bar indicates Atg21 peptide alone. Measurements using the VictorNiro Plate reader was assisted by Dr Alaa Shaikhqasem.

When determining the binding strength of two proteins, there are two states that these proteins can be in; a free state or a bound state [291], [292]. A binding reaction consists of a dynamic exchange between the bound and free states. The reaction proceeds to an equilibrium where the concentration of free proteins and bound proteins are held in a steady state. Once at equilibrium, binding can be further modelled using the law of mass action; as the rates of forward and reverse reactions are equal, it is possible to determine the binding affinity [293], [294].

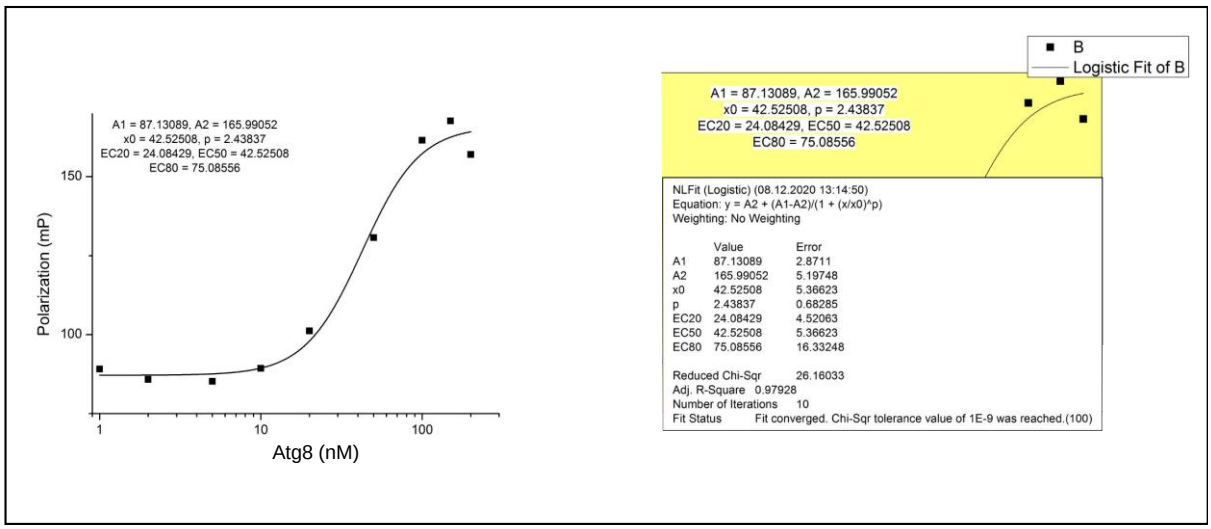

Figure 4-28: Full binding assay of Atg8 and Atg21.

1 µM of Atg21 peptide was incubated with Atg8 in concentrations ranging from 1 nM to 500 nM and incubated at room temperature for 5 mins before the fluorescence polarisation was measured at each concentration in triplicates. A sigmoidal curve can be seen with a K_d value of 42.5 nM. Measurements using the VictorNiro Plate reader was assisted by Dr Alaa Shaikhqasem.

For the complete binding assay, Atg8 concentrations ranged from 0.5 – 500 nM, with the Atg21 peptide concentration being kept the same as previous experiments at 1 µM. As the concentration of Atg8 increases, so does the fluorescence polarisation. At an Atg8 concentration of 20 nM it reaches the exponential phase before plateauing at a concentration of 500 nM. The dissociation constant value, K_d, was found to be 42.5 nM. This suggests that the binding between Atg8 and Atg21 is relatively weak.

4.2.3 Atg8 Crystallisation Trials

Once the binding affinity between Atg8 and the Atg21 peptide had been established, we determined the concentrations to use for crystallisation trials. Due to the binding being weak, we used a 20 fold molar excess of the Atg21 peptide and 800 µM Atg8. The solution was incubated at room temperature for 30 min before being plated on 12 x 96 well crystallisation plates.

Before the crystallisation screening conditions were added to the reaction, the solutions containing either Atg8 alone or Atg8 with the Atg21 peptides were tested for protein degradation or aggregation using dynamic light scattering (DLS). DLS is based on the Brownian motion of dispersed particles. When particles are dispersed in a solution, they move randomly

in all directions. The principle of Brownian motion is that particles are constantly colliding with molecules and these collisions cause a certain amount of energy to be transferred, inducing particle movement. The relation between the speed of the particles and the particle size is given by the Stokes-Einstein equation. A single-frequency laser is directed at a set angle into the solution, the diffraction of the laser light is recorded. This signal is used to determine the diffusion coefficient and the particle size using the Stokes-Einstein equation which is dependent on the refraction index of the oil applied to the sample [295]. DLS can be used to determine the homology of a given solution.

The dynamic light scattering of Atg8 alone shows suitable homology, with the majority of molecules having the same radius (Figure 4-12 (A)). This was further proof that the purification of Atg8 and the removal of all contaminants was successful. The analysis of Atg8 with the Atg21 peptide also showed acceptable levels of homology; this indicates low levels of protein precipitation or aggregation caused by the addition of the Atg21 peptide (Figure 4-12 (B)). Also, a slight shift in the radius of the molecules was seen, suggesting that Atg8 and the Atg21 peptide were binding in solution.

A total of 12 screening conditions were used, each with 96 unique crystallisation conditions; a total of 1,152 different conditions were tested. In order to obtain more information on the precipitation behaviour of the protein this systematic approach alters individual components of the crystallisation conditions, pH, anions and cations, independently from the others wells. Each well of the 96 well plate consists of four separate wells (Figure 3-2); a reservoir containing the screening condition, just the buffer, 1:1 and 2:1 ratios of protein to screening condition. The 96 well plates were stored at room temperature and checked every six weeks under the microscope for crystal growth. When crystals were seen, all four wells within the central well were also reviewed to determine whether the crystals were salt or protein-based. For the majority of cases, when crystals were located, they were located in both the 1:1 and 2:1 ratio wells. This ruled out random salt growth from either the buffer or the screening conditions. The preparation and checking of the crystallisation plates were assisted by Dr Alaa Shaikhqasem. The crystals that are seen in Figure 4-12 (C) were tested using X-Ray crystallography to determine whether they were formed of salt or protein with assistance

from Dr Piotr Neumann and Dr Alaa Shaikhqasem (Group of Prof. Dr R. Ficner, Molecular Structural Biology, Georg-August-University Göttingen).

The crystals were extracted from the well using a wire loop under the microscope and placed in a sucrose or glycerol solution and immediately frozen in liquid nitrogen. The crystals were placed in the X-Ray diffractor with a constant stream of liquid nitrogen, keeping the crystal frozen. Unfortunately, even with the detector as close to the crystal as possible, no X-rays could be detected. Crystals formed from salt diffract X-rays to a higher degree compared to protein based crystals. Therefore, crystals grown in the experiment were likely salt crystals. The screening conditions continued to be checked every few months in case crystals have formed, but so far this has not been successful, so we decided to perform computational modelling a go.

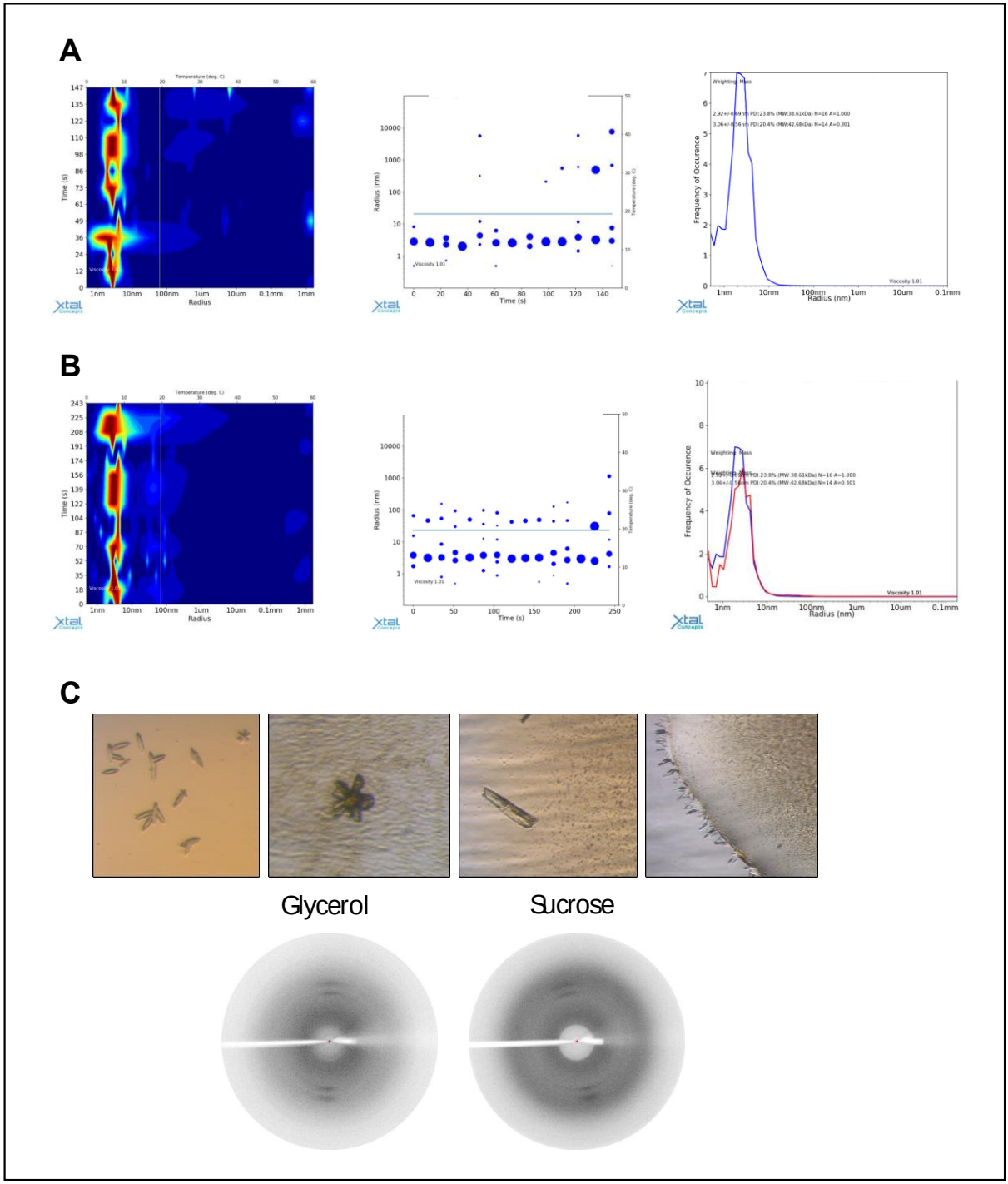

Figure 4-29: Crystallisation Trials of Atg8 and Atg21 peptide.

(A) Dynamic light scattering of S. cerevisiae Atg8 alone. (B) Dynamic light scattering of S. cerevisiae Atg8 with Atg21 peptide. 15 iterations, with each lasting 20 seconds. The line graph on the right shows an overlay of S. cerevisiae Atg8 alone (Blue) and S. cerevisiae Atg8 with the Atg21 peptide (Red). (C) Microscopic photos of the crystals grown under specific screening conditions. X-Ray crystallography of those crystals in glycerol or sucrose solutions. The experiment was assisted by Dr Alaa Shaikhqasem and Dr Piotr Neumann.

4.2.4 Protein Modelling

Following the work from Juris *et al. 2015* and Munzel *et al.* 2021, we wanted to further identify interacting regions of Atg21 while at the PAS. Previous work highlighted the conformation orientation of Atg21 and Atg16, where R151 of Atg21 was found to directly interact with D101 of Atg16. Additionally, the interaction of both proteins requires K152 of Atg21 and E102 of Atg16. Atg21 localisation is determined by the presence of PI3P at the autophagic membrane and also regulates the site of Atg8 lipidation [171]. Atg21 directly interacts with the Atg8-Atg3 conjugate via the conserved F5K6-motif of Atg8 and positions the Atg8 lipidation complex in close proximity to PE. Furthermore, the interaction between Atg16 and Atg21 allows for the recruitment of the Atg12-Atg5/Atg16 complex, thereby arranging the E3-like Atg12-Atg5 conjugate within reach of the E2-like enzyme Atg3 [62], [171].

Atg8 has a few regions that could be responsible for the interaction with Atg21. In the C-terminal ubiquitin-like domain of Atg8 is the AIM-binding site which is crucial for interaction with the WxxL-like motif in proteins such as Atg1, Atg3 and Atg19 [132], [296], [297]. The N-terminal helical domain (NHD) of Atg8 is flexible in solution and contains a FK-motif that mediates further interactions [298], [299].

Over the past decade, protein modelling and folding has excelled. Due to the difficulties of protein crystallisation, this has become a standard when looking at protein structure or protein-protein interactions. Many protein complexes are not stable enough to purify together, and computational analysis offers a far more straightforward approach.

Dr Piotr Neumann assisted in the crystallisation trials for ScAtg8 and the Atg21 peptide. As the structures of both proteins are known, Dr Neumann made computational modelling of the two proteins; using S. *cerevisiae* Atg8 and K. *lactis* Atg21. Crystallographic Object-Oriented Toolkit (C*oot*) is used for macromolecular model building and validation for protein modelling using X-ray data.

The superposition reveals that although the top surface of β-propellers is used for ubiquitin-binding, the residues participating in complex formation are not located on equivalent blades and form distinct patches on the protein surface. In contrast to Doa1 and Cdc48 β-propellers, the crystal structure of K. *lactis* Atg21 reveals several long and flexible loops on the top surface, implicating the possibility of loop-mediated interactions between Atg21 and Atg8 (Figure 4-13 (A)).

The residues 136-150 of ScAtg21, thought to be responsible for binding to Atg8, correspond to a highly conserved β-loop-β fragment, residues 88-102, in K. *lactis* Atg21, sharing 73% sequence similarity (Figure 4-14 (B)). This loop is well resolved in the crystal structure of K. *lactis* Atg21 and does not appear to be very flexible. The identified segment is not situated in a loop region, and Atg21 D146 could play an essential role in Atg8 binding, as seen in Figure 4-13.

The finding of only one site of interaction between Atg21 to Atg8 corelates well with the relatively weak K_d. If there were more interacting regions between Atg21 and Atg8 I would expect the K_d to be lower. This would also explain why Atg21 and Atg8 have not been purified in a complex. This could suggest the importance of Atg21 interacting with Atg16 in order to stabilise the binding with Atg8. Crosslinking experiments could help in further elucidating the interaction between Atg21 and Atg8.

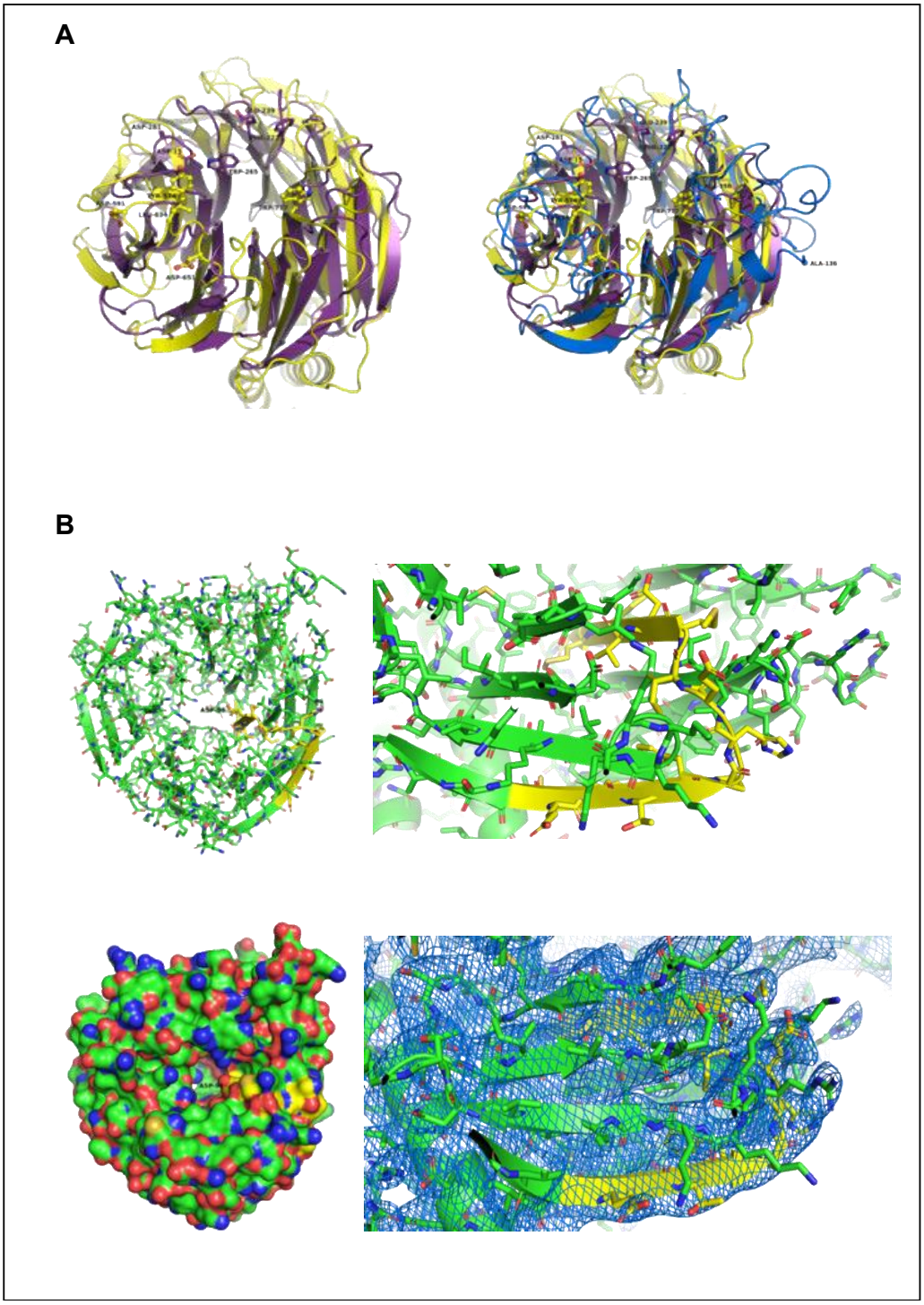

Figure 4-30: Structural modelling of Atg21.

(A) Left: Doa1, violet, and Cdc48, yellow, β-propeller (view from the "top" surface). Right: same as left plus K. lactis Atg21, blue. (B) K. lactis Atg21 structure, with the Atg21 fragment 88-102 coloured in yellow. Models were made using Coot by Dr Piotr Neumann.

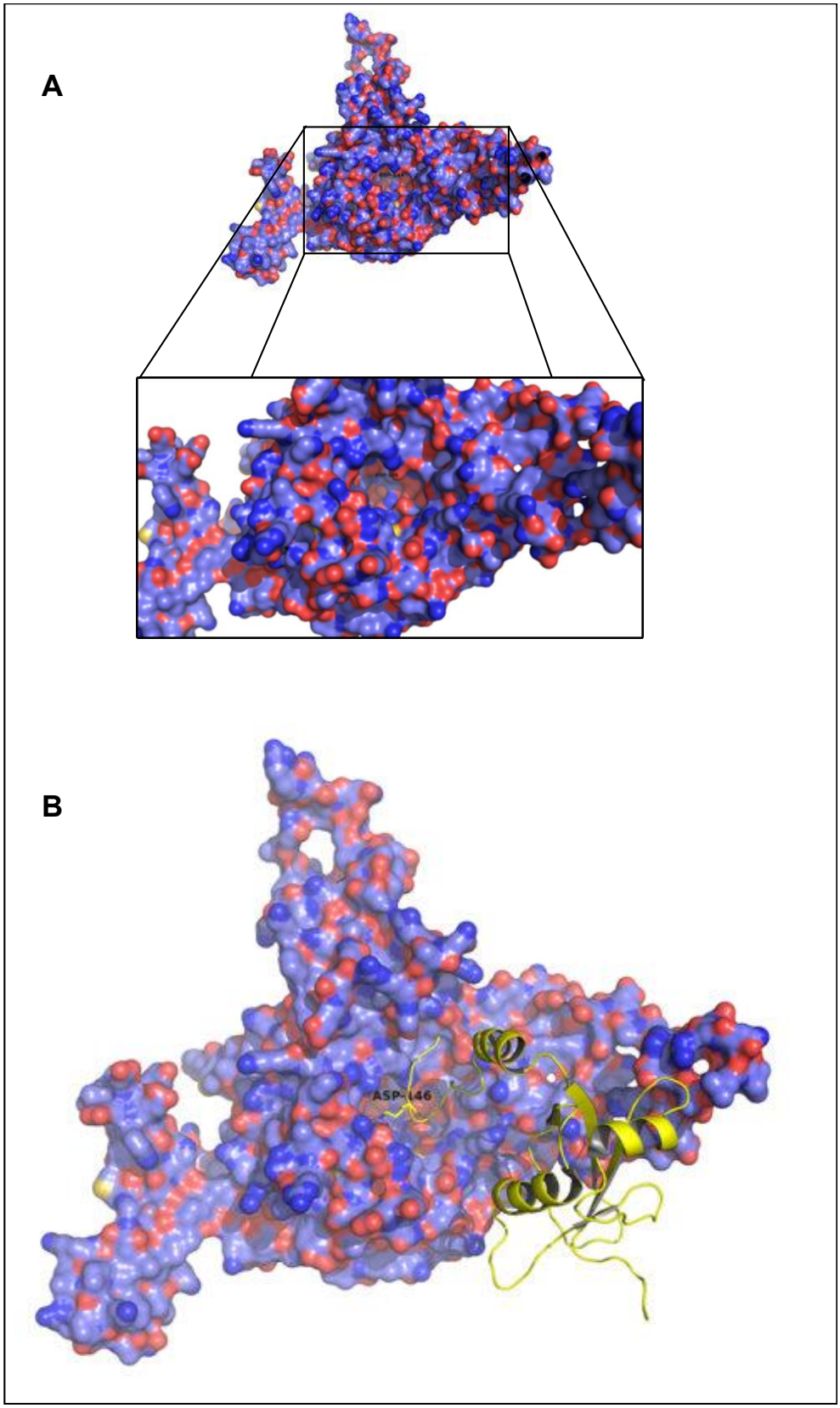

Figure 4-31: Modelling of Atg8.

(A) ScAtg8 with a magnified section showing the binding pocket. (B) Atg21 fragment, yellow, with aspartic acid at residue 146 in the binding pocket of Atg8. All models were made in Coot by Dr Piotr Neumann.

4.2.5 Atg8 and Atg21

The computational modelling of ScAtg8 and KlAtg21 agreed with our hypothesis that this fragment of Atg21 is vital for the binding to Atg8. We wanted to see if this would work using the physical proteins. ScAtg8 and KlAtg21 sample homology were checked using dynamic light scattering, assisted by Dr Achim Dickmann (Group of Prof. Dr R. Ficner, Molecular Structural Biology, Georg-August-University Göttingen).

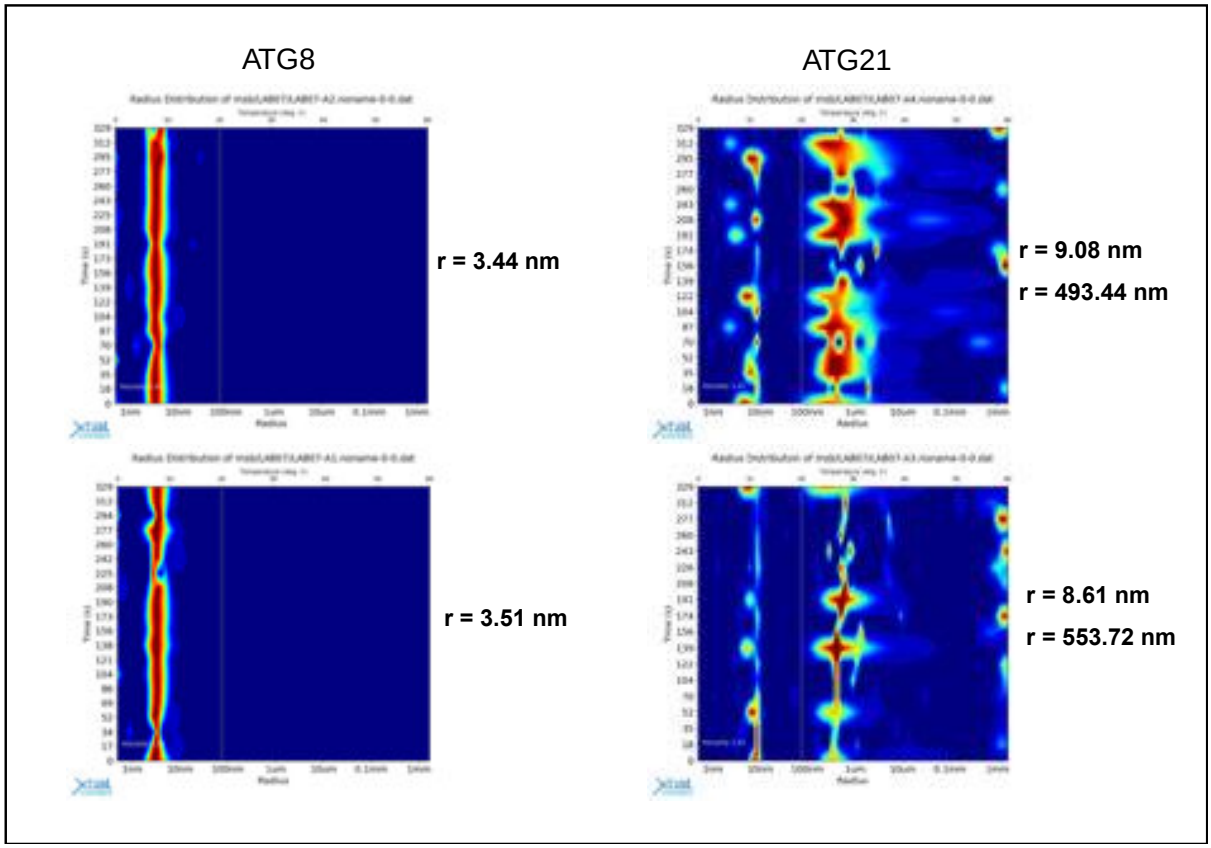

Figure 4-32: DLS of ScAtg8 and KlAtg21.

They are showing duplicate measurements of dynamic light scattering of ScAtg8 and KlAtg21 with the average radius of the molecules. Using the Xtal Concepts SpectroLight 600 was assisted by Dr Achim Dickmann.

The ScAtg8 samples looked very homogenous, with all the molecules being at a similar radius. Surprisingly, the KlAtg21 samples were not as homogenous, with two distinct bands at different radii. This could be due to the dimeric arrangement of Atg21 or that the sample still had contaminations or aggregates. Atg8 and Atg21 samples were then combined in a 1:1 and 2:1 ratio, respectively, and incubated for 5 mins before checking the samples again using DLS.

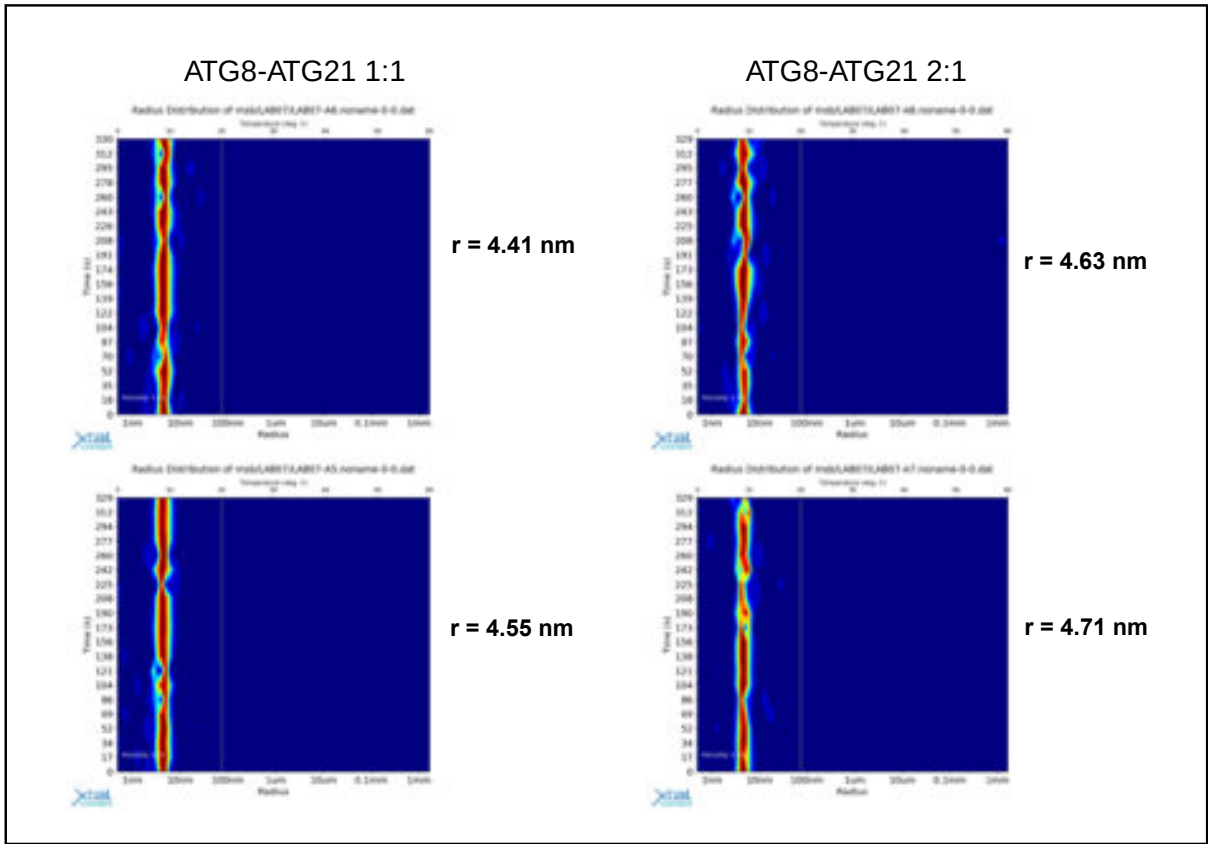

Figure 4-33: DLS of Atg8-Atg21 in 1:1 and 2:1 ratio.

The figure shows the duplicate dynamic light scattering experiments of ScAtg8 and KlAtg21 in a 1:1 and 2:1 ratio, respectively, with the average radius of the molecules. Using the Xtal Concepts SpectroLight 600 was assisted by Dr Achim Dickmann.

Interestingly, when ScAtg8 and KlAtg21 were combined together in a 1:1 and 2:1 ratio, respectively, the KlAtg21 sample appeared to stabilise. Each experiment led to a single band of molecules at a specific radius. When compared to S*c*Atg8 alone, there is an increase in radius of 1 nm when KlAtg21 was included. This indicates that the proteins interacted in solution as two separate bands were not seen supporting the possibility to get further insights by cross-linking.

4.3.1 Vacuolar Fragmentation

A member in our group, Dr Lisa Marquardt, has confirmed Atg18 plays a role in a novel type of retromer complex (Data not shown). Atg18 is an essential component of the core autophagic machinery. Additionally, it is known for regulating vacuolar morphology and in the recycling of vacuolar membrane proteins [148]. In yeast, the retromer complex consists of two subcomplexes: the cargo selective subcomplex (CSC) and a sorting nexin (SNX) dimer. The CSC is a trimer made up of Vps26, Vps29 and Vps35, and is essential for cargo selection

and sorting on the endosomal membrane. The SNX dimer is composed of Vps5 and Vps17 which are important in membrane remodelling. Another sorting nexin adaptor protein Snx3 also interacts with the CSC to regulate trafficking [210], [300]. All of these components are important for the recycling of cargo molecules from the endosome to the TGN. We aimed to determine which components of the retromer complex were responsible for vacuolar morphology.

Our unpublished data suggest a role of a complex composed of Atg18 and the CSC, but lacking the sorting nexins Vps5 and Vps17 in hyperosmotic stress induced vacuolar fragmentation. Thus fragmentation rates are measured in the respective deletion strains: *atg18Δ, vps35Δ, vps29Δ, vps26Δ, vps17Δ, vps5Δ, fab1Δ* and *snx3Δ.* The deletion strains missing an element of the retromer complex were grown in YPD until the log phase and stained with FM4-64 for 30 mins. Cells were then split, 50/50, into nutrient rich and hyperosmotic conditions and incubated for a further hour before imaging on the DeltaVision® microscope. 200 cells were imaged per condition, and analysis of the vacuoles was done using Fiji (seen in Figure 4-17).

As shown by Figure 4-17, the majority of deletion strains observed defects in vacuolar morphology irrespective of the osmotic stress. Where strains were either hyper-fragmented in both mediums or had very little vacuolar fragmentation. Except for *snx3Δ* that followed wildtype morphology.

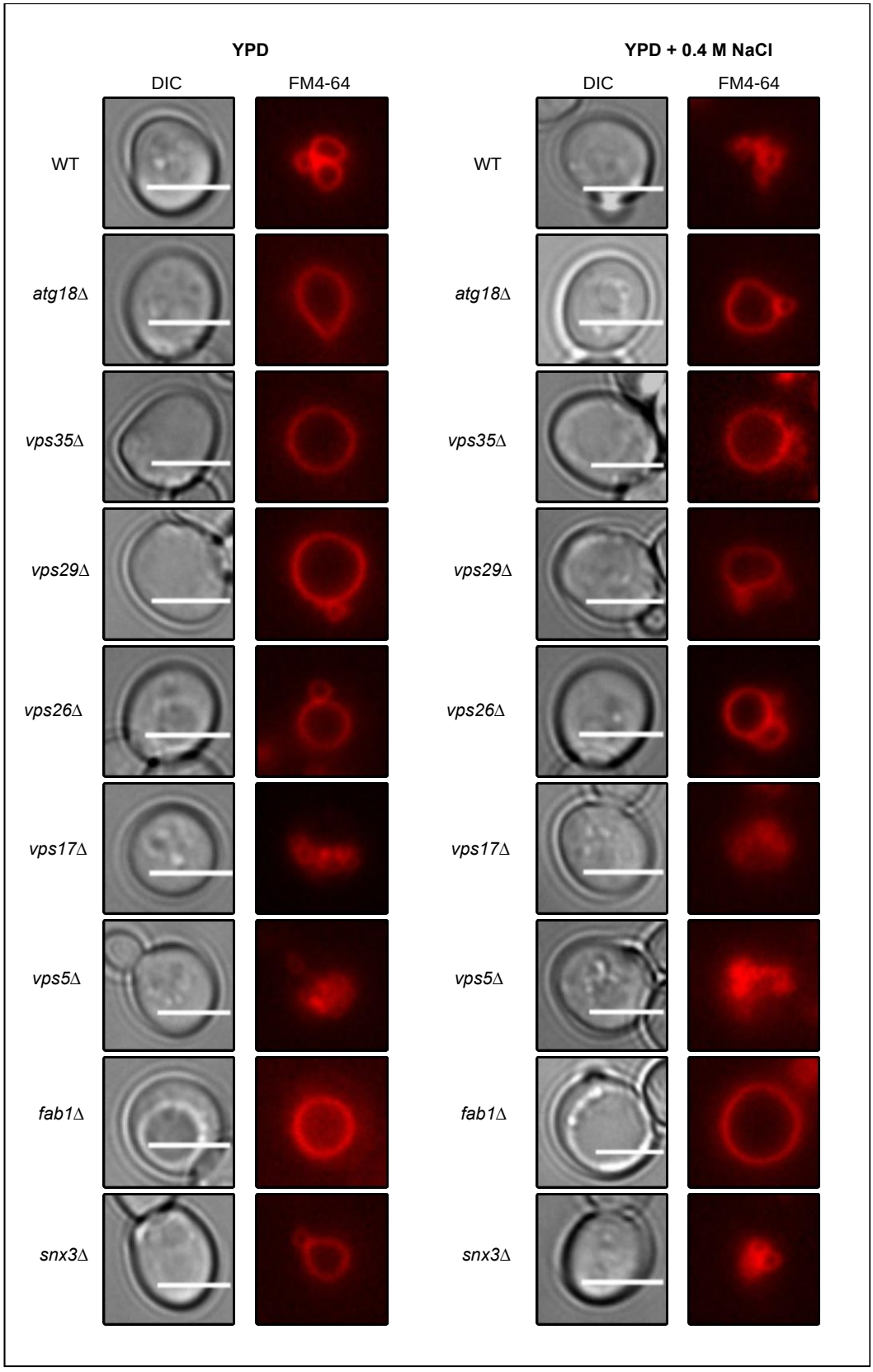

Figure 4-34: Vacuolar Fragmentation Images.

Yeast strains were grown in either YPD or YPD + 0.4 M NaCl and imaged using the DeltaVision®and showing DIC and FM4-64 images. 200 cells per condition were analysed using Fiji. The experiment was repeated three times and assisted by Florian Kramer.

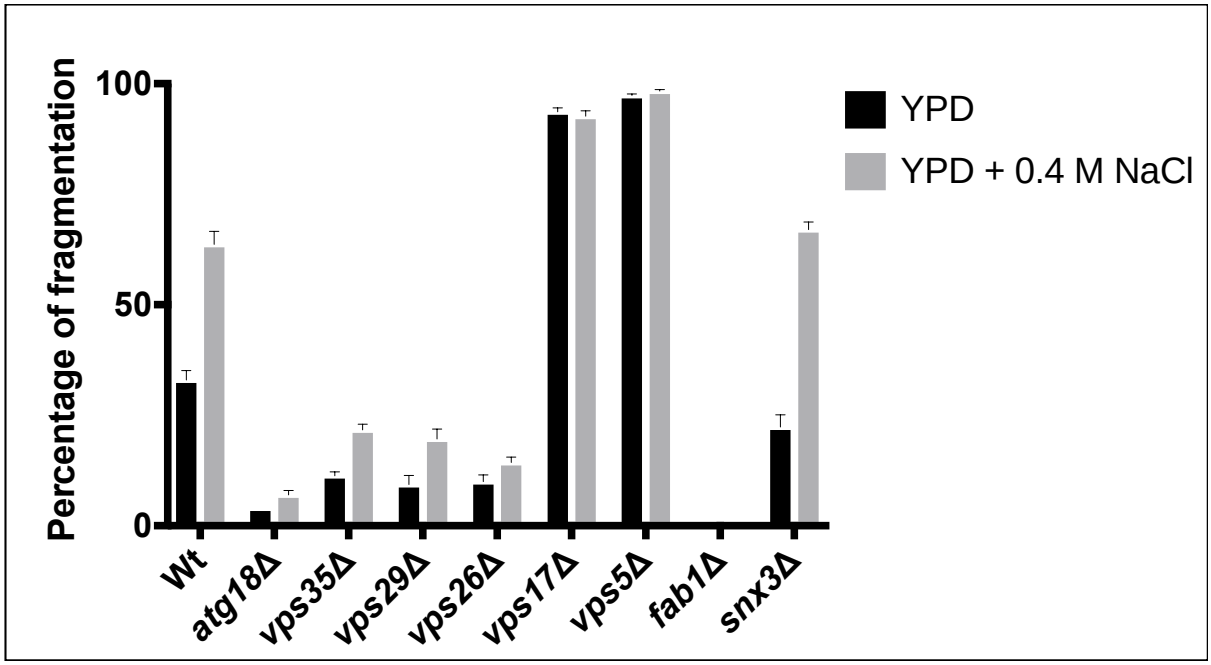

Figure 4-35: Vacuolar Fragmentation Analysis.

Bar graph showing the percentage of vacuolar fragmentation seen in each strain under each condition. Vacuolar fragmentation conditions were analysed on GraphPad Prism using a 2way ANOVA. All comparisons came back highly significant (****) except the comparison of Wt vs snx3Δ. Error bars show the standard error of the mean.

In agreement with published data, *atg18Δ* showed severe defects in vacuole fragmentation when compared to wildtype cells. Significant deficiencies in vacuolar fragmentation were also seen in CSC subcomplex components *vps35Δ, vps29Δ* and *vps26Δ* strains when compared to wildtype. On the contrary in the absence of the SNX-BAR subcomplex, *vps17Δ* and *vps5Δ* caused hyper-fragmentation of the vacuole before hyperosmotic stress; which indicates a general defect in vacuolar morphology. *snx3Δ* strain had similar vacuolar morphology to wildtype; this was to be expected as it has been previously described [301]. Defects in any components of the retromer complex cause altered vacuolar morphology compared to wildtype. Either they were severely lacking in fragmentation or completely hyper-fragmented. These observations strengthen our theory for the interaction between Atg18 and the retromer complex.

5. Discussion

In response to external environmental and internal homeostatic signals, cells must efficiently and successfully adapt to ensure survival during stress conditions. Autophagy is a highly conserved catabolic pathway that is vital for the development, cell survival and degradation of dysfunctional organelles and protein aggregates. Autophagy occurs in all eukaryotic cells [302], [303], underlying its importance. In this process, portions of the cytoplasm are sequestered within double-membrane vesicles known as autophagosomes. Autophagosomes form *de novo* within the cytoplasm to encompass the cargo. Autophagosomes fuse with the vacuole to release their cargo into the vacuolar lumen for degradation and recycling.

This study focused on the investigation of the molecular function of Hsv2, ascertaining how Atg21 binds to the ubiquitin-like protein Atg8 and determining the role of Atg18 within the retromer complex on vacuolar morphology. Firstly, to identify and characterise previously unknown interaction partners of Hsv2. Secondly, isolate and purify ScAtg8 for binding and crystallisation trails with KlAtg21. Lastly, knocking out components of the retromer complex to determine their role in regulating vacuolar morphology with Atg18.

An essential breakthrough in understanding the function of a protein within the cell is the identification of its interactome. Although PROPPINs are structurally well characterised, most of their functions remain elusive, especially in the case of Hsv2. For scaffold proteins such as the PROPPIN-family, which do not harbour an intrinsic enzymatic activity, it is crucial to understand their interactions in order to determine a function [127], [156], [160]. PROPPINs localise to various compartments within the cell, endosomes, vacuole, as well as the autophagic membrane; this suggests that they can exhibit a variety of potentially different functions [169]. This study primarily focused on the identification of interaction partners of Hsv2 to elucidate its role in cellular processes. Prior to this study, the only interacting partner identified of Hsv2 was Atg18 [169]. However, after a series of split ubiquitin assays and a BioID assay, we are able to expand the list of interacting proteins with Hsv2. The results obtained from these assays shed light on Hsv2 interacting with numerous SNAREs within the endosomal pathway and various transporters located at the vacuolar membrane.

5.1 Autophagic Function of Hsv2

Investigating the role of Hsv2 in unselective autophagy revealed that the absence of Hsv2 does not alter autophagic activity as the levels of matured Ape1 remained the same as wildtype. However, there does appear to be some cross-talk between the PROPPIN family. In the absence of Atg18 there should be no maturation of Ape1 as autophagy is completely blocked in this strain. In the double deletion *hsv2Δatg18Δ* there is no additional effect seen on the maturation of Ape1 as autophagy is blocked in the absence of Atg18. However, the double deletion *hsv2Δatg21Δ* strain showed a decrease in matured Ape1 compared to *atg21Δ* cells but only in the 2 hrs nitrogen starvation sample. This could be due to the Cvt pathway still being partially regulated via selective autophagy. Considering the PROPPINs share homology, in the absence of Atg21 it could be possible that Hsv2 partially substitutes in.

This hypothesis is further validated by the split ubiquitin assay. Where numerous Atg proteins were seen to interact with Hsv2, most notably Atg2, Atg8, Atg9, Atg13, Atg18 and Atg21. It has been well established that the Atg2-Atg18 complex is crucial for autophagosome formation and for the recycling of Atg9 [116], [127]. Atg2 is the largest protein in the autophagic core machinery and is essential for the localisation of Atg18 to the PAS. Recent studies have found that the loops of blade 2 and the 7AB loop on blade 7 of Atg18 are essential for binding with Atg2 and are required for the correct localisation of Atg2, as well as for autophagic flux [304]. Contrary to these results, it has also been observed that the deletion of the 7AB loop of Atg18 had no effect on its interaction with Atg2 [221]. In addition, mutations of the loops of blade 2 of Atg18 resulted in a significant decrease in binding to Atg2, confirming the importance of blade 2 of Atg18 in the binding to Atg2. A recent study has shown that the residues N78 and D100 on blade 2 of Hsv2 are required for binding to Atg2 and mutating one of these residues results in complete loss of binding [305]. Additionally, Bueno-Arribas *et al.,* show that Hsv2 mediates recruitment of a fraction of Atg2 to endosomes under basal conditions but not when autophagy is induced. Atg9 is the sole transmembrane protein among the core Atg proteins and is thought to provide the major source of membranes to the PAS for the formation of the isolation membrane [47], [116]. Atg9 localises to the expanding edge of the isolation membrane together with the Atg2-Atg18 complex. Shortly before the phagophore seals into an autophagosome, the Atg2-Atg18 complex

disassembles, leaving Atg18 on the outer membrane of the autophagosome, while Atg2 and Atg9 are recycled. The precise mechanism of how Atg9 is retrieved remains unclear but could require the retromer complex in conjunction with Atg18.

All PROPPINs are able to form an amphipathic α-helix in their 6CD loop, which can sense and induce membrane curvature. Both Atg18 and Atg21 localise to the edge of the growing phagophore but at distinct regions. Atg21 is restricted to the vacuole-phagophore contact site for the promotion of Atg8 lipidation, while Atg18 appears to be unequally distributed along the edge. It was found that in solution, PROPPINs are monomeric but upon binding to membranes they form oligomers [146], [306]. As all PROPPINs share homology, it would not be surprising if these oligomers contain different ratios of the three PROPPINs. Hsv2 is unable to fully take over another PROPPINs function as seen in the Ape1 assay but could potentially partially substitute in during oligomerisation, therefore aiding in membrane curvature or as a functional scaffold for other proteins to attach to.

5.1.1 Hsv2 in Selective Autophagy

A role for Hsv2 in selective autophagy was seen in PMN. During starvation for nitrogen, it was found that in *hsv2Δ* cells the micronucleophagic rate is reduced by approximately half of the wildtype rate [169]. More drastic reductions in micronucleophagic rate were seen in *atg18Δ* and *atg21Δ* cells, but this was the first time depletion of Hsv2 has been reported to affect autophagic activity. With more drastic reductions in PMN after deleting *ATG18* and *ATG21*, it is suggested that Hsv2 is required for efficient PMN activity but is not a crucial component of the micronucleophagic machinery. However, the absence of Hsv2 could affect vacuolar homeostasis and, as a secondary effect, PMN.

The split ubiquitin assay showed a strong interaction between Hsv2 and Atg13. Atg13 is a core autophagic protein that is crucial for both the Cvt pathway and autophagy. Under nitrogen starvation conditions, Atg13 interacts with Vac8 to form a protein complex on the vacuolar membrane. Interestingly, Vac8 also plays an important role in PMN, with direct interaction with Nvj1 mediating the formation of nucleus-vacuole contact sites [58]. The contact sites on Vac8 for interaction with Atg13 and Nvj1 share the same binding interface, and therefore

Atg13 and Nvj1 compete for binding with Vac8 [307]. This could potentially suggest a regulatory role for Hsv2 between macroautophagy and the microautophagic degradation of nuclear material. In the absence of Hsv2, Atg13 might outcompete Nvj1 for Vac8 binding and subsequently decreases the micronucleophagic rate.

Further involvement in selective autophagy could potentially occur in mitophagy, the selective process of mitochondrial degradation. The proteomic analysis of *hsv2Δ* cells compared to wildtype showed a down-regulation of *ATG33*, a mitochondrial mitophagy-specific protein. Unfortunately, the molecular mechanisms of Atg33 in mitophagy are poorly understood. Atg32 is a mitophagy-specific transmembrane protein on the outer membrane of the mitochondria. Typical for an autophagic cargo receptor, Atg32 interacts with Atg8 via the highly conserved W/YxxL/I motif in its cytosolic N-terminal region [31]. Atg32 further interacts with Atg11, a scaffold protein at the PAS; this interaction is mediated by the phosphorylation of Atg32 [308]. Atg33 is a polytopic mitochondrial outer membrane protein that was first identified as a factor required for stationary-phase mitophagy [309]. However, loss of Atg33 only blocked mitophagy to half the level of the wildtype during starvation, but it blocked mitophagy almost completely at the post-log phase. This suggests a specific role in quality-control signalling that identifies dysfunctional or aged mitochondria for mitophagy once cells have reached the post-log phase. Even though *ATG33* was greatly down-regulated in *hsv2Δ* cells, it is unlikely that Hsv2 is crucial for mitophagy but perhaps, like with PMN and the Cvt pathway, Hsv2 has a regulatory role that indirectly affects mitophagy.

5.1.2 Hsv2 in GOMED

GOMED was first described in 2016 as a form of alternative autophagy [173]. Hsv2 was observed to be essential for this process [180]. In *atg5Δhsv2Δ* cells there was a defect in processing GFP-pho8Δ60 compared to *atg5Δ* cells. Unexpectedly, this was not reproducible in our lab. Yamaguchi's lab gifted us the linearised plasmid they used for chromosomal integration of GFP-pho8Δ60. Additionally, both experiments used a SEY6210 background strain, ruling out the possibility of discrepancies between backgrounds. As the initial results were not reproducible we were unable to explore this process further.

5.2 Plasma Membrane to Endosomes Trafficking Involving Hsv2

The *trans*-SNARE complex at the plasma membrane consists of a combination of three proteins: Sso1/2, Sec9 and Snc1/2 [310]. The v-SNAREs Snc1 and Snc2 are 79% identical and are reported to be functionally redundant. The t-SNAREs Sso1 and its paralog Sso2, share 74% similarity, and were initially considered to be functionally redundant, although they have now been differentiated, with Sso1 playing a crucial role in sporulation [311]. An interaction between Hsv2 and Snc1, Sso1 and Tlg1 was observed in the split ubiquitin assay. These SNAREs function in the same recycling pathways, as shown in Figure 2-12. This strengthens the possibility that they are interacting partners of Hsv2.

Plasma membrane syntaxins, Sso1 and Sso2, together provide an essential function in vegetative cells, where they form a plasma membrane complex with the SNARE proteins Sec9 and Snc1/2 [312]–[314]. Sso1 is specifically required during sporulation, and this function cannot be provided by Sso2 [311]. Syntaxins belong to the t-SNARE subgroup, which are preferentially found on target membranes. In addition to the SNARE motif, syntaxins have an N-terminal domain that is made up of three shorter helices and a C-terminal transmembrane domain which is followed by a very short hydrophilic tail [315]. The N-terminal domain of Sso1 can interact with the SNARE motif and thus regulate the rate of SNARE complex assembly [316], [317]. Nicholson et al., 1998 showed that by truncating Sso1, lacking an N-terminal domain, complexes formed much more rapidly than full-length Sso1 with the regulatory N-terminal domain. In *S. cerevisiae,* the synaptobrevin homologues Snc1 and Snc2, the syntaxin 1 homologues Sso1 and Sso2, and the SNAP-25 homologue Sec9 form an analogous complex that mediates secretory vesicle fusion with the plasma membrane, see in Figure 2-12 [185], [310]. As an interaction between Hsv2 and Sso1 has been seen but not with Sso2, this suggests that Hsv2 could play an important role in sporulation and initiation of the prospore membrane; rather than the secretory pathway to the plasma membrane. It should be mentioned that the split ubiquitin assay was done using haploid cells and not diploid cells; knowing that the mechanisms of action differ between these, it may be beneficial to repeat this with diploid cells.

Snc1, a v-SNARE of secretory vesicles, cycles rapidly between the plasma membrane and endosomal/Golgi membranes and is required for fusion of secretory vesicles with the cell surface and is a widely studied endocytic cargo protein. The endocytosis of extracellular material and plasma membrane proteins is required to internalise nutrients, regulate the level of cell surface receptors, remove damaged proteins from the membrane, and recycle membrane proteins involved in exocytosis back to the secretory pathway. After Snc1 is delivered to the plasma membrane of the growing bud, it is rapidly internalised and transported to endosomal and Golgi compartments, where it is incorporated into new secretory vesicles [190]. For correct internalisation of Snc1 from the plasma membrane requires Yap1801 and Yap1802, acting as cargo-specific adaptors for the clathrin-mediated endocytosis of Snc1 [318]. Snc1 localises to the plasma membrane, sometimes restricted to the bud or generally to regions of polarised growth.

Snc1 is selectively incorporated into endocytic vesicles and becomes concentrated at the site of exocytosis [319], [320]. Snc1, a v-SNARE molecule, is a well-established retrograde cargo of the Snx4 pathway coming almost exclusively from the post-Golgi endosomes [321]. The SNX4-related subfamily of SNX-BARs is comprised of three members: Snx4/Atg24, Snx41 and Atg20/Snx42, which are proposed to function at early endosomes. Vps1, a dynamin-related GTPase, is required for retromer-dependent retrograde trafficking from the endosome, as well as proper trafficking of Snc1 a retrograde cargo of Snx4-Atg20 [322], [323]. A delay in fission activity has been seen in both Snx4 tubules, and Vps17 tubules in *vps1Δ* cells [320], suggesting that Vps1 promotes fission of SNX-BAR coated tubules from the endosome. The mechanism by which the Snx4-Atg20 recognises cargo is currently unclear. There are conflicting results on whether the Snx4 family and retromer SNX-BAR proteins operate on distinct populations [321], [324] or largely overlapping regions [320]. It has been suggested that the different SNX-BAR coated ETCs might mediate trafficking to distinct entry sites within the TGN, which would prevent the mixing of different cargo populations.

More recently, it has been shown that Snc1 is retrieved to the TGN via distinct, parallel pathways mediated by Snx4-Atg20, Rcy1/Drs2/COPI, and the retromer complex, as shown by Figure 5-1. In both *rcy1Δ* and *snx4Δ* cells, Snc1 was missorted along different stages of the recycling process. The *rcy1Δ* mutant caused accumulation at the vacuole, while the *snx4Δ*

mutant was able to retain Snc1 in intracellular compartments marked by Tlg1. In both single mutants, Snc1 recycling to the PM was unaffected. However, the double mutant *snx4Δrcy1Δ* nearly completely ablated recycling and most of Snc1 was localised to the vacuole. This phenotype was also seen in *vps35Δrcy1Δ* and *vps35Δsnx4Δ* double mutants, with Snc1 recycling completely defective in the triple mutant *snx4Δrcy1Δvps35Δ* [325]. These findings suggest that all three trafficking pathways are responsible for the recycling of Snc1. The results of the split ubiquitin assay suggest a strong interaction between Hsv2 and Snc1, a weak interaction with Snx4 and no interaction with Rcy1. This could indicate that Hsv2 is involved in the late stages of retrieval of Snc1 from the late endosome rather than from the TGN. Using a *hsv2Δ* strain transformed with GFP-Snc1 we could investigate if Snc1 accumulates at the vacuolar membrane. Additionally, whether the double deletions *hsv2Δsnx4Δ* or *hsv2Δvps25Δ* strains cause further defects in the recycling of Snc1.

Snc1 and Snc2 coimmunoprecipitated with Tlg1 and Tlg2 t-SNAREs, respectively [326]. These t-SNAREs confer retrograde protein transport from the cell surface and are required for Snc1 retrieval to the Golgi [190]. In cells lacking Tlg1 or Tlg2, Snc1 was unable to localise to the plasma membrane and accumulated on intracellular membranes, which may correspond to transport vesicles. Tlg1 is an unusual t-SNARE as it localises to multiple compartments and not just their resident membrane. An interaction was seen between Hsv2 and Tlg1 in the split ubiquitin assay; however, Hsv2 localises to late endosomes and the vacuolar membrane and not early endosomes or plasma membrane.

Tlg1 is a SNARE protein that localises to early endosomes and partially with the TGN [190], [327], [328]. Recently, Tlg1 was also found to colocalise with Snc1 [325]. Tlg1 is required for efficient degradation of the α factor receptor and for the retrieval of TGN resident proteins from the endocytic pathway [329]. All four endocytic syntaxins bind to the same v-SNARE Vti1 [330]. Tlg1 requires palmitoylation by Swf1; lack of palmitoylation results in its entry into MVBs and ultimately to its degradation in the vacuole. Nonacylated Tlg1 is recognised by the ubiquitin ligase Tul1 and becomes ubiquitinated, signalling entry into the MVB [331], [332]. Where and how these proteins interact needs to be explored further in order to understand a functional connection. It could be possible that Tlg1 and Snc1 are required for the correct localisation of Hsv2, and if we were to delete *TLG1* or *SNC1* we could see mislocalisation of

Hsv2. As SNARE proteins are important for the fusion of vesicles to membranes, it is unlikely that Hsv2 is required for the recycling of these SNAREs as a greater phenotype would be observed in the absence of Hsv2.

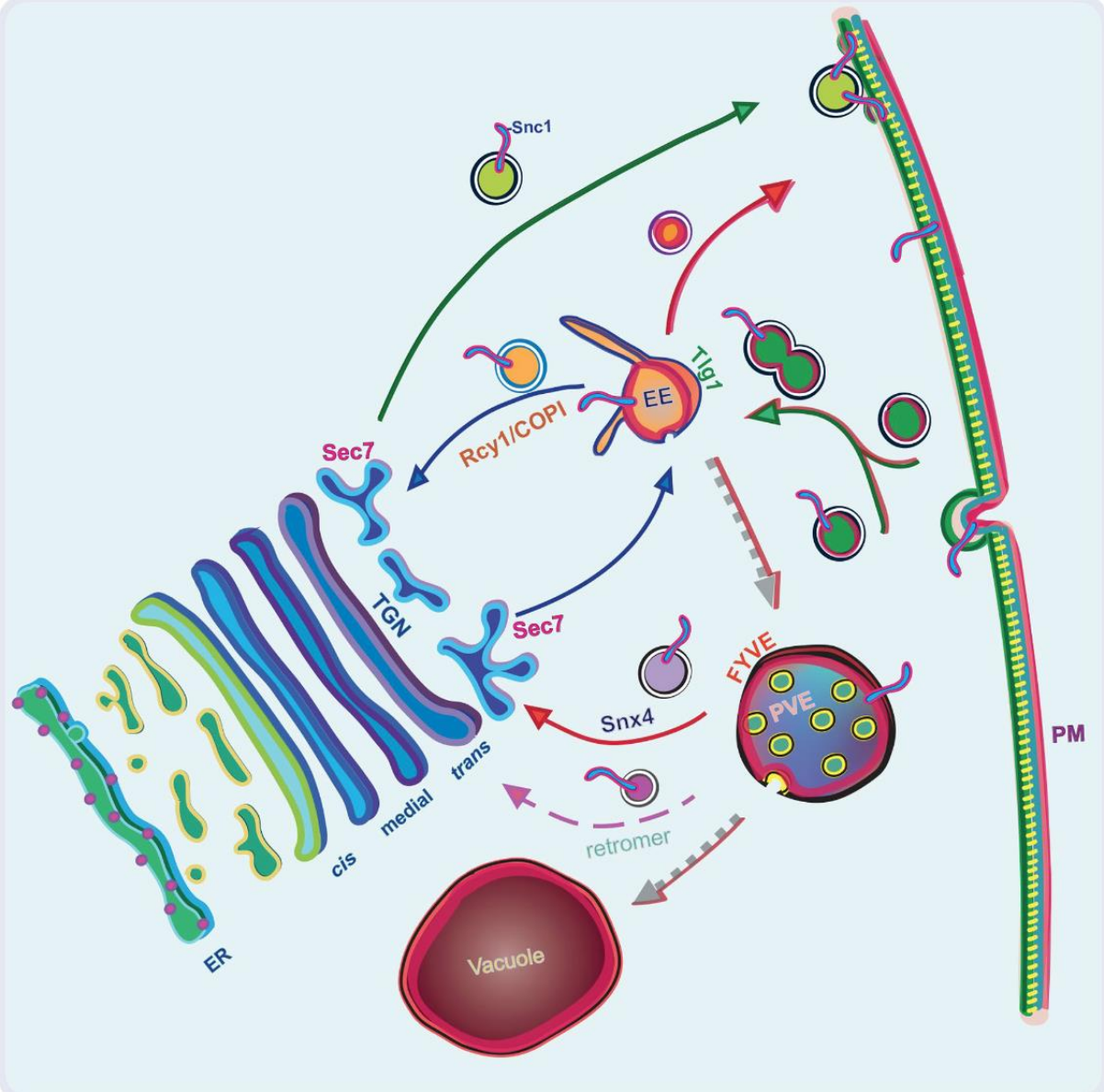

Figure 5-36: Cartoon schematic of the postendocytic recycling routes in yeast S. cerevisiae.

The main routes for Snc1 recycling include the Rcy1/COPI and Snx4 pathways. The cargoes are first packaged into Tlg1-positive early endosomes, where they are either selectively transported by Rcy1/COPI back to Sec7-positive TGN, directly recycled back to the PM, or remain in the early endosome as it matures into a PVE. At the PVE, specific cargoes are capable of retrieval by either the retromer complex or Snx4-dependant mechanisms. Taken from [325]

5.3 Late Endosomes to Vacuole Involving Hsv2

CPY is one of the many vacuolar hydrolases that are transported through the secretory pathway and can be easily monitored due to compartmental-specific posttranslational modifications. Following the translocation into the ER lumen, CPY is modified by the addition of four core oligosaccharides, generating the p1 precursor. As p1CPY moves through the Golgi complex, the core oligosaccharides are further modified by the addition of mannose residues, generating the Golgi-modified p2 precursor. p2CPY is then delivered to the vacuole, where its prosegment is cleaved, generating the mature vacuolar form of CPY [209].

In a proteomic analysis of wildtype cells vs *hsv2Δ* cells under nitrogen starvation conditions, it was found that after 8 hrs, the expression of the gene VPS15 was down-regulated in the *hsv2Δ* cells but after 24 hrs, it was up-regulated. However, no interaction between Hsv2 and Vps15 was observed in the split ubiquitin assay. Vps15 is a regulatory kinase in the class III PI3K complex involved in vacuolar protein sorting of CPY, general autophagic function and in pheromone signalling. Vps15 is composed of a kinase domain at its N-terminal for interaction with Vps34, a WD40 repeat region on the C-terminal or interacting with Vps30 and Atg14, and with a HEAT domain in the middle. Vps34 catalytic site is strongly influenced by the presence of Vps15, suggesting that Vps15 is essential in the assembly of the scaffolding complex [333]. Vps15 is thought to be the bridge between Vps34 and Atg14, whereby Vps15 communicates regulatory information from the Atg14-Vps30 subcomplex to Vps34. Electron microscopy studies have highlighted how conformational dynamics are a central feature of this complex. The catalytic domain of Vps34 undergoes a conformation change dislodging it from allosteric inhibition by the Vps15 kinase domain, which is required for maximum activity of Vps34 [333]. Although the split ubiquitin assay did not show an interaction between Hsv2 and Vps15, there was a mild interaction with Atg14 and Vps30/Atg6. This suggests that Hsv2 could interact with the PI3K complex I but does not come into contact with Vps15. CPY secretion was not observed in the absence of Atg18, Atg21 or Hsv2; however, overexpression of Atg21 lead to CPY secretion [169]. A recent study has shown that overexpression of Hsv2 caused CPY secretion to almost the same levels as *VPS13* deletion [305]. This suggests that Hsv2 does have a role in the endosomal trafficking pathway, however this could be due to the high level of redundancy of recycling pathways between the Golgi and endosomes.

Using the split ubiquitin assay, we saw a strong interaction between Hsv2 and the t-SNARE Pep12. Pep12 was the first member of the syntaxin family to be implicated in the transport to the vacuole from the Golgi and plasma membrane [329]. Pep12 is essential for the transport of luminal, but not membrane-bound, vacuolar hydrolases from the late Golgi to the vacuole [334]. The syntaxin-like t-SNARE may act as a receptor for the v-SNARE and allow transport vesicles to dock and fuse only with the appropriate target membrane [195]. Pep12 is also thought to be required for the closure of autophagosomes, with Vps21 and the CORVET complex. As Pep12 is recruited by Vps21, it is possible that the Vps21 module regulates a yet unknown step that follows autophagosome expansion and precedes closure. Following the internalisation of cargos, those destined for degradation continue to the pre-vacuolar endosome via *trans*-Golgi network-derived vesicles. The SNARE complex mediating this fusion step is thought to consist of the t-SNARE Pep12, Vti1 and Syn8 located on the pre-vacuolar compartment surface and the v-SNARE Ykt6 found on the TGN-derived vesicles [335]. Pep12 deletion has been shown to inhibit the transfer of vacuolar hydrolases from the Golgi to the vacuole but does not disrupt secretory protein transport [334]. Vti1 directly interacts with Pep12, as well as the intra-Golgi t-SNARE Sed5. Pep12 and Vti1 contribute to the formation of a functional SNAREpin with the t-SNARE Syn8 [330], [336]. Following the completion of the SNAREpin and the subsequent fusion of membranes, SNAREs need to be recycled from the pre-vacuolar endosomes before degradation in the vacuole.

Snx3 has been shown to be required for the recycling of Pep12 t-SNARE from the vacuolar membrane to the Golgi [321]; in the absence of Snx3, Pep12 accumulates on the vacuolar membrane. Within the same study, *vps5Δ and vps17Δ* cells showed a similar phenotype where Pep12 was accumulated on the vacuolar membrane. Although, these deletion strains have hyper fragmented vacuoles, and thus it is hard to determine what is vacuole and late endosomes. However, these results do suggest that the recycling of Pep12 is retromer dependent. It is still unclear if Pep12 is recognised by Snx3-retromer and relocated to SNX-BAR-retromer for recycling or how both these complexes are involved.

We have shown that Hsv2 affects the recycling of Pep12 in diploid cells but not haploid cells under nitrogen starvation conditions. Most studies investigating Pep12 recycling have seen

the accumulation of Pep12 on the vacuolar membrane and not within the vacuole lumen. With the confirmed interaction between Hsv2 and Vps35 via Co-IPs, this insinuates that like Atg18, Hsv2 can interact with the retromer cargo selection complex (CSC); explained in further detail in chapter 5.7. This could to be the mechanism by which Pep12 is recycled from late endosomes and the vacuolar membrane. However, further investigation needs to be done to determine why these mechanisms differ between haploid and diploid cells.

Hsv2 was also found to interact with Vps21 in the split ubiquitin assay. Vps21 localises to the PAS and is known for its role in early- to late-endosome transport [337], where *vps21Δ* mutant cells are defective in selective and nonselective autophagy, causing the accumulation of autophagosomal structures outside the vacuole. To accomplish its role in endocytosis, activated Vps21 recruits a group of factors that include CORVET, the tether Vac1, Pep12 and Vps45 [338], [339]. Mutations in all of the endocytic Vps21 downstream factors and the HOPS subunit cause defects in GFP-Atg8 and Ape1 processing under starvation conditions [340]. In endocytosis, Vps21 and Ypt7 function in a GTPase switch that coordinates two successive steps: early- to late-endosome maturation and the fusion of late endosomes with the vacuole, respectively [341], [342]. It has been suggested that autophagosomes require endocytic membranes in an early stage of their formation and therefore require the endosomal machinery for fusion with the vacuole. As Vps21 and Pep12 form a complex and both interact with Hsv2 in the split ubiquitin assay. This could suggest that either this complex regulates Hsv2 localisation at endosomes or that Hsv2 could have a redundant function involving the recycling of these proteins from the late endosome or vacuolar membrane. One of the difficulties of uncovering the potential function of Hsv2 with Vps21 and Pep12 is the variety of processes that is affected by these proteins. Discovering the site of interaction between these proteins and introducing mutations could help us determine the functional role of Hsv2 with Vps21 and Pep12.

Another SNARE that was found to interact with Hsv2 in the split ubiquitin assay was Vam3. Vam3 is a nonessential syntaxin required for homotypic fusion of vacuoles. Vam3 alone is sufficient to create vacuoles, which are thought to receive lipids via a specialised route from the Golgi [329], [343]. Together with the action of Rab GTPase Ypt7 and the HOPS tethering complex, the Vam3-Vti1-Vam7-Ykt6 SNARE bundle facilitates the efficient fusion of

autophagosomes with the vacuole [344]. In cells lacking Vam3, there was a defect in CPY trafficking where precursor CPY accumulated outside the vacuole.

All of these interactions suggest that Hsv2 could be important for the recycling of these SNAREs from the vacuolar membrane or late endosomes back to the TGN. There they can re-enter the autophagic pathway for CPY trafficking and autophagosome biogenesis. Alternatively, these SNAREs could be required for the correct localisation of Hsv2.

5.4 Cross-talk Between Autophagy and Sporulation

Autophagy and sporulation are both induced during stress conditions, and cells reprogram themselves by altering several cellular processes. It is known that the core Atg proteins are required for both autophagosome biogenesis and sporulation, but it is not clear how these Atg proteins are involved in the sporulation process [8], [345]. TOR is a negative regulator of both autophagy and sporulation, and it is unclear whether the effectors that repress autophagy are essential for sporulation or vice-versa. As rapamycin induces both autophagy and sporulation, it is very likely that these two processes share downstream proteins. Interestingly, when Atg13 is deleted, sporulation does not take place [255]. This suggests that Atg13 not only regulates autophagy via the Atg1 complex but also sporulation. In *S. pombe,* when diploid cells are cultivated in a medium lacking nitrogen, both autophagy and sporulation are induced [254]. Negative regulators of sporulation, including Yef3, Ald6 and Ego4 are degraded via autophagy suggesting that these two processes do take place simultaneously. Autophagy and sporulation both require the *de novo* formation of a double-layered structure. In the study by Matsuhara & Yamamoto, they observed that in *atg1Δ*, *atg7Δ* and *atg14Δ* strain in *S. pombe,* there was a defect in both autophagy and sporulation. Upon further investigation, these defects were specifically in SPB formation and elongation, which are necessary for PSM biogenesis. Sporulation requires the SNARE Sso1 for docking vesicles at MOP for PSM formation; Sso1 has also been shown to regulate Atg9 trafficking [121].

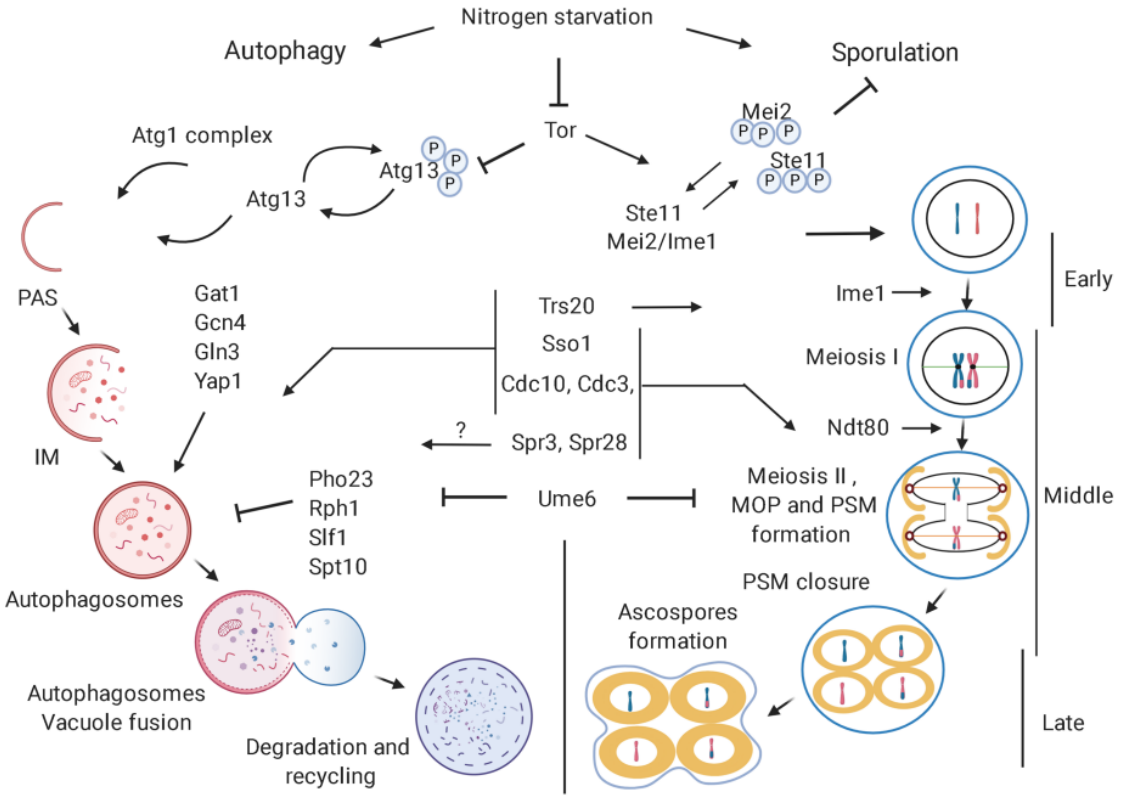

Figure 5-37: Cross-talk between Autophagy and Sporulation in yeast S. cerevisiae.

The left side represents the autophagic process, while the right side is sporulation. The inhibition of TOR promotes both autophagy and sporulation. In autophagy, the Atg1 complex recruits other proteins to the PAS to form the isolation membrane, which expands and captures cytosolic cargo. In sporulation, during the middle phase, MOP is formed, which leads to the biogenesis of the PSM. The PSM expands around the spindle pole bodies before fusing to complete the PSM. Modified from [346]

In vegetative cells, the fusion of post-Golgi secretory vesicles with the plasma membrane requires a SNARE complex formed by three components: Sso1/Sso2, Sec9, and Snc1/Snc2 [312], [314], [347]. Sso1/2 and Sec9 form a binary complex on the plasma membrane that interacts with Snc1/2 arriving with the vesicle to create the active fusogen [348]. Whereas at the prospore membrane, vesicle fusion requires Sso1, Snc1/2, and a sporulation-specific Sec9 paralog Spo20 [311]. The alteration of SNARE machinery by Spo20 seems to be the principal basis for diverting secretory vesicles to fuse with the prospore membrane instead of the plasma membrane.

The reduced levels of both D- and L-dityrosine in the spore wall of ascospores, the missorting of Pep12 and the sporulation defect observed in *hsv2Δ* diploid cells, would suggest Hsv2 plays an important role in sporulation. This could be in a similar way that Atg18 and Atg21 function in autophagy but on the PSM instead of the phagophore. As there are a lot of similarities

between these two processes, Hsv2's involvement would not be unexpected. Furthermore, if Hsv2 has a major role at the PSM, this can only occur in diploid cells, and so in haploid cells, we are potentially seeing secondary functions which would further the hypothesis that the PROPPINs can substitute in for one another when required.

5.5 Transporter Regulation with Hsv2

In fungi, phosphate is stored in the vacuolar lumen as polyphosphate. In *S. cerevisiae*, the vacuolar transporter chaperone (VTC) complex on vacuolar membranes synthesises polyphosphate into the vacuolar lumen using cytoplasmic ATP as a substrate [349]. The Vtc complex is enriched at the vacuolar membrane but also localises to other cellular compartments [285], [350]. All Vtc proteins contain three C-terminal transmembrane helices; Vtc1 is small and almost completely embedded in the membrane, whereas, Vtc2, Vtc3 and Vtc4 possess a large hydrophilic N-terminal domain that faces the cytosol [286]. Vtc proteins have also been implicated in several membrane-related processes, such as sorting of H^+ translocating ATPase, endocytosis, ER-Golgi trafficking, vacuole fusion and vacuolar polyphosphate homeostasis [350]–[352]. The interaction of calmodulin with the Vtc2 and Vtc3 is important in microautophagic vacuole invagination [353]. Vtc1 coprecipitated with Nvj1 and Sec18, suggesting a role in PMN and vesicle fusion with the vacuole, respectively [351]. Under nutrient limitation, the VTC complex is recruited to the vacuole along the autophagic tube, where it controls the distribution of membrane proteins over different compartments. Interactions have been seen between Hsv2 and Vtc1 in the split ubiquitin assay and Hsv2 and Vtc3 in the Bio ID. This further hints towards a regulatory role for Hsv2 in microautophagy. Whether Hsv2 is involved in the recycling of these components away from the vacuolar membrane and subsequently reducing the microautophagic rate, or if it potentially assists the VTC complex in compartmentalising these membrane proteins, is yet to be determined.

5.6 Hsv2 Involved in Sphingolipid Synthesis

The proteomic analysis of wildtype cells compared to *hsv2Δ* cells revealed that after 24 hrs of nitrogen starvation, *SKN1* is massively down-regulated when compared to wildtype. The

down-regulation of *SKN1* was not seen in the 8 hrs sample, suggesting that Hsv2 might be more important after prolonged starvation or stress conditions.

Skn1 has been shown to be a KRE6 homologue which is involved in the β-1,6-glucan biosynthesis, also, together with Ipt1, is involved in the biosynthesis of the sphingolipid class of mannosyl-di-inositol-phosphorylceremide ($M(IP)_2C$) from mannosyl-inositol-phosphorylceremide (MIPC) [354], [355]. The double deletion of *SKN1* and *KRE6* is lethal and causes deficiencies in cellular division, abnormal cell walls and decreased biofilm formation [356]. It has been suggested that both Skn1 and Ipt1 are negative regulators of autophagy, which could be mediated by sphingoid bases and might act in the same cascade as the PKA signalling pathway [357]. Although many factors involved in the biosynthesis of β-1,6-glucan have been identified, the mechanism of how this synthesis occurs remains unclear. Interestingly, Skn1 has been studied in cellular ageing of yeast *S. cerevisiae,* where they found that single deletions of either Skn1 or Ipt1 extended the chronological lifespan [358]. Each of these mutations caused the accumulation of excessive concentration of MIPC and impaired the synthesis of $M(IP)_2C$. It is unknown if MIPC plays a stimulatory role in regulating chronological lifespan and/or if $M(IP)_2C$ is a negative regulator of chronological lifespan.

The synthesis of sphingolipids was investigated to determine their involvement in autophagy. Using aureobasidin A (AbA), which inhibits inositol-phosphorylceremide (IPC) synthesis Yamagata et al., 2011 investigated various stages of autophagy to determine sphingolipid involvement. Nitrogen starvation conditions in combination with AbA treatment caused yeast cells to undergo rapid cell death. However, using a nitrogen- and carbon-deprived medium with AbA treatment did not induce apoptosis. Here, both the number and size of autophagic bodies was reduced in the presence of AbA treatment. A significant reduction in alkaline phosphatase activity was seen in cells treated with AbA. However, AbA treatment did not affect Atg12-Atg5 or Atg8-PE formation, vacuolar protease activity of Pep4 or Ape1, nor was the formation of the PAS affected [359]. These results imply that sphingolipids are components of the autophagosome membrane, but how these lipids are acquired or how they affect autophagosome formation, and autophagy progression is yet to be determined, as well as the role that Hsv2 has with sphingolipids. Trial experiments to confirm a change in Skn1 protein levels in *hsv2Δ* cells has so far been unsuccessful.

5.7 Atg8 & Atg21

Following the work from Dr Lena Munzel in investigating the role of Atg21 in the lipidation of Atg8, it was found that Atg21 during autophagy and the Cvt pathway organises the conjugation of Atg8 to PE at the autophagic membrane [360]. Atg21 recruits the Atg12-Atg5/Atg16 complex via the interaction with Atg16, and this interaction organises the E3-like Atg12-Atg5 conjugate within reach of the substrate E2-like enzyme Atg3. Atg21 localises to the autophagic membrane in a PI3P-dependant manner, and this positions the Atg8 lipidation complex in close proximity to PE [171]. More specifically, Atg21 is restricted to the phagophore edge near the vacuole, a region known as the vacuole isolation membrane contact site (VICS). Since PI3P is dispersed over the entire phagophore, additional mechanisms must restrict Atg21 to VICS; this restriction is thought to be due to the preferential binding to curved membranes. At the VICS, Vac8 was found to be enriched, while Vph1 was excluded [62]. Vac8 is a vacuolar membrane-associated protein involved in autophagy and is essential for the formation of NVJs in PMN [361], [362]. Whereas, Vph1 is a vacuolar ATPase required for the assembly of the ATPase V_0 domain and the activity of the vacuolar ATPase [363].

The crystal structure of Atg21 revealed that it folds into a seven-bladed β-propeller that exhibits a non-Velcro closure which has been observed for the other PROPPINs Atg18 and Hsv2 [146], [156], [162]. Munzel et al., 2021 solved the crystal structure of *K. lactis* Atg21 in complex with the *A. gossypii* Atg16 coiled-coil domain, in which the amino terminus of Atg16 points towards the PI3P binding sites of Atg21 and hence the membrane. In addition, the ScAtg16 residues I104, I108 and V112 were found to be essential for binding with ScAtg21. These same residues were reported to mediate the formation of a coat-like structure of Atg12-Atg5-Atg16 on the outer membrane of the phagophore [103], [114]. These observations suggest that Atg16 can either form a complex with Atg21 or part of a coat-like structure. The crystal structure also showed that the coiled-coil domain of one Atg16 dimer binds to two Atg21 molecules simultaneously, allowing for four PI3P binding sites for membrane association.

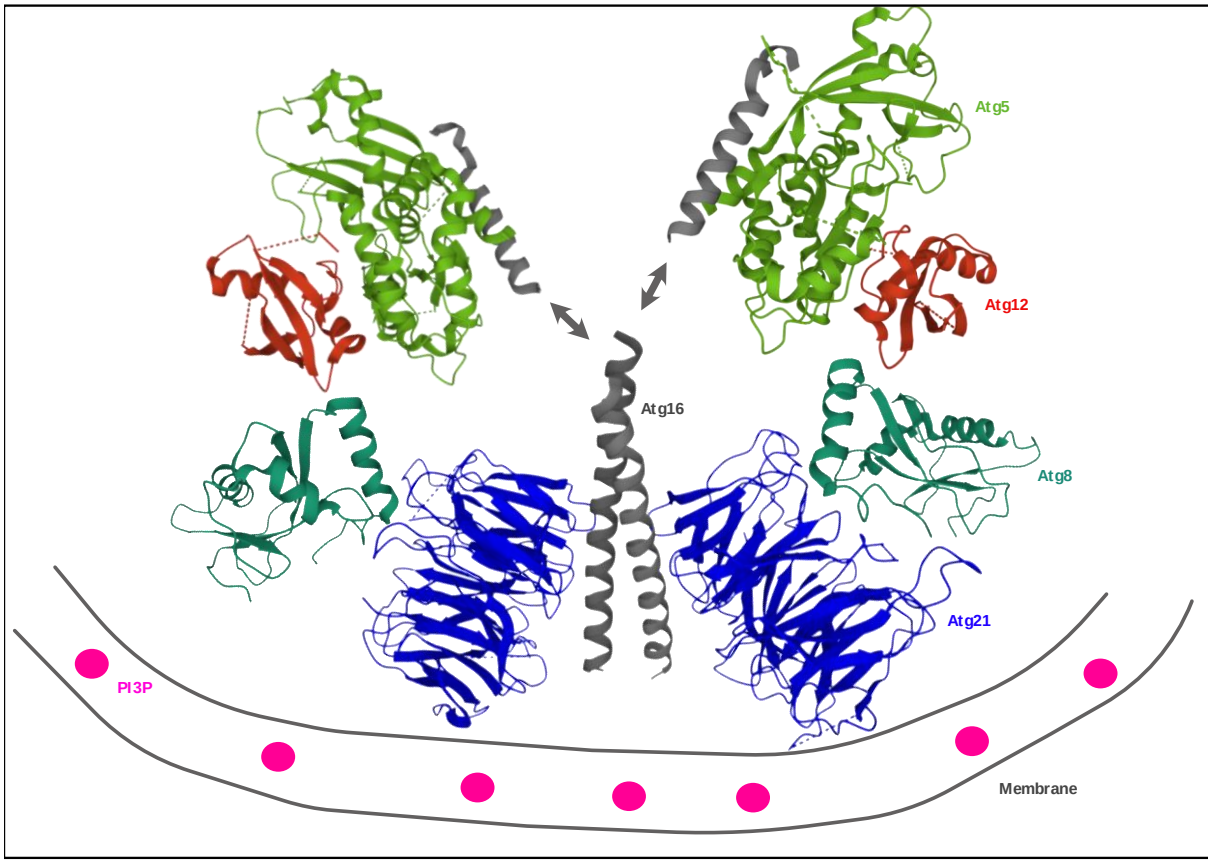

Figure 5-38: Hypothetical model for the assembly of the ubiquitin-like conjugation system at the membrane.

Proposed model of the spatial arrangement of the Atg8 lipidation complex. Superimposition of known crystal structures of Atg5 (green), Atg8 (teal), Atg12 (red), Atg16 (grey) and Atg21 (blue). The proposed binding of the complex to the concave side of PI3P positive membranes. Modified from [364].

The structure of the Atg16-Atg21 complex shows that the bottom side of the two Atg21 molecules are facing the Atg16 dimer in a reverse V shape, as shown in Figure 5-3. In contrast, Atg8 interacts with the top face of the Atg21 and the PI3P binding sites adjacent to the membrane. The computation modelling that Dr Piotr Neumann performed highlighted the D146 residue on Atg21 as vital for interacting with Atg8. D146 is located at the beginning of blade A at the entry of the central β-propeller channel, a site often involved in protein interaction [154]. This suggests that Atg8 interacts via its FK motif with the top face of the Atg21 propeller, where the D146 residue is required for the interaction. In the model proposed in Figure 5-3, Atg8 binds via the NHD-domain to the Atg21 propeller in an orientation such that the AIM-binding site of Atg8 faces away from the propeller. In this conformation, further interactions with Atg8 via the AIM-binding site can occur. The finding of only a single site of interaction between Atg21 and Atg8 correlate well with the weak binding affinity that was seen during the binding assays. This suggests the importance of

Atg21 binding to Atg16 in the Atg12-Atg5/Atg16 complex in order to stabilise Atg8 for conjugation with PE.

5.8 Atg18 and the Retromer Complex

Following the work from Dr Lisa Marquardt in investigating the role of Atg18 with the retromer complex, it was found that Atg18 interacts with Vps35, with both proteins localising to the endosomal membrane. Additionally, colocalisation experiments using confocal microscopy found 40% of Atg18-GFP puncta colocalised with Vps35-mCherry [221]. Following this, we wanted to determine the function of the retromer components on vacuolar morphology.

Cells that lack Vps5, missort and secrete soluble vacuolar proteins, contain fragmented vacuoles and mislocalise the CPY-sorting receptor, Vps10 [365]. Horazdovsky et al., 1997 found that the vast majority of CPY was missorted and secreted as the Golgi modified precursor p2CPY in *vps5Δ* cells. Vacuolar fragmentation was also seen in this study, although, Horazdovsky et al. suggested that this could be intermediates in vacuole biogenesis and not necessarily fragmentation of the vacuole. Regardless, these findings implicate Vps5 function, directly or indirectly, in the biogenesis or maintenance of vacuole morphology. These morphological defects were also seen in *vps17Δ* cells [209]. We observed hyperfragmentation of the vacuole in both *vps5Δ* and *vps17Δ* cells in nutrient rich and hyperosmotic conditions. This suggests that vacuolar fragmentation in these strains is not dependant on stress conditions. Together, these results complement the observations we saw in vacuolar fragmentation in *vps5Δ* and *vps17Δ* cells.

Ypt7 is a central regulator of this system via interactions with effectors, including the HOPS and CORVET tethering factors that promote fusion of endosomes to vacuoles [366], [367]. Loss of Ypt7 function results in the accumulation of endosomes and fragmented vacuoles [368]. It has been shown that the retromer CSC binds independently to the Vps5/Vps17 subcomplex and to Ypt7 suggesting a possible explanation for the fragmented vacuoles seen in *vps5Δ* and *vps17Δ*. In the absence of the SNX subcomplex, CSC interferes with Ypt7 regulation of endosome and vacuole-tethering factors [217], [369].

The maintenance of the vacuolar compartment must be tightly regulated to ensure that cargo receptors and membrane-associated proteins are cycled back to complete another round of trafficking and are not accumulated on the vacuolar membrane. With the absence of the retromer CSC components, defects in vacuolar fragmentation were seen, as shown in Figure 4-18. The single deletions of each component resulted in very similar phenotypes, where vacuolar fragmentation was significantly reduced when compared to wildtype. This suggests that without one component of the CSC, the complex is unable to retrieve cargo. Dr Marquardt also observed an interaction between Atg18 with Vps26 but only in the presence of Vps35, suggesting that the retromer components help stabilise one another and subsequent interactions with cargo or membranes. This might be solely due to the inability to bind Atg18 without all CSC components being present, as Atg18 is essential for vacuolar fragmentation and without correct localisation of Atg18 to the vacuolar membrane, no fission activity is observed. The CSC complex has a tendency to oligomerise which supports the formation of tubular endosomal carriers. If the CSC oligomerises when Atg18 is bound, this would concentrate multiple copies of Atg18 to a small area. With the hydrophobic 6CD loop of Atg18 forming a amphipathic α-helix when in contact with lipids, the concentration of several of these helices would be expected to enhance the curvature of the bilayer, making fission more efficient.

The sorting nexins performed very differently, with both *vps5Δ* and *vps17Δ* cells having hyper fragmented vacuoles in both nutrient-rich and hyperosmotic stress conditions when compared to wildtype. This could suggest a competitive binding for the CSC from Atg18 and the SNX-BAR proteins. Which would mean that the fission activity is regulated from both complexes. The Atg18-CSC is required for efficient fission of the vacuole under hyperosmotic stress. Conversely, the binding of SNX-BAR to CSC would reduce the fission activity as Atg18 can no longer bind to the CSC. A recent study by Courtellement et al., 2021, termed the complex between Atg18 and the retromer complex as CROP. Where CROP integrates Atg18 with part of the endosome- and vacuole-associated retromer complex to generate a membrane fission device of much higher potency. In the same study, it was found that the SNX-BAR subcomplex interferes with CROP formation or stability and directly competes with Atg18 for binding with the retromer complex [370]. In line with our results, when the SNX-

BAR proteins are absent, there is no competition of binding to the retromer complex, allowing for Atg18 binding with the CSC in the CROP complex to promote fission. This confirms the importance of Atg18, the CSC and the SNX-BAR proteins Vps5 and Vps17 in regulating vacuolar morphology.

6. Conclusion and Outlook

The main aim of this study was to discover previously unknown interaction partners of Hsv2. Several appealing and promising candidates were identified using the BioID with SILAC and split ubiquitin assays. Several of these candidates were further validated using Co-IPs, confirming the results from the assays. This provided us with novel insight into the potential function of Hsv2 in the recycling of SNARE and transporter proteins from the late endosome or vacuolar membrane. Further investigation is required to determine the role of Hsv2 in the recycling of these proteins and which transport pathways can interact with Hsv2. With the confirmation that Hsv2 interacts with Vps35, further experimentation should be done to understand the functional role of Hsv2 with the retromer complex.

There are striking similarities between the biogenesis of the autophagosome and the prospore membrane. With Atg18 and Atg21 having distinct roles at the autophagosome, it would be interesting to investigate if Hsv2 has a similar function at the prospore membrane. In addition, the missorting of Pep12 in diploid but not haploid cells suggests further investigation in diploid cells is required to understand the functional role of Hsv2.

The binding assays for Atg21 and Atg8 provided further evidence that the residue D146 of Atg21 is crucial for the binding to Atg8. This is strongly supported by the binding affinity of Atg21 and Atg8 being relatively weak, suggesting that there may only be one site of interaction. This supports the hypothesis that the interaction between Atg21 and Atg16 in the Atg12-Atg5/Atg16 complex is required to stabilise its interaction with Atg8 and its subsequent lipidation. We have planned a chemical crosslinking experiment with Prof. Henning Urlaub's group to further analyse the interaction between Atg21 and Atg8.

We also confirmed the importance of Atg18, the CSC and the SNX-BAR proteins, Vps5 and Vps17, of the retromer complex in regulating vacuolar morphology. Without a component of

the CSC complex, Atg18 cannot promote fission activity on the vacuole, suggesting that the CSC complex is crucial for Atg18 fission activity. Conversely, without the SNX-BAR proteins, Atg18 has no competition for binding with the CSC complex, and therefore unregulated fission activity is seen. Alternatively, without the SNX-BAR proteins the CSC binds more Ypt7 and in this complex Ypt7 cannot mediate vacuolar fusion leading to fragmented vacuoles.

7. Bibliography

[1] X. Wen and D. J. Klionsky, 'An Overview of macroautophagy in yeast', *Anal Chem.*, vol. 25, no. 4, pp. 368–379, 2017.

[2] C. López-Otín and G. Kroemer, 'Hallmarks of Health', *Cell*, vol. 184, no. 1, pp. 33–63, 2021.

[3] D. J. Klionsky *et al.*, 'Autophagy in major human diseases', *EMBO J.*, vol. 40, no. 19, pp. 1–64, 2021.

[4] S. . Clark, 'Newborn mice studied with the electron mircroscope', *Biophys. Biochem. Cytol.*, vol. 3, no. 3, pp. 349–362, 1957.

[5] A. B. Novikoff, 'The proximal tubule cell in experimental hydronephrosis', *J. Biophys. Biochem. Cytol.*, vol. 6, no. 1, pp. 136–138, 1959.

[6] A. B. Novikoff and E. Essner, 'Cytolysomes and mitochondrial degeneration.', *J. Cell Biol.*, vol. 15, pp. 140–146, 1962.

[7] K. Takeshige, M. Baba, S. Tsuboi, T. Noda, and Y. Ohsumi, 'Autophagy in yeast demonstrated with proteinase-deficient mutants and conditions for its induction', *J. Cell Biol.*, vol. 119, no. 2, pp. 301–312, 1992.

[8] M. Thumm *et al.*, 'Isolation of autophagocytosis mutants of Saccharomyces cerevisiae', *FEBS Lett.*, vol. 349, no. 2, pp. 275–280, 1994.

[9] T. M. Harding, A. Hefner-Gravink, M. Thumm, and D. J. Klionsky, 'Genetic and phenotypic overlap between autophagy and the cytoplasm to vacuole protein targeting pathway', *J. Biol. Chem.*, vol. 271, no. 30, pp. 17621–17624, 1996.

[10] A. M. Cuervo, E. Knecht, S. R. Terlecky, and J. F. Dice, 'Activation of a selective pathway of lysosomal proteolysis in rat liver by prolonged starvation', *Am. J. Physiol. - Cell Physiol.*, vol. 269, no. 5 38-5, pp. 200–208, 1995.

[11] C. Murakami and M. Kaeberlein, 'Quantifying yeast chronological life span by outgrowth of aged cells', *J. Vis. Exp.*, no. 27, pp. 3–9, 2009.

[12] R. Biddick and E. T. Young, 'The disorderly study of ordered recruitment', *Yeast*, pp. 205–220, 2009.

[13] M. B. Toledano, A. Delaunay, B. Biteau, and D. Azevedo, *6 Oxidative stress responses in yeast*, no. May 2016. 2004.

[14] S. Hohmann, M. Krantz, and B. Nordlander, *Yeast Osmoregulation*, vol. 428, no. 07.

Elsevier Masson SAS, 2007.

[15] H. P. Nasheuer, R. Smith, C. Bauerschmidt, F. Grosse, and K. Weisshart, 'Initiation of eukaryotic DNA replication: Regulation and mechanisms', *Prog. Nucleic Acid Res. Mol. Biol.*, vol. 72, 2002.

[16] C. Brocard-Masson and B. Dumas, 'The fascinating world of steroids: S. cerevisiae as a model organism for the study of hydrocortisone biosynthesis', *Biotechnol. Genet. Eng. Rev.*, vol. 22, no. 1, pp. 213–252, 2006.

[17] E. Owsianowski, D. Walter, and B. Fahrenkrog, 'Negative regulation of apoptosis in yeast', *Biochim. Biophys. Acta - Mol. Cell Res.*, vol. 1783, no. 7, pp. 1303–1310, 2008.

[18] L. Miller-Fleming, F. Giorgini, and T. F. Outeiro, 'Yeast as a model for studying human neurodegenerative disorders', *Biotechnol. J.*, vol. 3, no. 3, pp. 325–338, 2008.

[19] R. Matuo *et al.*, 'Saccharomyces cerevisiae as a model system to study the response to anticancer agents', *Cancer Chemother. Pharmacol.*, vol. 70, no. 4, pp. 491–502, 2012.

[20] A. Goffeau *et al.*, 'Life with 6000 Genes', *Science (80-.).*, vol. 274, no. October, pp. 546–567, 1996.

[21] M. Knop *et al.*, 'Epitope tagging of yeast genes using a PCR-based strategy: More tags and improved practical routines', *Yeast*, vol. 15, no. 10 B, pp. 963–972, 1999.

[22] C. Janke *et al.*, 'A versatile toolbox for PCR-based tagging of yeast genes: New fluorescent proteins, more markers and promoter substitution cassettes', *Yeast*, vol. 21, no. 11, pp. 947–962, 2004.

[23] M. S. Longtine *et al.*, 'Additional modules for versatile and economical PCR-based gene deletion and modification in Saccharomyces cerevisiae', *Yeast*, vol. 14, no. 10, pp. 953–961, 1998.

[24] J. Strathern, E. Jones, and J. Broach, 'The molecular biology of the yeast saccharomyces: Life cycle and inheritance', *Trends Biochem. Sci.*, vol. 7, no. 9, p. 339, 1981.

[25] J. S. Park and A. M. Neiman, 'VPS13 regulates membrane morphogenesis during sporulation in Saccharomyces cerevisiae', *J. Cell Sci.*, vol. 125, no. 12, pp. 3004–3011, 2012.

[26] M. Baba, K. Takeshige, N. Baba, and Y. Ohsumi, 'Ultrastructural analysis of the autophagic process in yeast: Detection of autophagosomes and their

characterization', *J. Cell Biol.*, vol. 124, no. 6, pp. 903–913, 1994.

[27] K. Takeshige, M. Baba, S. Tsuboi, T. Noda, and Y. Ohsumi, 'Autophagy in yeast demonstrated with proteinase-deficient mutants and conditions for its induction', *J. Cell Biol.*, vol. 119, no. 2, pp. 301–312, 1992.

[28] Z. Xie, U. Nair, and D. J. Klionsky, 'Atg8 Controls Phagophore Expansion during Autophagosome Formation', *Mol. Biol. Cell*, vol. 18, no. August, pp. 3250–3263, 2008.

[29] J. Geng, M. Baba, U. Nair, and D. J. Klionsky, 'Quantitative analysis of autophagy-related protein stoichiometry by fluorescence microscopy', *J. Cell Biol.*, vol. 182, no. 1, pp. 129–140, 2008.

[30] J. C. Farré, R. Manjithaya, R. D. Mathewson, and S. Subramani, 'PpAtg30 tags peroxisomes for turnover by selective autophagy.', *Dev. Cell*, vol. 14, no. 3, pp. 365–376, 2008.

[31] K. Okamoto, N. Kondo-Okamoto, and Y. Ohsumi, 'Mitochondria-Anchored Receptor Atg32 Mediates Degradation of Mitochondria via Selective Autophagy', *Dev. Cell*, vol. 17, no. 1, pp. 87–97, 2009.

[32] S. Schuck, C. M. Gallagher, and P. Walter, 'ER-phagy mediates selective degradation of endoplasmic reticulum independently of the core autophagy machinery', *J. Cell Sci.*, vol. 127, no. 18, pp. 4078–4088, 2014.

[33] C. Kraft, A. Deplazes, M. Sohrmann, and M. Peter, 'Mature ribosomes are selectively degraded upon starvation by an autophagy pathway requiring the Ubp3p/Bre5p ubiquitin protease', *Nat. Cell Biol.*, vol. 10, no. 5, pp. 602–610, 2008.

[34] H. Nakatogawa, Y. Ichimura, and Y. Ohsumi, 'Atg8, a Ubiquitin-like Protein Required for Autophagosome Formation, Mediates Membrane Tethering and Hemifusion', *Cell*, vol. 130, no. 1, pp. 165–178, 2007.

[35] V. Rogov, V. Dötsch, T. Johansen, and V. Kirkin, 'Interactions between Autophagy Receptors and Ubiquitin-like Proteins Form the Molecular Basis for Selective Autophagy', *Mol. Cell*, vol. 53, no. 2, pp. 167–178, 2014.

[36] K. Søreng, T. P. Neufeld, and A. Simonsen, 'Membrane Trafficking in Autophagy', *Int. Rev. Cell Mol. Biol.*, vol. 336, pp. 1–92, 2018.

[37] K. Suzuki, C. Kondo, M. Morimoto, and Y. Ohsumi, 'Selective transport of α-mannosidase by autophagic pathways: Identification of a novel receptor, Atg34p', *J. Biol. Chem.*, vol. 285, no. 39, pp. 30019–30025, 2010.

[38] A. Gubas and I. Dikic, ‘A guide to the regulation of selective autophagy receptors’, *FEBS J.*, vol. 289, no. 1, pp. 75–89, 2022.

[39] J. C. Farré, A. Burkenroad, S. F. Burnett, and S. Subramani, ‘Phosphorylation of mitophagy and pexophagy receptors coordinates their interaction with Atg8 and Atg11’, *EMBO Rep.*, vol. 14, no. 5, pp. 441–449, 2013.

[40] T. Kanki, K. Wang, Y. Cao, M. Baba, and D. J. Klionsky, ‘Atg32 Is a Mitochondrial Protein that Confers Selectivity during Mitophagy’, *Dev. Cell*, vol. 17, no. 1, pp. 98–109, 2009.

[41] K. Mochida *et al.*, ‘Receptor-mediated selective autophagy degrades the endoplasmic reticulum and the nucleus’, *Nature*, vol. 522, no. 7556, pp. 359–362, 2015.

[42] S. V. Scott, J. Guan, M. U. Hutchins, J. Kim, and D. J. Klionsky, ‘Cvt19 is a receptor for the cytoplasm-to-vacuole targeting pathway’, *Mol. Cell*, vol. 7, no. 6, pp. 1131–1141, 2001.

[43] T. Shintani, W. P. Huang, P. E. Stromhaug, and D. J. Klionsky, ‘Mechanism of cargo selection in the cytoplasm to vacuole targeting pathway’, *Dev. Cell*, vol. 3, no. 6, pp. 825–837, 2002.

[44] C. Kraft, M. Peter, and K. Hofmann, ‘Selective autophagy: Ubiquitin-mediated recognition and beyond’, *Nat. Cell Biol.*, vol. 12, no. 9, pp. 836–841, 2010.

[45] M. Yuga, K. Gomi, D. J. Klionsky, and T. Shintani, ‘Aspartyl aminopeptidase is imported from the cytoplasm to the vacuole by selective autophagy in Saccharomyces cerevisiae’, *J. Biol. Chem.*, vol. 286, no. 15, pp. 13704–13713, 2011.

[46] M. U. Hutchins and D. J. Klionsky, ‘Vacuolar Localization of Oligomeric α-Mannosidase Requires the Cytoplasm to Vacuole Targeting and Autophagy Pathway Components in Saccharomyces cerevisiae’, *J. Biol. Chem.*, vol. 276, no. 23, pp. 20491–20498, 2001.

[47] F. Reggiori, K. Tucker, P. E. Stromhaug, and D. J. Klionsky, ‘The Atg1-Atg13 complex regulates Atg9 and Atg23 retrieval transport from the pre-autophagosomal structure’, *Dev. Cell*, vol. 6, no. 1, pp. 79–90, 2004.

[48] M. Mari, J. Griffith, E. Rieter, L. Krishnappa, D. J. Klionsky, and F. Reggiori, ‘An Atg9-containing compartment that functions in the early steps of autophagosome biogenesis’, *J. Cell Biol.*, vol. 190, no. 6, pp. 1005–1022, 2010.

[49] C. He *et al.*, ‘Recruitment of Atg9 to the preautophagosomal structure by Atg11 is essential for selective autophagy in budding yeast’, *J. Cell Biol.*, vol. 175, no. 6, pp.

925–935, 2006.

[50] F. Reggiori, I. Monastyrska, T. Shintani, and D. J. Klionsky, 'The Actin Cytoskeleton Is Required for Selective Types of Autophagy, but Not Nonspecific Autophagy, in the Yeast Saccharomyces cerevisiae', *Mol. Biol. Cell*, vol. 16, no. November, pp. 5356–5372, 2005.

[51] I. Monastyrska, C. He, J. Geng, A. D. Hoppe, Z. Li, and D. J. Klionsky, 'Arp2 Links Autophagic Machinery with the Actin Cytoskeleton', *Mol. Biol. Cell*, vol. 18, no. May, pp. 3250–3263, 2008.

[52] D. Mijaljica, M. Prescott, and R. J. Devenish, 'Microautophagy in mammalian cells: Revisiting a 40-year-old conundrum', *Autophagy*, vol. 7, no. 7, pp. 673–682, 2011.

[53] M. Oku and Y. Sakai, 'Three Distinct Types of Microautophagy Based on Membrane Dynamics and Molecular Machineries', *BioEssays*, vol. 40, no. 6, pp. 1–6, 2018.

[54] J. A. Schäfer *et al.*, 'ESCRT machinery mediates selective microautophagy of endoplasmic reticulum in yeast', *EMBO J.*, vol. 39, no. 2, p. e102586, Jan. 2020.

[55] T. Sattler and A. Mayer, 'Cell-free reconstitution of microautophagic vacuole invagination and vesicle formation', *J. Cell Biol.*, vol. 151, no. 3, pp. 529–538, 2000.

[56] R. P. Bolender and E. R. Weibel, 'A morphometric study of the removal of phenobarbital-induced membranes from hepatocytes after cessation of treatment', *J. Cell Biol.*, vol. 56, no. 5, 1973.

[57] Y. Sakai, A. Koller, L. K. Rangell, G. a Keller, and S. Subramani, 'Peroxisome Degradation by Microautophagy in', *Cell*, vol. 141, no. 3, pp. 625–636, 1998.

[58] P. Roberts, S. Moshitch-Moshkovitz, E. Kvam, E. O'Toole, M. Winey, and D. S. Goldfarb, 'Piecemeal Microautophagy of Nucleus in Saccharomyces cerevisiae', *Mol. Biol. Cell*, vol. 13, no. January, pp. 4100–4109, 2003.

[59] I. Kiššova, B. Salin, J. Schaeffer, S. Bhatia, S. Manon, and N. Camougrand, 'Selective and non-selective autophagic degradation of mitochondria in yeast', *Autophagy*, vol. 3, no. 4, pp. 329–336, 2007.

[60] T. Van Zutphen *et al.*, 'Lipid droplet autophagy in the yeast Saccharomyces cerevisiae', *Mol. Biol. Cell*, vol. 25, no. 2, pp. 290–301, 2014.

[61] X. Pan *et al.*, 'Nucleus-vacuole junctions in Saccharomyces cerevisiae are formed through the direct interaction of Vac8p with Nvj1p', *Mol. Biol. Cell*, vol. 11, no. 7, pp. 2445–2457, 2000.

[62] L. Munzel *et al.*, 'Atg21 organizes Atg8 lipidation at the contact of the vacuole with the phagophore', *Autophagy*, vol. 17, no. 6, pp. 1458–1478, 2021.

[63] R. Krick *et al.*, 'Piecemeal Microautophagy of the Nucleus Requires the Core Macroautophagy Genes', *Mol. Biol. Cell*, vol. 20, no. October, pp. 2673–2683, 2008.

[64] F. B. Otto and M. Thumm, 'Mechanistic dissection of macro- and micronucleophagy', *Autophagy*, vol. 17, no. 3, pp. 626–639, 2021.

[65] T. Noda and Y. Ohsumi, 'Tor, a phosphatidylinositol kinase homologue, controls autophagy in yeast', *J. Biol. Chem.*, vol. 273, no. 7, pp. 3963–3966, 1998.

[66] Y. V. Budovskaya, J. S. Stephan, F. Reggiori, D. J. Klionsky, and P. K. Herman, 'The Ras/cAMP-dependent protein kinase signaling pathway regulates an early step of the autophagy process in Saccharomyces cerevisiae', *J. Biol. Chem.*, vol. 279, no. 20, pp. 20663–20671, 2004.

[67] Y. Fujioka *et al.*, 'Structural basis of starvation-induced assembly of the autophagy initiation complex', *Nat. Struct. Mol. Biol.*, vol. 21, no. 6, pp. 513–521, 2014.

[68] Y. Kamada, T. Funakoshi, T. Shintani, K. Nagano, M. Ohsumi, and Y. Ohsumi, 'Tor-mediated induction of autophagy via an Apg1 protein kinase complex', *J. Cell Biol.*, vol. 150, no. 6, pp. 1507–1513, 2000.

[69] Y. Kamada *et al.*, 'Tor Directly Controls the Atg1 Kinase Complex To Regulate Autophagy', *Mol. Cell. Biol.*, vol. 30, no. 4, pp. 1049–1058, 2010.

[70] Y. V. Budovskaya, J. S. Stephan, S. J. Deminoff, and P. K. Herman, 'An evolutionary proteomics approach identifies substrates of the cAMP-dependent protein kinase', *Proc. Natl. Acad. Sci. U. S. A.*, vol. 102, no. 39, pp. 13933–13938, 2005.

[71] J. S. Stephan, Y. Y. Yeh, V. Ramachandran, S. J. Deminoff, and P. K. Herman, 'The Tor and PKA signaling pathways independently target the Atg1/Atg13 protein kinase complex to control autophagy', *Proc. Natl. Acad. Sci. U. S. A.*, vol. 106, no. 40, pp. 17049–17054, 2009.

[72] N. Mizushima, T. Yoshimori, and Y. Ohsumi, 'The role of atg proteins in autophagosome formation', *Annu. Rev. Cell Dev. Biol.*, vol. 27, pp. 107–132, 2011.

[73] K. Suzuki, Y. Kubota, T. Sekito, and Y. Ohsumi, 'Hierarchy of Atg proteins in pre-autophagosomal structure organization', *Genes to Cells*, vol. 12, no. 2, pp. 209–218, 2007.

[74] Y. Rao, M. G. Perna, B. Hofmann, V. Beier, and T. Wollert, 'The Atg1-kinase complex

tethers Atg9-vesicles to initiate autophagy', *Nat. Commun.*, vol. 7, 2016.

[75] J. Sánchez-Wandelmer *et al.*, 'Atg4 proteolytic activity can be inhibited by Atg1 phosphorylation', *Nat. Commun.*, vol. 8, no. 1, pp. 1–9, 2017.

[76] M. J. Ragusa, R. E. Stanley, and J. H. Hurley, 'Architecture of the atg17 complex as a scaffold for autophagosome biogenesis', *Cell*, vol. 151, no. 7, pp. 1501–1512, 2012.

[77] G. Stjepanovic, C. W. Davies, R. E. Stanley, M. J. Ragusa, D. J. Kim, and J. H. Hurley, 'Assembly and dynamics of the autophagy-initiating Atg1 complex', *Proc. Natl. Acad. Sci. U. S. A.*, vol. 111, no. 35, pp. 12793–12798, 2014.

[78] L. H. Chew *et al.*, 'Molecular interactions of the Saccharomyces cerevisiae Atg1 complex provide insights into assembly and regulatory mechanisms', *Autophagy*, vol. 11, no. 6, pp. 891–905, 2015.

[79] H. Popelka and D. J. Klionsky, 'The molecular mechanism of Atg13 function in autophagy induction: What is hidden behind the data?', *Autophagy*, vol. 13, no. 3, pp. 449–451, 2017.

[80] H. Yamamoto *et al.*, 'The Intrinsically Disordered Protein Atg13 Mediates Supramolecular Assembly of Autophagy Initiation Complexes', *Dev. Cell*, vol. 38, no. 1, pp. 86–99, 2016.

[81] A. Matsuura, M. Tsukada, Y. Wada, and Y. Ohsumi, 'Apg1p, a novel protein kinase required for the autophagic process in Saccharomyces cerevisiae', *Gene*, vol. 192, no. 2, pp. 245–250, 1997.

[82] P. V. Schu, K. Takegawa, M. J. Fry, J. H. Stack, M. D. Waterfield, and S. D. Emr, 'Phosphatidylinositol 3-kinase encoded by yeast VPS34 gene essential for protein sorting', *Science (80-.).*, vol. 260, no. 5104, pp. 88–91, 1993.

[83] J. M. Backer, 'The regulation and function of Class III PI3Ks: Novel roles for Vps34', *Biochem. J.*, vol. 410, no. 1, pp. 1–17, 2008.

[84] A. Kihara, T. Noda, N. Ishihara, and Y. Ohsumi, 'Two distinct Vps34 phosphatidylinositol 3-kinase complexes function in autophagy and carboxypeptidase y sorting in Saccharomyces cerevisiae', *J. Cell Biol.*, vol. 153, no. 3, pp. 519–530, 2001.

[85] J. H. Stack, P. K. Herman, P. V. Schu, and S. D. Emr, 'A membrane-associated complex containing the Vps15 protein kinase and the Vps34 PI 3-kinase is essential for protein sorting to the yeast lysosome-like vacuole', *EMBO J.*, vol. 12, no. 5, pp. 2195–2204, 1993.

[86] J. H. Stack, D. B. DeWald, K. Takegawa, and S. D. Emr, 'Vesicle-mediated protein transport: Regulatory interactions between the Vps15 protein kinase and the Vps34 PtdIns 3-kinase essential for protein sorting to the vacuole in yeast', *J. Cell Biol.*, vol. 129, no. 2, pp. 321–334, 1995.

[87] S. Kametaka, T. Okano, M. Ohsumi, and Y. Ohsumi, 'Apg14p and Apg6/Vps30p form a protein complex essential for autophagy in the yeast, Saccharomyces cerevisiae', *J. Biol. Chem.*, vol. 273, no. 35, pp. 22284–22291, 1998.

[88] P. K. Herman, J. H. Stack, and S. D. Emr, 'A genetic and structural analysis of the yeast Vps15 protein kinase: Evidence for a direct role of Vps15p in vacuolar protein delivery', *EMBO J.*, vol. 10, no. 13, pp. 4049–4060, 1991.

[89] K. Obara and Y. Ohsumi, 'Atg14: A key player in orchestrating autophagy', *Int. J. Cell Biol.*, vol. 2011, 2011.

[90] A. C. Nascimbeni, P. Codogno, and E. Morel, 'Phosphatidylinositol-3-phosphate in the regulation of autophagy membrane dynamics', *FEBS J.*, vol. 284, no. 9, pp. 1267–1278, 2017.

[91] Ichimura Y *et al.*, 'A ubiquitin-like system mediates protein lipidation', *Nature*, vol. 408, no. 6811, pp. 488–92, 2000.

[92] T. Kirisako *et al.*, 'The reversible modification regulates the membrane-binding state of Apg8/Aut7 essential for autophagy and the cytoplasm to vacuole targeting pathway', *J. Cell Biol.*, vol. 151, no. 2, pp. 263–275, 2000.

[93] J. Kim, W. P. Huang, and D. J. Klionsky, 'Membrane recruitment of Aut7p in the autophagy and cytoplasm to vacuole targeting pathways requires Aut1p, Aut2p, and the autophagy conjugation complex', *J. Cell Biol.*, vol. 152, no. 1, pp. 51–64, 2001.

[94] I. Tanida *et al.*, 'Apg7p/Cvt2p: A novel protein-activating enzyme essential for autophagy', *Mol. Biol. Cell*, vol. 10, no. 5, pp. 1367–1379, 1999.

[95] I. Tanida, E. Tanida-Miyake, T. Ueno, and E. Kominami, 'The human homolog of Saccharomyces cerevisiae Apg7p is a protein-activating enzyme for multiple substrates including human Apg12p, GATE-16, GABARAP, and MAP-LC3', *J. Biol. Chem.*, vol. 276, no. 3, pp. 1701–1706, 2001.

[96] K. Suzuki, T. Kirisako, Y. Kamada, N. Mizushima, T. Noda, and Y. Ohsumi, 'The pre-autophagosomal structure organized by concerted functions of APG genes is essential for autophagosome formation', *EMBO J.*, vol. 20, no. 21, pp. 5971–5981, 2001.

[97] T. Hanada *et al.*, 'The Atg12-Atg5 conjugate has a novel E3-like activity for protein lipidation in autophagy', *J. Biol. Chem.*, vol. 282, no. 52, pp. 37298–37302, 2007.

[98] Noboru Mizushima *et al.*, 'A protein conjugation systemessential for autophagy', *Nature*, vol. 395, no. 6700, pp. 395–8, 1998.

[99] A. Kuma, N. Mizushima, N. Ishihara, and Y. Ohsumi, 'Formation of the ~350-kDa Apg12-Apg5·Apg16 multimeric complex, mediated by Apg16 oligomerization, is essential for autophagy in yeast', *J. Biol. Chem.*, vol. 277, no. 21, pp. 18619–18625, 2002.

[100] A. M. Taherbhoy *et al.*, 'Atg8 transfer from Atg7 to Atg3: A distinctive E1-E2 architecture and mechanism in the autophagy pathway', *Mol. Cell*, vol. 44, no. 3, pp. 451–461, 2011.

[101] T. Shintani, N. Mizushima, Y. Ogawa, A. Matsuura, T. Noda, and Y. Ohsumi, 'Apg10p, a novel protein-conjugating enzyme essential for autophagy in yeast', *EMBO J.*, vol. 18, no. 19, pp. 5234–5241, 1999.

[102] M. Yamaguchi *et al.*, 'Structural insights into Atg10-mediated formation of the autophagy-essential Atg12-Atg5 conjugate', *Structure*, vol. 20, no. 7, pp. 1244–1254, 2012.

[103] Y. Fujioka, N. N. Noda, H. Nakatogawa, Y. Ohsumi, and F. Inagaki, 'Dimeric coiled-coil structure of saccharomyces cerevisiae Atg16 and its functional significance in autophagy', *J. Biol. Chem.*, vol. 285, no. 2, pp. 1508–1515, 2010.

[104] N. Mizushima, T. Noda, and Y. Ohsumi, 'Apg16p is required for the function of the Apg12p-Apg5p conjugate in the yeast autophagy pathway', *EMBO J.*, vol. 18, no. 14, pp. 3888–3896, 1999.

[105] N. N. Noda, Y. Fujioka, T. Hanada, Y. Ohsumi, and F. Inagaki, 'Structure of the Atg12-Atg5 conjugate reveals a platform for stimulating Atg8-PE conjugation', *EMBO Rep.*, vol. 14, no. 2, pp. 206–211, 2013.

[106] Y. Cao, H. Cheong, H. Song, and D. J. Klionsky, 'In vivo reconstitution of autophagy in Saccharomyces cerevisiae', *J. Cell Biol.*, vol. 182, no. 4, pp. 703–713, 2008.

[107] C. Otomo, Z. Metlagel, G. Takaesu, and T. Otomo, 'Structure of the human ATG12~ATG5 conjugate required for LC3 lipidation in autophagy', *Nat. Struct. Mol. Biol.*, vol. 20, no. 1, pp. 59–66, 2013.

[108] S. E. Kaiser *et al.*, 'Noncanonical E2 recruitment by the autophagy E1 revealed by

Atg7-Atg3 and Atg7-Atg10 structures', *Nat. Struct. Mol. Biol.*, vol. 19, no. 12, pp. 1242–1249, 2012.

[109] H. Nakatogawa, 'Two ubiquitin-like conjugation systems that mediate membrane formation during autophagy', *Essays Biochem.*, vol. 55, no. 1, pp. 39–50, 2013.

[110] J. Romanov *et al.*, 'Mechanism and functions of membrane binding by the Atg5-Atg12/Atg16 complex during autophagosome formation', *EMBO J.*, vol. 31, no. 22, pp. 4304–4317, 2012.

[111] K. Harada *et al.*, 'Two distinct mechanisms target the autophagy-related e3 complex to the pre- autophagosomal structure', *Elife*, vol. 8, no. i, pp. 1–17, 2019.

[112] N. Kondo-Okamoto *et al.*, 'Autophagy-related protein 32 acts as autophagic degron and directly initiates mitophagy', *J. Biol. Chem.*, vol. 287, no. 13, pp. 10631–10638, 2012.

[113] T. Noda *et al.*, 'Apg9p/Cvt7p is an integral membrane protein required for transport vesicle formation in the Cvt and autophagy pathways', *J. Cell Biol.*, vol. 148, no. 3, pp. 465–479, 2000.

[114] A. Kaufmann, V. Beier, H. G. Franquelim, and T. Wollert, 'Molecular mechanism of autophagic membrane-scaffold assembly and disassembly', *Cell*, vol. 156, no. 3, pp. 469–481, 2014.

[115] Y. Ohashi and S. Munro, 'Membrane delivery to the yeast autophagosome from the golgi-endosomal system', *Mol. Biol. Cell*, vol. 21, no. 22, pp. 3998–4008, 2010.

[116] H. Yamamoto *et al.*, 'Atg9 vesicles are an important membrane source during early steps of autophagosome formation', *J. Cell Biol.*, vol. 198, no. 2, pp. 219–233, 2012.

[117] F. Reggiori, C.-W. Wang, U. Nair, T. Shintani, H. Abeliovich, and D. J. Klionsky, 'Early Stages of the Secretory Pathway, but Not Endosomes, Are Required for Cvt Vesicle and Autophagosome Assembly in Saccharomyces cerevisiae', *Mol. Biol. Cell*, vol. 14, no. December, pp. 5069–5081, 2004.

[118] C. He, M. Baba, Y. Cao, and D. J. Klionsky, 'Self-Interaction Is Critical for Atg9 Transport and Function at the Phagophore Assembly Site during Autophagy', *Mol. Biol. Cell*, vol. 20, no. December, pp. 2673–2683, 2008.

[119] F. Reggiori, T. Shintani, U. Nair, and D. J. Klionsky, 'Atg9 cycles between mitochondria and the pre-autophagosomal structure in yeasts.', *Autophagy*, vol. 1, no. 2, pp. 101–109, 2005.

[120] J. Geng, U. Nair, K. Yasumura-Yorimitsu, and D. J. Klionsky, 'Post-Golgi Sec Proteins Are Required for Autophagy in Saccharomyces cerevisiae', *Mol. Biol. Cell*, vol. 20, pp. 4524–4530, 2010.

[121] U. Nair *et al.*, 'SNARE proteins are required for macroautophagy', *Cell*, vol. 146, no. 2, pp. 290–302, 2011.

[122] M. Mari and F. Reggiori, 'Atg9 trafficking in the yeast Saccharomyces cerevisiae', *Autophagy*, vol. 3, no. 2, pp. 145–148, 2007.

[123] K. A. Tucker, F. Reggiori, W. A. Dunn, and D. J. Klionsky, 'Atg23 Is Essential for the Cytoplasm to Vacuole Targeting Pathway and Efficient Autophagy but Not Pexophagy', *J. Biol. Chem.*, vol. 278, no. 48, pp. 48445–48452, 2003.

[124] J. E. Legakis, W. L. Yen, and D. J. Klionsky, 'A cycling protein complex required for selective autophagy', *Autophagy*, vol. 3, no. 5, pp. 422–432, 2007.

[125] W. L. Yen, J. E. Legakis, U. Nair, and D. J. Klionsky, 'Atg27 Is Required for Autophagy-dependent Cycling of Atg9', *Mol. Biol. Cell*, vol. 18, no. December, pp. 986–994, 2007.

[126] S. W. Suzuki *et al.*, 'Atg13 HORMA domain recruits Atg9 vesicles during autophagosome formation', *Proc. Natl. Acad. Sci. U. S. A.*, vol. 112, no. 11, pp. 3350–3355, 2015.

[127] K. Obara, T. Sekito, K. Niimi, and Y. Ohsumi, 'The Atg18-Atg2 complex is recruited to autophagic membranes via phosphatidylinositol 3-phosphate and exerts an essential function', *J. Biol. Chem.*, vol. 283, no. 35, pp. 23972–23980, 2008.

[128] T. Shintani, K. Suzuki, Y. Kamada, T. Noda, and Y. Ohsumi, 'Apg2p Functions in Autophagosome Formation on the Perivacuolar Structure', *J. Biol. Chem.*, vol. 276, no. 32, pp. 30452–30460, 2001.

[129] S. R. Carlsson and A. Simonsen, 'Membrane dynamics in autophagosome biogenesis', *J. Cell Sci.*, vol. 128, no. 2, pp. 193–205, 2015.

[130] M. Graef, J. R. Friedman, C. Graham, M. Babu, and J. Nunnari, 'ER exit sites are physical and functional core autophagosome biogenesis components', *Mol. Biol. Cell*, vol. 24, no. 18, pp. 2918–2931, 2013.

[131] U. Nair *et al.*, 'A role for Atg8-PE deconjugation in autophagosome biogenesis', *Autophagy*, vol. 8, no. 5, pp. 780–793, 2012.

[132] H. Nakatogawa, J. Ishii, E. Asai, and Y. Ohsumi, 'Atg4 recycles inappropriately lipidated Atg8 to promote autophagosome biogenesis', *Autophagy*, vol. 8, no. 2, 2012.

[133] F. Reggiori and C. Ungermann, 'Autophagosome Maturation and Fusion', *J. Mol. Biol.*, vol. 429, no. 4, pp. 486–496, 2017.

[134] S. Abreu *et al.*, 'Conserved Atg8 recognition sites mediate Atg4 association with autophagosomal membranes and Atg8 deconjugation', *EMBO Rep.*, vol. 18, no. 5, pp. 765–780, 2017.

[135] E. Cebollero *et al.*, 'Phosphatidylinositol-3-phosphate clearance plays a key role in autophagosome completion', *Curr. Biol.*, vol. 22, no. 17, pp. 1545–1553, 2012.

[136] W. R. Parrish, C. J. Stefan, and S. D. Emr, 'Essential Role for the Myotubularin-related Phosphatase Ymr1p and the Synaptojanin-like Phosphatases Sjl2p and Sjl3p in Regulation of Phosphatidylinositol 3-Phosphate in Yeast', *Mol Biol Cell*, vol. 15, pp. 5318–5328, 2004.

[137] J. Cheng *et al.*, 'Yeast and mammalian autophagosomes exhibit distinct phosphatidylinositol 3-phosphate asymmetries', *Nat. Commun.*, vol. 5, pp. 1–10, 2014.

[138] R. S. Goody, M. P. Müller, and Y. W. Wu, 'Mechanisms of action of Rab proteins, key regulators of intracellular vesicular transport', *Biol. Chem.*, vol. 398, no. 5–6, pp. 565–575, 2017.

[139] R. Ho and C. Stroupe, 'The HOPS/class C Vps complex tethers membranes by binding to one Rab GTPase in each apposed membrane', *Mol. Biol. Cell*, vol. 26, no. 14, pp. 2655–2663, 2015.

[140] T. Darsow, S. E. Rieder, and S. D. Emr, 'A multispecificity syntaxin homologue, Vam3p, essential for autophagic and biosynthetic protein transport to the vacuole', *J. Cell Biol.*, vol. 138, no. 3, pp. 517–529, 1997.

[141] S. E. Rieder and S. D. Emr, 'A novel RING finger protein complex essential for a late step in protein transport to the yeast vacuole', *Mol. Biol. Cell*, vol. 8, no. 11, pp. 2307–2327, 1997.

[142] K. Meiling-Wesse, H. Barth, and M. Thumm, 'Ccz1p/Aut11p/Cvt16p is essential for autophagy and the cvt pathway', *FEBS Lett.*, vol. 526, no. 1–3, pp. 71–76, 2002.

[143] A. S. Polupanov, V. Y. Nazarko, and A. A. Sibirny, ' CCZ1 , MON1 and YPT7 genes are involved in pexophagy, the Cvt pathway and non-specific macroautophagy in the methylotrophic yeast Pichia pastoris ', *Cell Biol. Int.*, vol. 35, no. 4, pp. 311–319, 2011.

[144] U. D. Epple, I. Suriapranata, E. L. Eskelinen, and M. Thumm, 'Aut5/Cvt17p, a putative

lipase essential for disintegration of autophagic bodies inside the vacuole', *J. Bacteriol.*, vol. 183, no. 20, pp. 5942–5955, 2001.

[145] S. A. Teter, K. P. Eggerton, S. V. Scott, J. Kim, A. M. Fischer, and D. J. Klionsky, 'Degradation of lipid vesicles in the yeast vacuole requires function of Cvt17, a putative lipase', *J. Biol. Chem.*, vol. 276, no. 3, pp. 2083–2087, 2001.

[146] A. Scacioc, C. Schmidt, T. Hofmann, H. Urlaub, K. Kühnel, and Á. Pérez-Lara, 'Structure based biophysical characterization of the PROPPIN Atg18 shows Atg18 oligomerization upon membrane binding', *Sci. Rep.*, vol. 7, no. 1, pp. 1–15, 2017.

[147] P. E. Stromhaug, F. Reggiori, J. Guan, C.-W. Wang, and D. J. Klionsky, 'Atg21 Is a Phosphoinositide Binding Protein Required for Efficient Lipidation and Localization of Atg8 during Uptake of Aminopeptidase I by Selective Autophagy', *Mol. Biol. Cell*, vol. 16, no. 1, pp. 1–13, 2005.

[148] S. K. Dove *et al.*, 'Svp1p defines a family of phosphatidylinositol 3,5-bisphosphate effectors', *EMBO J.*, vol. 23, no. 9, pp. 1922–1933, 2004.

[149] R. Krick, J. Tolstrup, A. Appelles, S. Henke, and M. Thumm, 'The relevance of the phosphatidylinositolphosphat-binding motif FRRGT of Atg18 and Atg21 for the Cvt pathway and autophagy', *FEBS Lett.*, vol. 580, no. 19, pp. 4632–4638, 2006.

[150] H. K. W. Fong *et al.*, 'Repetitive segmental structure of the transducin', *Proc. Natl. Acad. Sci. U. S. A.*, vol. 83, no. 7, pp. 2162–2166, 1986.

[151] T. F. Smith, C. Gaitatzes, K. Saxena, and E. J. Neer, 'The WD repeat: A common architecture for diverse functions', *Trends Biochem. Sci.*, vol. 24, no. 5, pp. 181–185, 1999.

[152] L. Janda, P. Tichý, J. Spížek, and M. Petříček, 'A deduced Thermomonospora curvata protein containing serine/threonine protein kinase and WD-repeat domains', *J. Bacteriol.*, vol. 178, no. 5, pp. 1487–1489, 1996.

[153] T. F. Smith, 'Diversity of WD-repeat proteins', *Subcell. Biochem.*, vol. 48, pp. 20–30, 2008.

[154] C. U. Stirnimann, E. Petsalaki, R. B. Russell, and C. W. Müller, 'WD40 proteins propel cellular networks', *Trends Biochem. Sci.*, vol. 35, no. 10, pp. 531–538, 2010.

[155] R. B. Russell, P. D. Sasieni, and M. J. E. Sternberg, 'Supersites within superfolds. Binding site similarity in the absence of homology', *J. Mol. Biol.*, vol. 282, no. 4, pp. 903–918, 1998.

[156] R. Krick *et al.*, 'Structural and functional characterization of the two phosphoinositide binding sites of PROPPINs, a β-propeller protein family', *Proc. Natl. Acad. Sci.*, 2012.

[157] M. Thumm *et al.*, 'It takes two to tango: PROPPINs use two phosphoinositide-binding sites', *Autophagy*, vol. 9, no. 1, pp. 106–107, 2013.

[158] R. Krick *et al.*, 'Structural and functional characterization of the two phosphoinositide binding sites of PROPPINs, a β-propeller protein family', *Proc. Natl. Acad. Sci.*, vol. 109, no. 30, pp. E2042–E2049, 2012.

[159] S. Baskaran, M. J. Ragusa, E. Boura, and J. H. Hurley, 'Two-Site Recognition of Phosphatidylinositol 3-Phosphate by PROPPINs in Autophagy', *Mol. Cell*, vol. 47, no. 3, pp. 339–348, 2012.

[160] Y. Watanabe *et al.*, 'Structure-based analyses reveal distinct binding sites for Atg2 and phosphoinositides in Atg18', *J. Biol. Chem.*, vol. 287, no. 38, pp. 31681–31690, 2012.

[161] R. A. Busse, A. Scacioc, R. Krick, Á. Pérez-Lara, M. Thumm, and K. Kühnel, 'Characterization of PROPPIN-phosphoinositide binding and role of loop 6CD in PROPPIN-membrane binding', *Biophys. J.*, vol. 108, no. 9, pp. 2223–2234, 2015.

[162] Y. Watanabe *et al.*, 'Structure-based analyses reveal distinct binding sites for Atg2 and phosphoinositides in Atg18', *J. Biol. Chem.*, vol. 287, no. 38, pp. 31681–31690, 2012.

[163] N. Tamura, M. Oku, M. Ito, N. N. Noda, F. Inagaki, and Y. Sakai, 'Atg18 phosphoregulation controls organellar dynamics by modulating its phosphoinositidebinding activity', *J. Cell Biol.*, vol. 202, no. 4, pp. 685–698, 2013.

[164] H. Barth and M. Thumm, 'A genomic screen identifies AUT8 as a novel gene essential for autophagy in the yeast Saccharomyces cerevisiae', *Gene*, vol. 274, no. 1–2, pp. 151–156, 2001.

[165] J. A. Efe, R. J. Botelho, and S. D. Emr, 'Atg18 Regulates Organelle Morphology and Fab1 Kinase Activity Independent of Its Membrane Recruitment by Phosphatidylinositol 3,5-Bisphosphate', *Mol. Biol. Cell*, vol. 19, no. 1, pp. 308–317, 2007.

[166] N. Jin *et al.*, 'VAC14 nucleates a protein complex essential for the acute interconversion of PI3P and PI(3,5)P2in yeast and mouse', *EMBO J.*, vol. 27, no. 24, pp. 3221–3234, 2008.

[167] N. Gopaldass, B. Fauvet, H. Lashuel, A. Roux, and A. Mayer, 'Membrane scission driven by the PROPPIN Atg18', *EMBO J.*, vol. 36, no. 22, p. e201796859, 2017.

[168] K. Meiling-Wesse, H. Barth, C. Voss, E. L. Eskelinen, U. D. Epple, and M. Thumm, 'Atg21 is required for effective recruitment of Atg8 to the preautophagosomal structure during the Cvt pathway', *J. Biol. Chem.*, vol. 279, no. 36, pp. 37741–37750, 2004.

[169] Krick, S. Henke, J. Tolstrup, and M. Thumm, 'Dissecting the localization and function of Atg18, Atg21 and Ygr223c', *Autophagy*, vol. 4, no. 7, pp. 896–910, 2008.

[170] R. Krick and M. Thumm, 'Atg8 lipidation is coordinated in a PtdIns3P-dependent manner by the PROPPIN Atg21', *Autophagy*, vol. 12, no. 11, pp. 2260–2261, 2016.

[171] L. Juris, M. Montino, P. Rube, P. Schlotterhose, M. Thumm, and R. Krick, 'PI3P binding by Atg21 organises Atg8 lipidation', *EMBO J.*, vol. 34, pp. 955–973, 2015.

[172] S. Feyder, J. O. De Craene, S. Bär, D. L. Bertazzi, and S. Friant, 'Membrane trafficking in the yeast Saccharomyces cerevisiae model', *Int. J. Mol. Sci.*, vol. 16, no. 1, pp. 1509–1525, 2015.

[173] H. Yamaguchi *et al.*, 'Golgi membrane-associated degradation pathway in yeast and mammals', *EMBO J.*, vol. 35, no. 18, pp. 1991–2007, 2016.

[174] I. Fournier, J. Barwicz, and P. Tancrède, 'The structuring effects of amphotericin B on pure and ergosterol- or cholesterol-containing dipalmitoylphosphatidylcholine bilayers: A differential scanning calorimetry study', *Biochim. Biophys. Acta - Biomembr.*, vol. 1373, no. 1, pp. 76–86, 1998.

[175] R. Mouri, K. Konoki, N. Matsumori, T. Oishi, and M. Murata, 'Complex formation of amphotericin B in sterol-containing membranes as evidenced by surface plasmon resonance', *Biochemistry*, vol. 47, no. 30, pp. 7807–7815, 2008.

[176] C. T. Beh and J. Rine, 'A role for yeast oxysterol-binding protein homologs in endocytosis and in the maintenance of intracellular sterol-lipid distribution', *J. Cell Sci.*, vol. 117, no. 14, pp. 2983–2996, 2004.

[177] G. D'Angelo, M. Vicinanza, A. Di Campli, and M. A. De Matteis, 'The multiple roles of PtdIns(4)P - Not just the precursor of PtdIns(4,5)P2', *J. Cell Sci.*, vol. 121, no. 12, pp. 1955–1963, 2008.

[178] P. Mayinger, 'Phosphoinositides and vesicular membrane traffic', *Biochim. Biophys. Acta - Mol. Cell Biol. Lipids*, vol. 1821, no. 8, pp. 1104–1113, 2012.

[179] L. Demmel *et al.*, 'The Clathrin Adaptor Gga2p Is a Phosphatidylinositol 4-phosphate Effector at the Golgi Exit', *Mol. Biol. Cell*, vol. 18, no. December, pp. 986–994, 2008.

[180] H. Yamaguchi *et al.*, 'Wipi3 is essential for alternative autophagy and its loss causes neurodegeneration', *Nat. Commun.*, vol. 11, no. 1, pp. 1–5, 2020.

[181] T. Weimbs, S. H. Low, S. J. Chapin, K. E. Mostov, P. Bucher, and K. Hofmann, 'A conserved domain is present in different families of vesicular fusion proteins: A new superfamily', *Proc. Natl. Acad. Sci. U. S. A.*, vol. 94, no. 7, pp. 3046–3051, 1997.

[182] Y. A. Chen, R. H. Scheller, and H. H. Medical, 'SNARE-Mediated membrane fusion', vol. 2, no. February, pp. 98–106, 2001.

[183] R. Jahn, T. Lang, and T. C. Südhof, 'Membrane fusion', *Cell*, vol. 112, no. 4, pp. 519–533, 2003.

[184] T. Weber *et al.*, 'SNAREpins: Minimal machinery for membrane fusion', *Cell*, vol. 92, no. 6, pp. 759–772, 1998.

[185] D. Fasshauer, R. B. Sutton, A. T. Brunger, and R. Jahn, 'Conserved structural features of the synaptic fusion complex: SNARE proteins reclassified as Q- and R-SNAREs', *Proc. Natl. Acad. Sci. U. S. A.*, vol. 95, no. 26, pp. 15781–15786, 1998.

[186] L. Burri and T. Lithgow, 'A complete set of SNAREs in yeast', *Traffic Interchang.*, vol. 5, no. 1, pp. 45–52, 2004.

[187] H. Farhan, M. Kundu, and S. Ferro-Novick, 'The link between autophagy and secretion: A story of multitasking proteins', *Mol. Biol. Cell*, vol. 28, no. 9, pp. 1161–1164, 2017.

[188] S. K. G. Gadila and K. Kim, 'Cargo trafficking from the trans-Golgi network towards the endosome', *Biol. Cell*, vol. 108, no. 8, pp. 205–218, 2016.

[189] Y. Guo, D. W. Sirkis, and R. Schekman, 'Protein sorting at the trans-Golgi network', *Annu. Rev. Cell Dev. Biol.*, vol. 30, pp. 169–206, 2014.

[190] M. J. Lewis, B. J. Nichols, C. Prescianotto-Baschong, H. Riezman, and H. R. B. Pelham, 'Specific retrieval of the exocytic SNARE Snc1p from early yeast endosomes', *Mol. Biol. Cell*, vol. 11, no. 1, pp. 23–38, 2000.

[191] L. Hicke, B. Zanolari, M. Pypaert, J. Rohrer, and H. Riezman, 'Transport through the yeast endocytic pathway occurs through morphologically distinct compartments and requires an active secretory pathway and Sec18p/N-ethylmaleimide-sensitive fusion protein', *Mol. Biol. Cell*, vol. 8, no. 1, pp. 13–31, 1997.

[192] C. Prescianotto-Baschong and H. Riezman, 'Morphology of the yeast endocytic pathway', *Mol. Biol. Cell*, vol. 9, no. 1, pp. 173–189, 1998.

[193] F. R. Maxfield and T. E. McGraw, 'Endocytic recycling', *Nat. Rev. Mol. Cell Biol.*, vol. 5, no. 2, pp. 121–132, 2004.

[194] M. Baumert, P. R. Maycox, F. Navone, P. De Camilli, and R. Jahn, 'Synaptobrevin: An integral membrane protein of 18 000 daltons present in small synaptic vesicles of rat brain', *EMBO J.*, vol. 8, no. 2, pp. 379–384, 1989.

[195] T. Sollner *et al.*, 'SNAP receptors implicated in vesicle targeting and fusion', *Nature*, vol. 362, no. 6418, pp. 318–24, 1993.

[196] S. K. Lemmon and L. M. Traub, 'Sorting in the endosomal system in yeast and animal cells', *Curr. Opin. Cell Biol.*, vol. 12, no. 4, pp. 457–466, 2000.

[197] M. Babst, D. J. Katzmann, W. B. Snyder, B. Wendland, and S. D. Emr, 'Endosome-associated complex, ESCRT-II, recruits transport machinery for protein sorting at the multivesicular body', *Dev. Cell*, vol. 3, no. 2, pp. 283–289, 2002.

[198] D. J. Katzmann, G. Odorizzi, and S. D. Emr, 'Receptor downregulation and multivesicular-body sorting', *Nat. Rev. Mol. Cell Biol.*, vol. 3, no. 12, pp. 893–905, 2002.

[199] W. M. Henne, N. J. Buchkovich, and S. D. Emr, 'The ESCRT Pathway', *Dev. Cell*, vol. 21, no. 1, pp. 77–91, 2011.

[200] M. Vietri, M. Radulovic, and H. Stenmark, 'The many functions of ESCRTs', *Nat. Rev. Mol. Cell Biol.*, vol. 21, no. 1, pp. 25–42, 2020.

[201] M. Filimonenko *et al.*, 'Functional multivesicular bodies are required for autophagic clearance of protein aggregates associated with neurodegenerative disease', *J. Cell Biol.*, vol. 179, no. 3, pp. 485–500, 2007.

[202] K. Shirahama, T. Noda, and Y. Ohsumi, 'Mutational analysis of Csc1/Vps4p: Involvement of endosome in regulation of autophagy in yeast', *Cell Struct. Funct.*, vol. 22, no. 5, pp. 501–509, 1997.

[203] M. Alonso Y Adell, S. M. Migliano, and D. Teis, 'ESCRT-III and Vps4: a dynamic multipurpose tool for membrane budding and scission', *FEBS J.*, vol. 283, pp. 3288–3302, 2016.

[204] F. Zhou *et al.*, 'Rab5-dependent autophagosome closure by ESCRT', *J. Cell Biol.*, vol. 218, no. 6, pp. 1908–1927, 2019.

[205] F. Zhou, Z. Wu, M. Zhao, N. Segev, and Y. Liang, 'Autophagosome closure by ESCRT: Vps21/RAB5-regulated ESCRT recruitment via an Atg17-Snf7 interaction', *Autophagy*,

vol. 15, no. 9, pp. 1653–1654, 2019.

[206] W. Jiang *et al.*, 'Key regulators of autophagosome closure', *Cells*, vol. 10, no. 11, pp. 1–13, 2021.

[207] M. N. J. Seaman, E. G. Marcusson, J. L. Cereghino, and S. D. Emr, 'Endosome to Golgi retrieval of the vacuolar protein sorting receptor, Vps10p, requires the function of the VPS29, VPS30, and VPS35 gene products', *J. Cell Biol.*, vol. 137, no. 1, pp. 79–92, 1997.

[208] C. Burd and P. J. Cullen, 'Retromer: A master conductor of endosome sorting', *Cold Spring Harb. Perspect. Biol.*, vol. 6, no. 2, 2014.

[209] B. F. Horazdovsky, B. A. Davies, M. N. J. Seaman, S. A. McLaughlin, S. H. Yoon, and S. D. Emr, 'A sorting nexin-1 homologue, Vps5p, forms a complex with Vps17p and is required for recycling the vacuolar protein-sorting receptor', *Mol. Biol. Cell*, vol. 8, no. 8, pp. 1529–1541, 1997.

[210] K. E. Chen, M. D. Healy, and B. M. Collins, 'Towards a molecular understanding of endosomal trafficking by Retromer and Retriever', *Traffic*, vol. 20, no. 7, pp. 465–478, 2019.

[211] A. Hierro *et al.*, 'Functional architecture of the retromer cargo-recognition complex', *Nature*, vol. 449, no. 7165, pp. 1063–1067, 2007.

[212] J. D. Swarbrick *et al.*, 'VPS29 is not an active metallo-phosphatase but is a rigid scaffold required for retromer interaction with accessory proteins', *PLoS One*, vol. 6, no. 5, 2011.

[213] D. Wang *et al.*, 'Crystal structure of human vacuolar protein sorting protein 29 reveals a phosphodiesterase/nuclease-like fold and two protein-protein interaction sites', *J. Biol. Chem.*, vol. 280, no. 24, pp. 22962–22967, 2005.

[214] H. Shi, R. Rojas, J. S. Bonifacino, and J. H. Hurley, 'The retromer subunit Vps26 has an arrestin fold and binds Vps35 through its C-terminal domain', *Nat. Struct. Mol. Biol.*, vol. 13, no. 6, pp. 540–548, 2006.

[215] B. M. Collins *et al.*, 'Structure of Vps26B and mapping of its interaction with the retromer protein complex', *Traffic*, vol. 9, no. 3, pp. 366–379, 2008.

[216] M. S. Harrison, C. S. Hung, T. T. Liu, R. Christiano, T. C. Walther, and C. G. Burd, 'A mechanism for retromer endosomal coat complex assembly with cargo', *Proc. Natl. Acad. Sci. U. S. A.*, vol. 111, no. 1, pp. 267–272, 2014.

[217] L. K. Purushothaman and C. Ungermann, 'Cargo induces retromer-mediated membrane remodeling on membranes', *Mol. Biol. Cell*, vol. 29, no. 22, pp. 2709–2719, 2018.

[218] J. W. Yu and M. A. Lemmon, 'All Phox Homology (PX) Domains from Saccharomyces cerevisiae Specifically Recognize Phosphatidylinositol 3-Phosphate', *J. Biol. Chem.*, vol. 276, no. 47, pp. 44179–44184, 2001.

[219] M. Chandra *et al.*, 'Classification of the human phox homology (PX) domains based on their phosphoinositide binding specificities', *Nat. Commun.*, vol. 10, no. 1, 2019.

[220] T. I. Strochlic, T. G. Setty, A. Sitaram, and C. G. Burd, 'Grd19/Snx3p functions as a cargo-specific adapter for retromer-dependent endocytic recycling', *J. Cell Biol.*, vol. 177, no. 1, pp. 115–125, 2007.

[221] L. Marquardt, 'Identification and Characterization of autophagic and non-autophagic Interaction Partners of Atg18', 2021.

[222] S. C. Li and P. M. Kane, 'The yeast lysosome-like vacuole: Endpoint and crossroads', *Biochim. Biophys. Acta - Mol. Cell Res.*, vol. 1793, no. 4, pp. 650–663, 2009.

[223] J. D. Gary, A. E. Wurmser, C. J. Bonangelino, L. S. Weisman, and S. D. Emr, 'Fab1p is essential for PtdIns(3)P 5-kinase activity and the maintenance of vacuolar size and membrane homeostasis', *J. Cell Biol.*, vol. 143, no. 1, pp. 65–79, 1998.

[224] A. Yamamoto, D. B. DeWald, I. V. Boronenkov, R. A. Anderson, S. D. Emr, and D. Koshland, 'Novel PI(4)P 5-kinase homologue, Fab1p, essential for normal vacuole function and morphology in yeast', *Mol. Biol. Cell*, vol. 6, no. 5, pp. 525–539, 1995.

[225] T. R. Jeffries, S. K. Dove, R. H. Michell, and P. J. Parker, 'PtdIns-specific MPR Pathway Association of a Novel WD40 Repeat Protein, WIPI49', *Mol. Biol. Cell*, vol. 14, no. December, pp. 5069–5081, 2004.

[226] C. J. Bonangelino, N. L. Catlett, and L. S. Weisman, 'Vac7p, a novel vacuolar protein, is required for normal vacuole inheritance and morphology', *Mol. Cell. Biol.*, vol. 17, no. 12, pp. 6847–6858, 1997.

[227] C. J. Bonangelino *et al.*, 'Osmotic stress-induced increase of phosphatidylinositol 3,5-bisphosphate requires Vac14p, an activator of the lipid kinase Fab1p', *J. Cell Biol.*, vol. 156, no. 6, pp. 1015–1028, 2002.

[228] S. A. Rudge, D. M. Anderson, and S. D. Emr, 'Vacuole Size Control: Regulation of PtdIns(3,5)P2 Levels by the Vacuole-associated Vac14-Fig4 Complex, a PtdIns(3,5)P2-

specific Phosphatase', *Mol. Biol. Cell*, vol. 14, no. December, pp. 5069–5081, 2004.

[229] J. E. Duex, J. J. Nau, E. J. Kauffman, and L. S. Weisman, 'Phosphoinositide 5-phosphatase Fig4p is required for both acute rise and subsequent fall in stress-induced phosphatidylinositol 3,5-bisphosphate levels', *Eukaryot. Cell*, vol. 5, no. 4, pp. 723–731, 2006.

[230] E. B. Freese, M. I. Chu, and E. Freese, 'Initiation of Yeast sporulation by partial carbon, nitrogen, or phosphate deprivation', *J. Bacteriol.*, vol. 149, no. 3, pp. 840–851, 1982.

[231] B. Byers, 'Cytology of the yeast life cycle.', *Mol. Biol. Yeast Saccharomyceslife cycle inheritance.*, pp. 59–96, 1981.

[232] M. Kupiec, B. Byers, and R. E. Esposito, 'Meiosis and sporulation in Saccharomyces cerevisiae', *Mol. Cell. Biol. Yeast Saccharomyces*, vol. 3, pp. 889–1036, 1997.

[233] A. M. Neiman, 'Sporulation in the budding yeast Saccharomyces cerevisiae', *Genetics*, vol. 189, no. 3, pp. 737–765, 2011.

[234] K. L. Chung, R. Z. Hawirko, and P. K. Isaac, 'Cell wall replication in Saccharomyces cerevisiae.', *Can. J. Microbiol.*, vol. 11, no. 6, pp. 953–957, 1965.

[235] J. S. Tkacz and J. O. Lampen, 'Wall replication in saccharomyces species: use of fluorescein-conjugated concanavalin A to reveal the site of mannan insertion.', *J. Gen. Microbiol.*, vol. 72, no. 2, pp. 243–247, 1972.

[236] J. M. Sierra, R. Sentandreu, and J. R. Villanueva, 'Regulation of Wall Synthesis During Saccharomyces Cerevisiae Cell Cycle', *FEBS Lett.*, vol. 34, no. 2, 1973.

[237] P. Briza *et al.*, 'Systematic analysis of sporulation phenotypes in 624 non-lethal homozygous deletion strains of Saccharomyces cerevisiae', *Yeast*, vol. 19, no. 5, pp. 403–422, 2002.

[238] C. F. Robinow and J. Marak, 'A fiber apparatus in the nucleus of the yeast cell', *J. Cell Biol.*, vol. 29, no. 3, pp. 129–151, 1966.

[239] H. D. Agar and H. C. Douglas, 'Studies of budding and cell wall structure of yeast; electron microscopy of the sections.', *J. Bacteriol.*, vol. 70, no. 4, pp. 427–434, 1955.

[240] J. W. Bartholomew and T. Mittwer, 'Demonstration of yeast bud scars with the electron microscope.', *J. Bacteriol.*, vol. 65, no. 3, pp. 272–275, 1953.

[241] A. P. Mitchell, 'Control of meiotic gene expression in Saccharomyces cerevisiae', *Microbiol. Rev.*, vol. 58, no. 1, pp. 56–70, 1994.

[242] E. D. Shuster and B. Byers, 'Pachytene arrest and other meiotic effects of the start

mutations in Saccharomyes cerevisiae', *Genetics*, vol. 123, no. 1, pp. 29–43, 1989.

[243] M. J. Clancy, M. E. Shambaugh, C. S. Timpte, and J. A. Bokar, 'Induction of sporulation in Saccharomyces cerevisiae leads to the formation of N6-methyladenosine in mRNA: A potential mechanism for the activity of the IME4 gene', *Nucleic Acids Res.*, vol. 30, no. 20, pp. 4509–4518, 2002.

[244] P. B. Moens and E. Rapport, 'Spindles, spindle plaques, and meiosis in the yeast Saccharomyces Cerevisiae (Hansen)', *J. Cell Biol.*, vol. 50, no. 2, pp. 344–361, 1971.

[245] A. M. Neiman, 'Prospore membrane formation defines a developmentally regulated branch of the secretory pathway in yeast', *J. Cell Biol.*, vol. 140, no. 1, pp. 29–37, 1998.

[246] P. Briza, M. Breitenbach, A. Ellinger, and J. Segall, 'Isolation of two developmentally regulated genes involved in spore wall maturation in Saccharomyces cerevisiae', *Genes Dev.*, vol. 4, no. 10, pp. 1775–1789, 1990.

[247] A. Coluccio, E. Bogengruber, M. N. Conrad, M. E. Dresser, P. Briza, and A. M. Neiman, 'Morphogenetic pathway of spore wall assembly in Saccharomyces cerevisiae', *Eukaryot. Cell*, vol. 3, no. 6, pp. 1464–1475, 2004.

[248] T. Krishnamoorthy *et al.*, 'Phosphorylation of histone H4 Ser1 regulates sporulation in yeast and is conserved in fly and mouse spermatogenesis', *Genes Dev.*, vol. 20, no. 18, pp. 2580–2592, 2006.

[249] A. D. Roeder and J. M. Shaw, 'Vacuole Partitioning During Meiotic Division in Yeast', *Genet. Soc. Am.*, vol. 144, pp. 445–458, 1996.

[250] Y. Suda, H. Nakanishi, E. M. Mathieson, and A. M. Neiman, 'Alternative modes of organellar segregation during sporulation in Saccharomyces cerevisiae', *Eukaryot. Cell*, vol. 6, no. 11, pp. 2009–2017, 2007.

[251] H. E. Smith and A. P. Mitchell, 'A transcriptional cascade governs entry into meiosis in Saccharomyces cerevisiae', *Mol. Cell. Biol.*, vol. 9, no. 5, pp. 2142–2152, 1989.

[252] S. Chu and I. Herskowitz, 'Gametogenesis in yeast is regulated by a transcriptional cascade dependent on Ndt80', *Mol. Cell*, vol. 1, no. 5, pp. 685–696, 1998.

[253] Y. Kassir, D. Granot, and G. Simchen, 'IME1, a positive regulator gene of meiosis in S. cerevisiae', *Cell*, vol. 52, no. 6, pp. 853–862, 1988.

[254] H. Matsuhara and A. Yamamoto, 'Autophagy is required for efficient meiosis progression and proper meiotic chromosome segregation in fission yeast', *Genes to*

Cells, vol. 21, no. 1, pp. 65–87, 2016.

[255] A. H. Enyenihi and W. S. Saunders, 'Meiosis in Saccharomyces cerevisiae', *Genetics*, vol. 163, no. January, pp. 47–54, 2003.

[256] J. Schindelin *et al.*, 'Fiji: An open-source platform for biological-image analysis', *Nat. Methods*, vol. 9, no. 7, pp. 676–682, 2012.

[257] J. Cox and M. Mann, 'MaxQuant enables high peptide identification rates, individualized p.p.b.-range mass accuracies and proteome-wide protein quantification', *Nat. Biotechnol.*, vol. 26, no. 12, pp. 1367–1372, 2008.

[258] C. Kaiser, 'Methods in Yeast Genetics', *Bioelectrochemistry Bioenerg.*, vol. 19, no. 3, p. 599, 1994.

[259] D. Hanahan, 'Studies on transformation of Escherichia coli with plasmids', *J. Mol. Biol.*, vol. 166, no. 4, pp. 557–580, 1983.

[260] F. Sherman, 'Getting started with yeast', *Methods Enzymol.*, vol. 350, pp. 3–41, 2002.

[261] D. O. McClary, W. L. Nulty, and G. R. Miller, 'Effect of Potassium Versus Sodium in the Sporulation of Saccharomyces', *J. Bacteriol.*, vol. 78, no. 3, pp. 362–368, 1959.

[262] M. Straub, M. Bredschneider, and M. Thumm, 'AUT3, a serine/threonine kinase gene, is essential for autophagocytosis in Saccharomyces cerevisiae', *J. Bacteriol.*, vol. 179, no. 12, pp. 3875–3883, 1997.

[263] H. Barth, K. Meiling-Wesse, U. D. Epple, and M. Thumm, 'Mai1p is essential for maturation of proaminopeptidase I but not for autophagy', *FEBS Lett.*, vol. 512, no. 1–3, pp. 173–179, 2002.

[264] D. Mumberg, R. Muller, and M. Funk, 'Regulatable promoters of saccharomyces cerevisiae: Comparison of transcriptional activity and their use for heterologous expression', *Nucleic Acids Res.*, vol. 22, no. 25, pp. 5767–5768, 1994.

[265] F. Reggiori, M. W. Black, and H. R. B. Pelham, 'Polar transmembrane domains target proteins to the interior of the yeast vacuole', *Mol. Biol. Cell*, vol. 11, no. 11, pp. 3737–3749, 2000.

[266] R. K. Niedenthal, L. Riles, M. Johnston, and J. H. Hegemann, 'Green fluorescent protein as a marker for gene expression and subcellular localization in budding yeast', *Yeast*, vol. 12, no. 8, pp. 773–786, Jun. 1996.

[267] U. Gueldener, J. Heinisch, G. J. Koehler, D. Voss, and J. H. Hegemann, 'A second set of loxP marker cassettes for Cre-mediated multiple gene knockouts in budding yeast',

Nucleic Acids Res., vol. 30, no. 6, p. 23, 2002.

[268] R. S. Sikorski and P. Hieter, 'A system of shuttle vectors and yeast host strains designed for efficient manipulation of DNA in Saccharomyces cerevisiae.', *Genetics*, vol. 122, no. 1, pp. 19–27, 1989.

[269] H. W. Boyer, 'DNA restriction and modification mechanisms in bacteria', *F. C. Neidhardt (ed.), Escherichia coli Salmonella Cell. Mol. Biol.*, vol. 2, no. 0299, pp. 773–781, 1971.

[270] B. Weiss and C. C. Richardson, 'Enzymatic breakage and joining of deoxyribonucleic acid, I. Repair of single-strand breaks in DNA by an enzyme system from Escherichia coli infected with T4 bacteriophage.', *Proc. Natl. Acad. Sci. U. S. A.*, vol. 57, no. 4, pp. 1021–1028, 1967.

[271] U. K. Laemmli, 'Cleavage of Structural Proteins during the Assembly of the Head of Bacteriophage T4', *Nat. Publ. Gr.*, vol. 228, pp. 726–734, 1970.

[272] X. Wang, X. Li, and Y. Li, 'A modified Coomassie Brilliant Blue staining method at nanogram sensitivity compatible with proteomic analysis', *Biotechnol. Lett.*, vol. 29, no. 10, pp. 1599–1603, 2007.

[273] M. Pink, N. Verma, A. W. Rettenmeier, and S. Schmitz-Spanke, 'CBB staining protocol with higher sensitivity and mass spectrometric compatibility', *Electrophoresis*, vol. 31, no. 4, pp. 593–598, 2010.

[274] N. Opitz *et al.*, 'Capturing the Asc1p/Receptor for Activated C Kinase 1 (RACK1) Microenvironment at the head region of the 40s ribosome with quantitative BioID in Yeast', *Mol. Cell. Proteomics*, vol. 16, no. 12, pp. 2199–2218, 2017.

[275] S. V. Scott, M. Baba, Y. Ohsumi, and D. J. Klionsky, 'Aminopeptidase I is targeted to the vacuole by a nonclassical vesicular mechanism', *J. Cell Biol.*, vol. 138, no. 1, pp. 37–44, 1997.

[276] N. Johnsson and A. Varshavsky, 'Split ubiquitin as a sensor of protein interactions in vivo', *Proc. Natl. Acad. Sci. U. S. A.*, vol. 91, no. 22, pp. 10340–10344, 1994.

[277] S. Wittke, N. Lewke, S. Müller, and N. Johnsson, 'Probing the molecular environment of membrane proteins in vivo', *Mol. Biol. Cell*, vol. 10, no. 8, pp. 2519–2530, 1999.

[278] K. R. Parzych, A. Ariosa, M. Mari, and D. J. Klionsky, 'A newly characterized vacuolar serine carboxypeptidase, Atg42/Ybr139w, is required for normal vacuole function and the terminal steps of autophagy in the yeast Saccharomyces cerevisiae', *Mol. Biol.*

Cell, vol. 29, no. 9, pp. 1089–1099, 2018.

[279] L. H. Weaver, K. Kwon, D. Beckett, and B. W. Matthews, 'Corepressor-induced organization and assembly of the biotin repressor: A model for allosteric activation of a transcriptional regulator', *Proc. Natl. Acad. Sci. U. S. A.*, vol. 98, no. 11, pp. 6045–6050, 2001.

[280] J. E. Cronan, 'Biotination of proteins in vivo. A post-translational modification to label, purify, and study proteins', *J. Biol. Chem.*, vol. 265, no. 18, pp. 10327–10333, 1990.

[281] D. I. Kim, K. C. Birendra, W. Zhu, K. Motamedchaboki, V. Doye, and K. J. Roux, 'Probing nuclear pore complex architecture with proximity-dependent biotinylation', *Proc. Natl. Acad. Sci. U. S. A.*, vol. 111, no. 24, pp. 2453–2461, 2014.

[282] D. I. Kim *et al.*, 'An improved smaller biotin ligase for BioID proximity labeling', *Mol. Biol. Cell*, vol. 27, no. 8, pp. 1188–1196, 2016.

[283] N. Jin *et al.*, 'VAC14 nucleates a protein complex essential for the acute interconversion of PI3P and PI(3,5)P2 in yeast and mouse', *EMBO J.*, vol. 27, no. 24, pp. 3221–3234, 2008.

[284] U. Schulze *et al.*, 'The Vac14-interaction network is linked to regulators of the endolysosomal and autophagic pathway', *Mol. Cell. Proteomics*, vol. 13, no. 6, pp. 1397–1411, 2014.

[285] N. Ogawa, J. DeRisi, and P. O. Brown, 'New components of a system for phosphate accumulation and polyphosphate metabolism in Saccharomyces cerevisiae revealed by genomic expression analysis', *Mol. Biol. Cell*, vol. 11, no. 12, pp. 4309–4321, 2000.

[286] O. Müller, H. Neumann, M. J. Bayer, and A. Mayer, 'Role of the Vtc proteins in V-ATPase stability and membrane trafficking', *J. Cell Sci.*, vol. 116, no. 6, pp. 1107–1115, 2003.

[287] D. Secco, C. Wang, H. Shou, and J. Whelan, 'Phosphate homeostasis in the yeast Saccharomyces cerevisiae, the key role of the SPX domain-containing proteins', *FEBS Lett.*, vol. 586, no. 4, pp. 289–295, 2012.

[288] T. J. LaGrassa and C. Ungermann, 'The vacuolar kinase Yck3 maintains organelle fragmentation by regulating the HOPS tethering complex', *J. Cell Biol.*, vol. 168, no. 3, pp. 401–414, 2005.

[289] R. Russnak, D. Konczal, and S. L. McIntire, 'A Family of Yeast Proteins Mediating Bidirectional Vacuolar Amino Acid Transport', *J. Biol. Chem.*, vol. 276, no. 26, pp.

23849–23857, 2001.

[290] S. F. Nothwehr, S. A. Ha, and P. Bruinsma, 'Sorting of yeast membrane proteins into an endosome-to-Golgi pathway involves direct interaction of their cytosolic domains with Vps35p', *J. Cell Biol.*, vol. 151, no. 2, pp. 297–309, 2000.

[291] G. Scatchard, 'Attractions of Proteins for Small Molecules and Ions', *Ann. N. Y. Acad. Sci.*, vol. 51, no. 4, pp. 660–672, 1949.

[292] S. A. Berson and R. S. Yalow, 'Quantitative aspects of the reaction between insulin and insulin-binding antibody', *J. Clin. Invest.*, pp. 1996–2016, 1959.

[293] J. Chen, N. Sawyer, and L. Regan, 'Protein-protein interactions: General trends in the relationship between binding affinity and interfacial buried surface area', *Protein Sci.*, vol. 22, no. 4, pp. 510–515, 2013.

[294] E. C. Hulme and M. A. Trevethick, 'Ligand binding assays at equilibrium: Validation and interpretation', *Br. J. Pharmacol.*, vol. 161, no. 6, pp. 1219–1237, 2010.

[295] W. I. Goldburg, 'Dynamic light scattering', *Am. Assoc. Phys.*, vol. 67, no. 1999, p. 1093, 1999.

[296] N. N. Noda, Y. Ohsumi, and F. Inagaki, 'Atg8-family interacting motif crucial for selective autophagy', *FEBS Lett.*, vol. 584, no. 7, pp. 1379–1385, 2010.

[297] E. A. Alemu *et al.*, 'ATG8 family proteins act as scaffolds for assembly of the ULK complex: Sequence requirements for LC3-interacting region (LIR) motifs', *J. Biol. Chem.*, vol. 287, no. 47, pp. 39275–39290, 2012.

[298] R. Krick *et al.*, 'Cdc48/p97 and Shp1/p47 regulate autophagosome biogenesis in concert with ubiquitin-like Atg8', *J. Cell Biol.*, vol. 190, no. 6, pp. 965–973, 2010.

[299] M. Schwarten, M. Stoldt, J. Mohrlüder, and D. Willbold, 'Solution structure of Atg8 reveals conformational polymorphism of the N-terminal domain', *Biochem. Biophys. Res. Commun.*, vol. 395, no. 3, pp. 426–431, 2010.

[300] Y. S. Abubakar, W. Zheng, S. Olsson, and J. Zhou, 'Updated insight into the physiological and pathological roles of the retromer complex', *Int. J. Mol. Sci.*, vol. 18, no. 8, 2017.

[301] L. E. Dalton, B. D. M. Bean, M. Davey, and E. Conibear, 'Quantitative high-content imaging identifes novel regulators of Neo1 traffcking at endosomes', *Mol. Biol. Cell*, vol. 28, no. 11, pp. 1539–1550, 2017.

[302] D. J. Klionsky and S. D. Emr, 'Autophagy as a regulated pathway of cellular

degradation', *Science (80-.).*, vol. 290, no. 5497, pp. 1717–1721, 2000.

[303] S. Saha, D. P. Panigrahi, S. Patil, and S. K. Bhutia, 'Autophagy in health and disease: A comprehensive review', *Biomed. Pharmacother.*, vol. 104, no. April, pp. 485–495, 2018.

[304] Y. Lei *et al.*, 'The crystal structure of Atg18 reveals a new binding site for Atg2 in Saccharomyces cerevisiae', *Cell. Mol. Life Sci.*, vol. 78, no. 5, pp. 2131–2143, 2021.

[305] M. Bueno-Arribas, I. Blanca, C. Cruz-Cuevas, R. Escalante, M. A. Navas, and O. Vincent, 'A conserved ATG2 binding site in WIPI4 and yeast Hsv2 is disrupted by mutations causing β-propeller protein-associated neurodegeneration', *Hum. Mol. Genet.*, vol. 31, no. 1, pp. 111–121, 2022.

[306] S. Baskaran, M. J. Ragusa, E. Boura, and J. H. Hurley, 'Two-Site Recognition of Phosphatidylinositol 3-Phosphate by PROPPINs in Autophagy', *Mol. Cell*, vol. 47, no. 3, pp. 339–348, 2012.

[307] J. Park *et al.*, 'Quaternary structures of Vac8 differentially regulate the Cvt and PMN pathways', *Autophagy*, vol. 16, no. 6, pp. 991–1006, 2020.

[308] Y. Aoki *et al.*, 'Phosphorylation of serine 114 on Atg32 mediates mitophagy', *Mol. Biol. Cell*, vol. 22, no. 17, pp. 3206–3217, 2011.

[309] T. Kanki *et al.*, 'A Genomic Screen for Yeast Mutants Defective in Selective Mitochondria Autophagy', *Mol. Biol. Cell*, vol. 20, pp. 4524–4530, 2009.

[310] K. M. Fiebig, L. M. Rice, E. Pollock, and A. T. Brunger, 'Folding intermediates of snare complex assembly', *Nat. Struct. Biol.*, vol. 6, no. 2, pp. 117–123, 1999.

[311] J. Jäntti, M. K. Aalto, M. Öyen, L. Sundqvist, S. Keränen, and H. Ronne, 'Characterization of temperature-sensitive mutations in the yeast syntaxin 1 homologues Sso1p and Sso2p, and evidence of a distinct function for Sso1p in sporulation', *J. Cell Sci.*, vol. 115, no. 2, pp. 409–420, 2002.

[312] M. K. Aalto, H. Ronne, and S. Keranen, 'Yeast syntaxins Sso1p and Sso2p belong to a family of related membrane proteins that function in vesicular transport', *EMBO J.*, vol. 12, no. 11, pp. 4095–4104, 1993.

[313] V. Protopopov, B. Govindan, P. Novick, and J. E. Gerst, 'Homologs of the synaptobrevin/VAMP family of synaptic vesicle proteins function on the late secretory pathway in S. cerevisiae', *Cell*, vol. 74, no. 5, pp. 855–861, 1993.

[314] P. Brennwald, B. Kearns, K. Champion, S. Keränen, V. Bankaitis, and P. Novick, 'Sec9 is

a SNAP-25-like component of a yeast SNARE complex that may be the effector of Sec4 function in exocytosis', *Cell*, vol. 79, no. 2, pp. 245–258, 1994.

[315] I. Fernandez, J. Ubach, I. Dulubova, X. Zhang, T. C. Südhof, and J. Rizo, 'Three-dimensional structure of an evolutionarily conserved N-terminal domain of syntaxin 1A', *Cell*, vol. 94, no. 6, pp. 841–849, 1998.

[316] M. Munson, X. Chen, A. E. Cocina, S. M. Schultz, and F. M. Hughson, 'Interactions within the yeast t-SNARE Sso1p that control SNARE complex assembly', *Nat. Struct. Biol.*, vol. 7, no. 10, pp. 894–902, 2000.

[317] K. L. Nicholson, M. Munson, R. B. Miller, T. J. Filip, R. Fairman, and F. M. Hughson, 'Regulation of SNARE complex assembly by an N-terminal domain of the t- SNARE Sso1p', *Nat. Struct. Biol.*, vol. 5, no. 9, pp. 793–802, 1998.

[318] H. E. Burston *et al.*, 'Regulators of yeast endocytosis identified by systematic quantitative analysis', *J. Cell Biol.*, vol. 185, no. 6, pp. 1097–1110, 2009.

[319] J. Valdez-Taubas and H. R. B. Pelham, 'Slow Diffusion of Proteins in the Yeast Plasma Membrane Allows Polarity to Be Maintained by Endocytic Cycling', *Curr. Biol.*, vol. 13, p. ARTMED1118, 2003.

[320] M. Ma, C. G. Burd, and R. J. Chi, 'Distinct complexes of yeast Snx4 family SNX-BARs mediate retrograde trafficking of Snc1 and Atg27', *Traffic*, vol. 18, no. 2, pp. 134–144, 2017.

[321] E. H. Hettema, M. J. Lewis, M. W. Black, and H. R. B. Pelham, 'Retromer and the sorting nexins Snx4/41/42 mediate distinct retrieval pathways from yeast endosomes', *EMBO J.*, vol. 22, no. 3, pp. 548–557, 2003.

[322] I. I. Smaczynska-de Rooij, E. G. Allwood, S. Aghamohammadzadeh, E. H. Hettema, M. W. Goldberg, and K. R. Ayscough, 'A role for the dynamin-like protein Vps1 during endocytosis in yeast', *J. Cell Sci.*, vol. 123, no. 20, pp. 3496–3506, 2010.

[323] R. J. Chi, J. Liu, M. West, J. Wang, G. Odorizzi, and C. G. Burd, 'Fission of SNX-BAR-coated endosomal retrograde transport carriers is promoted by the dynamin-related protein Vps1', *J. Cell Biol.*, vol. 204, no. 5, pp. 793–806, 2014.

[324] Y. Shi, C. J. Stefan, S. M. Rue, D. Teis, and S. D. Emr, 'Two novel WD40 domain-containing proteins, Ere1 and Ere2, function in the retromer-mediated endosomal recycling pathway', *Mol. Biol. Cell*, vol. 22, no. 21, pp. 4093–4107, 2011.

[325] J. T. Best, P. Xu, J. G. McGuire, S. N. Leahy, and T. R. Graham, 'Yeast synaptobrevin,

Snc1, engages distinct routes of postendocytic recycling mediated by a sorting nexin, Rcy1-COPI, and retromer', *Mol. Biol. Cell*, vol. 31, no. 9, pp. 944–962, 2020.

[326] H. Abeliovich, E. Grote, P. Novick, and S. Ferro-Novick, 'Tlg2p, a yeast syntaxin homolog that resides on the Golgi and endocytic structures', *J. Biol. Chem.*, vol. 273, no. 19, pp. 11719–11727, 1998.

[327] R. H. Valdivia, D. Baggott, J. S. Chuang, and R. W. Schekman, 'The yeast clathrin adaptor protein complex 1 is required for the efficient retention of a subset of late Golgi membrane proteins', *Dev. Cell*, vol. 2, no. 3, pp. 283–294, 2002.

[328] C. Prescianotto-Baschong and H. Riezman, 'Ordering of compartments in the yeast endocytic pathway', *Traffic*, vol. 3, no. 1, pp. 37–49, 2002.

[329] J. C. M. Holthuis, B. J. Nichols, and H. R. B. Pelham, 'The syntaxin Tlg1p mediates trafficking of chitin synthase III to polarized growth sites in yeast', *Mol. Biol. Cell*, vol. 9, no. 12, pp. 3383–3397, 1998.

[330] G. F. Von Mollard, S. F. Nothwehr, and T. H. Stevens, 'The yeast V-SNARE Vti1p mediates two vesicle transport pathways through interactions with the t-SNAREs Sed5p and Pep12p', *J. Cell Biol.*, vol. 137, no. 7, pp. 1511–1524, 1997.

[331] F. Reggiori and H. R. B. Pelham, 'A transmembrane ubiquitin ligase required to sort membrane proteins into multivesicular bodies', *Nat. Cell Biol.*, vol. 4, no. 2, pp. 117–123, 2002.

[332] D. J. Katzmann, M. Babst, and S. D. Emr, 'Ubiquitin-dependent sorting into the multivesicular body pathway requires the function of a conserved endosomal protein sorting complex, ESCRT-I', *Cell*, vol. 106, no. 2, pp. 145–155, 2001.

[333] G. Stjepanovic, S. Baskaran, M. G. Lin, and J. H. Hurley, 'Vps34 Kinase Domain Dynamics Regulate the Autophagic PI 3-Kinase Complex', *Mol. Cell*, vol. 67, no. 3, pp. 528-534.e3, 2017.

[334] K. A. Becherer, S. E. Rieder, S. D. Emr, and E. W. Jones, 'Novel syntaxin homologue, Pep12p, required for the sorting of lumenal hydrolases to the lysosome-like vacuole in yeast', *Mol. Biol. Cell*, vol. 7, no. 4, pp. 579–594, 1996.

[335] J. H. Grissom, V. A. Segarra, and R. J. Chi, 'New perspectives on snare function in the yeast minimal endomembrane system', *Genes (Basel).*, vol. 11, no. 8, pp. 1–11, 2020.

[336] M. J. Lewis and H. R. B. Pelham, 'A new yeast endosomal SNARE related to mammalian syntaxin 8', *Traffic*, vol. 3, no. 12, pp. 922–929, 2002.

[337] B. Singer-Krüger *et al.*, 'Role of three rab5-like GTPases, Ypt51p, Ypt52p, and Ypt53p, in the endocytic and vacuolar protein sorting pathways of yeast', *J. Cell Biol.*, vol. 125, no. 2, pp. 283–298, 1994.

[338] J. H. Stack, B. Horazdovsky, and S. D. Emr, 'Receptor-mediated protein sorting to the vacuole in yeast: Roles for a Protein Kinase, a Lipid Kinase and GTP-Binding Proteins', *Annu. Rev. Cell Dev. Biol.*, vol. 11, pp. 1–33, 1995.

[339] G. G. Tall, H. Hama, D. B. DeWald, and B. F. Horazdovsky, 'The phosphatidylinositol 3-phosphate binding protein Vac1p interacts with a Rab GTPase and a Sec1p homologue to facilitate vesicle-mediated vacuolar protein sorting', *Mol. Biol. Cell*, vol. 10, no. 6, pp. 1873–1889, 1999.

[340] Y. Chen *et al.*, 'A Vps21 endocytic module regulates autophagy', *Mol. Biol. Cell*, vol. 25, no. 20, pp. 3166–3177, 2014.

[341] T. Noda, N. Fujita, and T. Yoshimori, 'The late stages of autophagy: How does the end begin?', *Cell Death Differ.*, vol. 16, no. 7, pp. 984–990, 2009.

[342] D. Poteryaev, S. Datta, K. Ackema, M. Zerial, and A. Spang, 'Identification of the switch in early-to-late endosome transition', *Cell*, vol. 141, no. 3, pp. 497–508, 2010.

[343] R. C. Piper, N. J. Bryant, and T. H. Stevens, 'The membrane protein alkaline phosphatase is delivered to the vacuole by a route that is distinct from the VPS-dependent pathway', *J. Cell Biol.*, vol. 138, no. 3, pp. 531–545, 1997.

[344] L. Bas, D. Papinski, and C. Kraft, 'Ykt6 mediates autophagosome-vacuole fusion', *Mol. Cell. Oncol.*, vol. 5, no. 6, pp. 1–3, 2018.

[345] M. Tsukada and Y. Ohsumi, 'Isolation and characterization of autophagy-defective mutants of Saccharomyces cerevisiae', *FEBS Lett.*, vol. 333, no. 1–2, pp. 169–174, 1993.

[346] G. Barve and R. Manjithaya, 'Cross-talk between autophagy and sporulation in Saccharomyces cerevisiae', *Yeast*, vol. 38, no. 7, pp. 401–413, 2021.

[347] J. E. Gerst, L. Rodgers, M. Riggs, and M. Wigler, 'SNCI, a yeast homolog of the synaptic vesicle-associated membrane protein/synaptobrevin gene family: Genetic interactions with the RAS and CAP genes', *Proc. Natl. Acad. Sci. U. S. A.*, vol. 89, no. 15, p. 7287, 1992.

[348] J. A. McNew *et al.*, 'Compartmental specificity of cellular membrane fusion encoded in SNARE proteins', *Nature*, vol. 407, no. 6801, pp. 153–159, 2000.

[349] M. Hothorn *et al.*, 'Catalytic core of amembrane-associated eukaryotic polyphosphate polymerase', *Science (80-.).*, vol. 324, no. 5926, pp. 513–516, 2009.

[350] A. Cohen, N. Perzov, H. Nelson, and N. Nelson, 'A novel family of yeast chaperons involved in the distribution of V- ATPase and other membrane proteins', *J. Biol. Chem.*, vol. 274, no. 38, pp. 26885–26893, 1999.

[351] O. Müller, M. J. Bayer, C. Peters, J. S. Andersen, M. Mann, and A. Mayer, 'The Vtc proteins in vacuole fusion: Coupling NSF activity to Vo trans-complex formation', *EMBO J.*, vol. 21, no. 3, pp. 259–269, 2002.

[352] N. Nelson, N. Perzov, A. Cohen, K. Hagai, V. Padler, and H. Nelson, 'The cellular biology of proton-motive force generation by V-ATPases', *J. Exp. Biol.*, vol. 203, no. 1, pp. 89–95, 2000.

[353] A. Uttenweiler, H. Schwarz, H. Neumann, and A. Mayer, 'The Vacuolar Transporter Chaperone (VTC) Complex Is Required for Microautophagy', *Mol. Biol. Cell*, vol. 18, no. December, pp. 986–994, 2007.

[354] R. C. Dickson, E. E. Nagiec, G. B. Wells, M. M. Nagiec, and R. L. Lester, 'Synthesis of mannose-(inositol-P)2-ceramide, the major sphingolipid in Saccharomyces cerevisiae, requires the IPT1 (YDR072c) gene', *J. Biol. Chem.*, vol. 272, no. 47, pp. 29620–29625, 1997.

[355] K. Thevissen *et al.*, 'SKN1, a novel plant defensin-sensitivity gene in Saccharomyces cerevisiae, is implicated in sphingolipid biosynthesis', *FEBS Lett.*, vol. 579, no. 9, pp. 1973–1977, 2005.

[356] T. Roemer, S. Delaney, and H. Bussey, 'SKN1 and KRE6 define a pair of functional homologs encoding putative membrane proteins involved in beta-glucan synthesis', *Mol. Cell. Biol.*, vol. 13, no. 7, pp. 4039–4048, 1993.

[357] K. Thevissen *et al.*, 'Skn1 and Ipt1 negatively regulate autophagy in Saccharomyces cerevisiae', *FEMS Microbiol. Lett.*, vol. 303, no. 2, pp. 163–168, 2010.

[358] A. M. Aerts *et al.*, 'Level of M(IP)2C sphingolipid affects plant defensin sensitivity, oxidative stress resistance and chronological life-span in yeast', *FEBS Lett.*, vol. 580, no. 7, pp. 1903–1907, 2006.

[359] M. Yamagata, K. Obara, and A. Kihara, 'Sphingolipid synthesis is involved in autophagy in Saccharomyces cerevisiae', *Biochem. Biophys. Res. Commun.*, vol. 410, no. 4, pp. 786–791, 2011.

[360] L. Munzel, ‘Atg21 restricts Atg8 lipidation to a novel vacuole-phagophore contact site’, 2018.

[361] Y. X. Wang, N. L. Catlett, and L. S. Weisman, ‘Vac8p, a vacuolar protein with armadillo repeats, functions in both vacuole inheritance and protein targeting from the cytoplasm to vacuole’, *J. Cell Biol.*, vol. 140, no. 5, pp. 1063–1074, 1998.

[362] E. Kvam and D. S. Goldfarb, ‘Nucleus-vacuole junctions and piecemeal microautophagy of the nucleus in S. cerevisiae’, *Autophagy*, vol. 3, no. 2, pp. 85–92, 2007.

[363] M. F. Manolson *et al.*, ‘The VPH1 gene encodes a 95-kDa integral membrane polypeptide required for in vivo assembly and activity of the yeast vacuolar H+-ATPase’, *J. Biol. Chem.*, vol. 267, no. 20, pp. 14294–14303, 1992.

[364] J. Metje, ‘Structural characterization of autophagy related protein complexes’, 2017.

[365] L. M. Banta, J. S. Robinson, D. J. Klionsky, and S. D. Emr, ‘Organelle assembly in yeast: characterization of yeast mutants defective in vacuolar biogenesis and protein sorting.’, *J. Cell Biol.*, vol. 107, no. 4, pp. 1369–1383, 1988.

[366] D. F. Seals, G. Eitzen, N. Margolis, W. T. Wickner, and A. Price, ‘A Ypt/Rab effector complex containing the Sec1 homolog Vps33p is required for homotypic vacuole fusion’, *Proc. Natl. Acad. Sci. U. S. A.*, vol. 97, no. 17, pp. 9402–9407, 2000.

[367] K. Peplowska, D. F. Markgraf, C. W. Ostrowicz, G. Bange, and C. Ungermann, ‘The CORVET Tethering Complex Interacts with the Yeast Rab5 Homolog Vps21 and Is Involved in Endo-Lysosomal Biogenesis’, *Dev. Cell*, vol. 12, no. 5, pp. 739–750, 2007.

[368] E. S. Seeley, M. Kato, N. Margolis, and W. Wickner, ‘Genomic Analysis of Homotypic Vacuole Fusion’, *Mol. Biol. Cell*, vol. 13, no. March, pp. 782–794, 2002.

[369] T. T. Liu, T. S. Gomez, B. K. Sackey, D. D. Billadeau, and C. G. Burd, ‘Rab GTPase regulation of retromer-mediated cargo export during endosome maturation’, *Mol. Biol. Cell*, vol. 23, no. 13, pp. 2505–2515, 2012.

[370] T. Courtellemont, M. G. De Leo, N. Gopaldass, and A. Mayer, ‘CROP: A Retromer-PROPPIN complex mediating membrane fission in the endo-lysosomal system’, *bioRxiv*, p. 2021.09.06.459059, 2021.